Unravelling Synthesis and Transport Phenomena in Emulsion Systems with Small Angle Scattering

Yi-Ting Lee

A dissertation

submitted in partial fulfillment of the

requirements for the degree of

Doctor of Philosophy

University of Washington

2019

Reading Committee:

Lilo D. Pozzo, Chair

Matthew O'Donnell

Cole A. DeForest

Vincent C. Holmberg

Program Authorized to Offer Degree:

Chemical Engineering

University of Washington

Abstract

Unravelling Synthesis and Transport Phenomena in Emulsion Systems
with Small Angle Scattering

Yi-Ting Lee

Chair of the Supervisory Committee:
Associate Professor Lilo D. Pozzo
Department of Chemical Engineering

Emulsions are a dispersion of two immiscible liquids that can be found in a variety of products frequently used in our daily lives. These dispersions of droplets are intrinsically unstable and would phase separate if no stabilizers were present. Even if the emulsions are stabilized, the emulsion system is still extremely dynamic and multiple phenomena could occur simultaneously to affect the stability of the dispersion. Therefore, fundamentally understanding how the droplets interact with each other is crucial when designing emulsion-based products.

Small angle scattering is a unique technique that can provide information of a sample in its native environment. Moreover, custom-built sample environments could also be utilized with this technique to provide additional controllable parameters such as the application of acoustic forces

to alter the dynamics in emulsion system. Thus, small angle scattering is an optimal method for characterizing emulsion systems. In this dissertation, three different fundamental interactions that occur in emulsion systems are probed using both small angle X-ray scattering and small angle neutron scattering.

The role of acoustic forces in solid particle stabilized Pickering emulsion formation using sonication is first investigated. Cavitation events are found to be crucial in inducing particle adsorption onto the oil-water interface. Mass transport kinetics between emulsions are also presented in this dissertation. When the emulsions are at rest, oil molecules can exchange between oil droplets spontaneously by directly diffusing through the aqueous phase or via direct emulsion contact. When emulsions are sonicated, the acoustic-force induced cavitation can significantly accelerate the oil exchange process. Moreover, the electrostatic repulsion, Gibbs elasticity of the oil-water interface provided by the presence of surfactants, and the emulsion size all played a role in the acoustic force induced oil exchange process. This dissertation will demonstrate our work towards understanding the interactions in emulsion systems on a molecular scale to provide a fundamental knowledge on how to design an emulsion-based system.

TABLE OF CONTENTS

LIST OF FIGURES

LIST OF TABLES

ACKNOWLEDGEMENTS

I would like to thank my advisor Dr. Lilo Pozzo for her mentoring and guidance. She was always available to meet and discuss even about very minor details in experimental designs or results. I am always impressed by her expertise and ability to instantly provide feedback and suggestions. She can always provide directions which motivates me to develop and grow to be a better scientist. I would also like to thank the members of my committee, Dr. Cole DeForest, Dr. Vincent Holmberg, and Dr. Matthew O'Donnell for their intellectual guidance, kindness for allowing me to make mistakes and to provide the opportunity to show improvement.

I am also lucky to have the opportunities to meet and work with several researchers at different national labs. Specifically, I am grateful for Dr. Jan Ilavsky and Dr. Ivan Kuzmenko from the Argonne national lab, Dr. John Barker and Dr. Yun Liu at NIST Center for Neutron Research for all their help executing experiments and analyzing our scattering data. Most importantly, for willing to show up no matter what time it is and help us troubleshoot. Without them, none of the work presented here would be possible.

I would also like to thank all of my current and past lab mates including, Dr. Greg Newbloom, Dr. David S. Li, Dr. Yeneneh Yimer, Dr. Pablo De La Iglesia, Dr. Yuyin Xi, Ryan Kastilani, Kiran Kanekal, Caitlyn Wolf, Jamie Rodrigues, Canfeng Wei, Ziwei Zhou, Kacper Lachowski, Sage Scheiwiller, Shrilakshmi Bonageri, and all of the basement friends (past and present) for all of the technical conversations and moral support. I would especially like to thank Greg and David for their patience when helping me go over my thoughts and proving their insights base on their experience and Dr. Jared Shadish for exploring a lot of Seattle with me. Without everyone, I would have been able to keep my sanity with the countless hours in Benson Hall.

DEDICATION

To my family and friends

Chapter 1. INTRODUCTION

1.1 EMULSIONS

Emulsions are dispersions of liquid droplets in another type of continuous liquid solvent in which the two liquids are not miscible with each other. This dissertation is restricted to emulsions of water and oil, either as oil-in-water or water-in-oil emulsions (Figure 1.1), and these emulsions have several applications in the food, agriculture, chemical manufacturing, and biomedical fields.[1–3] Some examples of commonly used emulsion products used in our daily lives include mayonnaise, butter, milk, paint, skin care products, pesticides, and drugs.

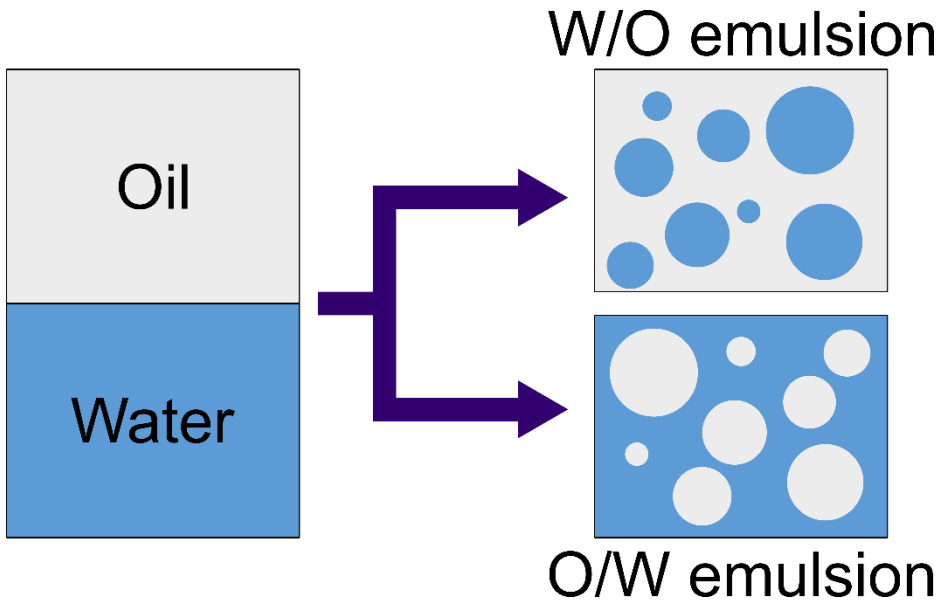

Figure 1.1. Example of using two immiscible liquids to form emulsions. Based on the amount of the phases and the stabilizer used, one can form either water-in-oil (W/O) or oil-in-water (O/W) emulsions.

Emulsions can be roughly divided and described as macroemulsions, microemulsions, and nanoemulsions based on their size and stability.[4] Macroemulsions are droplets with sizes greater than 500 nm in diameter and the dispersion is usually milky white and turbid. On the other hand,

nanoemulsion and microemulsions are special cases where the dispersions are less turbid, sometimes event transparent. These droplets usually have sizes ranging from 5 to 500 nanometers in diameter. The main difference between nanoemulsion and microemulsion is their stability. Microemulsions are thermodynamically stable swollen micelles whereas nanoemulsions are metastable dispersions that are kinetically stable but thermodynamically unstable.[4] Therefore, if given enough time, nanoemulsions will ultimately phase separate into the original two immiscible liquids.

Based on the definition of different types of emulsion systems, it is clear that these dispersions are rarely thermodynamically stable. This is because emulsion systems are very dynamic and multiple processes could occur simultaneously to induce instability. These interactions are similar to lyophobic (hydrophobic) colloidal systems where the colloids undergo particle size disproportionation (Oswald ripening), phase segregation, flocculation, and coalescence.[5,6] Ostwald ripening occurs through the dissolution of the dispersed molecules through the continuous phase, which would result in a growth of the larger and the disappearance of smaller droplets. If emulsion samples are allowed to sit over time, gravitational forces could cause emulsion phase segregation. Depending on the density differences between the dispersed and continuous phase, the droplets would either sediment or cream. Flocculation can also occur due to the attraction between droplets or the presence of other colloids (e.g. polymers/micelles/particles) in the dispersion, resulting in droplet clustering. Both phase segregation and flocculation will concentrate droplets in emulsion system and could potentially result in merging of droplets or 'coalescence'. Forming larger droplets further decreases interfacial area between immiscible liquids. Moreover, these droplets also have a larger tendency to sediment or cream due to the buoyance forces and the reduced diffusivity of larger droplets. As a result, further droplet

coalescence can occur and can ultimately lead to phase-separation, which is the minimal achievable interfacial area.

Still, in order to induce coalescence, the thin liquid film between droplet interfaces must be drained. Draining the liquid films to a certain thickness 'h_c' will destabilize and ruptures the oil-water interface thus inducing coalescence. However, whether the film will thicken or thins is correlated to the disjoining pressure, which is the differences between the pressure in the liquid film and the bulk solution. Disjoining pressure is affected by interfacial properties, therefore, one could alter the intermolecular forces (i.e. van der Waals attraction, repulsion from surfactants, and hydrogen bonding) to either synthesize a stable emulsion or demulsify the emulsion dispersion.[7]

1.2 Emulsifiers for Stabilizing Emulsions

In order to increase the shelf life of emulsions for potential applications, emulsifiers are often added to increase the kinetic stability of dispersions. Emulsifiers are stabilizing agents that can interact with both types of liquid, lowering the interfacial tension between the two insoluble liquids, and increasing the kinetic stability of the emulsions (Figure 1.2).[8,9] When properly stabilized, emulsions can remain stable for many years.

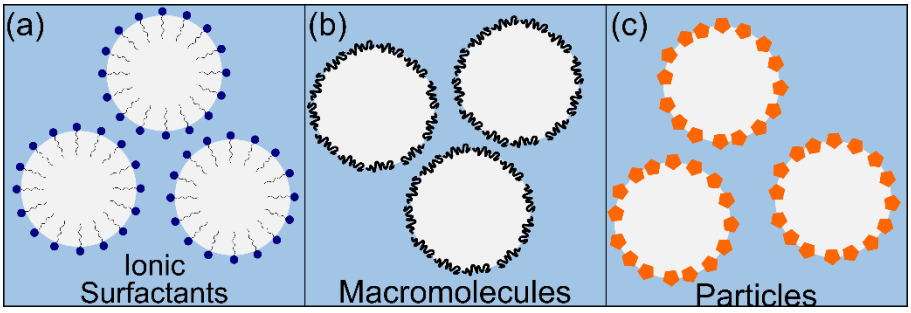

Figure 1.2. Emulsions stabilized by different types of emulsifiers.

Common surfactants that are used in our daily lives are small molecules that contain both hydrophobic and hydrophilic characteristics, such as anionic surfactant sodium dodecyl sulfate (SDS) or cationic surfactant cetrimonium bromide (CTAB). The hydrocarbon tail of surfactants can interact favorably with hydrophobic liquids whereas the hydrophilic head will be attracted to the aqueous phase. Thus, these small molecules can tightly pack onto oil-water interfaces and create repulsive forces between droplets due to the presence of charged hydrophilic head groups for oil in water emulsion systems (i.e. sulfate head groups), making the compounds useful as a detergent.

Another method to stabilize an emulsion system is the use of non-ionic surfactants, such as macromolecules or polymers. These molecules can also contain hydrophobic blocks which interacts with the hydrophobic liquids and hydrophilic blocks that interacts with the aqueous phase. Adsorbed non-ionic surfactants can produce steric repulsion forces between droplets that are also stabilized by non-ionic surfactants, thus physically preventing the droplets from coalescing.[10] Examples of non-ionic surfactants include Tween®, Triton®, polysaccharides, and Span® commercial products, as well as polymers such as polyethylene glycol and Pluronic®.[11–14]

Finally, solid particles can also be used to stabilize emulsion droplets in what is known as a Pickering emulsion. Pickering emulsions were first observed in 1907 by S.U. Pickering.[15] One advantage of Pickering emulsions over traditional surfactant-stabilized emulsions is that the presence of particles at the oil-water interface produces a shell that significantly increases the droplet's resistance to coalescing.[16,17] Moreover, the amount of energy required to remove a particle from this oil-water interface tends to be significantly higher than of surfactant stabilized systems.[18] Pickering emulsions have also been shown to have less toxicity, making them attractive

candidates for biomedical applications.[16,17] Other applications for Pickering emulsions are found in the food synthesis, wastewater treatment, and oil recovery.[1,16,19,20]

1.3 EMULSION SYNTHESIS

A simplified schematic diagram of emulsion formation and breakup thermodynamics is shown in Figure 1.3. The free energy associated with forming emulsion dispersions from the separate liquid state could be expressed using equation (1.1), where ΔG_{area} is the interfacial free energy, T is the temperature, and $\Delta S_{configuration}$ is the configurational entropy. Moreover, the interfacial free energy at a constant temperature and pressure can be expressed as the total free energy of the increasing interfacial surfaces (equation (1.2)), where γ is the interfacial tension at the oil-water interphase and ΔA is the increased total contact area. The configurational entropy depends on the number of oil droplets formed in the dispersion and can be expressed using equation (1.3), where N is the number of emulsion droplets formed, k is the Boltzmann constant, and Φ_0 is the oil volume fraction in the system. The free energy change $\Delta G_{emulsion}$ between the emulsion dispersion state versus the separated bulk liquids state is generally greater than zero (e.g. macroemulsions and nanoemulsions) but there are systems where it is less than zero (e.g. microemulsions). However, as can be seen in Figure 1.3 there is an additional energy, the activation energy, separating the two states. This activation energy is usually significantly greater than the free energy change. Therefore, large amounts of mechanical energy are usually required to form stable emulsions.

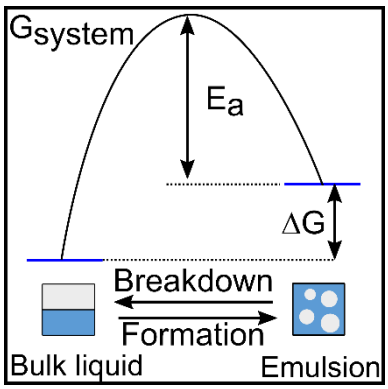

Figure 1.3. Simplified thermodynamic diagram of emulsion formation and breakup.

$$\Delta G_{emulsion} = \Delta G_{area} - T\Delta S_{configuration} \quad (1.1)$$

$$\Delta G_{area} = \gamma \Delta A \quad (1.2)$$

$$\Delta S_{configuration} = -Nk\left[\ln \emptyset_0 + \left(\frac{1-\emptyset_0}{\emptyset_0}\right)\ln(1-\emptyset_0)\right] \quad (1.3)$$

As indicated above, mechanical energy is generally required to de-stabilize the interfaces between the two liquid phases to 'break' these down into smaller droplets during emulsification. The amount of energy that is required to form emulsions can range from as small as just shaking and mixing a sample by hand to using specialized equipment to induce high shear fields in the system to break down large droplets and to form smaller ones. Some of the techniques commonly used for synthesizing emulsions include high shear mixing, high pressure homogenization (i.e. Avestin), liquid jet breakup and sonication.

On the other hand, emulsions can also form spontaneously and without the application of external forces. One example of spontaneous emulsification is the synthesis of microemulsions, where $\Delta G_{emulsion}$ is less than zero and no energy barriers (i.e. activation energy) exists. Another example is the 'ouzo effect' in reference to the Greek alcoholic drink.[21] In the latter case, the formation of emulsions can't be explained using classical thermodynamics. Moreover, the

synthesized emulsions are still thermodynamically unstable and will phase-separate with enough time. The main mechanism behind this effect is that some hydrophobic oils have a finite solubility in solvents like ethanol. When a miscible bad solvent (i.e. water) is added into the system, the solubility of the oil decreases and oil is forced out of solution to form small droplets without any mechanical energy input. This method can synthesize very small and monodisperse emulsion droplets but requires three types of liquids which can be problematic for some systems.

Phase inversion methods including phase inversion temperature (PIT) and catastrophic phase inversion (CPI) are also techniques that can be used to synthesize emulsions spontaneously. PIT takes advantage of the temperature dependent solubility of non-ionic surfactants (i.e. polyethoxylated surfactants) in water, where higher temperatures generally result in a decrease in the polymer's affinity with water.[22–24] For example, increasing temperatures for O/W emulsions stabilized by polyethylene glycol will result in inverting the system to W/O emulsions. Lowering the temperature could invert the system back to the O/W emulsion state. CPI, on the other hand, uses the volume fraction of the water and oil in the system for synthesizing emulsions. By adding water to an oil system containing surfactant, W/O emulsions can be initially formed. Increasing water volume fraction would result in forming more W/O emulsion droplets which will eventually coalesce and phase invert to an O/W system.[25,26] Both phase inversion techniques have the advantage of being able to synthesize small monodisperse emulsion droplets and can be easily scaled up for manufacturing processes.[23] However, these methods usually require the use of high concentrations of surfactants, which would potentially be problematic for some applications.

1.4 ULTRASOUND

Ultrasound is defined as acoustic waves where the frequency is greater than the standard human audible limit (> 20k Hz). It is often associated with uses in the medical field for imaging or therapy (i.e. ablation) but it is also commonly used in other fields for applications including sonar, nondestructive testing, and ultrasonic humidifiers among many others. The application of ultrasound (sonication) is also one of the most commonly used techniques in chemical labs for glassware cleaning, re-suspension of dispersed material, and for emulsification.

When acoustic waves are propagating through the medium, they will result in constant compressing and pulling of liquid regions within the sample (Figure 1.4). The displacement relative to equilibrium can be expressed as equation (1.4), where A is the maximum amplitude, f is the frequency of the acoustic wave, and t is time. If the acoustic pressure is higher than a certain threshold, the local negative pressure could overcome the saturated vapor pressure of the solvent (or droplet) and result in the formation of vapor cavities. Vapor cavities can then oscillate with the acoustic pressure waves or collapse during the positive pressure phase.[27] This formation and collapse of vapor bubbles is called cavitation and it has been demonstrated to be able to provide high local stresses, pressures, and temperatures up to 5000K.[28–30] Stresses resulting from cavitation are the important contributors to many of the previously mentioned applications.

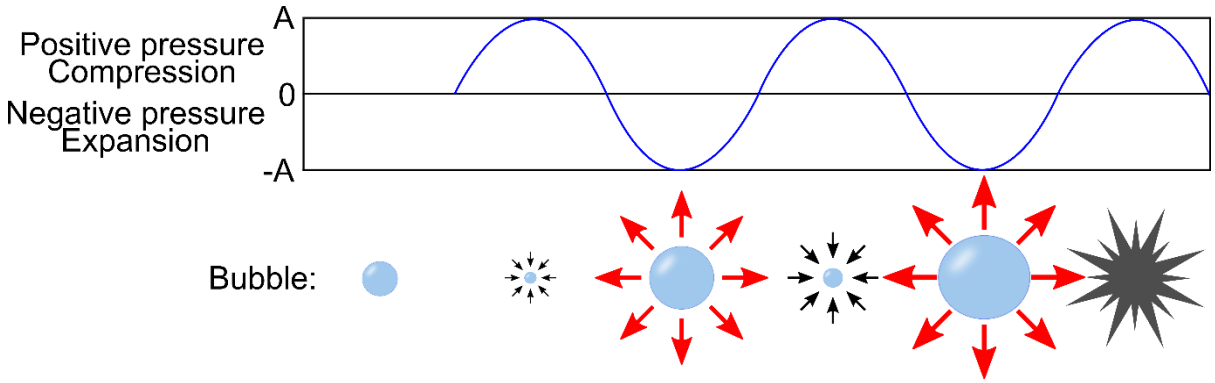

Figure 1.4. Oscillating acoustic waves can induce formation and collapse of vapor cavities (cavitation) which can provide high stresses and temperatures.

$$a = A \sin 2\pi f t \tag{1.4}$$

As mentioned previously, sonication is one of the most frequently used methods for synthesizing emulsions. It has been demonstrated that ultrasound induced emulsification is a two stage process.[31] The applied acoustic wave first induces a Rayleigh-Taylor instability at the interface between the bulk oil and water phase, resulting in the formation of large droplets (~100 μm in diameter). The second step is when cavitation occurs near the oil-water interfaces, further breaking down the droplets to very fine sizes with diameters as small as on the order of a couple of nanometers.[32]

The final synthesized droplet size is affected by various parameters including the type and concentration of the surfactants used, the viscosity of the liquids, the oil volume fraction in the system, and the applied acoustic parameters.[27,33,34] Using higher ultrasound frequencies have been shown to create marginally smaller emulsion droplets.[32,35] However, the cavitation threshold also increases when using higher frequency acoustic sources. Therefore, this will require greater energy input for emulsification at higher frequencies.[36] The effects of insonication time and applied acoustic power (intensity) on synthesized emulsion size (Sauter mean diameter $d_{3,2}$) can be expressed using a power law equation (equation (1.5)), where P_w is the applied power density and

t_s is sonication time. The decrease in emulsion size during sonication is more pronounced in the initial stage of sonication and the dispersion will eventually reach an equilibrium size. Increasing the input power will result in less sonication time required to reach the final equilibrium size.[37] Other parameters related to the ultrasound waves that will affect the emulsification process include the amount of dissolved gas and particles in the medium, the temperature, and the hydrostatic pressure of the system.[27,38,39]

$$d_{3,2} = P_w^{-a} t_s^{-b} \tag{1.5}$$

The use of ultrasound in emulsion systems is not only restricted to emulsion synthesis. One example is the use of sonication to induce particle adsorption onto emulsion interfaces to form of Pickering emulsions.[16,40,41] Acoustic forces are also often used in sonochemistry, using emulsions as micro reactors for chemical synthesis.[42–44] In these cases, the extreme conditions provided by the cavitation events can break chemical bonds (i.e. hydrogen bonds in water) to form radicals to initiate reactions in processes including emulsion polymerization and nanomaterial synthesis.[42,45] The application of ultrasound is also common in the oil industry for demulsifying W/O emulsions.[46–48] Reports for these processes often use acoustic standing waves and demulsifiers to induce phase separation. The demulsifiers can displace the particles stabilizing the emulsion interface, the acoustic standing waves can concentrate the droplets to the antinodes, and the cavitation events can disrupt the oil-water interface to induce emulsion coalescence.

1.5 Goal and Objectives

The main goal of this thesis is to fundamentally examine interactions at emulsion interfaces. The approach taken in this dissertation is to use of both small angle X-ray scattering

and small angle neutron scattering to examine emulsion systems in their native dispersion state. To this end, a custom-built ultrasound sample environment is used in portions of the studies to examine acoustic-force induced interactions. Two different interactions at emulsion interfaces will be examined in this dissertation. First, we examine the role of acoustic forces in inducing the formation of particle stabilized emulsions. The second portion of this dissertation discusses mass transport phenomena that occurs in emulsion systems both at rest and under the influence of acoustic forces.

The first system that will be examined is the formation of gold nanoparticle stabilized Pickering emulsions (Chapter 3). Despite having several advantages over the classical surfactant stabilized emulsions and having potential in numerous applications, there are still challenges associated with their synthesis process. One key challenge is the limitations in the synthesis of particles that are capable of forming Pickering emulsions. Another main challenge is the presence of energy barriers that may be present to prevent adsorption of particles onto the emulsion interface. In Chapter 3 we will examine an amphiphilic gold nanoparticle stabilized emulsion model system to determine which acoustic parameters are most crucial in overcoming existing energy barriers. Here we used ultra-small angle X-ray scattering to characterize structural changes occurring during the sonication process. We also developed a Debye scattering model to better fit the acquired scattering data. This model allows us to obtain important Pickering emulsion parameters including emulsion size, surface coverage, and amount of unbounded particles in the system. With this new approach, we show that cavitation events occurring during sonication are crucial to overcoming energy barriers to induce Pickering emulsion formation. In addition, different types of emulsions are used to synthesize Pickering emulsion and we show that there are

no substantial differences in the estimated cavitation thresholds. However, significant oil loss is also observed for lower boiling point emulsions, which can be an important consideration.

In Chapters 4 and 5 we use time-resolved small angle neutron scattering with a combination of contrast variation to examine the transport of oil molecules between oil droplets at rest and under the influence of acoustic forces. The basis on the technique used in both of these chapters is the design of an emulsion system that would be contrast matched when oil molecules are fully exchanged between the different droplets. The main advantage of this technique is the ability to use only one chemical composition to examine mass transport in emulsion systems. In short, a mixture containing two different populations of emulsions, one with a higher scattering length density and one with a lower scattering length density, were allowed to exchange oil molecules either at rest or under the influence of acoustic forces. Any oil exchange occurring between different oil droplets resulted in a net decrease in contrast and thus a decrease in the recorded scattering intensities. Moreover, a relaxation function was defined and used to measure the extent of oil exchanged between droplets, providing a standardized method to quantify and compare oil exchange kinetics between various emulsion systems.

The transport of oil molecules between oil droplets in emulsion systems at rest is first examined in Chapter 4. In this study, parameters including the concentration of stabilizing anionic surfactant (i.e. sodium dodecyl sulfate, hexyl sulfate sodium salt, and tetradecyl sulfate sodium salt), temperature of the samples, concentration of salt in the emulsion system, and the solubility of the oil phase was varied to examine its effects on the oil exchange kinetics. With this approach, we showed that the oil exchange kinetics is significantly faster when surfactants are present and when the samples were held at a higher temperature. Moreover, the concentration of surfactant present, the type of anionic surfactants used, and the addition of salt in emulsion systems showed

little effects on the exchange kinetics. However, it was also observed that the presence of surfactant micelles would minimally accelerate the oil exchange kinetics through depletion interactions. The main driving force to the observed oil exchange was hypothesized to be a combination of direct oil molecule diffusion through the aqueous phase and a direct emulsion contact mechanism. In contrast, direct oil diffusion mechanisms would dominate in emulsion systems when using higher solubility oils. Direct emulsion contact oil exchange would be the primary exchange mechanisms for insoluble emulsion systems.

Acoustic force induced oil exchange in emulsion systems is further investigated in Chapter 5. In this study, hexadecane emulsions stabilized by different concentrations of SDS were sonicated at various acoustic pressures. It was observed that the oil exchange process is greatly accelerated when sonicated but only when cavitation events occurred. Moreover, the presence of stabilizing surfactants at oil-water interfaces showed an opposite trend when compared to the results obtained for emulsion systems at rest. Surfactant stabilized emulsions exchanged oil molecules at a significantly slower rate and the exchange kinetics is strongly affected by the concentration of stabilizing surfactants (non-linear correlation). The mechanism driving the oil exchange process is hypothesized to be reversible droplet coalescence. Moreover, the droplet size, the electrostatic repulsion provided by the stabilizing surfactants, and the Gibbs elasticity provided by the surfactants decorating the emulsions played significant roles in deterring the rate of emulsion coalescence. Work in Chapters 4 and 5 demonstrates that mass transport in emulsion systems is extremely complex and time resolved small angle neutron scattering is a unique tool that can provide the ability to probe this type of system.

1.6 REFERENCES

(1) Berton-Carabin, C. C.; Schroën, K. *Annu. Rev. Food Sci. Technol.* **2015**, *6* (1), 263–297.

(2) Koo, O. M.; Rubinstein, I.; Onyuksel, H. *Nanomedicine Nanotechnology, Biol. Med.* **2005**, *1* (3), 193–212.

(3) Skerget, M.; Kotnik, P.; Hadolin, M.; Hras, A. R.; Simonic, M.; Knez, Z. *Food Chem.* **2005**, *89* (2), 191–198.

(4) McClements, D. J. *Soft Matter* **2012**, *8* (6), 1719–1729.

(5) Berg, J. C. *An Introduction to Interfaces and Colloids*; WORLD SCIENTIFIC, **2009**.

(6) Ivanov, I. B.; Kralchevsky, P. A. *Colloids Surfaces A Physicochem. Eng. Asp.* **1997**, *128* (1–3), 155–175.

(7) Aveyard, R.; Clint, J. H. *Curr. Opin. Colloid Interface Sci.* **1996**, *1* (6), 764–770.

(8) Binks, B. P. *Curr. Opin. Colloid Interface Sci.* **2002**, *7* (1–2), 21–41.

(9) Aveyard, R.; Binks, B. P.; Clint, J. H. *Adv. Colloid Interface Sci.* **2003**, *100–102*, 503–546.

(10) Manor, O.; Chau, T. T.; Stevens, G. W.; Chan, D. Y. C.; Grieser, F.; Dagastine, R. R. *Langmuir* **2012**, *28* (10), 4599–4604.

(11) Zhang, T.; Marchant, R. E. *J. Colloid Interface Sci.* **1996**, *177* (2), 419–426.

(12) Weiss, J.; McClements, D. J. *Langmuir* **2000**, *16* (14), 5879–5883.

(13) Joscelyne, S. M.; Trägårdh, G. **2000**, *169* (April 1999), 107–117.

(14) Burguera, J. L.; Burguera, M. *Talanta* **2012**, *96*, 11–20.

(15) Pickering, S. U. *J. Chem. Soc., Trans.* **1907**, *91*, 2001–2021.

(16) Wu, J.; Ma, G.-H. *Small* **2016**, *12* (34), 4633–4648.

(17) Kaewsaneha, C.; Tangboriboonrat, P.; Polpanich, D.; Eissa, M.; Elaissari, A. *Colloids*

Surfaces A Physicochem. Eng. Asp. **2013**, *439*, 35–42.

(18) Tu, F.; Park, B. J.; Lee, D. *Langmuir* **2013**, *29* (41), 12679–12687.

(19) Chevalier, Y.; Bolzinger, M.-A. *Colloids Surfaces A Physicochem. Eng. Asp.* **2013**, *439*, 23–34.

(20) Wang, X.; Shi, Y.; Graff, R. W.; Lee, D.; Gao, H. *Polymer.* **2015**, *72*, 361–367.

(21) Vitale, S. a.; Katz, J. L. *Langmuir* **2003**, *19* (10), 4105–4110.

(22) Shinoda, K.; Saito, H. *J. Colloid Interface Sci.* **1968**, *26* (1), 70–74.

(23) Anton, N.; Vandamme, T. F. *Int. J. Pharm.* **2009**, *377* (1–2), 142–147.

(24) Anton, N.; Benoit, J.-P.; Saulnier, P. *J. Control. Release* **2008**, *128* (3), 185–199.

(25) Binks, B. P.; Lumsdon, S. O. *Langmuir* **2000**, *16* (6), 2539–2547.

(26) Anton, N.; Benoit, J. P.; Saulnier, P. *J. Control. Release* **2008**, *128* (3), 185–199.

(27) Canselier, J. P.; Delmas, H.; Wilhelm, A. M.; Abismaïl, B. *J. Dispers. Sci. Technol.* **2002**, *23* (1–3), 333–349.

(28) Flint, E. B.; Suslick, K. S. *Science,* **1991**, *253* (5026), 1397–1399.

(29) Doktycz, S.; Suslick, K. *Science,* **1990**, *247* (4946), 1067–1069.

(30) Suslick, K. S.; Price, G. J. *Annu. Rev. Mater. Sci.* **1999**, *29* (1), 295–326.

(31) Kentish, S.; Wooster, T. J.; Ashokkumar, M.; Balachandran, S.; Mawson, R.; Simons, L. *Innov. Food Sci. Emerg. Technol.* **2008**, *9* (2), 170–175.

(32) Li, M. K.; Fogler, H. S. *J. Fluid Mech.* **1978**, *88* (03), 513.

(33) Mujumdar, S.; Senthil Kumar, P.; Pandit, A. B. *Indian J. Chem. Technol.* **1997**, *4* (6), 277–284.

(34) Gaikwad, S. G.; Pandit, A. B. *Ultrason. Sonochem.* **2008**, *15* (4), 554–563.

(35) Kaci, M.; Arab-Tehrany, E.; Desjardins, I.; Banon-Desobry, S.; Desobry, S. *J. Food Eng.*

2017, *194*, 109–118.

(36) Apfel, R. E.; Holland, C. K. *Ultrasound Med. Biol.* **1991**, *17* (2), 179–185.

(37) Cucheval, A.; Chow, R. C. Y. *Ultrason. Sonochem.* **2008**, *15* (5), 916–920.

(38) Bondy, C.; Söllner, K. *Trans. Faraday Soc.* **1935**, *31* (C), 843–846.

(39) Bondy, C.; Söllner, K. *Trans. Faraday Soc.* **1935**, *31*, 835–843.

(40) Larson-Smith, K.; Pozzo, D. C. *Langmuir* **2012**, *28* (32), 11725–11732.

(41) Yang, Y.; Fang, Z.; Chen, X.; Zhang, W.; Xie, Y.; Chen, Y.; Liu, Z.; Yuan, W. *Front. Pharmacol.* **2017**, *8* 1–20.

(42) Xu, H.; Zeiger, B. W.; Suslick, K. S. *Chem. Soc. Rev.* **2013**, *42* (7), 2555–2567.

(43) Entezari, M. H.; Ghows, N. *Ultrason. Sonochem.* **2011**, *18* (1), 127–134.

(44) Bhanvase, B. A.; Sonawane, S. H. *Chem. Eng. Process. Process Intensif.* **2014**, *85*, 86–107.

(45) Bradley, M.; Grieser, F. *J. Colloid Interface Sci.* **2002**, *251* (1), 78–84.

(46) Hamidi, H.; Mohammadian, E.; Asadullah, M.; Azdarpour, A.; Rafati, R. *Ultrason. Sonochem.* **2015**, *26*, 428–436.

(47) A Issaka, S. *J. Pet. Environ. Biotechnol.* **2015**, *06* (02).

(48) Kokal, S. L. *SPE Prod. Facil.* **2005**, *20* (01), 5–13.

Chapter 2. THEORY AND METHODS

2.1 SMALL ANGLE SCATTERING

Small angle scattering is a non-destructive technique that can be used to examine structures within samples. Advantages of scattering as a characterization method include its ability to analyze samples in their original environment (e.g. nanoparticles dispersed in liquid) and the ability to provide structural information over a wide range of length scales (from 1 to 10000 nm) depending on the instrument that is used. Moreover, based on use of the different irradiation sources (i.e. light, neutron or X-ray), small angle scattering can be used to highlight and characterize different material structures and thus can be applied to a variety of areas including colloids, polymers, and biology.[1,2]

2.1.1 *Small Angle Scattering Theory*

Small angle scattering introduces a collimated irradiation source, either X-ray or neutron beam, through a sample. While most of the irradiation source passes and transmits through the sample undisturbed, a small portion interacts with the sample and is scattered as shown in Figure 2.1. The intensity of the scattered beam is a function of angle and this contains information on the structure of the sample. The scattering is also a function of incident wavelength. Therefore, a scattering vector q is often used instead in order to compare data from instruments with sources that may have variable incident wavelengths. The scattering vector q, or momentum transfer vector, is defined as the difference between the incident vector (k_i) and the scattered vector (k_s) as shown in equation (2.1). Moreover, scattering data is the Fourier transform of the scattering length density distribution and has a unit of one over length. As a result, scattering data at regions of large

q provide information on smaller length scales whereas lower q section of the data has information on features spanning larger length scales.

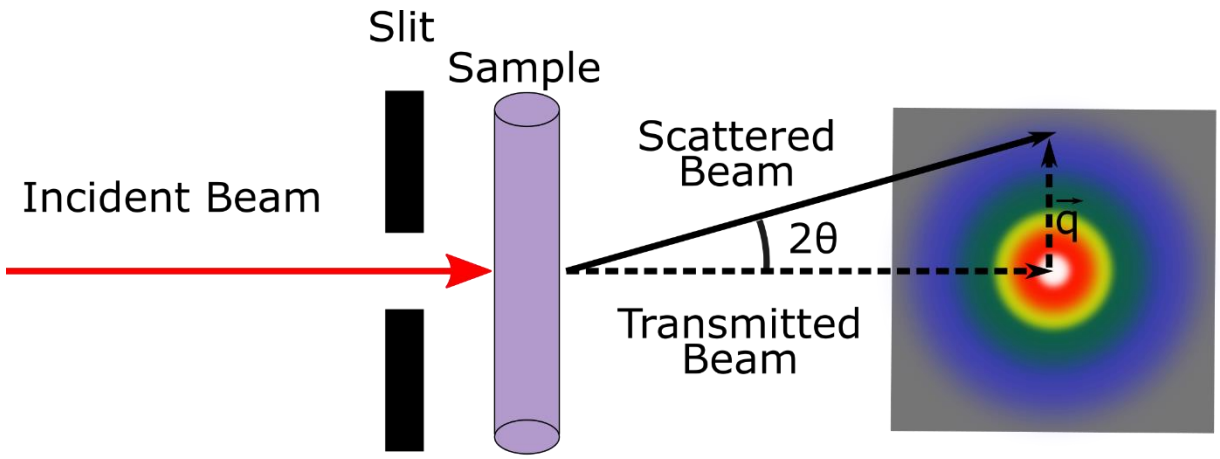

Figure 2.1. Schematic diagram of small angle scattering experimental setups.

$$q \equiv |\vec{q}| = |k_s - k_i| = \frac{4\pi}{\lambda} sin\frac{\theta}{2} \tag{2.1}$$

For small angle X-ray scattering (SAXS), the scattering signals acquired by the detector arise from elastic interactions between an incident X-ray photon and the electron clouds within the sample. Materials containing atoms with higher electron densities would have a higher probability of interacting with the incident X-ray and would scatter more, producing a higher scattering intensity. Thus, metal particles tend to scatter X-rays much more than organic molecules such as polymers or solvent molecules like water. On the other hand, scattering in small angle neutron scattering (SANS) originates from interactions between the incident neutron beam and the nucleus of atoms in the material, which also varies widely with different elements or isotopes. As a result, the amplitude of the interaction can differ significantly when compared to X-ray scattering

To quantify a material's ability to scatter due to an incident beam containing either X-rays or neutrons, a parameter called the scattering length density (SLD) is defined. For a material with a composition of A_mB_n, its scattering length density is shown in equation (2.2) where *b* is the scattering length contribution of each atom type and *m* and *n* are the numbers of atoms in a unit volume *v* of material. The SLD value of a chemical can be estimated using the National Institute of Standards and Technology SLD calculator by providing information on the chemical composition and the density of the material.[3]

$$scatter\ length\ density\ (SLD) = \rho = \frac{mb_A + nb_B}{v} \qquad (2.2)$$

Knowing the SLD value for all of the components in a system, including the solvent, all dispersed materials, and the dissolved components is critical to planning or conducting small angle scattering experiments. This is because the recorded scattering data contains scattering signals from all components within the examined sample. Thus, if the material of interest has a similar scattering length density to the continuous phase, the contrast would be very low and very little scattering will be observed. As a result, the scattering data will be noisy, would require longer integration times and, at the same time, may provide inadequate data for analysis.

Another crucial factor that needs to be considered when designing small angle scattering experiments is the amount of the incident beam that will transmit through the sample. Transmission intensity, which is measured at $\theta = 0^o$, decays exponentially as a function of the sample thickness (d) and attenuation (Λ) as shown in equation (2.3). Attenuation of X-rays and neutrons is from a combination of absorption and scattering from the sample. The attenuation coefficient for neutron scattering is also called the total scattering cross-section and will vary with the wavelength of the neutrons used to perform the experiment. Total scattering cross-sections for different materials can

be estimated using information in the evaluated nuclear data file (ENDF), which is a database that provides nuclear reaction data (e.g. neutron cross-sections). The total scattering cross-section of a sample can be assumed to be a linear combination the different materials present weighed by their volume fraction.[4] An example of estimating the neutron transmission through a sample in a small angle neutron scattering (SANS) experiment design while varying the amount of H_2O/D_2O in the solvent and sample thickness is shown in Figure 2.2. As can be seen in the figure, the transmission through the sample significantly decreases with an increase in sample thickness and the amount of H_2O in the solvent due to its high incoherent scattering cross-section. Therefore, to obtain the maximum neutron transmission through the samples when a SANS experiment, one would ideally use a deuterated solvent and a short sample pathlength. However, in order to obtain strong scattering signals in SANS experiments the contrast between the structures characterized and solvent also has to be accounted for. For example, minimal scattering intensities would be recorded from a sample containing deuterated structures (with similar SLD values to the solvent) in a fully deuterated solvent despite having the great sample transmission. Thus, depending on the samples characterized, there may be a conflict between trying to promote a higher contrast within the sample and also having a higher transmission signal when designing a neutron scattering experiment. An example of having to optimize sample contrast versus transmission is shown in Chapters 4 and 5, where a long pathlength sample holder was used in SANS experiments.

$$T = \frac{I_{\theta=0}}{I_0} = e^{-d/\Lambda} \tag{2.3}$$

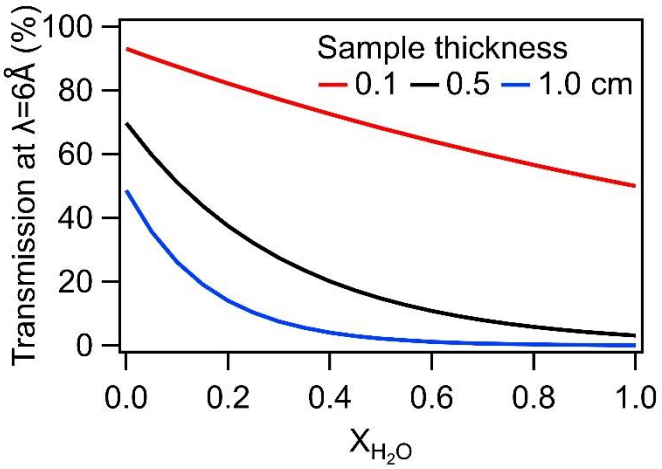

Figure 2.2. Example of sample transmission when using a 6 Å wavelength neutron as irradiation source. The transmitted intensity is a function of thickness and total scattering cross-section of the sample.

2.1.2 *Contrast Matching*

Although in most small angle scattering experiments it is ideal to have a sample where the contrast between the characterized material and the solvent is significant, having no contrast for portions of the analyzed system can also be beneficial. The use of zero contrast to highlight different parts of the sample is a technique called contrast matching (or contrast variation) and it is a unique method that is often used in SANS experiments.[2] One simple way of achieving the contrast matching condition is to vary the solvent that is used to dissolve the material. Another method is to take advantage of the substantial SLD differences between hydrogen and deuterium to make a solvent using both types of isotopes to tune the solvent's SLD. For example, when performing experiments in an aqueous solution, the SLD of the solvent could be tuned by mixing different ratios of H_2O/D_2O to obtain a solvent SLD ranging from -0.561×10^{-6} Å^{-2} (100% H_2O) to $6.363x \times 10^{-6}$ Å^{-2} (100%D_2O).[3]

One simplified example of using the contrast matching technique is when researchers are characterizing a sample that contains two different structures (e.g. squares and pentagons). The SLD of the solvent could be varied such that it matches one of the structure to highlight the other

(Figure 2.3 (a)). Contrast matching could also be applied to characterize portions of a structure within the same sample (e.g. a core-shell structure) to highlight either the shell thickness or the core size (Figure 2.3 (b)).

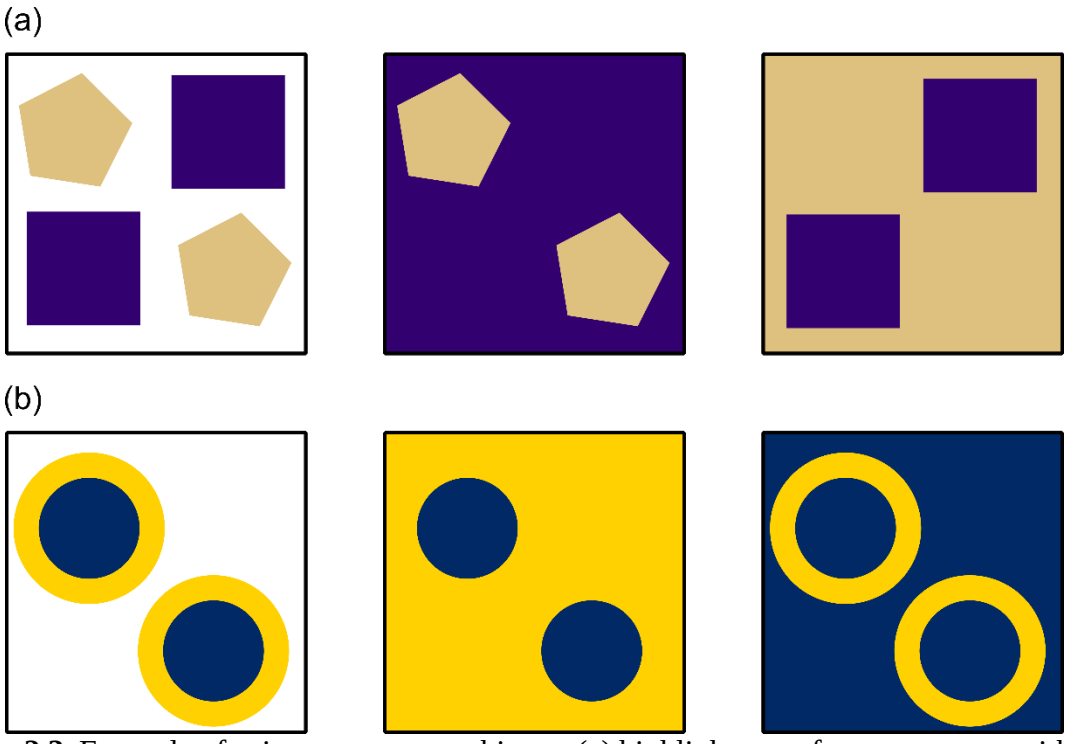

Figure 2.3. Example of using contrast matching to (a) highlight one of two structures within the system and (b) examine the shell thickness/core size in a core-shell structure.

Another example is also shown in Chapters 4 and 5 where contrast variation is used to examine the kinetics of oil exchange between oil in water emulsions using initial stock emulsions with different SLDs. This type of experiment is known as time-resolved SANS. Here, the system was designed to start with a mixture of higher SLD and lower SLD oil identical droplets with equal contrast to the solvent. Any oil exchange occurring in the system would result in a decrease in the contrast in the system and when the two emulsions are sufficiently exchanged, ideally no (or minimal) scattering would be detected from the sample (Figure 2.4).

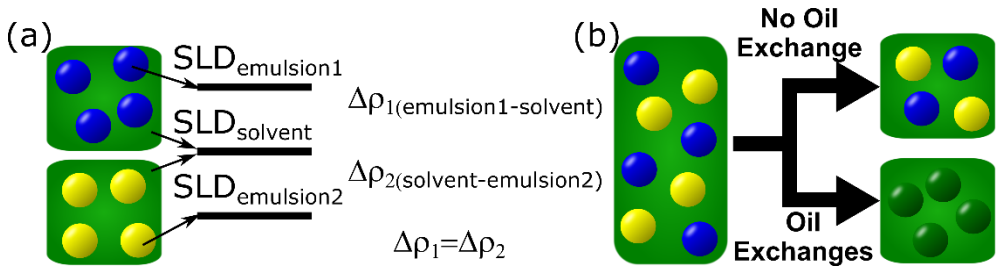

Figure 2.4. Schematic diagram of oil in water emulsion oil exchange experiment. (a) Deuterated and partially deuterated droplets have relative equal contrast to the solvent. (b) Oil exchange between emulsions would result in forming a perfect contrast matching system.

2.1.3 *Example of Optimizing Sample Contrast Versus Transmission*

The overall measured scattering intensity is correlated with the sample transmission (T) and contrast (Δρ) as shown in equation (2.4). Moreover, the contrast of the two stock emulsion systems can be expressed as equation (2.5), where $SLD_{emulsion1}$ and $SLD_{emulsion2}$ are scattering length densities (SLD) of the two populations of emulsion that are consistent with hydrogenated/deuterated hexadecane and $SLD_{solvent}$ is the scattering length density of the solvent (H_2O and D_2O mixture).

Ideally one would choose to use a fully deuterated hexadecane as the high SLD emulsion (SLD = 6.66×10^{-6} Å^{-2}) and fully hydrogenated hexadecane as the low SLD emulsion (SLD = -0.43×10^{-6} Å^{-2}) as the two initial emulsion stocks because this maximizes contrast. Based on this emulsion composition, the corresponding SLD of the solvent could then be estimated to be 3.11×10^{-6} Å^{-2}, which consists of 46 vol% H_2O and 54 vol% D_2O. However, if oil exchange experiments were performed using this contrast matching condition and a long pathlength sample cell (i.e. 1 cm), the large absorption cross-section of H_2O in the solvent would absorb nearly all of the neutrons passing through the system and minimal scattering intensities would be detected (transmission ~3%). Thus, a balance between the emulsion contrast and sample transmission must

be considered to optimize contrast matching of the emulsion systems for any given sample thickness.

$$I \propto T * \Delta\rho^2 \tag{2.4}$$

$$\Delta\rho^2 = (SLD_{Emulsion1} - SLD_{solvent})^2 = (SLD_{solvent} - SLD_{Emulsion2})^2 \tag{2.5}$$

The first step for estimating the optimized contrast matching condition is to simplify equation (2.5) to minimize the number of parameters used in the calculation. The equation can be re-organized to express the fully exchanged system that is contrast matched. In addition, the amount of deuterated hexadecane (D-hexadecane) and hydrogenated hexadecane (H-hexadecane) in this system can be expressed in its corresponding volume fraction. For example, the fully mixed emulsion contains X_{hex} H-hexadecane and $X_{D\text{-}hex}$ D-hexadecane, which can also be expressed as (1- X_{hex}). The same process can also be performed to the solvent such that the mixture is expressed only using the volume fraction of H_2O (equation (2.6)). The SLD values of the different components are constants that can be estimated using the NIST neutron activation and scattering calculator.[3] Thus, the emulsion contrast matching condition can be simplified to using only one parameter (either in X_{hex} or X_{H2O}) as shown in equation (2.7).

$$X_{hex} * SLD_{hex} + (1 - X_{hex}) * SLD_{D-hex} = X_{H_2O} * SLD_{H_2O} + (1 - X_{H_2O}) * SLD_{D_2O} \tag{2.6}$$

$$X_{H_2O} = 1.022X_{Hex} - 0.0417 \tag{2.7}$$

The other part of the optimization process is to account for the sample transmission (T) using equation (2.3). The value of the total cross section used in this equation can be estimated using a linear combination of the cross sections of H_2O (6.93 cm^{-1} for a 6 Å source) and D_2O (0.72 cm^{-1}). For example, a solvent containing 25% H_2O and 75% D_2O results in a total solvent cross section of 2.27 cm^{-1}.

The theoretical scattering intensity can then be estimated using equation (2.4). The estimated contrast, transmission, and scattering intensities are shown in Figure 2.5. As can be seen in the figure, the optimal sample configuration should contain a contrast matched oil that consists of 30% H-hexadecane and 70% D-hexadecane. The corresponding solvent mixture would contain roughly 26.5% H_2O and 73.5% D_2O, which would provide 9% neutron transmission through a 1 cm pathlength sample.

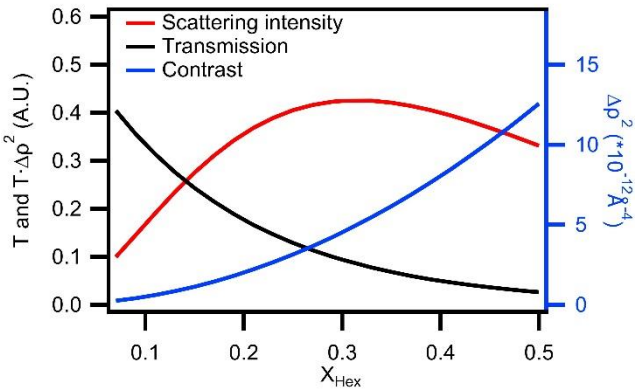

Figure 2.5. Optimizing the detected scattering intensity by varying the transmission and contrast of the system.

While the contrast matching configuration for the emulsion system could be estimated using the equations above, using the estimated values of the hydrogenated/deuterated material to make the sample could result in synthesizing a system that is not perfectly contrast matched. The mismatch between the calculation and the experimental measurement is due to variations in the

quality of raw materials that are purchased. The purity of the components affects the actual scattering length of the samples. Therefore, the estimated SLD of the different materials may not be entirely identical to the theoretically estimated value. Thus, it is crucial to validate that the synthesized system is actually contrast matched before conducting any time-resolved contrast matching experiments.

The experimental contrast matching condition can be obtained by synthesizing the theoretically estimated contrast matching oil mixture (30% H-hexadecane and 70% D-hexadecane) in solvents with various amounts of H_2O/D_2O. The scattering profiles for each sample can be collected and the actual contrast matching point would be the condition where minimal scattering is observed. An alternative method for estimating the contrast matching point is to plot out the square root of the scattering intensity at a specific q versus the volume fraction of D_2O in the solvent. The obtained result should resemble a 'V' shape since any contrast mismatch in the emulsion system would result in a higher observed scattering intensity.

The curve can be further modified such that the contrast matching condition could be mathematically estimated. In short, the curve was linearized by multiplying half of the 'V' data point values by '-1' as shown in Figure 2.6. The contrast matching point of the system would be the condition in which the line crosses the x-axis. For our system, the actual experimental contrast matching point occurred when the solvent contained 73.1% D_2O and 26.9% H_2O, which is relatively close to the theoretical calculation of 73.5% D_2O and 26.5% H_2O. Additional contrast matching validation experiments are also required when performing experiments that uses other oils as the dispersion phase (e.g. dodecane or octane).

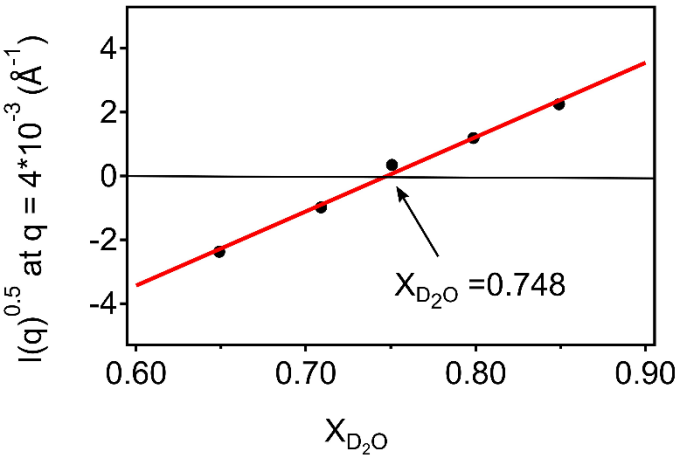

Figure 2.6. Contrast matching validation for hexadecane emulsion systems showing that the synthesized sample based on the theoretically calculated value is close to the actual experimental contrast matching point.

2.1.4 *Scattering Data Fitting and Data Analysis*

The main method of analyzing a set of scattering data is to fit profiles with suitable scattering models. Small angle scattering data provides information not only on the shape and size of individual particles but also how these particles are arranged. This is because scattering signals are sensitive to interference of scattering events from each individual particle and its surrounding neighbors. For a system consisting of only one type of particle, the scattering intensity can be expressed using equation (2.8), where N is the number density of particles, V_p is the volume of a single particle, $\Delta\rho$ is the scattering length density difference between the particle and the solvent, $P(q)$ is the form factor of a single particle, and $S(q)$ is the structure factor which takes into consideration the inter-particle correlations.

$$I(q) = N * V_p^2 \Delta\rho^2 P(q) S(q) + background \qquad (2.8)$$

Since the form factor corresponds to the scattering of an isolated particle, it provides information on the shape of the particles. Mathematically, this can be expressed as the summation of the intensity of all the scattering waves within one particle as shown in equation (2.9), where r_i is the vector defining the distance between pairs of atoms within a particle.

$$P(q) = \left[\frac{1}{V_p}\int_{V_p} e^{iqr_i} dr_i\right]^2 \tag{2.9}$$

2.1.4.1 Sphere Model

The spherical model is the simplest scattering model and it was derived by Gunier.[5] It is a fundamental model that is also the basis for modeling gold stabilized Pickering emulsion systems (Chapter 3). For a monodisperse spherical system with uniform electron density, the form factor of a sphere can be expressed using equation (2.10) where *r* is the radius of the spherical particle.

$$P(q) = \left[3 * \frac{\sin(qr) - qR\cos(qr)}{(qr)^3}\right]^2 \tag{2.10}$$

For isolated (i.e. dilute) spherical particles in a dispersion, the structure factor has a value of 1 and the scattering intensity is expressed as shown in equation (2.11), where *V* is the total volume of the sample and φ_p is the volume fraction of scattering particles.

$$I(q) = \frac{\varphi_p}{V} * \left[3 * V_p * \Delta\rho * \frac{\sin(qr) - qR\cos(qr)}{(qr)^3}\right]^2 + background \tag{2.11}$$

The spherical model is a good representation for colloidal gold nanoparticles presented in this dissertation because the particles are synthesized in very dilute concentrations. Therefore, it

can be used to accurately measure the radius of the particles and to assess the dispersion stability and polydispersity. When using this model for fitting, the background and scattering length density for gold particles and water is kept constant since they are known or subtracted during data reduction process. The only variables are then the radius, volume fraction, and the polydispersity (if this is included in the model) of the particles. The estimated particle size can also be compared to the results obtained from transmission electron microscopy to determine if the modeled results are accurate. If the scattering profiles are reduced and plotted in absolute units, the scale parameter in the model represents the volume fraction.

2.1.4.2 Raspberry model

The first model used to analyze the synthesized Pickering emulsions in Chapter 3 is the Raspberry model developed by Larson-Smith *et. al*.[6] This model describes a system where several small spherical particles decorate the surface of a large sphere (oil droplet). In addition, it assumed that the small particles are immersed on the oil-water interface and based on the wettability of the nanoparticles the particle contact angle on the interface would vary. The scattering intensity of a Pickering emulsion is summarized in equation (2.12), assuming the oil droplets and nanoparticles in the system are monodisperse.

$$I_{Total}^{Mono}(q) = I_{op}^{Mono}(q) + I_{p}^{Mono}(q) \qquad (2.12)$$

Equation (2.12) can be expanded to the following equations, where P_{op} is the form factor of the Pickering emulsion, M is the scattering length of the overall Pickering emulsion, S_{op} is the structure factor or the Pickering emulsion, S_{pp} is the structure factor for the particles, and δ is where the particle is at the interface ($-1 \leq \delta \leq 1$).

$$I_{op}^{Mono}(q) = \left(\varphi_o(\Delta\rho_o)^2 V_o + \varphi_p^T \varphi_p^a N_p \left(\Delta\rho_p\right)^2 V_p\right) P_{op} \tag{2.13}$$

$$I_p^{Mono}(q) = \varphi_p^T (1 - \varphi_p^a)\left(\Delta\rho_p\right)^2 V_p \psi_p^2 \tag{2.14}$$

$$\psi_p = \frac{3\left[\sin\left(qR_p\right) - qR\cos\left(qR_p\right)\right]}{(qR_p)^3} \tag{2.15}$$

$$\psi_o = \frac{3[\sin(qR_o) - qR\cos(qR_o)]}{(qR_o)^3} \tag{2.16}$$

$$P_{op} = \frac{1}{M^2}\begin{bmatrix} (\Delta\rho_o)^2 V_o^2 \psi_o^2 + N_p\left(\Delta\rho_p\right)^2 V_p^2 \psi_p^2 \\ +N_p\left(N_p - 1\right)\left(\Delta\rho_p\right)^2 V_p^2 S_{pp} + 2N_p \Delta\rho_o \Delta\rho_p V_o V_p S_{op} \end{bmatrix} \tag{2.17}$$

$$M = \Delta\rho_o V_o + N_p \Delta\rho_p V_p \tag{2.18}$$

$$S_{op} = \psi_o \psi_p \frac{\sin(q(R_o + \delta R_p))}{q(R_o + \delta R_p)} \tag{2.19}$$

$$S_{pp} = \psi_p^2 \left[\frac{\sin(q(R_o + \delta R_p))}{q(R_o + \delta R_p)}\right]^2 \tag{2.20}$$

Where:
R_o: Radius of the oil droplet
R_p: Radius of the particle
φ_o: Volume fraction of the emulsion phase
φ_p^T: Volume fraction of the particles
φ_p^a: Volume fraction of the particles adsorbed onto the emulsion
N_p: Number of particles at the surface of a single emulsion
V_o: Volume of a single emulsion
V_p: Volume of a single particle
ρ_o: Scattering length density of the emulsion phase
ρ_p: Scattering length density of the particles
ρ_s: Scattering length density of the solvent
$\Delta\rho_o = (\rho_o - \rho_s)$: Scattering contrast between the emulsion and solvent
$\Delta\rho_p = (\rho_p - \rho_s)$: Scattering contrast between the particles and solvent

When using the Raspberry model, parameters including background (set as 0), δ (set at 0 which assumes that 50% of the particle is in each liquid phase), the particle radius, SLDs for the particle, solvent, and the emulsions were kept constant to simplify the modeling process. The initial input of the size of the emulsion is obtained from DLS. By using the raspberry model, one can estimate the emulsion size, emulsion surface coverage of the particles, polydispersity, volume fraction of the particles and emulsions in the Pickering emulsion system.

2.1.4.3 Debye Model

A Debye model consisting of 'N' smaller spheres (GNP) surrounding a large sphere (emulsion) was used to represent synthesized Pickering emulsions. All spheres were assumed to be hard spheres; therefore, they would not overlap with each other.[7] The schematic of the Pickering emulsion is shown in Figure 2.7. The scattering intensity of a Pickering emulsion was divided into multiple terms, including scattering intensity of the individual GNPs, emulsion droplets, scattering due to the interactions between GNPs vs the emulsion droplets, and GNP-GNP interactions. Since both GNPs and emulsions in the system were all spheres, their form factors were expressed as the following equations, where q is the scattering vector, r and R are the radii of the GNPs and emulsion droplets, and ρ the scattering length density of the components or water.

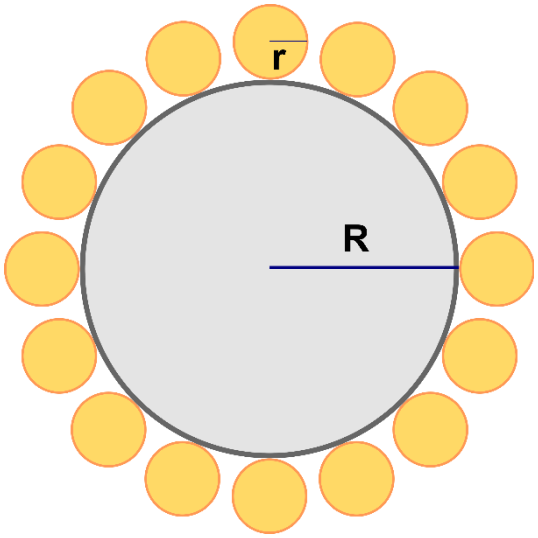

Figure 2.7. Schematic figure of a Debye model used to fit Pickering emulsion scattering data. A spherical emulsion droplet with a radius R is evenly coated by N spherical GNPs with a radius r.

$$F_{partilce} = (\rho_p - \rho_{solvent})V_p \frac{3[\sin(qr) - qr\cos(qr)]}{(qr)^3} \tag{2.21}$$

$$F_{oil} = (\rho_o - \rho_{solvent})V_o \frac{3[\sin(qR) - qR\cos(qR)]}{(qR)^3} \tag{2.22}$$

$$V_p = \frac{4}{3}\pi r^3 \tag{2.23}$$

$$V_o = \frac{4}{3}\pi R^3 \tag{2.24}$$

The scattering intensities of the individual components and the interactions between these components was then calculated using equations (2.25) through (2.28).

$$P_{particle} = \left(F_{particle}\right)^2 \tag{2.25}$$

$$P_{oil} = (F_{oil})^2 \tag{2.26}$$

$$P_{op} = 2NF_{oil}F_{particle}\frac{\sin\left(q(R+r)\right)}{q(R+r)} \tag{2.27}$$

$$P_{pp} = 2\left(F_{particle}\right)^2 \sum_{i=1}^{N-1}\sum_{j=i+1}^{N}\frac{\sin\left[q\left(\hat{r_i} - \hat{r_j}\right)\right]}{q\left(\hat{r_i} - \hat{r_j}\right)} \tag{2.28}$$

The scattering intensity of one Pickering emulsion was then expressed as the summation of all the individual components with a weighing factor, where ρ_o is the scattering length density (SLD) of the emulsion core, $\rho_{solvent}$ is the SLD of the solvent, and $\rho_{particle}$ is the SLD of the gold nanoparticles

$$P_{Pickering} = \frac{1}{M^2}\left(P_{particle} + P_{oil} + P_{op} + P_{pp}\right) \tag{2.29}$$

$$M = (\rho_o - \rho_{solvent})V_o + N\left(\rho_p - \rho_{solvent}\right)V_p \tag{2.30}$$

However, since there were some particles not bound to the emulsion interface and free floating in the system, the final scattering intensity of a monodisperse Pickering emulsion with some excess particle in the system was then expressed as the following equation, where ϕ_o is the volume fraction of the oil phase, ϕ_p^{total} is the dosed total volume fraction of the particles, and ϕ_{ex} is the estimated ratio of excess particles in the system.

$$I_{sys} = \begin{bmatrix} \phi_o(\rho_o - \rho_{olvent})V_o + \\ \phi_p^{total}(1-\phi_{ex})N(\rho_p - \rho_{solvent})V_p \end{bmatrix} P_{Pickering} + \phi_p^{total}\phi_{ex}\frac{P_{particle}}{V_p} \quad (2.31)$$

Polydispersity of the Pickering emulsions was included by assuming their size distribution to be log-normal. The probability of each size within a bin size was estimated using the standard normal table on a log scale. Using more bins to express the lognormal distribution would provide a better estimation of the distribution but the scattering intensity calculation time also significantly increases with the increasing number of bins; therefore, a total of 5 bins was used for all modeling results shown in Chapter 3.

The model was verified by changing the parameters and observing how scattering intensity characteristics varied. To simplify the system, a model where there were only Pickering emulsions and no 'free' excess particles was first examined to determine which parameters had the most effect on the scattering curve (Figure 2.8). Parameters including Pickering emulsion radius, amount of emulsion surface covered, and emulsion polydispersity were then varied while other parameters were kept constant. Based on the modeling results, increasing the Pickering emulsion radius resulted in a shift of the Guinier region into lower q. Increasing emulsion surface coverage gave rise to a shift of the characteristic peak, the GNP-GNP interaction peak, into higher q regions. Finally, increasing the polydispersity of the emulsion droplet smoothed the scattering curve.

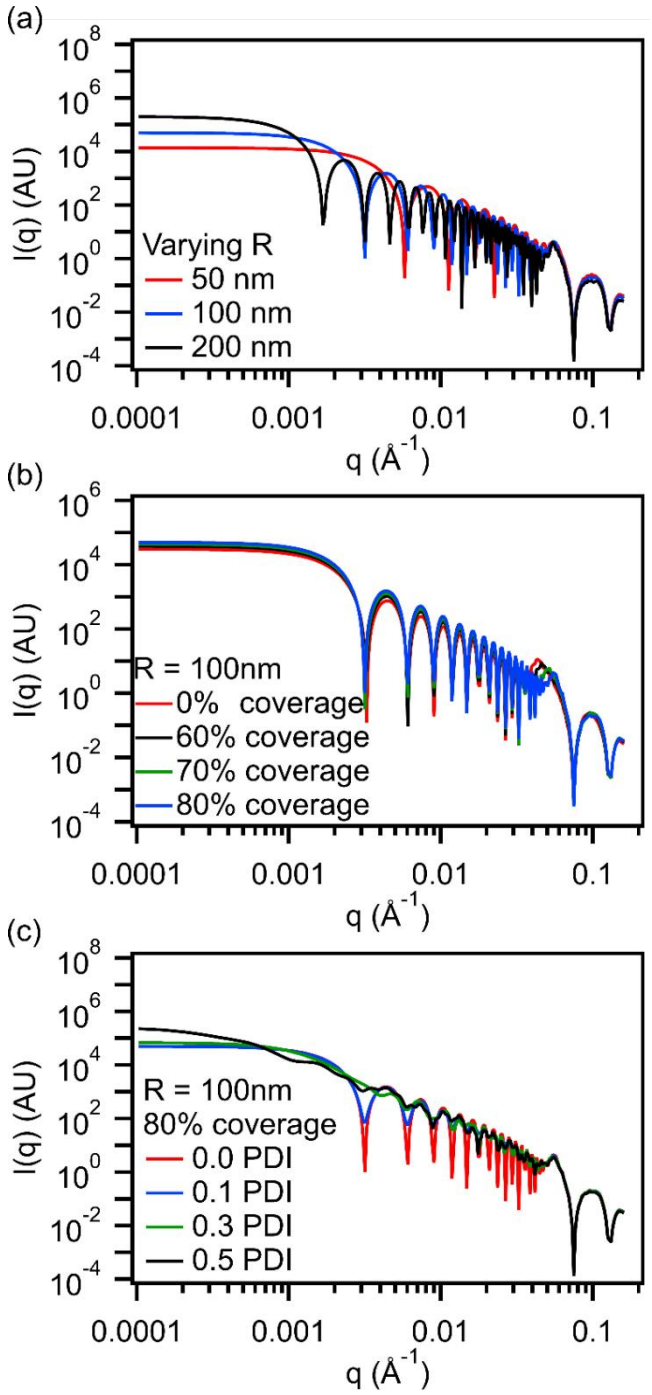

Figure 2.8. Debye model of Pickering emulsions varying emulsion (a) radius, (b) surface coverage, and (c) polydispersity. No instrumental smearing or polydispersity is included in these models. Scattering length densities were fixed for water (9.47×10^{-6} Å^{-2}), gold (124.69×10^{-6} Å^{-2}) and emulsion (14.47×10^{-6} Å^{-2}).

An example of fitting an obtained Pickering emulsion scattering profile with both the raspberry and Debye model is shown in Figure 2.9. As can be seen in the figure, the Debye

modeled fit provides a better estimation of the gold particle-particle interaction peak. Another advantage of using the Debye model is the ability to calculate a non-perfect system containing multiple size distributions of gold nanoparticles and Pickering emulsions. Thus, the Debye model was used for modeling the acquired scattering profiles containing Pickering emulsions.

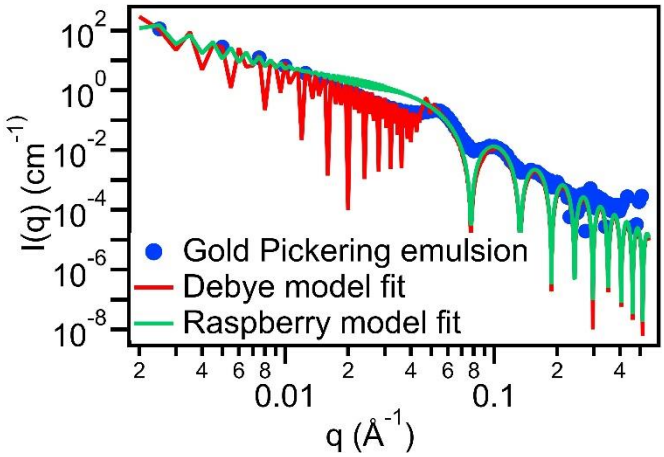

Figure 2.9. Example of fitting Pickering emulsion data using the Debye model versus the raspberry model.

2.1.4.4 Estimating Exchange Kinetics Using a Relaxation Function

For analyzing time-resolved SANS on the other hand, the important information that one aims to obtain from the scattering profiles is the overall contrast of the emulsion system and not necessarily the size/shape of the oil droplets. One method to measure contrast in emulsion system is to model every single scattering profile while assuming the emulsion size distribution remains constant. This method is limited however, when analyzing larger sized emulsion systems where the size distribution may not be adequately modeled due to a limited q range. Thus, another method of obtaining the same information is to use a relaxation function to characterize the amount of mass that is transferred between oil droplets in an emulsion system.

As mentioned previously, the recorded scattering intensity of a sample could be expressed using equation (2.8). If the emulsion size distribution within the sample does not change over time

and the droplets are dilute, the recorded scattering intensity is now only correlated to the square of the system's contrast. The extent of the oil exchange can then be expressed as a relaxation function (R(t)) as shown in equation (2.32). *I(t)* is the integrated scattering intensity at any given time, I_0 is the integrated scattering intensity at time zero which can be obtained using the control emulsion sample where the system contrast remained constant, and I_∞ is the integrated scattering intensity at infinite time which is obtained from the pre-mixed control sample. Additional details on the emulsion systems, analysis, and models used to fit the relaxation functions are further discussed in Chapters 4 and 5.

$$R(t) = \left(\frac{I(t) - I_\infty}{I_0 - I_\infty}\right)^{1/2} \tag{2.32}$$

2.1.5 *Ultrasound Sample Environment*

An ultrasound sample environment was custom built to allow us to simultaneously probe acoustic force induced changes within a sample during sonication while performing small angle scattering experiments. The sample environment consists of a sample holder that can be sandwiched be two chambers containing water and focused ultrasound transducers (1.24 MHz Sonic Concepts H-102, f-number 0.98, 64 mm diameter, Sonic Concepts Inc., Bothell, WA, USA). The transducers have a well-defined acoustic beam and acoustic parameters including the applied acoustic pressure, duty cycle, and pulse repetition frequency could be controlled. The sample environment could also be modified for only one transducer as the acoustic source by using an empty water chamber or switching out one of the water chambers with a spherical reflector fixed onto the sample holder (in Chapter 5). Perpendicular to the acoustic source axis is a Kapton window that allows neutron and X-ray beams to pass through. Beneath the sample holder is a custom-made wide-band polyvinylidene difluoride (PVDF) transducer that receives any acoustic

waves passing through the sample, which would be used for acoustic cavitation analysis. Liquid samples can be loaded or removed through a threaded hole on top of the sample holder. The assembly of the sample environment is shown in Figure 2.10.

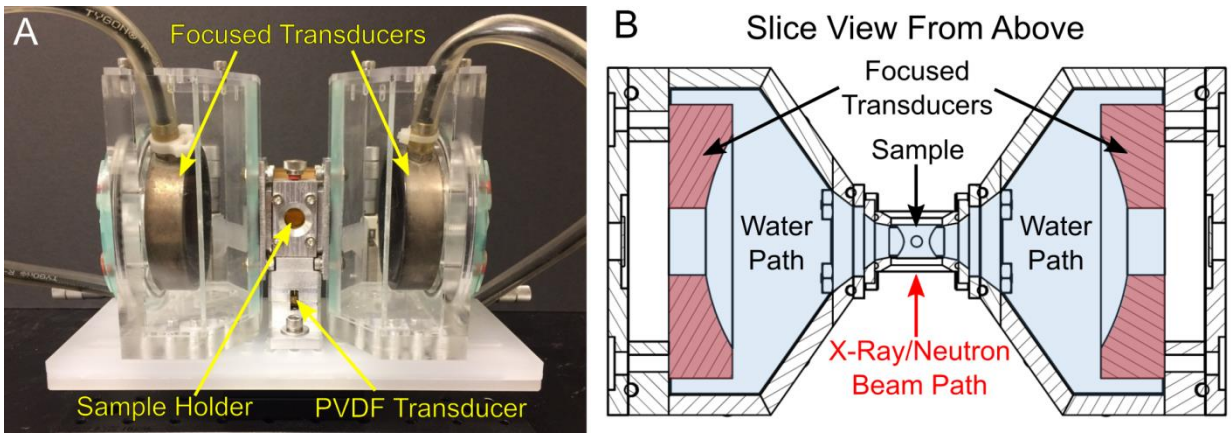

Figure 2.10. (a) sample environment assembled and (b) top down slice view of the sample environment.[8]

The wiring of the acoustic setup is shown in Figure 2.11. In short, a laptop using MATLAB codes is used to control a dual-channel arbitrary waveform generator (4154, BK Precision, Yorba Linda, CA, USA) to select acoustic parameters including waveform, frequency, wave amplitude, and pulse length that are applied to the transducer. The signals are passed through a linear amplifier (A150, ENI, Rochester, NY, USA) to amplify the signals by 55dB. The amplified signal is then passed through a pre-amplifier (matching network) for the transducer and to the transducer which would then generate acoustic waves. Ultrasound signals passing through the sample holder are received by the PVDF transducer connected to a wideband preamplifier (Precision Acoustics, Dorchester, UK), oscilloscope (2190D, BK Precision) and finally saved on the computer. The laptop is also synchronized with the X-ray or neutron scattering instrument using a data acquisition card (USB-6001, National Instruments, TX, USA). Pictures of mounting the ultrasound sample environment onto a Bonse-Hart instrument configuration at beamline 9-ID-C (ultra-small angle X-ray scattering) in Advanced Photon Source-Argonne National Lab are shown in Figure 2.12.

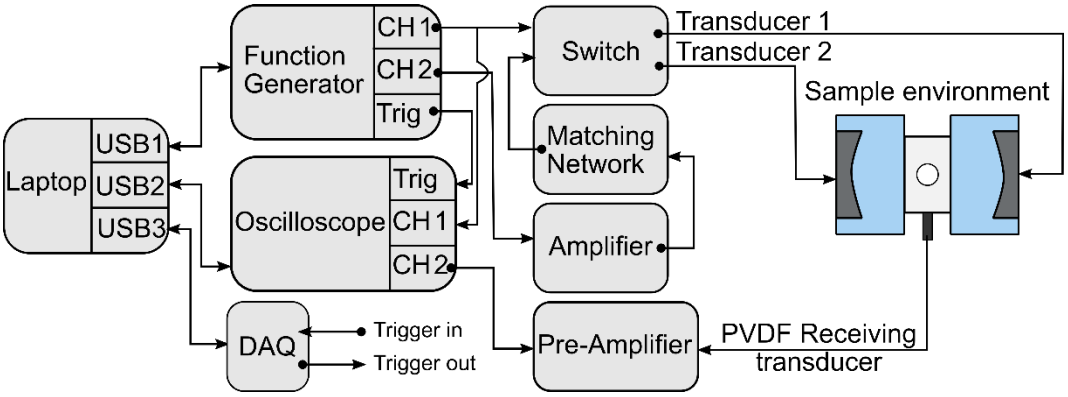

Figure 2.11. Block diagram of ultrasound sample environment. Image is adapted based off of an image from Li *et al.*[8]

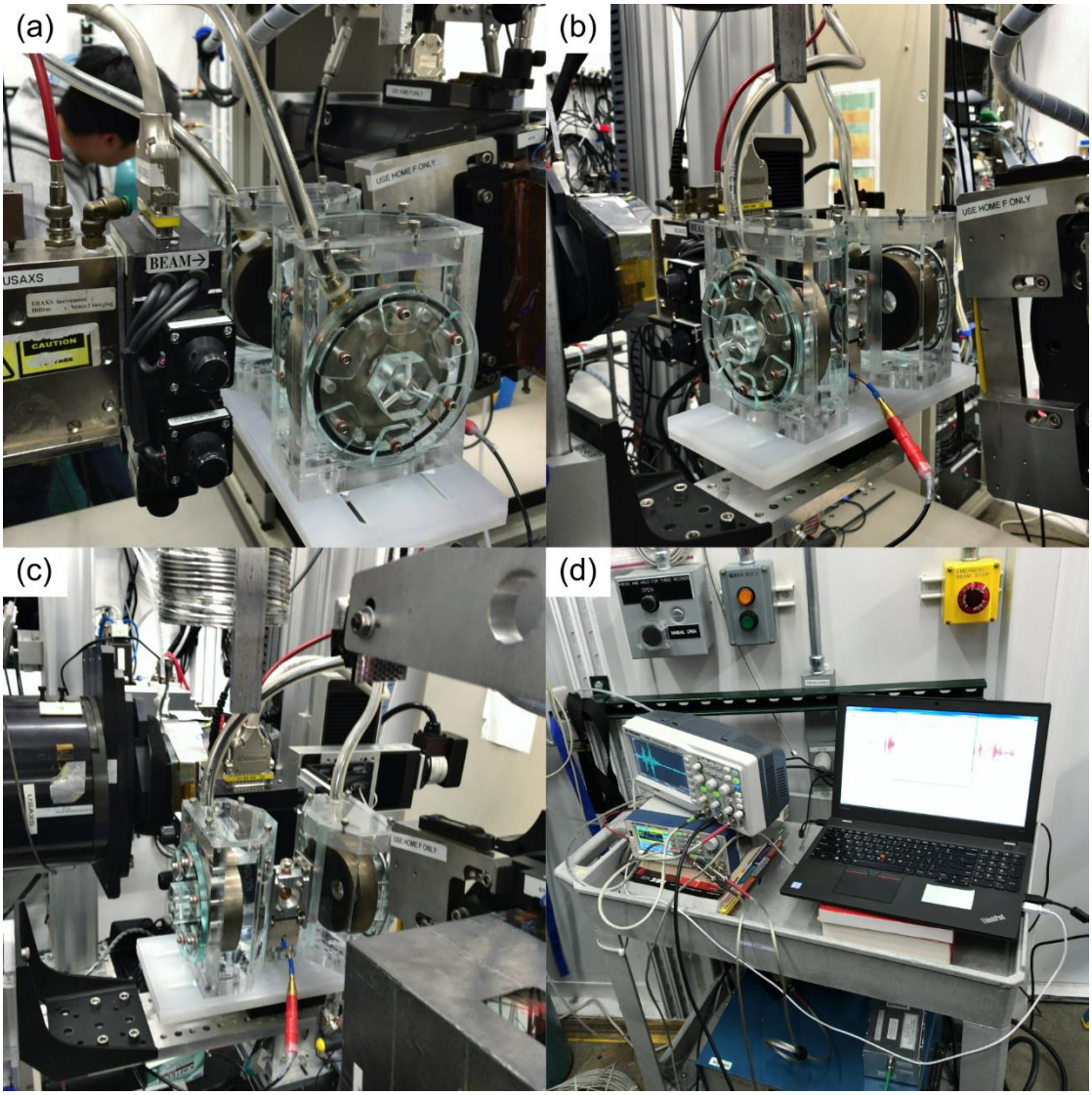

Figure 2.12. Example pictures of ultrasound sample environment mounted onto the Bonse-Hart instrument and device wiring at beamline 9-ID-C in Argonne National Lab.

2.1.5.1 Acoustic Signal Analysis to Detect Cavitation Events

The recorded acoustic signals were analyzed using a method adapted from Fabiilli, *et al*.[9] In short, the average power of the recorded acoustic waves was obtained by applying a Hamming window and transferring the recorded data to the frequency domain using Fast Fourier transforms (FFTs). Background signals were then removed from the data by subtracting the average power that was estimated at high acoustic frequencies. The cavitation power of the sample was then estimated by summing the power values between 0.1 to 0.5 MHz. The sample mean power was then compared to the mean power obtained from a water sample sonicated at low sonication pressures (no cavitation). If the estimate sample cavitation power was 4 times greater than the value estimated from the water sample, it was defined to have a cavitation event occurring in that system. Cavitation probability could then be estimated by summing the total number of cavitation events and dividing that number by the total number of incident acoustic waves. The cavitation threshold was obtained from the acoustic pressure versus cavitation probability curve using a sigmoidal model to obtain the half way point as shown in the result section in the report. An example frequency spectrum for an emulsion sample sonicated below and above the cavitation threshold is shown in Figure 2.13. Additional details on ytthe cavitation analysis method is discussed in Chapter 3.

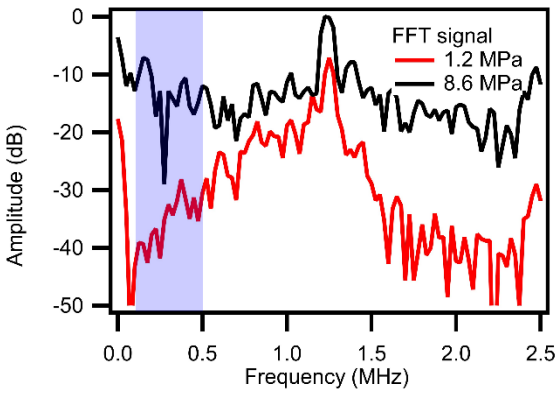

Figure 2.13. Example frequency spectrum of sonicating an emulsion sample below (1.2 MPa) and above (8.6 MPa) the cavitation threshold.

2.2 ULTRAVIOLET-VISIBLE SPECTROSCOPY

There are several ways to characterize the optical properties of a material in dispersion. UV-Vis spectroscopy is one of the most straightforward and simple characterization techniques which provides information related to material's optical properties. UV-Vis spectroscopy provides information on the extinction of a material at specific wavelengths in the range of 200-1100 nm. UV-Vis spectrometers work by passing monochromatic light through a sample and measures the amount of that light transmitted through the sample using a photodetector. The extinction of the sample at a specific wavelength can then be calculated using Beer-Lambert's law (equation (2.33)) where A_b is the extinction, A_0 is the intensity of the incident light, and A_t is the intensity of the transmitted light detected.

$$A_b = log_{10}\left(\frac{A_0}{A_t}\right) \tag{2.33}$$

The Beer-Lambert's law is also often expressed as equation (2.34), which accounts for the concentration (c) of the absorbing substrate in a solution, the path-length (L) of light through the sample and the extinction coefficient (ε) of the absorbing material.

$$A_b = \varepsilon cL \tag{2.34}$$

By applying the principle of conservation of energy, the incident light can also be described as $A_0 = A_{absorbed}+A_{scattered}+A_{transmitted}$. Since the equipment cannot discriminate between absorption and scattering, the only information that is accurately provided is the attenuation of intensity by the inserted sample (i.e. $A_{absorbed}+A_{scattered}$) as a function of wavelength. For small nanoparticles, the absorption of light is generally more significant than the fraction of scattered light but may not be true for all cases.[10] The maximum absorbance wavelength of a plasmonic material can also be related to the arrangement of nanoparticles in solution.[11]

One example of using UV-Vis spectroscopy to obtain insight into material properties is the characterization of gold nanoparticles since gold nanoparticles have unique optical properties. Studies have shown that UV-Vis spectroscopy can effectively provide information on the size and shape of gold nanoparticles due to differences in localized surface plasmon resonance.[11] For example, depending on the size of the particles, spherical gold nanoparticles usually exhibit one maximum absorbance peak at wavelengths ranging from 510-570 nm. On the other hand, rod-shaped gold nanoparticles tends to have two absorbance peaks due to the existence of two different characteristic dimensions (i.e. radius and length).[12]

The clustering of gold nanoparticles can also contribute to changes in maximum absorbance wavelength in the UV-Vis spectrum.[13] For example, the 12 nanometer diameter gold nanospheres show a narrow characteristic maximum absorbance peak at 520 nm. However, after functionalizing the gold particles to form amphiphilic gold nanoclusters, the maximum peak wavelength of the spectrum red-shifts due to the plasmon coupling effects between adjacent gold particles in a nanocluster. Pickering emulsion droplets decorated with adsorbed gold nanoparticles show further redshifts into the near-IR region and the absorbance spectrum broadens as shown in Figure 2.14.[14] Although contact between particles is not necessary to induce plasmon coupling, particles do need to be very close to each other (usually within a few nm) to maximize the shift.

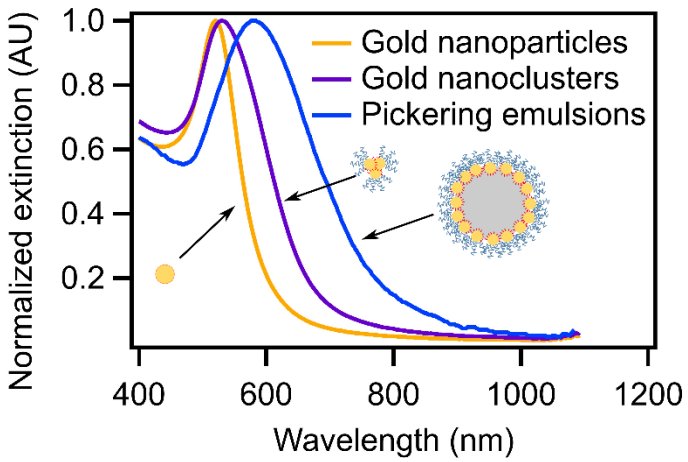

Figure 2.14. Example UV-vis spectrum of (a) gold nanoparticles (b) gold nanoclusters and (c) Pickering emulsions.

2.3 DYNAMIC LIGHT SCATTERING (DLS)

Dynamic light scattering (Quasi-Elastic Light Scattering) is yet another technique that can be used to obtain size distributions of dispersed materials. One advantage of this method is that it can characterize a sample in dispersion with a small volume size.[15] Another advantage of DLS is its ability to characterize samples with sizes ranging from a couple of nanometers up to a few micrometers. DLS measurements are obtained by measuring the Brownian motion of the objects (e.g. particles and droplets) in dispersion and using the sample's diffusivity to predict its size distribution. In short, a monochromic laser is applied through a sample and the scattered light intensity fluctuations are detected at a specific angle (i.e. 175° backscattering) relative to the incident beam. The fluctuating intensities are used to calculate the autocorrelation function g_2 and this is further fit to obtain the object's diffusion coefficient. Smaller objects have faster Brownian motions compared to more massive objects and therefore, would move out of the observing window faster and results in a more rapid decrease in the autocorrelation function. The size of the objects can then be obtained by using the Stoke-Einstein equation (equation (2.35)), where D is the diffusion coefficient, k_B is the Boltzmann constant, T is sample temperature, η is the viscosity

of the solvent, and r_h is the hydrodynamic radius of the object. One main assumption applied when using the Stokes-Einstein equation is that all of the objects in the system are spherical.

$$D = \frac{k_B T}{6\pi\eta r_h} \tag{2.35}$$

The size obtained using dynamic light scattering is the hydrodynamic radius, which is based on the movement of the objects in the solution and thus can easily be affected by the object's surface characteristics. If the object's surface is able to drag solvent molecules along while diffusing through the solvent, the obtained size distribution tends to be overestimated. For example, synthesized colloidal gold nanospheres in Chapter 3 were characterized using other techniques including transmission electron microscopy and small angle X-ray scattering, which both shows that the spherical particles have a diameter of 12 nanometers. However, the hydrodynamic diameter obtained from DLS was around 18 nanometers which is significantly larger than the actual particle size. The overestimation of size is due to the presence of surface-capping molecules that increases the hydrodynamic drag of the particle and affects its diffusion coefficient.

Another parameter that the DLS can provide is the polydispersity (PDI) of a system. It is extremely challenging to perform any synthesis and to be able to obtain uniformly sized objects. Usually, the materials in the system would have a distribution of various sizes and the degree of non-uniformity is provided by the PDI, which can be expressed as the square of the standard deviation divided (σ) by the mean of the size distribution (d_{mean}) as shown in equation (2.36). Based on experience, the typical polydispersity of the gold nanoparticles synthesized in our lab using the Turkevich method is around 0.2, indicating that the synthesized nanoparticles are relatively monodisperse. On the other hand, synthesizing oil in water emulsions without the presence of surfactants usually results in forming samples with a PDI greater than 0.5.

$$PDI = \left(\frac{\sigma}{d_{mean}}\right)^2 \tag{2.36}$$

Despite only being able to obtain the hydrodynamic radius/diameter and not the true size of a structure with DLS, this technique is still a useful tool since it provides a quick way of measuring the size of a dispersion and its polydispersity. Moreover, DLS can also be used to check changes in the structure of materials at each step during a synthesis process.[14] For example in our gold nanoparticle system, once gold nanoparticles are functionalized with a hydrophilic thiol-terminated poly(ethylene glycol) methyl ether (i.e. PEG-thiol), the hydrodynamic diameter of the functionalized particles would be close to 60 nanometers due to the presence of polymer chains on the gold particle surface. When gold nanoclusters are formed, the estimated cluster size is related to the amount of PEG-thiol on the gold particles and the number of particles in a cluster. This size distribution is usually on the order of 60 to100 nanometers. If the Pickering emulsions were synthesized successfully, the measured size distribution would further increase, primarily dominated by the oil droplet size, and can vary from a hundred nanometer up to microns in diameter (Figure 2.15).

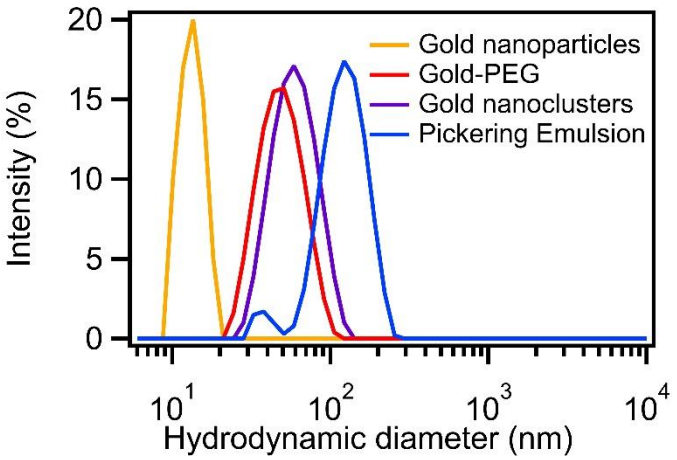

Figure 2.15. Example result obtained for dynamic light scattering showing the hydrodynamic diameter of gold nanoparticles, hydrophilic gold-PEG, gold nanoclusters, and Pickering emulsions.

2.4 TRANSMISSION ELECTRON MICROSCOPY (TEM)

Characterization techniques such as UV-vis spectroscopy and DLS indirectly provide information on the structure of the system. On the other hand, TEM can directly visualize samples under high magnification/resolution and can provide information including the shape, size, polydispersity, structural arrangement, and surface features.[16] The working principle of TEM is similar to optical microscopy however instead of normal visible light, high energy electrons beams are passed through the samples. When electrons are passed through a thin slice of a sample, it can either pass through the grid unaffected, be absorbed or scatter off the sample. The electrons are then focused by several lenses and displaced onto a fluorescent screen or CCD camera.

Figure 2.16 (a) is an example of a relatively monodisperse gold nanoparticle sample that was synthesized. Larger amphiphilic gold nanoclusters (Figure 2.16 (b)) are formed when the nanoparticles are functionalized with hydrophilic poly(ethylene glycol) methyl ether thiol and hydrophobic alkanethiol (i.e. octanethiol). When Pickering emulsions are formed (Figure 2.16 (c)) the nanostructure further increases in size and forms a more spherical structure. It can also be seen that not all of the gold nanoparticles are at the emulsion interface and that there are some excess particles present in the system.

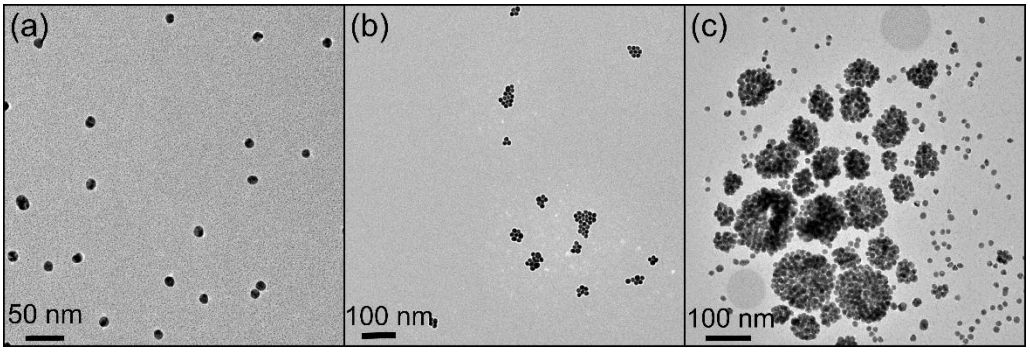

Figure 2.16. Example TEM image acquired for (a) gold nanoparticles (b) gold nanoclusters and (c) Pickering emulsions.

2.5 REFERENCES

(1) Hammouda, B. **2008**.

(2) *Neutron, X-Rays and Light: Scattering Methods Applied to Soft Condensed Matter*, 1st ed.; Lindner, P., Zemb, T., Eds.; North Holland, **2002**.

(3) NIST neutron activation and scattering calculator https://www.ncnr.nist.gov/resources/activation/.

(4) Rose, P. F. *ENDF-201: ENDF/B-VI Summary Documentation*; Upton, NY, **1991**.

(5) Guinier, A and Fournet, G. *John Wiley & Sons, Inc*. **1955**.

(6) Larson-Smith, K.; Jackson, A.; Pozzo, D. C. *J. Colloid Interface Sci.* **2010**, *343* (1), 36–41.

(7) Debye, P. *J. Phys. Colloid Chem.* **1946**, *18* (1), 18–32.

(8) Li, D. S.; Lee, Y.-T.; Xi, Y.; Pelivanov, I.; O'Donnell, M.; Pozzo, L. D. *Soft Matter* **2018**, 5283–5293.

(9) Fabiilli, M. L.; Haworth, K. J.; Fakhri, N. H.; Kripfgans, O. D.; Carson, P. L.; Fowlkes, J. B. *IEEE Trans. Ultrason. Ferroelectr. Freq. Control* **2009**, *56* (5), 1006–1017.

(10) Jain, P. K.; Lee, K. S.; El-Sayed, I. H.; El-Sayed, M. A. *J. Phys. Chem. B* **2006**, *110*, 7238–7248.

(11) Haiss, W.; Thanh, N. T. K.; Aveyard, J.; Fernig, D. G. **2007**, *79* (13), 4215–4221.

(12) Link, S.; Mohamed, M. B.; El-Sayed, M. A. *J. Phys. Chem. B* **1999**, *103* (16), 3073–3077.

(13) Larson-Smith, K.; Pozzo, D. C. *Soft Matter* **2011**, *7* (11), 5339–5347.

(14) Larson-Smith, K.; Pozzo, D. C. *Langmuir* **2012**, *28* (32), 11725–11732.

(15) Bruce J. Berne, R. P. *Dynamic Light Scattering: With Applications to Chemistry, Biology, and Physics*; **1976**.

(16) David B. Williams, C. B. C. *The Transmission Electron Microscope*; **1996**.

Chapter 3. ULTRASOUND-BASED FORMATION OF NANO-PICKERING EMULSIONS INVESTIGATED VIA IN-SITU SAXS

Sonication is one of the most commonly used methods to synthesize Pickering emulsions. Yet, the process of emulsion sonication is rarely characterized in detail and acoustic conditions are largely determined by experimenter's personal experience. In this study, the role of sonication in the formation of Pickering emulsions from amphiphilic gold nanoparticles was investigated using a new sample environment combining ultrasound delivery with ultra-small-angle X-ray scattering (USAXS) measurements. The detection of acoustic cavitation and the simultaneous analysis of structural data via USAXS demonstrated direct correlation between Pickering emulsion formation and cavitation events. There was no evidence of spontaneous adsorption of particles onto the oil-water interface without ultrasound, which suggests the presence of a stabilizing force. Acoustically detected cavitation events could originate in the bulk solvent and/or inside the emulsion droplets. These events helped overcome energy barriers to induce particle adsorption.

3.1 INTRODUCTION

Emulsions are metastable dispersions of two immiscible liquids that form an apparently homogeneous material (i.e. macroscopically). Without stabilizers, emulsions are intrinsically unstable and ultimately will separate into two different phases.[1] Although surfactants commonly stabilize emulsions, solid particles have also been demonstrated to be effective stabilizers producing systems called Pickering emulsions.[2–4] Based on the wettability of the particles, either oil-in-water or water-in-oil Pickering emulsions are formed.[3] Other advantages of Pickering emulsions include a significant increase in the emulsion’s resistance to coalescence, increased

energy barriers to eject particles from the emulsion interface (i.e. nearly irreversible adsorption), and decreased toxicity to living cells.[5–7] Consequently, Pickering emulsions can be used effectively in fields such as food science & engineering, oil recovery, cosmetics, and biomedical technologies.[6,8–12]

Despite the wide range of potential applications, Pickering emulsions have not always been used extensively because of the challenges in controlling their synthesis. The formation of Pickering emulsions is known to be sensitive to particle shape, size, surface properties, and concentrations.[6] Further, even if particles have adequate properties to stabilize an emulsion interface, factors such as energy barriers can prevent spontaneous adsorption.[13,14]

Electrostatic repulsion is one such known energy barrier that can effectively prevent spontaneous particle adsorption. Still, it can be overcome by altering the charge on the particle surface using surface chemical functionalization or by altering the solvent's environment (e.g. pH or ionic strength).[15–17] Another possible barrier is steric repulsion, which is common for polymer-functionalized particles acting as stabilizing agents. In this case, polymer layers form a physical barrier preventing particle adsorption.[18,19] Steric repulsion can be overcome by applying mechanical forces such as high shear mixing, high-pressure homogenization, or sonication.[20–22] In this work we carefully analyze the role of acoustic cavitation in overcoming such energy barriers using controlled sonication.

Of all methods for applying mechanical forces to synthesize Pickering emulsions, sonication is the most frequently used. Bath or probe-type sonicators are common tools in most colloid laboratories. These emit strong acoustic waves in the ultrasound frequency range (>20 kHz) for mechanical agitation, redispersion, emulsification, and/or glassware cleaning. Sonication is also effective in Pickering emulsion synthesis because it can simultaneously emulsify and force

particle adsorption onto droplet interfaces. However, laboratory sonicators are rarely calibrated and acoustic settings and sonication times are usually selected by personal experience and/or trial and error resulting in widely variable results. Moreover, most of these instruments produce poorly defined acoustic fields and do not provide information on important acoustic parameters (e.g. local acoustic pressure). Furthermore, differences in experimental parameters including probe/bath geometry, sample positioning, sample volume and vessel material, affect acoustic conditions and produce drastic variations in sonication results from system to system and sample to sample. For most studies reported in the literature, sonication is often treated as a 'black box' with little attention given to the underlying physics controlling these processes.

In controlled ultrasound experiments, the acoustic frequency, pressure (intensity), duration, and pulse repetition frequency (or duty cycle) are carefully controlled. Acoustic radiation force, which scales proportionally with the square of acoustic pressure, could provide nanoparticles with the momentum necessary to both move in the dispersion and overcome energy barriers between the nanoparticle and the emulsion interface. Alternatively, cavitation could form and violently collapse vapor cavities in the liquid, producing locally high pressures, stresses, and temperatures that would induce the formation of Pickering emulsions.[23,24]

This work uses *in-situ* scattering methods to understand the process of Pickering emulsion synthesis under controlled acoustic fields. The model system examined here consists of oil-in-water emulsions insonated in the presence of polymer-coated amphiphilic gold nanoparticles (GNP). In previous studies, our lab has shown that these types of GNPs are effective in stabilizing both hydrocarbon and perfluorocarbon emulsions.[22,25] This work mainly focuses on the use of perfluorinated oils for Pickering emulsion formation due to the increased interest in utilizing Pickering emulsion contrast agents for medical imaging. Previously, we have shown that Pickering

emulsions with perfluorinated cores can be a potential theranostic agents for sono-photoacoustic imaging.[25–30] These Pickering emulsions can be activated using a combination of ultrasound and laser pulses to provide significant contrast for sono-photoacoustic imaging and can simultaneously break blood clots.[26] Nevertheless, hydrogenated alkane oils such as hexadecane, are also included in this study in order to compare observations with Pickering emulsions that are of general interest for other applications.[31–34]

Structural changes occurring within the samples are characterized using ultra-small angle X-ray scattering (USAXS) during sonication within a custom build focused ultrasound sample environment.[35,36] Compared to other techniques which can only characterize the samples before and after the formation of Pickering emulsions, USAXS is a unique technique because it provides us with the ability to quantitatively examine structural changes during the application of acoustic forces. Moreover, the custom build sample environment enables user defined control over the transmitted acoustic settings (e.g. acoustic pressure, pulse duration, and pulse repetition frequency) while simultaneously monitoring for cavitation events. By varying the acoustic pressures, sonication times and the types of oils, we systematically explore the role of sonication parameters and emulsion composition in the formation of Pickering emulsions.

3.2 Materials and Methods

3.2.1 *Sample Preparation*

Gold (III) chloride trihydrate, sodium citrate dihydrate (>99.9%, CAS: 16961-25-4), hexadecane (99%, CAS:544-76-3), butanethiol (99%, CAS: 109-79-5), and sulfuric acid (98%, CAS: 7664-93-9) were purchased from Sigma-Aldrich (St. Louis, MO, USA). 10 kDa thiol-terminated poly (ethylene glycol) methyl ether (95%, PEG-thiol) was purchased from Polymer

Source (Dorval, Quebec, Canada). Perfluoroalkanes including perfluorononane (99%, CAS:375-96-2), perfluorooctane (90%, CAS:307-34-6), and perfluorohexane (98%, CAS:355-42-0) were obtained from Synquest Laboratories (Alachua, FL, USA). Colloidal gold nanoparticles of ~12 nm average diameter were synthesized using methods described by Frens.[37] All alkane and perfluoroalkane oils were fully linear with no branching. All glassware used in synthesizing gold nanoparticles was cleaned with a critical cleaning detergent Liquinox® (Alconox, Inc., NY, USA), sonicated in a sonication bath for 30 minutes, and set in an acid bath with Nochromix solution (Nochromix® powder, Godax Labs Inc., MD, USA, dissolved in pure sulfuric acid) for an hour to remove any potential residual organic material. GNPs with a dosing of 8 PEG-thiol chains/nm^2 and 20 butanethiol chains/nm^2 were synthesized using methods adapted by Larson-Smith *et al*.[26,38]

Coarse oil-in-water emulsions were prepared in a separate container by sonicating 1 vol% of oil (i.e. perfluorinated oils or hexadecane) in deionized water using a Branson Digital Sonifier S-450 with a 3 mm tapered microtip (Branson Ultrasonics, CT, USA) at 30% amplitude 50% duty cycle (i.e. 0.1 seconds on and 0.1 seconds off) for a total of 20 seconds of sonication time. The coarse surfactant-free emulsions were then added to GNP dispersions to form a 50:1 oil to gold volume ratio. The final volume fraction of oil in the sample was $3.4x10^{-3}$. Each emulsion sample was freshly prepared before conducting experiments to avoid coarsening due to coalescence. The dispersions of oil droplets and nanoparticles were then sonicated using a focused ultrasound sample environment at various acoustic conditions. GNPs without emulsions and emulsions without nanoparticles were also sonicated as controls. An overall schematic diagram of the process for functionalizing GNP and synthesizing Pickering emulsion using ultrasound is shown in Figure 3.1.

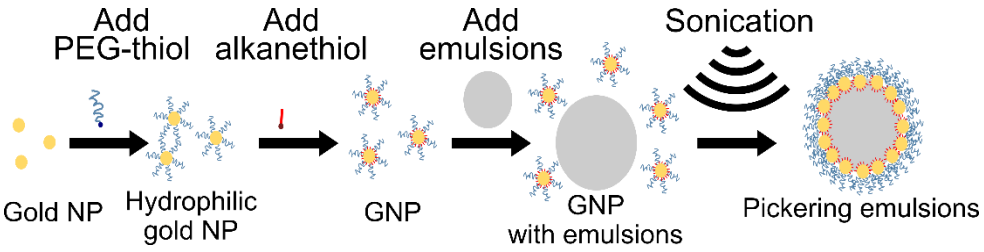

Figure 3.1. Overall schematic diagram of functionalizing GNP and Pickering emulsion formation.

3.2.2 *USAXS Measurements and Data Analysis*

USAXS experiments were performed using a custom designed acoustic sample environment.[35] For each acoustic experiment, 2 coaxially aligned 1.24 MHz focused ultrasound transducers (Sonic Concepts H-102, f-number 0.98, 64 mm diameter, Sonic Concepts Inc., Bothell, WA, USA) were pulsed at acoustic pressures ranging from 0 to 7.2 MPa, at a repetition frequency (PRF) of 6.2 kHz and a 20% duty cycle. Samples were insonated for a total of 3 minutes at each USAXS time-point measurement unless otherwise specified. The two face-to-face transducers were alternated at a rate of 1 Hz to prevent material buildup at one side of the sample holder due to acoustic radiation forces. All USAXS experiments were performed in a standard Bonse-Hart instrument configuration at beamline 9-ID-C in Advanced Photon Source-Argonne National Lab.[39] The energy of the X-ray beam was 21 keV.

The recorded USAXS scattering data was reduced to an absolute scale and desmeared using Indra module of SAS software.[40,41] The desmeared scattering data was then modeled with two different models to describe these complex system, which may contain multiple coexisting components (e.g. 'free' particles, undecorated oil droplets, and droplets with adsorbed particles). In the first model, a sum of two polydisperse sphere populations, was used for samples containing GNPs and emulsions when no particle adsorption occurred (i.e. Pickering emulsions were not being formed). For these samples, it was assumed that GNPs and emulsion droplets were not

interacting with each other, which is a good assumption in the dilute conditions used in this study. Therefore, this was considered as a system containing two independent populations of spheres. The modeling of this 2-sphere system was performed using Irena to obtain size distributions (log-normal) and volume fractions for each component.

For samples and conditions that would form Pickering emulsions, a generalized scattering model developed by Debye was used to fit the scattering profiles. The Debye model can be used to model any arbitrary shape as long as it is composed of spherical subunits with known relative position.[42] For Pickering emulsion systems, this was constructed as a large sphere (i.e. droplet) evenly decorated by smaller spheres (i.e. gold nanoparticles) corresponding to a certain area coverage. Model details were included in the Chapter 2. This model is similar to a raspberry model that has been previously described but it is better suited to describe the correlations between particles at the emulsion-water interface (i.e. curved spherical interface) at the expense of more expensive computations.[43] Specific modeling parameters were found using a least squares routine coded into MATLAB. Size, surface coverage, volume fraction of the Pickering emulsion, and the amount of remaining non-adsorbed gold nanoparticles could be obtained using the Debye model.

3.3 CAVITATION ANALYSIS

Ultrasound signal analysis was performed using MATLAB to implement methods adapted from Fabiilli, *et al*.[44] In short, a Hamming window was applied centered on the acoustic time of flight from the focused transducer to the sample. Fast Fourier transforms (FFTs) of windowed signals were calculated and an average power for the signal at high frequencies (background signal) was subtracted. Cavitation power was then obtained by summing power values between 0.1 to 0.5 MHz to highlight non-linear signals that emerge due to the effects of cavitation when this is present.

The mean acoustic power was also obtained for a water sample at low acoustic pressures without cavitation. A cavitation threshold was defined to correspond to signals larger than 4 times the mean acoustic power of the water sample within this frequency window. The cavitation probability was then calculated by summing the number of signals whose cavitation power was greater than the cavitation threshold and dividing this by the total number of incident acoustic pulses. The cavitation threshold for each sample was found by fitting a sigmoid curve to a plot of the acoustic pressure versus cavitation probability and calculating the 50% crossing point.

3.3.1 *UV-Vis Characterization*

Optical extinction spectra were measured over the range of 300-1100 nm using ultraviolet-visible (UV-Vis) spectroscopy (Thermo Scientific Evolution 300, Thermo Fisher Scientific, MA, USA). All samples were diluted 20 times in deionized water to avoid surpassing an extinction value greater than 2.

3.3.2 *TEM Analysis*

Samples before and after sonication were also dried and imaged using a FEI Tecnai G2 F20 Transmission Electron Microscope (TEM) operating at 200 kV. TEM samples were prepared by diluting gold nanoparticle or Pickering emulsion dispersions 50 times in deionized water to prevent particle clustering during drying. The diluted dispersion was then deposited on a carbon TEM grid and allowed to dry in a desiccator for at least 24 hours before performing measurements.

3.4 RESULTS

GNPs, such as those used in this study, have been previously shown to form Pickering emulsions when sonicated in the presence of oil.[22,38] Yet, we also found that these GNPs would

not spontaneously form Pickering emulsions by direct adsorption (e.g. simply mixing particles and oil emulsions) or by applying moderate shear (e.g. magnetic stirring). Under these conditions, optical extinction spectra showed no significant changes compared to those obtained from GNPs alone, which had a narrow peak at 520 nm characteristic of gold nanoparticle plasmonic resonance (Figure 3.2). The formation of Pickering emulsions usually red shifts the optical extinction spectrum as nanoparticles are packed in close proximity and interparticle plasmonic resonance begins to dominate.[22,45] Of all methods tested, sonication was the only one that reliably produced Pickering emulsions.

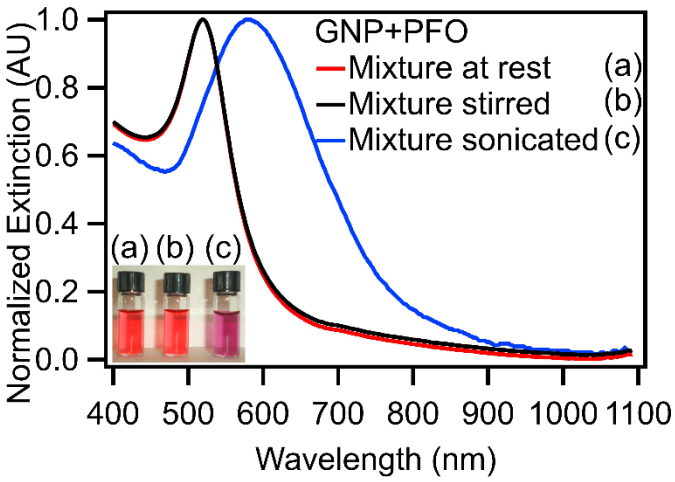

Figure 3.2. UV-Vis extinction spectra of GNP with perfluorooctane emulsions (a) allowed to rest, (b) magnetically stirred, and (c) sonicated. Insert: Photographs of the corresponding samples.

To further explore the role of sonication in Pickering emulsion synthesis, a sample containing GNPs and perfluorooctane was sonicated in the acoustic sample environment at various acoustic pressures. Scattered acoustic signals were also recorded for cavitation detection. An example of the frequency spectrum for a sample with and without cavitation events is shown in Figure 3.3 (a). When there is no cavitation, the only peak is found at the transducer fundamental

frequency. At higher acoustic pressures, peak intensities at the carrier frequency (and its harmonics) increase proportionally. In addition, inertial cavitation from bubble collapse produced additional broadband noise, which is especially evident at lower frequencies. The cavitation probability curve was plotted for each sample using the calculated cavitation probability at each pressure (Figure 3.3 (b)). The cavitation threshold was estimated to be 6.4 MPa for this sample. Cavitation analysis of pure water shows that the emulsions reduced the cavitation threshold from 7.3 to 6.4 MPa.

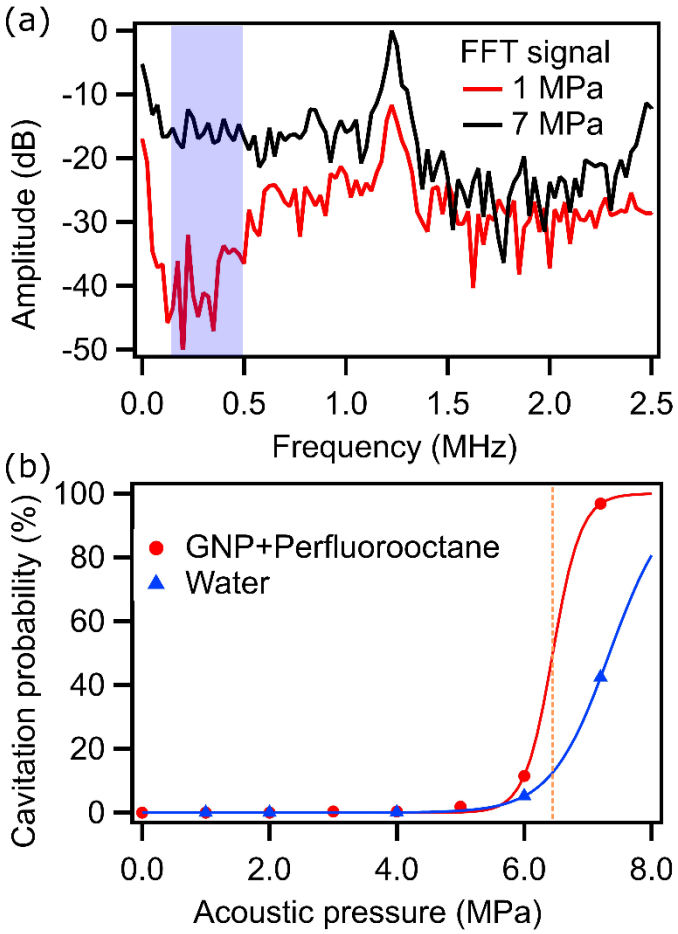

Figure 3.3. (a) An example frequency spectrum of GNP with perfluorooctane sonicated above (7.2 MPa) and below (1.0 MPa) the cavitation threshold. Cavitation detection was performed using amplitudes in the highlighted area. (b) Cavitation probability curves for GNP with perfluorooctane and pure water as obtained from acoustic analysis.

TEM images of samples sonicated at various acoustic pressures further showed that Pickering emulsions would only form by sonicating GNPs and emulsions at cavitation pressures of 7.2 MPa (Figure 3.4). Regardless of aging time, GNP particles did not spontaneously adsorb onto the perfluorooctane droplet interface to form Pickering emulsions. Moreover, Pickering emulsion formation did not appear to scale proportionally with acoustic pressure, indicating a cavitation-based mechanism was essential for this sample.

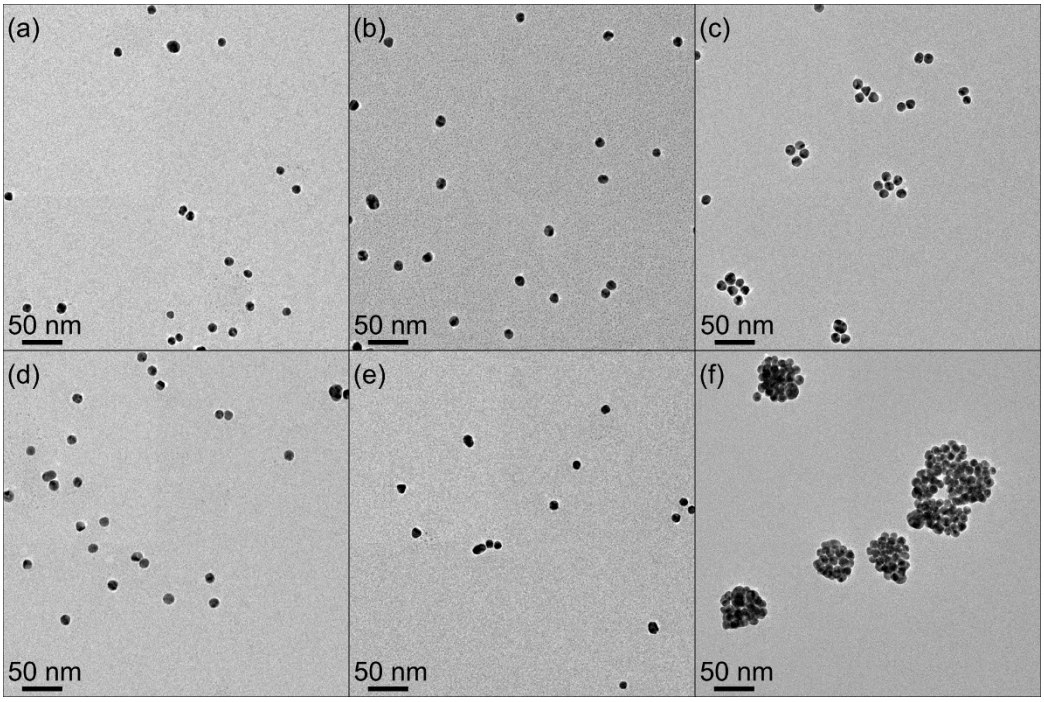

Figure 3.4. TEM images of GNP (i.e. no oil present) (a) before sonication, (b) sonicated at 1 MPa (no cavitation), (c) sonicated at 7.2 MPa (cavitation). Images of GNP in the presence of perfluorooctane emulsions (d) before sonication, (e) sonicated at 1 MPa, and (f) sonicated at 7.2 MPa.

Structural changes were also quantified using USAXS during sonication. USAXS can probe material structures over multiple length scales (1-10,000 nm) and in their native dispersed state during ultrasound manipulation. This removes potential structural changes due to aging or drying that may occur when preparing TEM samples, which requires high vacuum. Two main changes in scattering profiles were observed with increasing acoustic pressure; one in the low-q ($q < 0.01$ Å^{-1}) and the other in the mid-q regions ($0.01 < q < 0.07$ Å^{-1}) shown in Figure 3.5 (a). Low-q changes are typically associated with a change in the droplet size distribution while changes in the mid-q region are characteristic features for Pickering emulsion formation.[22] Based on the collected scattering data, only samples sonicated at 7.2 MPa showed this characteristic inflection.

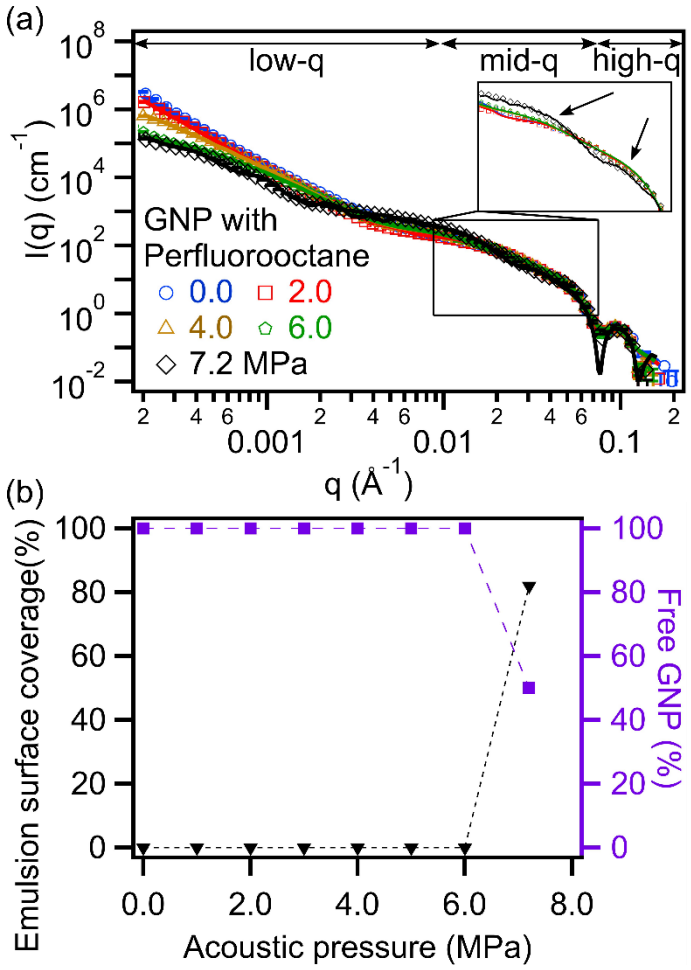

Figure 3.5. (a) Desmeared USAXS profiles of GNP with perfluorooctane sonicated at various acoustic pressures. A model containing 2 spheres was used to fit the sample sonicated at acoustic pressures lower than the cavitation threshold (<6.4 MPa), and a Debye model was used to fit the sample sonicated at 7.2 MPa. Scattering length densities were fixed for water (9.47×10^{-6} Å^{-2}), gold (124.69×10^{-6} Å^{-2}) and perfluorooctane (14.47×10^{-6} Å^{-2}). (b) Quantification of the emulsion surface coverage and amount of excess 'free' GNPs.

The sizes and volume fractions of GNPs in the sample were obtained by modeling the scattering curves before sonication. Based on modeling results, GNPs consisted mostly of particles of 6.0 nm radii with a polydispersity (PDI, non-uniformity of the particles) of 0.12 (78.5 vol% of the total GNPs). PDI provides information on the non-uniformity of the particles and in our model was defined as the square of the standard deviation divided by the mean radius. However, a smaller

fraction (21.5 vol%) of larger particles (13.3 nm radii with a PDI of 0.19) were also present. The total GNP volume fraction was estimated based on the scattering to be 5.8×10^{-5}.

For samples sonicated below 7.2 MPa, TEM images and USAXS scattering curves suggest that no Pickering emulsions would be formed. Therefore, the system was modelled as a non-interacting combination of individual GNPs and emulsions. Results from modeling the samples confirm, as expected, that the size and volume fraction of GNPs did not change when varying the applied acoustic pressure. On the other hand, perfluorooctane emulsion sizes, distributions, and volume fractions changed, as demonstrated in Figure 3.6.

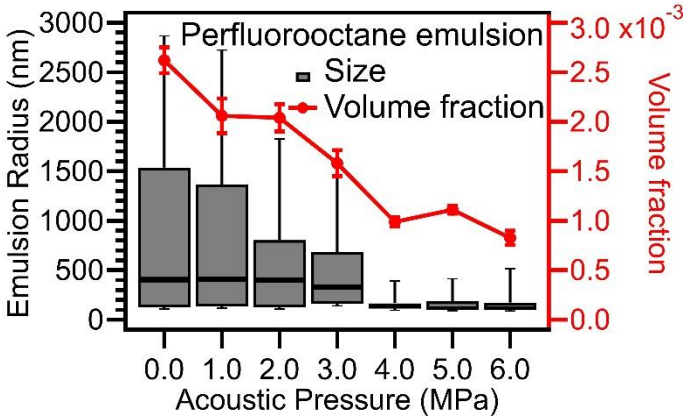

Figure 3.6. Perfluorooctane emulsion size distribution (box plot) obtained from USAXS modeling showing emulsion size and emulsion volume fraction both decreased with increasing applied acoustic pressures. For the box and whisker plot, the box portion, from bottom to top, represents the 25th percentile, median, and 75th percentile of the distribution. The whisker portion represents the 10% percentile and 90% percentile

Based on these modeling results, it was determined that the sizes of polydisperse emulsions significantly decreased with increasing applied acoustic pressures. The estimated emulsion volume fraction also decreased, suggesting that there was a significant loss of oil through vaporization during sonication. Additional details and modeling of GNP with perfluorooctane emulsions are provided in the supplemental information chapter (Chapter 7).

A Debye model was used to fit 1-D scattering curves to reproduce important scattering features of Pickering emulsions. Based on the modeled results, it was determined that two populations of Pickering emulsions of different sizes were present in the sample sonicated at 7.2 MPa (Figure 3.5 (a)). For this sample, 60.9 vol% of the Pickering emulsions had a mean radius of 19.7 nm and 39.1 vol% had a mean radius of 213.2 nm. A single emulsion size distribution would not fit the data. The remaining volume fraction of emulsion droplets in the system at these conditions was 5.0×10^{-4} (i.e. equivalent to 79.9% volume loss). All droplets were densely packed with GNPs with a surface coverage of ~82%, close to maximum packing and consistent with results observed in TEM images. However, not all GNPs were bound to an emulsion interface. Despite a GNP volume fraction of 5.8×10^{-5}, approximately 59% of the particles were still un-bound and diffusing freely in the continuous phase. The surface coverage and excess of 'free' GNPs as a function of acoustic pressure is plotted in Figure 3.5 (b). All major changes coincided with crossing the cavitation threshold for this sample. In contrast, the size of the perfluorooctane droplets changes well before reaching the cavitation threshold. This suggests that cavitation was not necessary to alter the original droplet size distribution but it is indeed essential to induce the adsorption of the GNPs to the emulsion interface. One disadvantage of our explicit Debye model was that the PDI of GNPs was not considered since it greatly increased computation times and required assumptions to be made on the relative adsorption of large and small particles at the oil-water interface.

Sonication time was also investigated to determine whether total time or the presence of cavitation was more important in Pickering emulsion formation. Two different samples of GNPs containing perfluorooctane emulsions were sonicated at different acoustic pressures, one above and one below the cavitation threshold. The sub-threshold sample did not show any characteristic

features of Pickering emulsion regardless of sonication time (Figure 3.7). The only observed changes in the scattering profile were due to changes in the perfluorooctane emulsion size distribution. On the other hand, the sample sonicated at 7.2 MPa showed an immediate change in the scattering profile.

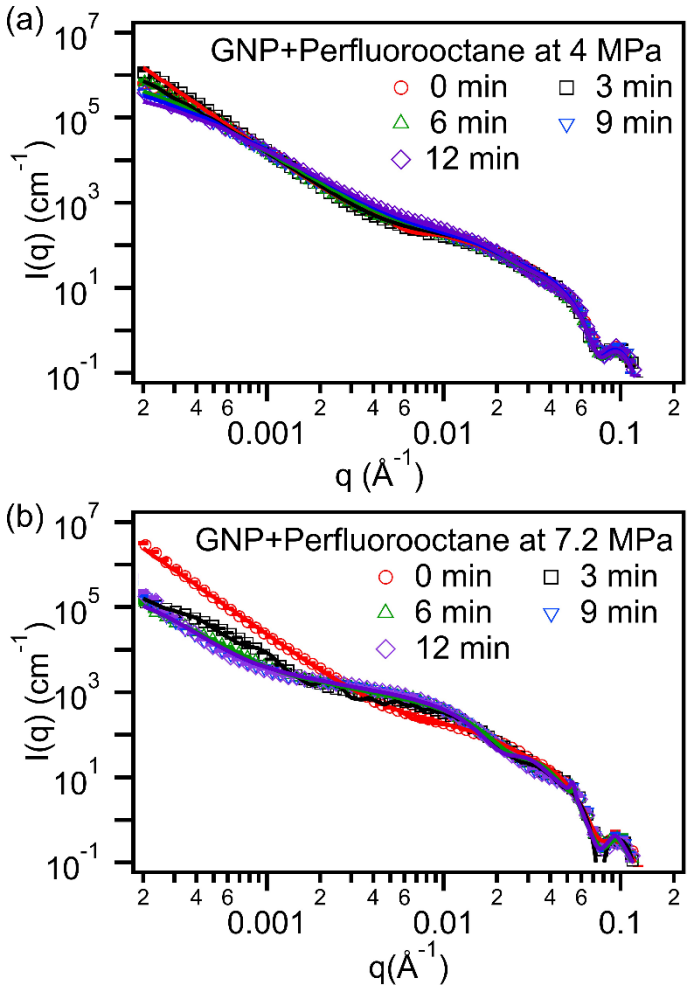

Figure 3.7. Scattering profiles of GNP with perfluorooctane sonicated at (a) 4 MPa (no cavitation) and (b) 7.2 MPa (cavitation) with increasing sonication time.

All data obtained with perfluorooctane as the emulsion core suggests that cavitation events were crucial for Pickering emulsion formation. To further test this, we also analyzed oils with different boiling points including perfluorohexane (b.p,= 56°C), perfluorononane (b.p.=124°C), and hexadecane (b.p.= 287°C). The cavitation probability curves for these emulsions (Figure 3.8) showed that despite using oils of different boiling point, all of the samples had similar cavitation thresholds.

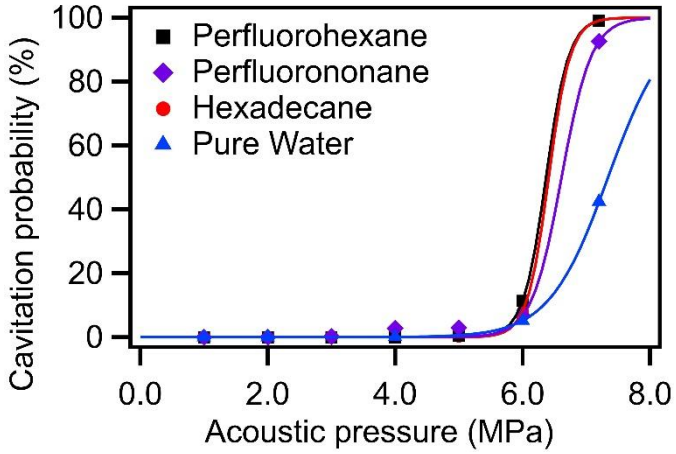

Figure 3.8. Cavitation probability curves for GNPs with perfluorohexane ($T_{boiling}$ = 56°C), perfluorononane ($T_{boiling}$ = 125°C), and hexadecane ($T_{boiling}$ = 286.8°C) emulsions versus pure water.

The corresponding USAXS profiles for samples sonicated at acoustic pressures above (7.2 MPa) or below (6 MPa) the cavitation threshold are shown in Figure 3.9. Results for all of the samples showed that Pickering emulsions were only formed when sonicated above the cavitation threshold. The fine details observed in the calculated models were due to the assumption that all GNPs are monodisperse and evenly distributed at the emulsion interface. This created large intensity fluctuations in the model that were 'smeared' out in the experimental USAXS data. However, the most important parameters (i.e. emulsion size, emulsion packing density, and amount of free GNP) in Pickering emulsion system were adequately captured and were unaffected

by these intensity fluctuations. The estimated values of the important Pickering emulsion parameters, boiling point of the emulsions, and estimated cavitation thresholds are summarized in Table 3.1. All samples were prepared using the same batch of GNPs. Therefore, when modeling the scattering profiles, GNP particle size distributions were kept constant. The GNP volume fraction on the other hand was not constant due to possible small variations when pipetting.

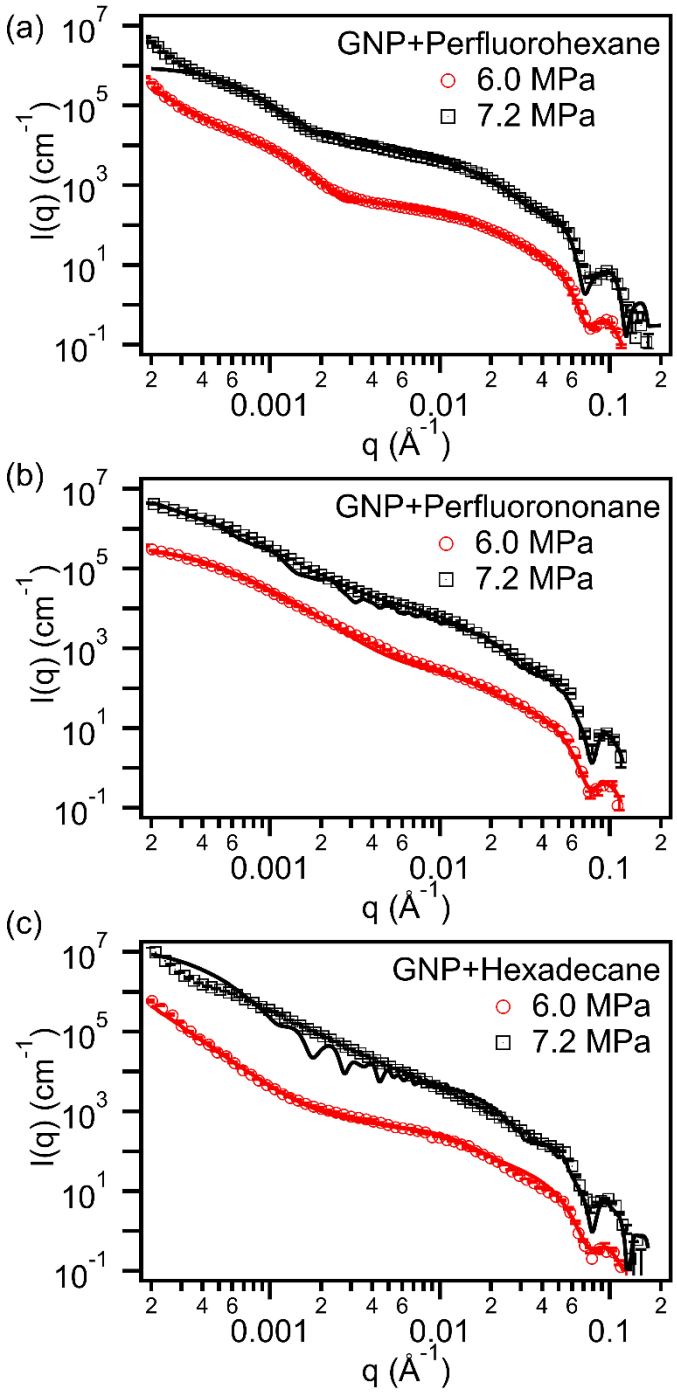

Figure 3.9. USAXS data for GNP with (a) perfluorohexane, (b) perfluorononane, and (c) hexadecane emulsions sonicated at acoustic pressures below (6 MPa) and above (7.2 MPa) the cavitation threshold (Scattering data was shifted in the vertical direction by 1.5×10^{6} cm^{-1} to show the changes in the scattering curve). The scattering length densities of perfluorohexane (13.76×10^{-6} $Å^{-2}$), perfluorononane (14.74×10^{-6} $Å^{-2}$), and hexadecane (7.55×10^{-6} $Å^{-2}$), were kept constant during the modeling process.

Based on USAXS modeling results, most samples produced two polydisperse size distributions of Pickering emulsions. Using lower boiling point oils resulted in forming smaller Pickering emulsions and in more emulsion volume loss due to vaporization. Only the scattering fits for the hexadecane sample, which has the highest boiling point, suggested that there was only one size distribution of droplets with a high PDI. Nevertheless, regardless of the emulsion boiling point there is always a large amount of 'free' GNPs remaining within the system. Additional details on the Debye model and the explanation on how the different parameters (i.e. free GNP%) were estimated were discussed in Chapter 2.

Table 3.1. Boiling point, cavitation threshold, and Debye parameters obtained for different Pickering emulsions.

Emulsion core	Boiling point (°C)	Cavitation threshold (MPa)	GNP volume fraction	Pickering emulsion radius: $R+2r_{small}$ (nm)	PDI	Emulsion volume fraction	Excess 'Free' GNP (%)
PFH	56	6.4	6.4×10^{-5}	17.1 (76.5 vol%)	0.5	6.0×10^{-4} (73.5% loss)	59.7
				217.2 (23.5 vol%)	0.3		
PFO	104	6.4	5.8×10^{-5}	19.7 (60.9 vol%)	0.1	5.0×10^{-4} (79.9% loss)	59.0
				213.2 (39.1 vol%)	0.4		
PFN	124	6.6	7.2×10^{-5}	29.2 (36.0 vol%)	0.4	3.1×10^{-3} (12.2% loss)	45.9
				223.2 (64.0 vol%)	0.5		
Hexadecane	287	6.4	6.9×10^{-5}	362.2	0.3	3.5×10^{-3} (12.5% loss)	56.0

3.5 DISCUSSION

Based on the results it was clear that cavitation was required to produce Pickering emulsions in these systems. Although TEM is useful for directly visualizing the nanostructure, it could only be performed *ex-situ* and under high vacuum leading to the evaporation of the solvents. Moreover, TEM could only provide a limited field of view and the nanostructures can be affected by the drying process (e.g. GNP aggregation or deflated Pickering emulsion due to oil evaporation). For example, emulsion droplets decorated by particles are deflated and appear as dense aggregates of particles (Figure 3.4 (f)). On the other hand, when oil is not present, very small levels of aggregation is observed. The formation of small aggregates in samples that do not have oil (Figure 3.4 (c)) is likely triggered by cavitation events that may also provide enough mechanical energy to overcome the steric stabilization that is provided by the surface-bound PEG chains. Still, the extend of aggregation is clearly limited and much smaller than what is observed in the presence of oil.

In contrast to TEM, USAXS is better suited to provide a direct structural analysis of the ensemble-averaged nanostructures directly from the dispersion state and while the sample is being manipulated with acoustic fields. Scattering profile for the same GNP control samples were acquired (Chapter 7 supplemental information, Figure 7.5) and results demonstrated that large aggregates were formed during sonication when oil was not present. Thus, USAXS was chosen as our main characterization technique to examine the formation of Pickering emulsions. Other techniques including UV-vis, TEM and Fourier-transform infrared spectroscopy (Chapter 7 supplemental information, Figure 7.6) were performed to support observations made from the scattering measurements and to guide in the selection of a suitable scattering model for quantitative analysis.

Although bubbles are known to have large contrast due to their low density, cavitation bubbles are not detected using USAXS due to the long measurement times. This was further explained by Li *et al.* by evaluating the cavitation of pure water and pure ethanol during similar USAXS measurements.[46] Since cavitation bubble nucleation and collapse occurs over microsecond time scales, the short bubble lifetimes, relative to the total USAXS scan time (3 minutes), means that the total contribution of cavitation bubbles to the scattering is negligible.

USAXS results also showed that applying acoustic fields without cavitation resulted in a decrease in emulsion size and, for some samples, a significant loss of oil. The observed emulsion size change suggests that shear forces provided by just the acoustic fields, without cavitation, are sufficient to destabilize the interface to break emulsions into smaller droplets. This phenomenon was also observed by Kaci *et al*. where they synthesized sunflower oil emulsions in water using a high-frequency acoustic source.[47] The oil loss detected during sonication of perfluorocarbon samples is likely due to the volatility of these oils, which are of significant interest for ultrasound and photoacoustic contrast agents.[48] Lower boiling point perfluorocarbons (e.g. perfluorohexane, vapor pressure: 27 kPa at 25°C) are incredibly volatile and can evaporate at room temperature even in emulsified form. Thermal heating in samples due to acoustic forces can further facilitate emulsion vaporization. Thus, sonicating samples to induce droplet vaporization without achieving re-condensation results in irreversible vaporization. The applied acoustic pressure and time-scales may not be sufficient to achieve re-condensation of some bubbles back into droplets for the more volatile oils. This results in the irrecoverable loss of oil. In this study, we used a family of oils of variable susceptibility to vaporization in order to evaluate the influence of this effect on the way Pickering emulsions are typically synthesized.

Fortunately, *in-situ* analysis of these processes via USAXS enables quantification of droplet size distributions and volume fractions directly with only one technique. This observation is also similar to results from Fabiilli *et al*., who examined the process of sonicating perfluorocarbons with focused acoustic waves.[44] They showed that the emulsion vaporization threshold and the inertial cavitation threshold could be different. For lower boiling point perfluorocarbon emulsions (i.e. perfluorohexane and perfluoropentane), the irreversible oil vaporization threshold could be significantly lower than the reversible cavitation threshold. Schad *et al.* later did a similar study using two receiving transducers to record reflected acoustic signals.[49] They revealed that the difference between the two thresholds is a function of both emulsion size and the applied acoustic frequency. Smaller droplets and lower acoustic frequencies prevented irreversible vaporization of emulsion droplets.

After analyzing the acoustic data for all samples, it was also found that all samples had similar cavitation thresholds regardless of the oil that was used. This finding is similar to results obtained by Giesecke and Hynynen, who compared cavitation thresholds for various fluorinated emulsions.[50] Several studies have also showed that the Laplace pressure, from interfacial tension, plays a significant role in stabilizing micro/nano-droplets and in increasing the boiling point of the droplets.[51,52] Because of this enhanced droplet stability, it is difficult to conclusively determine if cavitation nucleated exclusively from the droplet core, from the bulk fluid or in both phases. Moreover, the ~3 minute acquisition rate of the USAXS prevented us from resolving the transient nature of cavitation bubble growth and collapse.

It is logical that cavitation of the oil core is more likely to occur with low boiling point oil droplets (e.g. perfluorohexane), while cavitation of the solvent phase would be more likely with high boiling point oils (e.g. hexadecane). However, when also taking into account the low volume

fraction of the emulsions that were used here, it would be expected that there will be a higher probability of cavitation events initiating in the solvent phase than within droplets.

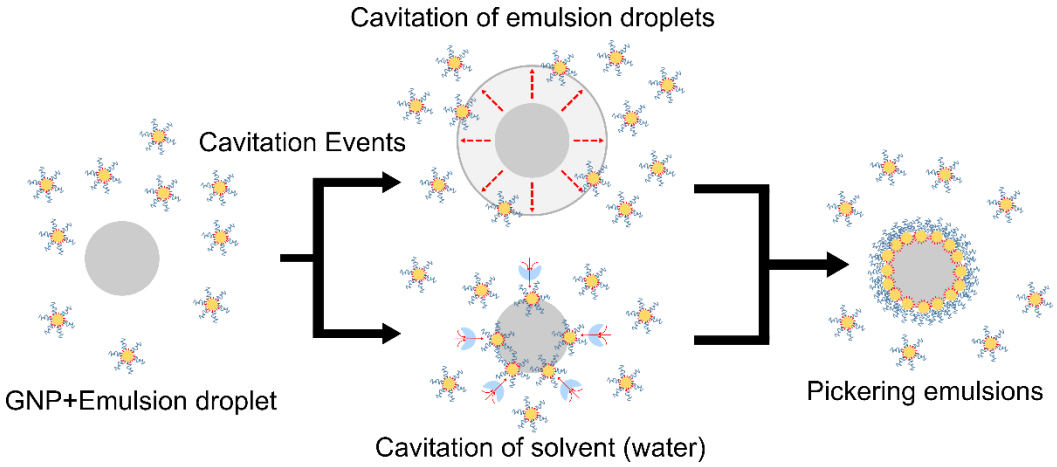

Figure 3.10. Schematic depiction of possible mechanisms for Pickering emulsion synthesis. Cavitation events in either the oil phase (top route) or the solvent phase (bottom route) could provide sufficient energy to overcome energy barriers for particle adsorption.

Given two potential sources of cavitation, we hypothesize two possible ultrasound assisted Pickering emulsion formation mechanisms (Figure 3.10). The first assumes that cavitation events occur in the bulk fluid (i.e. water). Momentum transfer from the fluid to the particles and droplets due to surrounding random cavitation events could overcome the stabilizing energy barriers that otherwise prevent spontaneous adsorption of the nanoparticles to the oil-water interface. The second potential mechanism would be due to droplet or oil cavitation. During the rapid expansion (i.e. vaporization) and subsequent collapse (i.e. re-condensation) of oil micro/nano-droplets reversibly converting to gas bubbles, droplets expand up to an order of magnitude in diameter (three orders of magnitude in volume). The high interfacial velocities and large displacements during abrupt bubble expansion steps could entrap and induce GNPs in the surrounding medium

to adsorb onto the droplet interface. Unfortunately, we are currently unable to differentiate between cavitation of the solvent versus the droplet phase due to the different time scales. However, this may be possible to study in the future with faster X-ray scattering techniques such as time resolved SAXS, which can provide scattering profiles on a sub microsecond time scale, using synchronization to acoustic pulses. The sample composition could also be altered to further favor where the cavitation events will occur. An example of a future experiment may include using a more volatile solvent (i.e. ethanol/water mixture) and smaller sized high boiling point emulsions (i.e. perfluorodecalin). Using the proposed samples could potentially prevent emulsions from cavitating and examine a system where cavitation events only occur in the continuous phase.

Finally, we find that all synthesized Pickering emulsions had the same estimated surface coverage regardless of the type of oil used. The estimated value was similar to the theoretical maximum achievable surface coverage (~82%) when accounting for the butanethiol film thickness on gold surfaces.[53] Having a surface coverage close to the theoretical maximum was reasonable given the strong adsorption energy. GNPs can also pack onto any 'open' emulsion surface until maximum surface coverage is reached during sonication. Interestingly, the results also show that 45-60% of the GNPs would remain 'free' in dispersion without adsorption to the oil-water interface. This value seemed to be somewhat insensitive to the oil type or to the sonication process. One explanation for the presence of excess free particles was due to the statistical nature of droplet breakup and interfacial stabilization. In order to achieve 100% particle adsorption, it would be necessary for ultrasound to produce new interfaces (i.e. breaking droplets) that were rapidly decorated with 'free' nanoparticles before any coalescence could take place. However, in reality particle adsorption and interface formation processes may have widely variable time scales. In addition, ultrasound may also act to expel particles from interfaces in the same way that it may

also act to mechanically push 'free' particles to induce adsorption. Another potential explanation for this observation is from the emulsion stability standpoint. According to Binks *et al.*, droplet surfaces that are not fully decorated by particles and that lacking an excess of 'free' particles would coalesce until reaching maximum surface coverage or would otherwise result in the formation of macroscopic oil films covering the walls of the sample holder.[54] Our results suggest a potential steady state between adsorbed and excess 'free' particles in the system. This would need to be further investigated with other emulsion systems.

Based on these results, a few strategies can be suggested to improve the cavitation conditions for Pickering emulsion synthesis, which is crucial when designing Pickering emulsions for use as medical contrast agents or for other applications.[25–28,55] The frequency used in this experiment (i.e. 1.24 MHz) was higher than that commonly used in traditional laboratory sonication (i.e. 20-75 kHz). Although a higher frequency allowed us to sonicate the samples at a relatively high pressure without cavitation, it also resulted in significant oil evaporation, up to 80 volume percent of the dosed low boiling point emulsions, throughout the 30-minute sonication time. A lower frequency source (e.g. sonication bath or probe sonicator) could achieve a lower cavitation thresholds and insonate a larger volume.

Another method to minimize emulsion loss is to use smaller initial droplets for Pickering emulsion synthesis. Nano-sized emulsions prepared using techniques such as high-pressure homogenization or spontaneous emulsification will produce higher Laplace pressures that can stabilize emulsions and prevent them from vaporizing during sonication. One example of spontaneous emulsification is the ouzo method where oil is first dissolved in a solvent (e.g. ethanol) and water is then added to induce the formation of small emulsion droplets. This spontaneous emulsification method is a reliable way to produce monodisperse nanoemulsions from

volatile oils.[56] In general, direct analysis of emulsification via *in-situ* scattering presents a unique opportunity to understand the complex physics at play in these processes.

3.6 CONCLUSION

In this study, we provide a direct analysis of Pickering emulsion synthesis using amphiphilic gold nanoparticles and several different perfluorinated and hydrogenated alkanes. A specially designed acoustic system, producing fields of well-defined shape and controllable intensity, was used along with ultra-small angle X-ray scattering (USAXS) to provide direct structural information on emulsion systems during simultaneous sonication. All previous works have only been able to characterize Pickering emulsions before and after synthesis but not during synthesis.[4,8,22,31,33] Significantly, this work demonstrates, for the first time, that the formation of Pickering emulsions using sterically stabilized particles requires cavitation to occur due to the application of acoustic fields. No particle adsorption could be detected under weak acoustic fields that resulted in no cavitation. Moreover, we also demonstrate that there is significant loss of oil occurring during the sonication process when the volatility of the oil is high. In contrast, the loss becomes minimal when using high boiling point oils. Additionally, results show that there is also an excess of 'free' un-adsorbed particles (45-60%) present in all cases and conditions explored in this work. This suggests that processes leading to interface generation (i.e. drop breakup), interface destruction (i.e. drop coalescence), particle adsorption and particle desorption are all likely occurring simultaneously during ultrasound application and an excess of particles seems to always remain. USAXS results also show that Pickering emulsions were densely coated with gold nanoparticles achieving surface coverage that is near the close-packing limit. Interestingly, the boiling point of the core oil did not correlate with changes to the cavitation threshold or with surface coverage of the synthesized Pickering emulsion. However, this parameter did affect the

final droplet size distribution and the volume fraction of Pickering emulsion droplets remaining in the system.

The main finding of this report is that structural changes could be correlated to cavitation events and that spontaneous particle adsorption did not occur in any case. This finding is extremely pertinent when designing Pickering emulsion systems for use in applications such as medical contrast agents, cosmetics and/or consumer products. Interestingly, cavitation events were detected at similar pressures regardless of the emulsion boiling point. Two potential mechanisms were also proposed to describe how different cavitation sources could induce adsorption of amphiphilic gold nanoparticles onto emulsion surfaces. Future experiments include the use of time resolved SAXS to differentiate between cavitation of the solvent versus the droplet phase.

3.7 REFERENCES

(1) Solans, C.; Izquierdo, P.; Nolla, J.; Azemar, N.; Garciacelma, M. *Curr. Opin. Colloid Interface Sci.* **2005**, *10* (3–4), 102–110.

(2) Pickering, S. U. *J. Chem. Soc., Trans.* **1907**, *91*, 2001–2021.

(3) Binks, B. P.; Clint, J. H. *Langmuir* **2002**, *18* (4), 1270–1273.

(4) Aveyard, R.; Binks, B. P.; Clint, J. H. *Adv. Colloid Interface Sci.* **2003**, *100–102*, 503–546.

(5) Tu, F.; Park, B. J.; Lee, D. *Langmuir* **2013**, *29* (41), 12679–12687.

(6) Wu, J.; Ma, G.-H. *Small* **2016**, *12* (34), 4633–4648.

(7) Kaewsaneha, C.; Tangboriboonrat, P.; Polpanich, D.; Eissa, M.; Elaissari, A. *Colloids Surfaces A Physicochem. Eng. Asp.* **2013**, *439*, 35–42.

(8) Berton-Carabin, C. C.; Schroën, K. *Annu. Rev. Food Sci. Technol.* **2015**, *6* (1), 263–297.

(9) Skerget, M.; Kotnik, P.; Hadolin, M.; Hras, A. R.; Simonic, M.; Knez, Z. *Food Chem.* **2005**, *89* (2), 191–198.

(10) Chevalier, Y.; Bolzinger, M.-A. *Colloids Surfaces A Physicochem. Eng. Asp.* **2013**, *439*, 23–34.

(11) Wang, X.; Shi, Y.; Graff, R. W.; Lee, D.; Gao, H. *Polymer* **2015**, *72*, 361–367.

(12) Tang, J.; Quinlan, P. J.; Tam, K. C. *Soft Matter* **2015**, *11* (18), 3512–3529.

(13) Stocco, A.; Rio, E.; Binks, B. P.; Langevin, D. *Soft Matter* **2011**, *7* (4), 1260.

(14) Garbin, V.; Crocker, J. C.; Stebe, K. J. *J. Colloid Interface Sci.* **2012**, *387* (1), 1–11.

(15) Larson-Smith, K.; Jackson, A.; Pozzo, D. C. *Langmuir* **2012**, *28* (5), 2493–2501.

(16) Simovic, S.; Prestidge, C. A. *Langmuir* **2003**, *19* (9), 3785–3792.

(17) Whitby, C. P.; Djerdjev, A. M.; Beattie, J. K.; Warr, G. G. *J. Colloid Interface Sci.* **2006**,

301 (1), 342–345.

(18) Dolan, A. K.; Edwards, S. F. *Proc. R. Soc. A Math. Phys. Eng. Sci.* **1974**, *337* (1611), 509–516.

(19) Li, F.; Pincet, F. *Langmuir* **2007**, *23* (25), 12541–12548.

(20) Köhler, K.; Santana, A. S.; Braisch, B.; Preis, R.; Schuchmann, H. P. *Chem. Eng. Sci.* **2010**, *65* (10), 2957–2964.

(21) Yamanaka, K.; Nishino, S.; Naoe, K.; Imai, M. *Colloids Surfaces A Physicochem. Eng. Asp.* **2013**, *436*, 18–25.

(22) Larson-Smith, K.; Pozzo, D. C. *Langmuir* **2012**, *28* (32), 11725–11732.

(23) Doktycz, S.; Suslick, K. *Science* **1990**, *247* (4946), 1067–1069.

(24) Flint, E. B.; Suslick, K. S. *Science* **1991**, *253* (5026), 1397–1399.

(25) Wei, C. W.; Lombardo, M.; Larson-Smith, K.; Pelivanov, I.; Perez, C.; Xia, J.; Matula, T.; Pozzo, D.; O'Donnell, M. *Appl. Phys. Lett.* **2014**, *104*, 0–4.

(26) Wei, C.; Xia, J.; Lombardo, M.; Perez, C.; Arnal, B.; Larson-Smith, K.; Pelivanov, I.; Matula, T.; Pozzo, L.; O'Donnell, M. *Opt. Lett.* **2014**, *39* (9), 2599–2602.

(27) Arnal, B.; Perez, C.; Wei, C.; Xia, J.; Lombardo, M.; Pelivanov, I.; Matula, T. J.; Pozzo, L. D.; Donnell, M. O. *Photoacoustics* **2015**, *3* (1), 3–10.

(28) Arnal, B.; Wei, C.-W.; Xia, J.; Pelivanov, I. M.; Lombardo, M.; Perez, C.; Matula, T. J.; Pozzo, D.; O'Donnell, M. In *SPIE BiOS*; Oraevsky, A. A., Wang, L. V., Eds.; 2014; Vol. 8943, p 89433E.

(29) Arnal, B.; Perez, C.; Wei, C.-W.; Xia, J.; Lombardo, M.; Pelivanov, I.; Matula, T. J.; Pozzo, L. D.; O'Donnell, M. *Photoacoustics* **2015**, *3* (1), 3–10.

(30) Arnal, B.; Wei, C.-W.; Perez, C.; Nguyen, T.-M.; Lombardo, M.; Pelivanov, I.; Pozzo, L.

D.; O'Donnell, M. *Photoacoustics* **2015**, *3* (1), 11–19.

(31) Guillot, S.; Bergaya, F.; de Azevedo, C.; Warmont, F.; Tranchant, J.-F. *J. Colloid Interface Sci.* **2009**, *333* (2), 563–569.

(32) Skelhon, T. S.; Grossiord, N.; Morgan, A. R.; Bon, S. A. F. *J. Mater. Chem.* **2012**, *22* (36), 19289.

(33) Gould, J.; Garcia-Garcia, G.; Wolf, B. *Materials* **2016**, *9* (9), 791.

(34) Marto, J.; Ascenso, A.; Gonçalves, L. M.; Gouveia, L. F.; Manteigas, P.; Pinto, P.; Oliveira, E.; Almeida, A. J.; Ribeiro, H. M. *Drug Deliv.* **2016**, *23* (5), 1594–1607.

(35) Li, D. S.; Lee, Y.-T.; Xi, Y.; Pelivanov, I.; O'Donnell, M.; Pozzo, L. D. *Soft Matter* **2018**, *14* (25), 5283–5293.

(36) Xi, Y.; Li, D. S.; Newbloom, G. M.; Tatum, W. K.; O'Donnell, M.; Luscombe, C. K.; Pozzo, L. D. *Soft Matter* **2018**, 4963–4976.

(37) Frens, G. *Nat. Phys. Sci.* **1973**, *241* (105), 20–22.

(38) Larson-Smith, K.; Pozzo, D. C. *Soft Matter* **2011**, *7*, 5339.

(39) Ilavsky, J.; Zhang, F.; Andrews, R. N.; Kuzmenko, I.; Jemian, P. R.; Levine, L. E.; Allen, A. J. *J. Appl. Crystallogr.* **2018**, *51* (3), 867–882.

(40) Ilavsky, J.; Jemian, P. R. *J. Appl. Crystallogr.* **2009**, *42* (2), 347–353.

(41) Zhang, F.; Ilavsky, J.; Long, G. G.; Quintana, J. P. G.; Allen, A. J.; Jemian, P. R. *Metall. Mater. Trans. A* **2010**, *41* (5), 1151–1158.

(42) Debye, P. *Ann. Phys.* **1915**, *351* (6), 809–823.

(43) Larson-Smith, K.; Jackson, A.; Pozzo, D. C. *J. Colloid Interface Sci.* **2010**, *343* (1), 36–41.

(44) Fabiilli, M. L.; Haworth, K. J.; Fakhri, N. H.; Kripfgans, O. D.; Carson, P. L.; Fowlkes, J.

B. *IEEE Trans. Ultrason. Ferroelectr. Freq. Control* **2009**, *56* (5), 1006–1017.

(45) Lamprecht, B.; Schider, G.; Lechner, R. T.; Ditlbacher, H.; Krenn, J. R.; Leitner, A.; Aussenegg, F. R. *Phys. Rev. Lett.* **2000**, *84* (20), 4721–4724.

(46) Li, D. S.; Lee, Y.-T.; Xi, Y.; Pelivanov, I.; O'Donnell, M.; Pozzo, L. D. *Soft Matter* **2018**, 5283–5293.

(47) Kaci, M.; Meziani, S.; Arab-Tehrany, E.; Gillet, G.; Desjardins-Lavisse, I.; Desobry, S. *Ultrason. Sonochem.* **2014**, *21* (3), 1010–1017.

(48) Sheeran, P. S.; Matsunaga, T. O.; Dayton, P. A. *Phys. Med. Biol.* **2014**, *59* (2), 379–401.

(49) Schad, K. C.; Hynynen, K. *Phys. Med. Biol.* **2010**, *55* (17), 4933–4947.

(50) Giesecke, T.; Hynynen, K. *Ultrasound Med. Biol.* **2003**, *29* (9), 1359–1365.

(51) Matsunaga, T. O.; Sheeran, P. S.; Luois, S.; Streeter, J. E.; Mullin, L. B.; Banerjee, B.; Dayton, P. A. *Theranostics* **2012**, *2* (12), 1185–1198.

(52) Mountford, P. A.; Borden, M. A. *Adv. Colloid Interface Sci.* **2016**, *237*, 15–27.

(53) Porter, M. D.; Bright, T. B.; Allara, D. L.; Chidsey, C. E. *J. Am. Chem. Soc.* **1987**, *109* (12), 3559–3568.

(54) Binks, B. P.; Clint, J. H.; Fletcher, P. D. I.; Lees, T. J. G.; Taylor, P. *Langmuir* **2006**, *22* (9), 4100–4103.

(55) Arnal, B.; Wei, C.; Perez, C.; Nguyen, T.; Lombardo, M.; Pelivanov, I.; Pozzo, L. D.; Donnell, M. O. *Photoacoustics* **2015**, *3* (1), 11–19.

(56) Li, D. S.; Yoon, S. J.; Pelivanov, I.; Frenz, M.; O'Donnell, M.; Pozzo, L. D. *Nano Lett.* **2017**, *17* (10), 6184–6194.

Chapter 4. CONTRAST-VARIATION TIME-RESOLVED SANS ANALYSIS OF OIL EXCHANGE KINETICS BETWEEN OIL-IN-WATER EMULSIONS STABILIZED BY ANIONIC SURFACTANTS

Contrast-variation time-resolved small angle neutron scattering (CV-SANS) was used to examine oil exchange kinetics between identical mixtures of hydrogenated/deuterated hexadecane emulsion systems without a net change in droplet size occurring within the timeline of the experiment. Oil exchange rates were estimated by transforming recorded scattering profiles to a relaxation function and by fitting to exponential decay models. We find the oil exchange process was accelerated when the droplets were stabilized by anionic surfactants even at concentrations well below the surfactant critical micelle concentration. Moreover, the exchange rate was not significantly accelerated when surfactant micelles were present. This suggests that micellar-mediated transport mechanisms do not play the dominant role in these systems. Screening electrostatic repulsion by increasing the ionic strength of the medium also had a negligible effect on oil exchange kinetics. In contrast, the use of oils with shorter alkane chain lengths (e.g. dodecane), having a higher solubility in water, significantly accelerated rates of oil transport between droplets. Oil transport rates for hexadecane were also found to increase with temperature and to follow Arrhenius behavior. These results were rationalized as an increase in the droplet collision frequency due to Brownian motion that results in direct oil transport without irreversible coalescence. Thus, primary mechanisms for oil exchange in insoluble anionic surfactant-stabilized emulsion systems is hypothesized to be through direct emulsion contact, reversible coalescence and/or direct oil permeation through thin liquid films. CV-SANS is also demonstrated as a powerful technique for the study of transport kinetics in all kinds of emulsion systems.

4.1 INTRODUCTION

Emulsion systems are dynamic and several phenomena can induce mass transport between dispersed oil droplets. Understanding how oil molecules exchange between droplets in emulsion systems is also crucial to designing emulsion-based drug-delivery vehicles, modifying properties (e.g. fragrance or flavor) of emulsion-based food products, or for utilizing droplets as microreactors for polymer and/or nanoparticle synthesis.[1–7] Of all possible transport mechanisms, emulsion coalescence and Ostwald ripening are probably among the best understood.[8–14] When emulsions are unstable, coalescence can occur due to colloidal forces and interactions. Droplet coalescence leads to size increases (i.e. coarsening) that ultimately cause water/oil macroscopic phase-separation. Ostwald ripening occurs in metastable emulsion systems through the dissolution of oil molecules in the continuous phase.[9,15,16] The driving force for this mechanism originates from differences in oil solubility and chemical potential at the oil-water interface, which is correlated to a droplet's radius of curvature.[17] Smaller droplets lead to higher oil solubilities, which results in a net diffusion of oil molecules towards larger emulsion droplets. As a result, the size distribution changes over time with larger droplets growing at the expense of smaller ones.

On the other hand, several studies have shown that poorly soluble oil molecules can also exchange between stabilized droplets, even without Ostwald ripening or coalescence, resulting in an equilibrium oil exchange without a net size change.[10,11,18–24] For example, transport mechanisms between droplets stabilized by non-ionic surfactants have been previously examined using differential scanning calorimetry (DSC).[10,18,19,25] In these studies, it was revealed that the oil exchange process only occurred when surfactant micelles were present at concentrations above the critical micelle concentration (CMC).[23] Surfactant micelles can be excellent molecular carriers by helping to solubilize insoluble oils in their hydrophobic core and accelerating transport across the

continuous phase. An alternative oil-exchange mechanism was also proposed in studies using microscopy, pulse gradient NMR, fluorescence, and turbidity measurements.[20,21] Here, the primary mechanism for oil exchange was based on direct emulsion contact where reversible collisions cause direct oil permeation through thin liquid films between the droplets as they collide due to Brownian motion.

Recently, time-resolved contrast variation small angle neutron scattering (CV-SANS) was also used to examine oil exchange rates between insoluble oil droplets.[22] In this study, Roger *et al.* examined the coarsening of nanosized hexadecane emulsions without the presence of additional surfactant micelles. It was observed that oil exchange rates occurred over a time scale that was significantly faster than that of any droplet size change. Moreover, the droplet growth rate also decreased with increasing chain length of the polyoxyethylene alkyl ether surfactants that were used to stabilize the droplets. These authors suggested that the main mechanism for oil exchange was due to droplet contact ripening.

Although few reports use time-resolved CV-SANS to study emulsion transport kinetics, this powerful technique has been more widely used to examine the kinetics of exchange of molecules in lipid vesicle or block copolymer micelle systems.[26–30] For example, time-resolved CV-SANS was used to distinguish the kinetic exchange rates of isotopically labelled lipids between different vesicles and within individual vesicles (e.g. lipid 'flip-flop' transitions).[26,28,29,31] Studies showed that lipids exchange between vesicles at faster time-scales than the rate of 'flipping' within the bilayers of unilamellar systems. In contrast, the opposite trend was observed in supported lipid bilayer systems (i.e. lipid coated nanoparticles). In block copolymer micelle systems, studies have shown that the escape of unimers from micelles was the rate limiting step in

the exchange kinetics.[30] For example, it was revealed that the molecular weight of the block copolymer, the degree of polymerization of the hydrophobic core-forming block, the interfacial tension between the solvent and hydrophobic block, and the sample temperature all played significant roles in mediating exchange kinetics.[32–37]

The main advantage of CV-SANS as a molecular transport characterization tool originates from differences in scattering length densities (SLD) between hydrogenated and deuterated versions of identical molecules (e.g. block copolymers, lipids, and oils). This allows researchers to directly examine exchange kinetics using nearly identical molecular isotopes without the need for any additional labelling. For emulsion systems, this eliminates any potential confounding of oil exchange kinetics that may be due to differences in chemical composition and/or solubility of components in the continuous phase.[21,24,25]

A schematic of CV-SANS experiments performed on emulsion systems in this work is shown in Figure 4.1. Two identical batches of deuterated/hydrogenated hexadecane emulsions are prepared with equal contrast to the solvent and the same size distribution. They are then mixed in equal proportions (1 to 1) at time zero and CV-SANS profiles are continuously collected. Any oil exchange that occurs after the initial mixing step would result in a decrease in contrast between the droplets and the solvent, which would ultimately decrease the scattering intensity. If all of the oil molecules are fully exchanged, minimal scattering should be detected.

In this work we use time-resolved CV-SANS to examine transport processes in oil-in-water (e.g. hexadecane) emulsions stabilized by anionic surfactants (e.g. sodium dodecyl sulfate). By varying the stabilizing surfactant concentration, temperature, ionic strength, types of anionic

surfactant, and alkane chain length, we systematically examine oil exchange processes and identify dominant transport mechanisms.

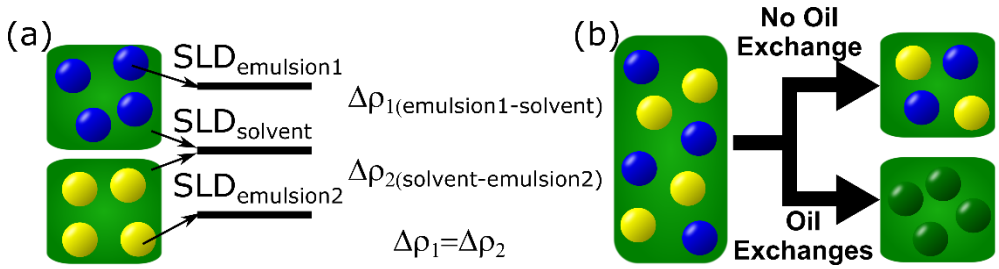

Figure 4.1. Schematic oil-in-water emulsion oil exchange CV-SANS experiment. (a) Identical emulsions containing deuterated oil and partially-deuterated oil are prepared to have opposite scattering length densities and equal contrast with the solvent. (b) When oil exchanges between droplets, a decrease in intensity is observed due to contrast matching. If no oil exchanges, the scattering intensity remains constant with time.

4.2 Materials And Methods

Hexadecane (>99%, CAS: 544-76-3), dodecane (>99%, CAS: 112-40-3), octane (>99%, CAS: 111-65-9), sodium dodecyl sulfate (SDS, CAS: 151-21-3), hexyl sulfate sodium salt (SHS, CAS: 2207-98-9), tetradecyl sulfate sodium salt (STS, CAS: 1197-50-0), and sodium chloride (CAS: 7647-14-5) were purchased from Sigma-Aldrich (St. Louis, MO, USA). Deuterated hexadecane (D34, 99%, CAS: 15716-08-2), deuterated dodecane (D26, 98%, CAS: 16416-30-1), deuterated octane (D18, 99%, CAS: 17252-77-6), and deuterium oxide (99.9%, CAS: 7789-20-0) were purchased from Cambridge Isotope Laboratories, Inc. (Tewksbury, MA, USA). Aerosil® R816 was obtained as a gift from Evonik Industries (Essen, Germany).

Fully deuterated (high SLD) and partially deuterated (low SLD, 60 vol% hydrogenated and 40 vol% deuterated) alkane emulsion stocks with equal contrast to the solvent were prepared identically and subsequently mixed, right before an experiment, to monitor the oil exchange

kinetics. In short, concentrated stock emulsions were first synthesized by sonicating 1.2 volume percent oil in the solvent using a Branson Digital Sonifier S-450 with a 3 mm sonicating microtip (Branson Ultrasonics, CT, USA) at 30% amplitude 50% duty cycle (1 seconds on and 1 seconds off) for a total of 25 minutes of sonication time. The solvents used in this study for synthesizing the emulsion stocks contain small concentrations of surfactants (i.e. 1 mM of anionic surfactants), with the exception of the samples where no surfactants were present. The details on the SLDs of the stock emulsions and the exact composition of the solvents for different contrast matched emulsion systems are summarized in Table 4.1 and Table 4.2. Emulsion stocks in the presence of a desired surfactant concentration (e.g. 20 mM SDS) were then prepared by using the initial emulsion stock, high concentrations of stabilizing agents (e.g. 100 mM SDS) and additional H_2O/D_2O solvent. Using this method to synthesize samples allowed us to form identically sized emulsions having variable surfactant concentrations. The final composition of the emulsion stocks contained 1 vol % of alkane droplets in solvents containing surfactant at concentrations ranging from 0 to 20 mM. Solid fumed silica particles (Aerosil® R816) were also used as the stabilizing agent in some samples of this study. The particle-stabilized Pickering emulsion stocks were synthesized by directly sonicating 1 vol% percent of stock oil with 1 wt% of silica particles. The two stock oil-in-water emulsions with the same stabilizing agent concentrations were then mixed at a 1:1 volume ratio prior to loading the sample into a 0.4 cm pathlength NIST titanium demountable sample cell with quartz windows

Table 4.1. Details on the dispersed phase (oil) used for contrast matched emulsion systems.

Oil Type	High SLD Emulsion (100 vol% D-Hexadecane)		Low SLD Emulsion (40 vol% D-Hexadecane)	
	SLD ($x10^{-6}$ Å^{-2})	Density (g/mL)	SLD ($x10^{-6}$ Å^{-2})	Density (g/mL)
Hexadecane	6.66	0.88	2.41	0.85
Dodecane	6.56	0.86	2.35	0.79
Octane	6.36	0.81	2.23	0.75

Table 4.2. Continuous phase (water) compositions for contrast matched emulsion systems.

Oil type in emulsion system	Hydrogenated water (vol%)	Deuterated water (vol%)	Solvent SLD ($x10^{-6}$ $Å^{-2}$)
Hexadecane	26.5	73.5	4.54
Dodecane	27.7	72.3	4.46
Octane	30.0	70.0	4.29

Pre-mixed emulsions, prepared from the two high/low SLD components, were also synthesized to quantify any residual scattering in 'perfectly mixed' samples containing different surfactant species and concentrations. Running such control samples was important since the surfactants and interfacial stabilizers that were used in this study were not contrast matched to the solvent. This resulted in some residual scattering in CV-SANS profiles even after 'perfect' oil mixing. These control samples were synthesized by pre-mixing a 1:1 ratio of high and low SLD stock oils at a total of 1 vol% prior to adding to the solvents containing different concentrations of the stabilizing agents. The pre-mixed emulsions were then further sonicated using the tip sonicator with identical acoustic parameters to those used for other emulsions. This resulted in fast and effective mixing of the oil molecules to achieve the equivalent to samples that are left to exchange oil over an infinitely long period of time.

It is important to note that a fully hydrogenated alkane emulsion could not be used as the lower SLD emulsion due to the large absorption cross-section of the solvent, which prevented the use of thicker samples. The contrast matching condition was carefully designed and optimized for a system with a sample pathlength of 1 cm, which was used in a parallel study investigating the effects of acoustic forces inducing emulsion mixing. Additional information on the optimization of the contrast matching condition was provided in Chapter 2.

4.2.1 *Small Angle Neutron Scattering (SANS)*

Small angle neutron scattering (SANS) experiments were conducted at the National Institute of Standards and Technology Center for Neutron Research (NCNR) using the 45-meter-long very small angle neutron scattering (VSANS) instrument. Two detector configurations (i.e. sample-to-detector distances) were used simultaneously during experiments to simultaneously acquire scattering intensities spanning from a q range of $1.9x10^{-3}$ to $1.7x10^{-1}$ $Å^{-1}$. In each experiment, up to 17 samples could be loaded onto the instrument and each sample was exposed to neutrons at 1- or 5-minute intervals to collect the full-range scattering profile. VSANS was uniquely suited for this study because it allowed for full q-range collection at once as a function of time.

4.2.2 *SANS Data Analysis*

The recorded SANS data were reduced using standard VSANS Igor reduction protocols.[38] The extent of oil exchange could be expressed using the relaxation function (equation (4.1)) since the contrast of the emulsion system was proportional to the square root of the scattering intensity.[30] *I(t)* is the integrated scattering intensity at any given time, I_0 is the integrated scattering intensity at time zero which can be obtained using the unmixed 100% deuterated alkane control sample, and I_∞ is the integrated scattering intensity at infinite time which is obtained from the pre-mixed control sample. An assumption for utilizing the relaxation function was that the size distribution did not change over time (constant I_0). To check this, scattering profiles of the unmixed 100% deuterated alkane emulsion systems were also tracked over the duration of an experiment. These profiles showed little or no change over time (Chapter 7 supplemental information) suggesting that the assumption of constant I_0 is reasonable for these systems. A few samples showed small scattering changes over time that suggested some slight change in size. For these samples, additional analyses

were performed using the control sample (unmixed 100% deuterated samples) to estimate the corresponding I_0. The effect of accounting for these small changes in droplet size was negligible and this is further discussed in the results section.

$$R(t) = \left(\frac{I(t) - I_\infty}{I_0 - I_\infty}\right)^{1/2} \tag{4.1}$$

The kinetic oil exchange parameters were then estimated by fitting the relaxation function *R(t)* to an exponential decay model (equation (4.2)), where *k* is a decay constant, *t* is time and *a* is a final plateau value or residual scattering that persists due to slow oil exchange processes that occur outside of the measurement window. For samples without any added surfactants, the plateau value *a* was fixed at 0 since it was not necessary to include in order to obtain good model fits.

$$R(t) = (1 - a) \cdot e^{-kt} + a \tag{4.2}$$

4.2.3 *Emulsion Size Estimation*

The size of the synthesized emulsions was obtained either through dynamic light scattering (DLS) using a Malvern Zetasizer Nano ZS, (Malvern Instruments Ltd., Worcestershire, United Kingdom) or by fitting a simple sphere model to the CV-SANS scattering data when it was possible. Unfortunately, due to the limited q range of the instrument, the size distribution of some of the larger droplets could not be estimated using solely the recorded CV-SANS profiles. Therefore, for consistency purposes, all reported sizes are obtained from DLS. The size distribution obtained from fitting the scattering data was only used to qualitatively assess for possible emulsion size changes during an experiment with the control samples.

4.3 RESULTS

The kinetics of oil exchange between hexadecane droplets in emulsions with and without the presence of SDS was examined first. The emulsions without the presence of surfactants had a hydrodynamic diameter of 603 nm with a polydispersity index (PDI) of 0.3 while emulsions containing stabilizing surfactants had a mean diameter of 113 nm with a PDI of 0.2. The DLS measurements for the emulsions are provided in the supplemental information chapter (Chapter 7). Examples of the obtained SANS profiles at 25°C are shown in Figure 4.2. As can be seen in the figures, all of the samples showed a decrease in scattering intensities over time, indicating that oil molecules were able to exchange between droplets regardless of whether or not surfactants were present. Interestingly, the decrease in scattering intensity was extremely slow for samples without stabilizing surfactants. Still, ultimately the emulsion systems would reach a fully mixed state where minimal scattering intensities were recorded in the pre-mixed control samples.

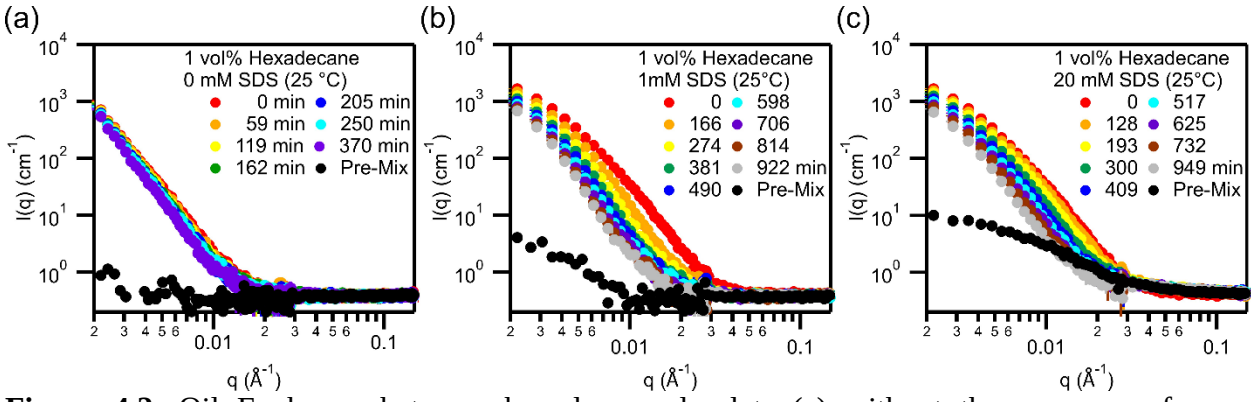

Figure 4.2. Oil Exchange between hexadecane droplets (a) without the presence of any surfactants, stabilized by (b) 1 mM and (c) 20 mM SDS at 25 °C. Emulsions stabilized by surfactant shows a significant faster oil exchange process.

When surfactants were present, the recorded scattering intensities decreased at a significantly faster rate. Moreover, it was observed that the scattering intensities of samples

containing lower (1 mM) and higher (20 mM) surfactant concentrations seemed to decrease at a similar rate. The main difference between the two systems was only observed in fully exchanged scattering profiles of pre-mixed control samples, where the sample containing 20 mM of SDS had a significantly higher residual scattering intensity due to the presence of greater amount of the non-contrast matched surfactant. Oil exchange experiments for emulsion systems containing other concentrations of SDS (i.e. 2.5, 5, 10, and 15 mM) were also performed and the corresponding scattering profiles are provided in the supplemental information chapter (Chapter 7). In general, the scattering profiles for emulsion systems stabilized by various concentrations of SDS, above and below its critical micelle concentration (CMC_{SDS} in presence of emulsion = ~11.94 mM) all showed similar rates of decrease in the scattering intensities. The CMC of SDS in the presence of emulsion droplets was estimated through conductivity measurements. This resulted in a slightly higher CMC value (theoretical CMC_{SDS} = 8.2 mM) due to the adsorption of some SDS molecules onto the oil-water interface.[39,40] Additional information on the measurements is provided in the supplemental information chapter (Chapter 7).

Another parameter that could significantly affect the oil exchange kinetics was the sample temperature. Example scattering profiles of oil exchange between emulsions stabilized by 1 mM SDS at various sample temperatures is shown in Figure 4.3. As can be seen in the figure, increasing the sample temperature resulted in a significantly faster scattering intensity decay. This trend, where increasing the temperature results in faster oil exchange, was also observed in samples containing other surfactant concentrations (Chapter 7 supplemental information).

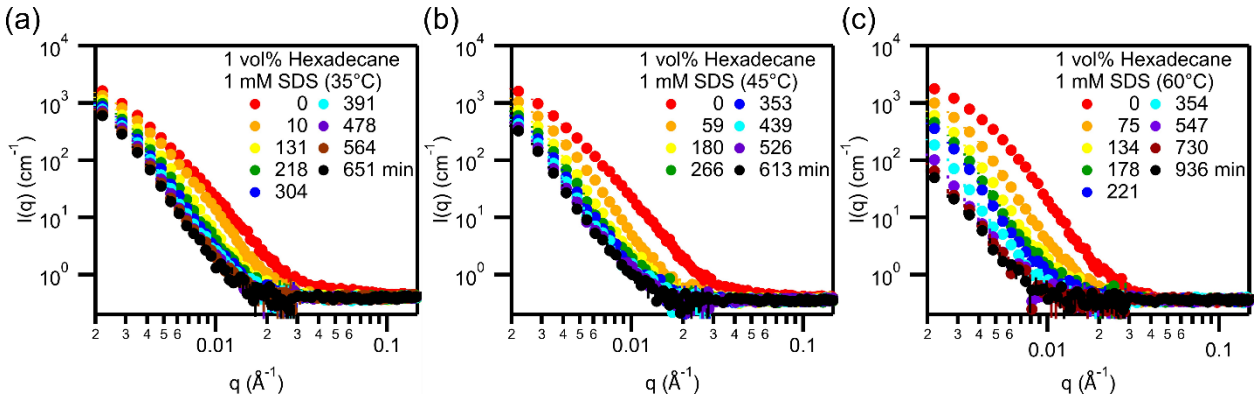

Figure 4.3. Scattering profiles of droplet oil exchange at (a) 35 °C, (b) 45 °C, and (c) 60 °C of a 1 vol% hexadecane emulsions stabilized by 1 mM SDS sample. Increasing sample environment temperature results in a faster decrease in scattering intensities.

To quantitatively compare the oil exchange kinetics between emulsion samples containing different concentrations of surfactants and at different sample temperatures, the scattering profiles were transformed using a relaxation function (equation (4.1)) to express the average normalized contrast of the emulsion systems. An advantage of using the relaxation function for analysis is that it automatically accounts for differences in residual scattering and that it provides a standardized method for comparing oil transport kinetics between different samples. Figure 4.4 is an example of the estimated relaxation functions for emulsion samples stabilized by 1 mM SDS at various temperatures.

The estimated relaxation decay functions were then fit to an exponential decay model (equation (4.2)) to obtain important oil exchange kinetic parameters. The exponential decay model contains a plateau value ‘a’ to accommodate the observation that some relaxation functions for samples at the highest temperatures studied (60 °C) still did not fully decay to 0 even after very long elapsed times (Figure 4.4, blue curve). Using a simple exponential decay to fit the relaxation function would otherwise consistently overestimate the decays at longer time points. On the other hand, fitting the relaxation functions of emulsion systems at lower temperatures using exponential

decay models either with/without a plateau had little effects on the time constant of the exponential decay. Still, for consistency, we chose to use the exponential decay model with an added plateau to fit all the estimated relaxation functions. In addition, the plateau value used in all of the modeling was kept constant and based on the estimated value obtained from samples measured at the highest temperatures (i.e. 60 °C). The only exceptions are the samples where the experiments were only performed at 25 °C (i.e. 2.5 and 15 mM SDS) and not at elevated temperatures.

Based on the modeled fits, the plateau value for emulsion systems containing 1 mM SDS is around 0.12 and the estimated decay constants are 9.7×10^{-4} (25 °C), 1.3×10^{-3} (35 °C), 2.1×10^{-3} (45 °C) and 6.3×10^{-3} min^{-1} (60 °C). The effect of accounting for emulsion size change on the estimated relaxation function value was also investigated and was found to have little consequence in the parameters extracted from the relaxation decay curve. Therefore, since emulsion sizes showed little to no variation in DLS and in CV-SANS over the time-scales of experiments, they were assumed to remain constant in our analysis. Additional details are provided in the supplemental information chapter (Chapter 7).

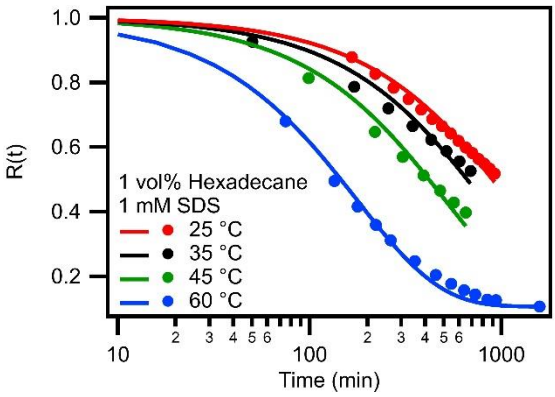

Figure 4.4. Example emulsion oil exchange kinetic curve with modeled fits for hexadecane mixtures stabilized at 1 mM SDS.

The relaxation functions with corresponding fits at various surfactant concentrations and temperatures are shown in Figure 4.5. The results again confirm the observation that the presence of surfactants and the increase in sample temperature accelerated the oil exchange process. The modeling results also suggest that temperature has a more significant effect on the oil exchange kinetics for emulsion systems stabilized by surfactants. It was also observed that the relaxation function of the emulsion sample containing 20 mM SDS decayed slightly faster than the other samples, especially at elevated temperatures.

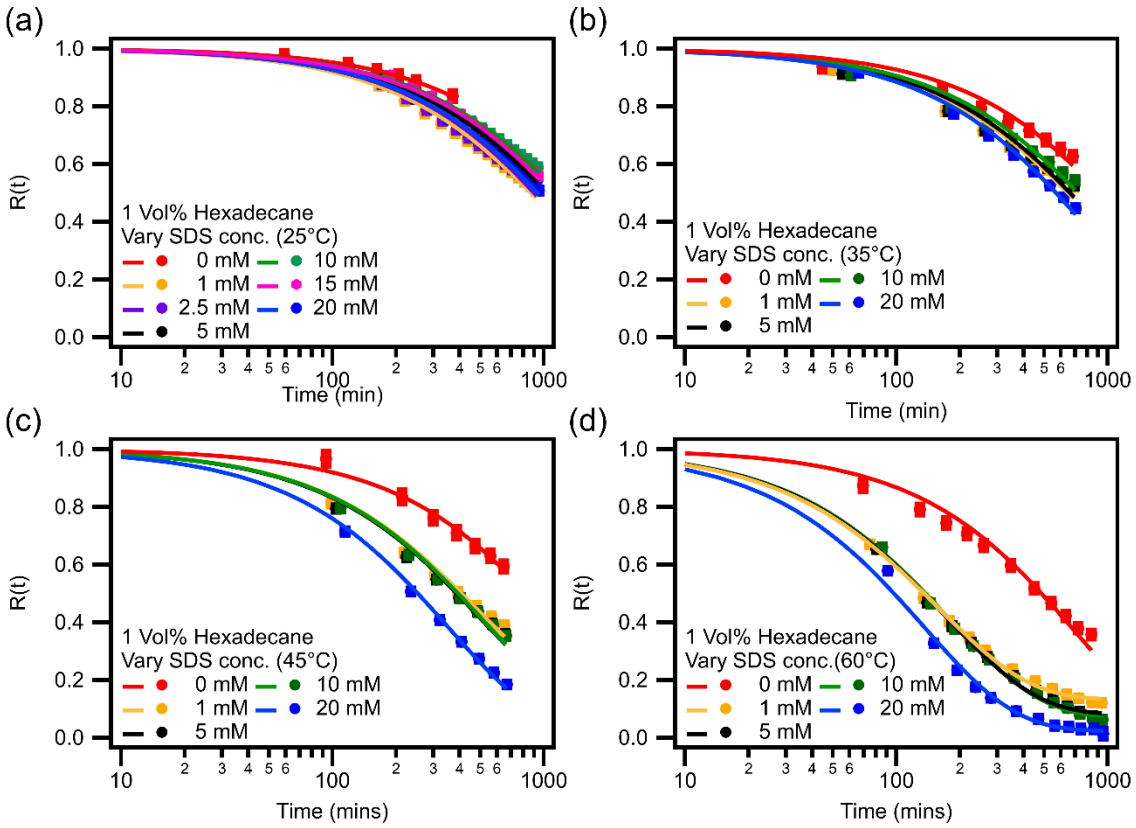

Figure 4.5.. Relaxation function of emulsion systems stabilized by various SDS concentration and held at different temperatures. The results show that the oil exchange kinetics is similar across most SDS concentrations at all temperatures. The exception are samples with 20 mM SDS, where a slightly accelerated decay is observed at elevated temperatures. Samples without added surfactant are also included for comparison (red).

The estimated decay constants for the different emulsion systems could be fit with an Arrhenius equation (equation (4.3)), where k is the estimated decay constant, A is the pre-exponential factor, E_a is the activation energy, R is the gas constant, and T is the absolute temperature. The results are shown in Figure 4.6 and the summary of the parameters estimated from the Arrhenius plot is shown in Table 4.3. The estimated Arrhenius parameters for emulsion systems without any stabilizing surfactants were different from those with stabilizers. However, little variation was observed for samples with different concentrations of SDS above and below the CMC.

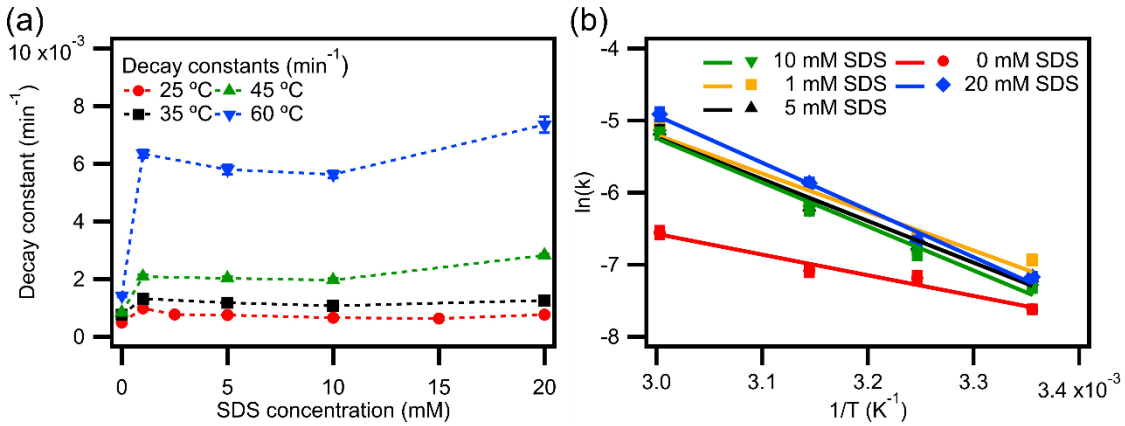

Figure 4.6. (a) Estimated kinetic decay constants for samples with variable SDS concentration and at various temperatures. Parameters were obtained from fits to (4.2), where the plateau constant *(a)* was fixed and estimated from experiments at 60 °C. (b) Arrhenius plot for the kinetic decay constant for emulsion systems at variable surfactant concentrations.

$$\ln(k) = \ln(A) - \frac{E_a}{R}\left(\frac{1}{T}\right) \tag{4.3}$$

Table 4.3. Kinetic parameters estimated from the Arrhenius analysis.

SDS concentration (mM)	ln(A) (min^{-1})	Ea (kJ/mol-k)
0	2.0 ±1.2	23.8±3.2
1	10.8±2.8	44.4±7.4
5	12.1±1.8	48.1±4.8
10	13.1±1.6	50.8±4.2
20	14.7±1.4	54.5±3.7

Emulsion oil exchange experiments were also performed for anionic surfactants with identical head groups but longer and shorter alkyl tails, STS (C14) and SHS (C6), to further examine the role of surfactant structure and the presence of micelles on oil exchange kinetics. All surfactants have the same polar head group and the only difference between the surfactants is the hydrophobic tail length, which resulted in a significant difference in the surfactant's critical micelle concentrations (i.e. theoretical CMC for STS = 2 mM and for SHS = 300 mM). This portion of the experiment was carried out at 45 °C due to the poor solubility of STS at 25 °C. Example oil exchange scattering profiles obtained SHS and STS stabilized emulsion systems are shown in Figure 4.7 (a) and (b). As can be seen in the figure, the size distribution of the as-synthesized emulsions is different for different surfactants. Emulsions stabilized by STS have a mean hydrodynamic diameter of 105 nm and PDI of 0.2, similar to emulsions samples where SDS was used as the stabilizing agent. On the other hand, emulsions in the sample with SHS present are larger and have a mean hydrodynamic of 261 nm and PDI of 0.4. Additional scattering profiles of emulsion systems stabilized by SHS and STS is provided in the supplemental information chapter (Chapter 7). The estimated relaxation functions and decay constants are shown in Figure 4.7 (c) and (d). As can be seen in the figure, the emulsion systems stabilized by STS showed similar decay rates to the results obtained from SDS systems and is not affected by the concentration of stabilizing surfactant. Results obtained from emulsion systems stabilized by SHS also showed little correlation between surfactant concentration and rate of oil exchange. However, the estimated decay constant had a value much lower than for emulsion systems containing SDS and STS. The difference in the decay rate was likely due to differences in emulsion size that affected droplet diffusion rates, collision probabilities and total interfacial area.

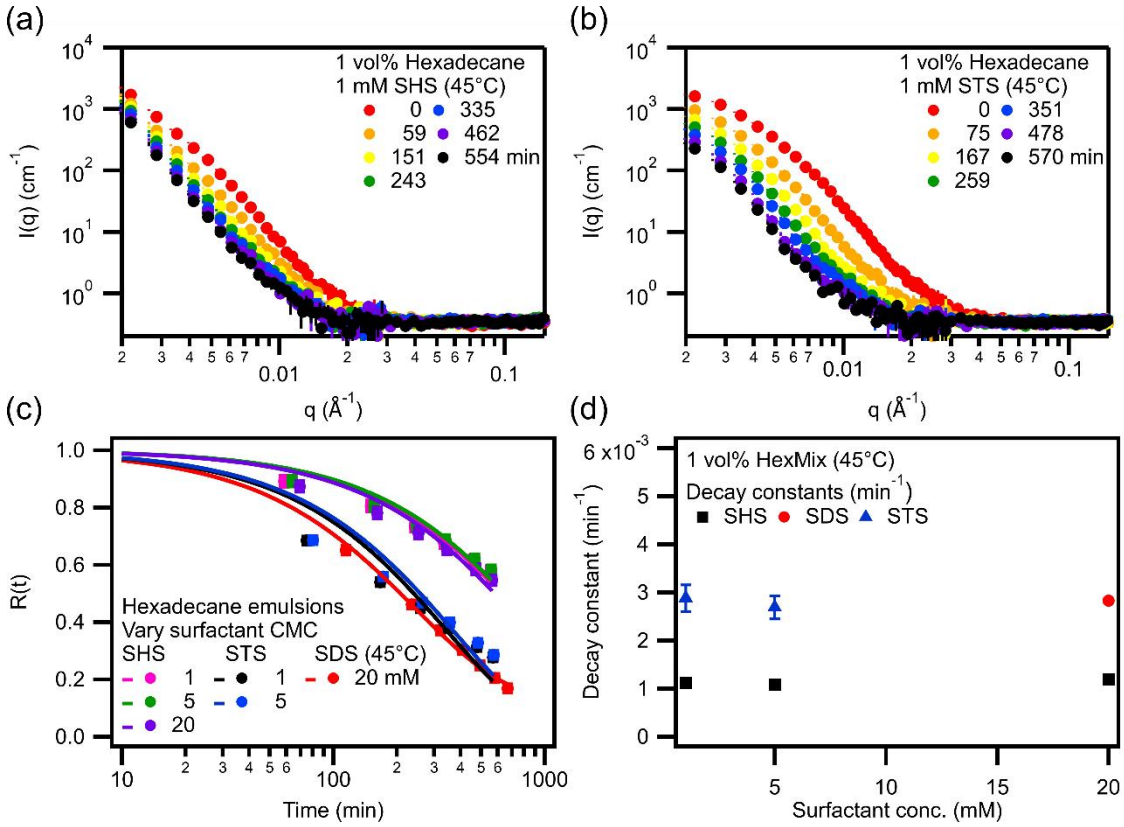

Figure 4.7. (a) CV-SANS scattering profiles for 1 vol% hexadecane emulsion stabilized by 1 mM SHS as a function of time. (b) CV-SANS scattering profiles for emulsions stabilized by 1 mM STS. (c) Relaxation function of emulsions stabilized by anionic surfactants SHS, SDS and STS. The kinetics of oil transport is also not significantly affected by the concentration of the stabilizing surfactants. (d) Estimated decay constants for emulsion systems with different surfactants.

We also performed an experiment to determine if the ionic strength of the continuous water phase affected the oil exchange kinetics. One hypothesis to explain the insignificant effect of surfactant concentrations on oil exchange kinetics was that strong electrostatic repulsion forces provided by the dense packing of charged ionic head groups at the interface of oil droplets could prevent micelles from approaching the droplet. Adding salt into the system, increasing the ionic strength, could screen this repulsive force and potentially accelerate micelle-driven oil exchange. However, relaxation functions in Figure 4.8 show that screening the electrostatic repulsion forces in emulsion systems with the presence of micelles (20 mM SDS) did not significantly affect oil

exchange kinetics in any form. The estimated decay constants for samples containing 0 mM, 5 mM and 50 mM NaCl were identical ($k = 1.2x10^{-3}$). Results from this experiment again suggest that perhaps the main driving force inducing oil exchange in anionic surfactant stabilized emulsion systems was not micelle driven and that another dominant form of oil exchange is present.

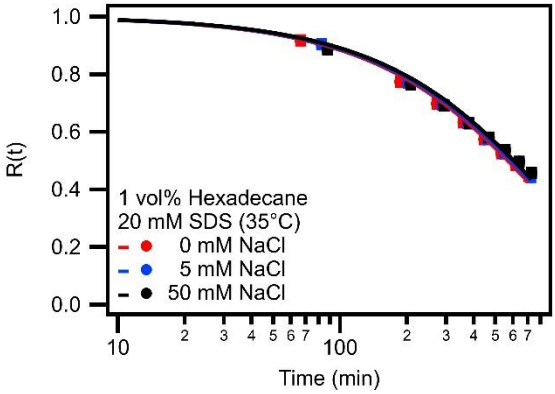

Figure 4.8. Oil exchange kinetics for identical SDS emulsion samples prepared with varying NaCl concentration at 35°C. Results show that screening electrostatic repulsion in the system has little effect on the oil mixing kinetics.

The last parameter that was examined was the effect of oil type on the oil exchange kinetics. Figure 4.9 (a) shows an example scattering profile for oil exchanging between dodecane emulsions, stabilized by 1 mM of SDS at 25°C. The synthesized dodecane emulsion droplets were 142 nm in diameter with a PDI of 0.1, slightly larger than the emulsions in the hexadecane system. However, as can be seen in its relaxation curve (Figure 4.9 (b)), the dodecane emulsion system exchanges oil molecules over a time scale of minutes. In contrast, hexadecane emulsion systems, with the same stabilizing surfactant concentration and sample temperature, would need to exchange oil over a period of several hours to achieve similar mixing states. The estimated decay constant was 1.8×10^{-1} min^{-1} and the plateau was 0.095. Oil exchange between dodecane droplets stabilized at other SDS concentrations at 25°C was also performed and also showed that oil exchanges significantly faster (Chapter 7 supplemental information). Clearly, the oil molecule size

has a significant effect on the oil exchange kinetics. In fact, it was so significant that dodecane droplets still exchange oil at faster rates at 5°C than hexadecane droplets at 60°C. The kinetic decay constants for dodecane droplets stabilized by 5 and 20 mM SDS were $2.0x10^{-2}$ and $2.7x10^{-2}$ respectively.

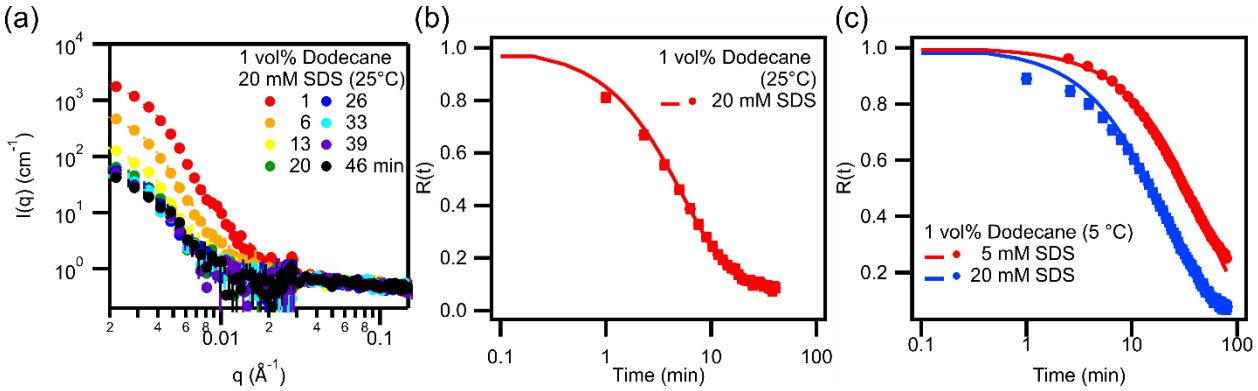

Figure 4.9. (a) CV-SANS profiles of oil exchange between dodecane droplets stabilized by 20 mM SDS at 25°C. Oil exchanges significantly faster than for hexadecane emulsion systems. (b) Estimated relaxation curve at 25°C. (c) Relaxation function of dodecane emulsions stabilized by either 5 or 20 mM SDS at 5°C.

The effects of the solubility of oil molecules in the continuous water phase on the kinetics of exchange was further examined by using solid particles as stabilizing agents in lieu of anionic surfactants. The purpose of using particle stabilized emulsions (Pickering emulsions) to study oil exchange kinetics was that solid particles provide a steric barrier against coalescence and also prevent the formation of thin liquid films through which the oil molecules could permeate. However, such emulsion droplets still have significant interfacial areas exposing oil directly to the continuous water phase for transport through the bulk. Thus, for these samples, the only possible oil exchange mechanism is through direct molecular solubilization and diffusion across the continuous phase. Example scattering profiles with hexadecane as the oil phase are shown in Figure 4.10 (a). The scattering profiles only show slight changes in the recorded scattering

intensities over time that can be captured in the corresponding relaxation curve Figure 4.10 (b). Moreover, the estimated relaxation decay of the more soluble emulsion systems shows that the oil exchange kinetics significantly accelerate with decreasing alkane chain length (i.e. increasing solubility). The kinetic decay constants increase from 2.4×10^{-4} min^{-1} (hexadecane) to 1.3×10^{-2} min^{-1} (dodecane) and 1.9×10^{-1} min^{-1} (octane) with decreasing oil molecule size.

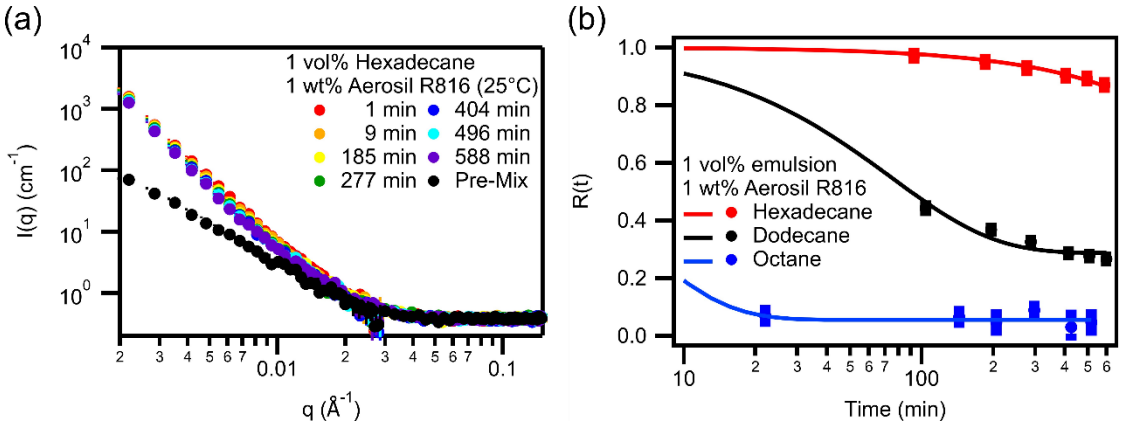

Figure 4.10. (a) CV-SANS profiles of oil exchange between Pickering emulsions with hexadecane as the oil phase. The exchange is extremely slow due to the low solubility of hexadecane in water. (b) Relaxation functions for Pickering emulsions prepared with hexadecane, dodecane, and octane as the oil phase.

4.4 Discussion

All of the recorded SANS data and estimated relaxation functions shown here suggest that the concentration of the stabilizing anionic surfactant had minimal effect on the oil exchange kinetics. Therefore, micelle-dominated oil exchange can be ruled out as a main contributor since significant transport was observed in emulsion systems stabilized by surfactants at concentrations well under the critical micelle concentration of the surfactant. These observations are also similar to other reports examining Ostwald ripening processes.[12,41] One example is a report by Kabalnov *et al.* where the authors observed that the concentration of SDS, ranging from 33 mM to 1 M, had minimal effect on the undecane emulsion ripening rate. Screening the electrostatic repulsion

between the micelles and emulsions also did not result in an increased oil exchange rate. It was suggested that perhaps the micelles provided a minimal contribution to oil mass transport since these had a limited ability to solubilize oil molecules from the continuous phase.

Additional oil exchange mechanisms, including direct molecular diffusion through the continuous phase and direct emulsion contact, could simultaneously occur in emulsion systems. Experiments using Pickering emulsions were performed to isolate the two exchange mechanisms, providing the ability to only examine the oil exchange that was induced by bulk molecular diffusion of oil through water. For the relatively insoluble hexadecane emulsion system, it was observed that relaxation function decayed minimally, suggesting that almost no oil molecules were exchanged due to its extremely low solubility in water ($2.1x10^{-5}$ mg/L at 25°C). On the other hand, changing the solubility of the emulsion core from hexadecane to dodecane ($3.7x10^{-3}$ mg/L) and octane ($6.6x10^{-1}$ mg/L) resulted in accelerating the oil exchange kinetics by orders of magnitudes, allowing emulsion systems to reach exchange equilibrium within minutes. Based on these observations, it is clear that direct oil molecule diffusive transport across the continuous aqueous phase occurs in emulsion systems. Furthermore, this oil exchange mechanism would become the primary method of transport in emulsion systems when using more soluble oils in the dispersed emulsion phase. Direct molecular transport and how this is affected by oil solubility has been examined in other reports, primarily in relation to the stability of emulsions. For example, prior reports have shown that the Ostwald ripening rate in emulsion systems decreases when using longer alkane chain length molecules as the dispersed emulsion phase.[9,22]

On the other hand, our results show that oil molecules still exchanged in insoluble emulsion systems where the direct oil diffusion mechanisms were severely hindered due to poor oil

solubility. In such systems, including hexadecane emulsion systems, the mechanisms that likely dominate oil exchange processes are through direct emulsion contacts. When two droplets collide without undergoing coalescence, oil molecules could still exchange via direct permeation through thin liquid films, by reversible emulsion coalescence, or by a combination of the two. Spontaneous contact between dispersed droplets occurs via Brownian motion. When contact happens, thin liquid films can form between the two curved interfaces as the droplets move close to each other as shown in Figure 4.11. The lifetime of these liquid films is a function of the disjoining pressure between the droplets, the salt concentration, pH, and temperature.[13,42–44] Examples of droplets undergoing reversible coagulation have been captured using video enhanced microscopy.[45] Under certain conditions, the thin liquid film can be stable and persist for long periods of time. For example, reports have shown that SDS stabilized emulsions can form stable flocs of adhesive emulsions when the systems contain high concentrations of salt and the samples are held at elevated temperatures.[13,46–49] However, further varying the environmental conditions resulted in disruptions to this balance and droplets separated from each other.[49] The presence of liquid thin films, regardless their lifetime, can provide an environment where oil molecules can diffuse through a much shorter distance across the continuous phase and exchange faster between droplets. Direct permeation of oil molecules through the liquid film has been observed and proposed as the main driving force for inducing oil exchange in multiple emulsion systems examining oil exchange between dissimilar oil emulsions.[14,22,50,51] This work shows that direct permeation induced oil exchange can also occur spontaneously for homogeneous emulsion systems.

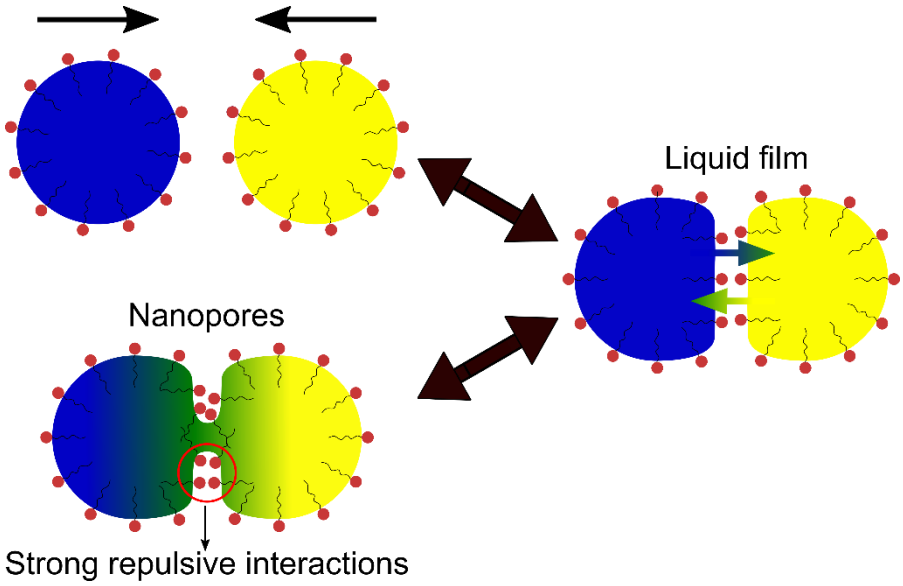

Figure 4.11. Schematic diagram of emulsions forming thin liquid films and nanopores when moving close to each other.

Transient holes or pores in the liquid thin film could also form if the droplets were able to continue moving closer to each other, inducing partial emulsion coalescence and allowing oil molecules to rapidly exchange between the droplets directly through nanopores. The formation of these transient holes should be temporary for surfactant stabilized emulsions since the surfactant molecules around the nucleated pores would be packed with an unfavorable curvature.[52,53] As a result, surfactant molecules at these highly curved interfaces would exhibit strong repulsive forces between each other and form a high activation energy barrier for further emulsion coalescence as shown in lower portion of Figure 4.11. Unless this activation energy barrier is surpassed, the droplets would detach from the doublet form back to two individual drops. While reversible coalescence of stabilized emulsions seemed counterintuitive, this mechanism has been proposed as a primary mechanism for transport between droplets in multiple water-in-oil microemulsion systems.[53–55] For example, Fletcher *et al.* examined mass exchange between thermodynamically stable water in heptane microemulsions by observing the quenching of fluorescent molecules that

were dissolved in their core.[53] The observed exchange kinetics between microemulsions was not affected by the size of the fluorescent molecules that were used, suggesting the exchange process was not due to the permeation of the solutes through liquid thin films. Moreover, the authors also observed that mixing two sizes of microemulsions together resulted in an intermediate size shortly after adding the two together. If reversible coalescence can occur in thermodynamically stable systems, this process may also occur in kinetically stable emulsion systems. Unfortunately, both contact-induced mechanisms occur over time scales that are significantly faster than the timescales of our characterization technique. Thus, it is not yet possible with our data to distinguish and determine which mechanism is dominating the observed oil exchange for insoluble oils.

Another important observation stemming from our work was that hexadecane emulsion systems containing 20 mM of SDS showed a slightly faster decay in the estimated relaxation function. We hypothesize that this small increase in transport may be due to depletion interactions arising due to the presence of excess surfactant micelles. Depletion forces can occur between large particles (e.g. droplets) when they are suspended in a solution with other non-adsorbing components (e.g. micelles) present. Studies on depletion interactions between surfaces using light scattering, electron microscopy, and atomic force microscopy showed that depletion forces can oscillate and can either be attractive or repulsive, depending on the distance between the surfaces and the concentration of the surfactant micelles that are present.[52,56–60] For systems containing small concentrations of micelles, depletion forces generally result in attractive interactions between emulsion surfaces, allowing droplets to be closer with their neighbors and to have a higher probability of inducing direct emulsion contact-based oil exchange.

When modeling oil exchange kinetics, it was observed that a simple exponential decay was not able to fit the relaxation decay function when surfactant was present. Adding a small plateau constant to the model fit was required to fit the data points at longer time points. The presence of a non-zero plateau value could be due to some chemical impurities in the system, resulting in slight contrast mismatch. However, the relaxation function was normalized to a pre-mixed sample which should already account for any residual scattering intensities due to contrast mismatch. Moreover, the model fits also showed slight deviations between the fits and the estimated relaxation function even when adding the plateau constant to the model. One proposed explanation is that polydisperse emulsion systems exhibit a relaxation function that consisted of more than one exponential decay.[20] Another hypothesis is that oil exchange consists of multiple processes where a fast decay is due to direct exchange between droplets that dominates in the initial phases of transport. The slower exchange process could potentially be due to complexation of longer oil molecules within emulsion droplets. It is possible that such molecular complexes may only break when significant energy is added to the system (e.g. via sonication during pre-mixing). These small complexes of oil molecules may bundle together and transport as a group, rather than as single molecules, unless a certain energy threshold is exceeded. If the diffusion of stable oil complexes is much slower than that of isolated oil molecules a slower relaxation process would be measured. As a result, there is a small portion of oil that will take much longer to fully exchange and to reach the contrast matching conditions. On the other hand, this mismatch in oil composition is not observed in the pre-mix sample since the complexation of oil molecules may be broken by the large acoustic energies that are applied to the system during the pre-mixing process. It should be noted, however, that the plateau constant was a low value that usually represented ~10% of the signal.

A third potential explanation for this plateau relates to the coupling of hydrogenated/deuterated alkane molecules to the hydrophobic tails of surfactants. As a result, the hydrogenated and deuterated oil molecules could diffuse across surfactant-oil interfaces at different rates. This hypothesis may be supported by a molecular simulation study by Ahn *et al.* on the oil transport through non-ionic surfactant coated oil-water interfaces.[61] In their study, it was shown that the origin of the transport energy barrier was due to the inhomogeneity of the surfactant monolayers at the oil and water interface. It was observed that the transport barrier was affected by the size of solute, but mainly due to the size differences in the molecule's cross section and not the length of the solute. Although their study was performed on non-ionic surfactant stabilized emulsion systems, the effect of solute size on the transport barrier should be a universal phenomenon.

The impacts of hydrogenated/deuterated molecules on mass transport kinetics was also observed in a study by Fletcher *et al.*.[53] It was noted that deuterated water-in-oil emulsions had a slightly slower transport rate compared to the rate that was recorded in hydrogenated water-in-oil emulsion systems. Moreover, the estimated decay constant decreased with the increase in the volume fraction of deuterated water in the inverse emulsion system. The difference in hydrogenated/deuterated hexadecane molecular diffusion rates could also slightly affect the oil exchange rates in our reported emulsion system. However, it shouldn't affect the overall observed trends between the different emulsion systems since all samples were all prepared from the same stocks of oil-in-water emulsions. One potential experiment that could be performed in the future to determine if the chemical compositions had a significant effect on the oil exchange kinetics is to synthesize emulsion systems with the same concentration of stabilizing surfactants but with different starting ratios of hydrogenated/deuterated alkane oils.

Based on the observation that the oil exchange process in hexadecane emulsion systems is one of direct contact, the results obtained from the Arrhenius equation can be explained as follows. The values of the pre-exponential factor and activation energy are both higher in emulsion systems containing surfactants. The activation energy represents the amount of energy required to overcome the transport barrier. Thus, observing larger transport energy barriers when surfactant monolayers are present is logical. On the other hand, the pre-exponential factor is correlated to the frequency of droplet collisions.

Our results suggest that stabilized emulsions had a significantly higher collision frequency which was counter intuitive since anionic surfactant stabilized emulsions carry a more negative zeta-potential when compared to the bare emulsions. However, the collision frequency is also correlated to the oil concentration and the size of the droplets that are present in the system. The bare emulsions synthesized in our experiments were significantly larger (~600 nm in diameter) than those prepared with stabilizing surfactants (~100 nm in diameter). As a result, the bare emulsion systems had significantly fewer droplets in the sample and lower diffusion coefficients that resulted in a lower collision rate. Additional experiments could be performed by synthesizing emulsions of differing size and concentration followed by systematic Arrhenius analyses. Nevertheless, the use of time-resolved SANS with contrast matching presents a unique opportunity to fundamentally understand the kinetics of mass transport between droplets in emulsion systems.

4.5 CONCLUSION

In this study, we directly examined oil exchange kinetics between emulsions using contrast variation small angle neutron scattering (CV-SANS). Parameters including the type and concentration of stabilizing agent used, the sample temperature, the solubility of the oil phase, and

the ionic strength in the emulsion system were varied to examine its effects on the oil exchange kinetics. The rate of oil exchange was estimated using a relaxation function. Oil exchange kinetic results obtained from several emulsion systems suggest that two different oil exchange mechanisms occurred within the system. For emulsion systems containing shorter alkane chains and more soluble oils, the oil exchange was dominated by the direct diffusion of oil molecules through the aqueous phase.

On the other hand, insoluble systems such as hexadecane emulsions, exchange through direct droplet contact mechanisms consisting of reversible coalescence or permeation through transient holes in the thin liquid films. The estimated relaxation function also showed that the presence of surfactants and the increase of the sample temperature would result in an accelerated oil exchange. Moreover, the estimated kinetic decay constants follow Arrhenius behavior. On the other hand, the concentration of anionic surfactant and the concentration of salt in the emulsion system had little effect on oil exchange kinetics.

Modeling of the relaxation decay functions suggest that other processes could be involved in the oil exchange, resulting in a deviation from a single exponential decay. A fast exchange between droplets dominates the initial stages of oil transport. However, the presence of a slower oil exchange process was also observed at longer time points and it is hypothesized to originate from either molecular complexation and/or from differences in transport rate between hydrogenated and deuterated hexadecane molecules (i.e. molecular interaction effects due to isotopic substitution).

Importantly, contrast variation time-resolved small angle neutron scattering (CV-SANS) is not limited to examining oil exchange rates between droplets stabilized by anionic surfactants.

It can also be extended to examine exchange rates between emulsions stabilized by other interfacial agents and under variable conditions. Moreover, time-resolved CV-SANS also provides a unique ability to examine transport induced by external fields (e.g. shear) in real time, which is not possible with other characterization techniques.

4.6 REFERENCES

(1) Hettiarachchi, K.; Zhang, S.; Feingold, S.; Lee, A. P.; Dayton, P. A. *Biotechnol. Prog.* **2009**, *25* (4), 938–945.

(2) Thickett, S. C.; Gilbert, R. G. *Polymer* **2007**, *48* (24), 6965–6991.

(3) Mao, L.; Roos, Y. H.; Biliaderis, C. G.; Miao, S. *Crit. Rev. Food Sci. Nutr.* **2017**, *57* (15), 3173–3187.

(4) Dan, N. *J. Food Eng.* **2016**, *175*, 136–144.

(5) Antonietti, M. *Prog. Polym. Sci.* **2002**, *27* (4), 689–757.

(6) Chern, C. S. *Prog. Polym. Sci.* **2006**, *31* (5), 443–486.

(7) Teo, B. M.; Prescott, S. W.; Ashokkumar, M.; Grieser, F. *Ultrason. Sonochem.* **2008**, *15* (1), 89–94.

(8) Peña, A. A.; Miller, C. A. *Adv. Colloid Interface Sci.* **2006**, *123–126* (SPEC. ISS.), 241–257.

(9) Kabalnov, A. .; Makarov, K. .; Pertzov, A. .; Shchukin, E. . *J. Colloid Interface Sci.* **1990**, *138* (1), 98–104.

(10) Weiss, J.; Canceliere, C.; McClements, D. J. *Langmuir* **2000**, *16* (17), 6833–6838.

(11) Weiss, J.; Herrmann, N.; McClements, D. J. *Langmuir* **1999**, *15* (20), 6652–6657.

(12) Hoang, T. K. N.; La, V. B.; Deriemaeker, L.; Finsy, R. *Phys. Chem. Chem. Phys.* **2004**, *6* (7), 1413–1422.

(13) Leal-Calderon, F.; Poulin, P. *Curr. Opin. Colloid Interface Sci.* **1999**, *4* (3), 223–230.

(14) Schmitt, V.; Cattelet, C.; Leal-Calderon, F. *Langmuir* **2004**, *20* (1), 46–52.

(15) Binks, B. P.; Clint, J. H.; Fletcher, P. D. I.; Rippon, S.; Lubetkin, S. D.; Mulqueen, P. J. *Langmuir* **1998**, *14* (19), 5402–5411.

(16) Voorhees, P. W. *J. Stat. Phys.* **1985**, *38* (1–2), 231–252.

(17) Taylor, P. *Adv. Colloid Interface Sci.* **1998**, *75* (2), 107–163.

(18) McClements, D. J.; Dungan, S. R.; German, J. B.; Kinsella, J. E. *Top. Catal.* **1992**, *6* (5), 415–422.

(19) Weiss, J.; McClements, D. J. *Langmuir* **2000**, *16* (14), 5879–5883.

(20) Malassagne-Bulgarelli, N.; McGrath, K. M. *Soft Matter* **2009**, *5* (23), 4804.

(21) Taisne, L.; Walstra, P.; Cabane, B. *J. Colloid Interface Sci.* **1996**, *184* (2), 378–390.

(22) Roger, K.; Olsson, U.; Schweins, R.; Cabane, B. *Angew. Chemie Int. Ed.* **2015**, *54* (5), 1452–1455.

(23) McClements, D. J.; Dungan, S. R. *J. Phys. Chem.* **1993**, *97* (28), 7304–7308.

(24) Drelich, A.; Grossiord, J. L.; Gomez, F.; Clausse, D.; Pezron, I. *J. Colloid Interface Sci.* **2012**, *386* (1), 218–227.

(25) McClements, D. J.; Dungan, S. R.; German, J. B.; Kinsella, J. E. *Colloids Surfaces A Physicochem. Eng. Asp.* **1993**, *81* (C), 203–210.

(26) Gerelli, Y.; Porcar, L.; Lombardi, L.; Fragneto, G. *Langmuir* **2013**, *29* (41), 12762–12769.

(27) Wah, B.; Breidigan, J. M.; Adams, J.; Horbal, P.; Garg, S.; Porcar, L.; Perez-Salas, U. *Langmuir* **2017**, *33* (14), 3384–3394.

(28) Nakano, M.; Fukuda, M.; Kudo, T.; Endo, H.; Handa, T. *Phys. Rev. Lett.* **2007**, *98* (23), 30–33.

(29) Nakano, M.; Fukuda, M.; Kudo, T.; Matsuzaki, N.; Azuma, T.; Sekine, K.; Endo, H.; Handa, T. *J. Phys. Chem. B* **2009**, *113* (19), 6745–6748.

(30) Lund, R.; Willner, L.; Richter, D. In *Advances in Polymer Science*; 2013; pp 51–158.

(31) Nguyen, M. H. L.; DiPasquale, M.; Rickeard, B. W.; Stanley, C. B.; Kelley, E. G.;

Marquardt, D. *Biophys. J.* **2019**, *116* (5), 755–759.

(32) Zinn, T.; Willner, L.; Lund, R.; Pipich, V.; Richter, D. *Soft Matter* **2012**, *8* (3), 623–626.

(33) Lund, R.; Willner, L.; Richter, D.; Dormidontova, E. E. *Macromolecules* **2006**, *39* (13), 4566–4575.

(34) Choi, S. H.; Lodge, T. P.; Bates, F. S. *Phys. Rev. Lett.* **2010**, *104* (4), 1–4.

(35) Lu, J.; Choi, S.; Bates, F. S.; Lodge, T. P. *ACS Macro Lett.* **2012**, *1* (8), 982–985.

(36) Lund, R.; Willner, L.; Pipich, V.; Grillo, I.; Lindner, P.; Colmenero, J.; Richter, D. *Macromolecules* **2011**, *44* (15), 6145–6154.

(37) Zinn, T.; Willner, L.; Pipich, V.; Richter, D.; Lund, R. *ACS Macro Lett.* **2016**, *5* (7), 884–888.

(38) Kline, S. R. *J. Appl. Crystallogr.* **2006**, *39* (6), 895–900.

(39) Moroi, Y.; Motomura, K.; Matuura, R. *J. Colloid Interface Sci.* **1974**, *46* (1), 111–117.

(40) Chang, H.-C.; Lin, Y.-Y.; Chern, C.-S.; Lin, S.-Y. *Langmuir* **1998**, *14* (23), 6632–6638.

(41) Kabalnov, A. S. *Langmuir* **1994**, *10* (3), 680–684.

(42) Ivanov, I. B.; Kralchevsky, P. A. *Colloids Surfaces A Physicochem. Eng. Asp.* **1997**, *128* (1–3), 155–175.

(43) Zapryanov, Z.; Malhotra, A. K.; Aderangi, N.; Wasan, D. T. *Int. J. Multiph. Flow* **1983**, *9* (2), 105–129.

(44) Valkovska, D. S.; Ivanov, I. B. *J. Colloid Interface Sci.* **1999**, *211* (2), 291–303.

(45) Holt, Ø.; S¨ther, Ø.; Sjo¨blom, J.; Dukhin, S. S.; Mishchuk, N. A. *Colloids Surfaces A Physicochem. Eng. Asp.* **1997**, *123–124*, 195–207.

(46) Poulin, P.; Nallet, F.; Cabane, B.; Bibette, J. *Phys. Rev. Lett.* **1996**, *77* (15), 3248–3251.

(47) Bibette, J.; Mason, T. G.; Gang, H.; Weitz, D. A.; Poulin, P. *Langmuir* **1993**, *9* (12),

3352–3356.

(48) Destribats, M.; Rouvet, M.; Gehin-Delval, C.; Schmitt, C.; Binks, B. P. *Soft Matter* **2014**, *10* (36), 6941–6954.

(49) Aronson, M. P.; Princen, H. M. *Nature* **1980**, *286* (5771), 370–372.

(50) Malassagne-Bulgarelli, N.; McGrath, K. M. *Soft Matter* **2013**, *9* (1), 48–59.

(51) Taisne, L.; Cabane, B. *Langmuir* **1998**, *14* (17), 4744–4752.

(52) Aveyard, R.; Clint, J. H. *Curr. Opin. Colloid Interface Sci.* **1996**, *1* (6), 764–770.

(53) Fletcher, P. D. I.; Howe, A. M.; Robinson, B. H. *J. Chem. Soc. Faraday Trans. 1 Phys. Chem. Condens. Phases* **1987**, *83* (4), 985–1006.

(54) Fletcher, P. D. I.; Horsup, D. I. *J. Chem. Soc. Faraday Trans.* **1992**, *88* (6), 855–864.

(55) Clark, S.; Fletcher, P. D. I.; Ye, X. *Langmuir* **1990**, *6* (7), 1301–1309.

(56) Christov, N. C.; Danov, K. D.; Zeng, Y.; Kralchevsky, P. A.; von Klitzing, R. *Langmuir* **2010**, *26* (2), 915–923.

(57) Petsev, D. N.; Denkov, N. D.; Kralchevsky, P. A. *J. Colloid Interface Sci.* **1995**, *176* (1), 201–213.

(58) Lucassen-Reynders, E. H.; Cagna, A.; Lucassen, J. *Colloids Surfaces A Physicochem. Eng. Asp.* **2001**, *186* (1–2), 63–72.

(59) Mondain-Monval, O.; Leal-Calderon, F.; Phillip, J.; Bibette, J. *Phys. Rev. Lett.* **1995**, *75* (18), 3364–3367.

(60) Marinova, K. G.; Gurkov, T. D.; Dimitrova, T. D.; Alargova, R. G.; Smith, D. *Langmuir* **1998**, *14* (8), 2011–2019.

(61) Ahn, J.-H.; Kim, H.-S.; Lee, K. J.; Jeon, S.; Kang, S. J.; Sun, Y.; Nuzzo, R. G.; Rogers, J. A. *Science* **2006**, *314* (5806), 1754–1757.

Chapter 5. KINETIC ANALYSIS OF ULTRASOUND INDUCED OIL EXCHANGE IN OIL-IN-WATER EMULSIONS THROUGH CONTRAST VARIATION TIME-RESOLVED SANS

Ultrasound is one of the most commonly used methods for synthesizing and processing emulsion systems. In this study, the kinetics of acoustically induced emulsion oil exchange was examined using contrast variation time-resolved small angle neutron scattering (CV-SANS). A custom-built sample environment was used to deliver acoustic forces while simultaneously performing CV-SANS experiments. It was observed that the oil exchange rate was significantly accelerated when sonicating at high acoustic pressures, where violent cavitation events can induce droplet coalescence and breakup. No significant oil exchange occurred at acoustic pressures below the cavitation threshold.

It was also observed that the oil exchange kinetics was deterred when emulsions were stabilized by surfactants. In addition, oil exchange rates varied non-linearly with the concentration of surfactants present and exchange was slowest when the emulsions were stabilized by an intermediate concentration of surfactant. It is hypothesized that emulsion size, electrostatic repulsion and Gibbs elasticity of the oil-water interface play significant roles in the observed trends. The observed trends in oil exchange rates versus surfactant concentration coincides well with theoretical models for the fluctuation of the elasticity of the interface. Acoustically induced oil exchange was most inefficient when the interfacial elasticity was at its maximum value.

5.1 INTRODUCTION

Immiscible liquids, such as oil and water, can be mixed to form metastable dispersions or emulsions for use in numerous applications. The dynamics of the emulsion system is significantly affected by the conditions of its environment. For example, the type and concentration of stabilizing agents that are present in the system, the temperature and the ionic strength can affect droplet stability through Ostwald ripening and/or by inducing coalescence over time.[1–6] Even if an emulsion system is apparently stable over an extended period of time, mass transport of oil between droplets can still occur.[7–12] Understanding the dynamics of transport in emulsion systems is, therefore, critical to designing improved droplet-based systems, processes and applications.[13–17] One example relates to the use of droplets as microreactors for synthesizing high molecular weight polymers (i.e. emulsion polymerization), where transport of radical initiators dictates the rate of polymerization, the molecular weight of the synthesized polymers, and the synthesis yield.[13,17–20] Another example is the use of droplets as drug carriers, where an improved understanding in the transport of the water insoluble drugs could help better predict the bioavailability at a desired location and its corresponding pharmacokinetics.[21–23]

In the past, researchers have taken advantage of compositional variations in properties to fundamentally examine oil exchange kinetics between droplets in emulsions.[8,9,11,12,24] For example, researchers have used differential scanning calorimetry (DSC) to examine oil exchange processes between oil droplets that have different melting points.[11,12,24,25] Most of these studies examined emulsion systems stabilized by non-ionic surfactants and found that the main mechanism for inducing oil exchange between the droplets was related to excess surfactant micelles that were present in the dispersion. Other examples of using compositional differences to characterize oil exchange include the use of hydrophobic fluorescent dyes, chemical quenching of fluorescent

compounds, and turbidity measurements for emulsion systems containing droplets with different refractive indices.[8,9,26,26–30]

Contrast variation time-resolved small angle neutron scattering (CV-SANS) has also been used as an alternative technique to examine mass transport in colloidal systems including the exchange of oil molecules in emulsion systems, unimer exchange in block-copolymer micelles, and lipid exchange between/within vesicles.[31–36] The main advantage for using this method relates to its ability to examine transport between nearly identical chemical compositions due to the vast differences in scattering length densities (SLD) between the hydrogenated versus deuterated versions of molecular isotopes. An example of CV-SANS used to examine oil exchange processes was recently reported by Roger *et al.,* where they examined oil transport between non-ionic surfactant stabilized hexadecane droplets.[31] In their study, both Ostwald ripening and emulsion coalescence were hindered, and no excess surfactant micelles were present. The hydrophobic and hydrophilic properties of polyoxyethylene alkyl ether surfactants used to stabilize the emulsions were also varied, and the author examined the growth rate of the droplet size over time and compared it to the oil exchange rates. It was observed that oil molecules exchanged efficiently between the droplets well before any measurable change in droplet size was apparent. This suggested that droplet contact ripening was the main mechanism for the observed exchange.

This work aims to further demonstrate the use CV-SANS to examine variations in oil exchange rates in emulsion systems under the influence of externally applied acoustic forces. We focus on ultrasound because sonication is frequently applied to synthesize and process emulsion systems. Moreover, acoustic forces have also been shown to be able to enhance mass and heat transfer in various systems.[37–41] For example, in ultrasound enhanced emulsion polymerization and in sonochemistry, the application of acoustic forces to emulsion systems was shown to improve

the transport of chemical species (e.g. radicals or ions) to accelerate reaction processes and/or to produce a higher product yields.[42–44]

In this report, we examine ultrasound induced oil exchange in model systems consisting of hexadecane-in-water emulsions. Experiments presented here are performed using a custom-built ultrasound sample environment that allows for direct probing of oil exchange kinetics in well-characterized and controlled acoustic fields with simultaneous collection of time-resolved SANS data (Figure 5.1 (a)).[45,46] In short, two emulsion stocks with the same contrast to the solvent were individually synthesized and mixed together right before initiating CV-SANS data collection (Figure 5.1 (b)). Any oil exchange between droplets would result in a decrease in the overall contrast within the emulsion system and thus minimal contrast would be observed when emulsions fully exchange their oil. By varying the applied acoustic pressure and the concentration of surfactants stabilizing the emulsion interface, we can have a better fundamental understanding of how oil exchanges under the influence of acoustic forces.

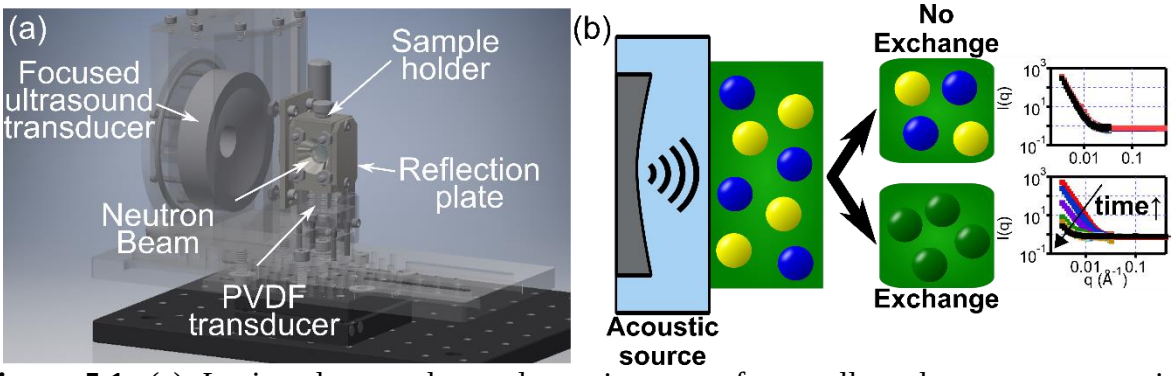

Figure 5.1. (a) *In-situ* ultrasound sample environment for small angle neutron scattering experiments. (b) Schematic diagram of ultrasound induced oil exchange where oil molecules exchanging between droplets would result in a decrease in the detected scattering intensity.

5.2 MATERIALS AND METHODS

Hexadecane (>99%, CAS: 544-76-3) and sodium dodecyl sulfate (SDS, CAS: 151-21-3) were purchased from Sigma-Aldrich (St. Louis, MO, USA). Deuterated hexadecane (D34, 99%, CAS: 15716-08-2), deuterated sodium dodecyl sulfate (98%), and deuterium oxide (99.9%, CAS: 7789-20-0) were purchased from Cambridge Isotope Laboratories, Inc. (Tewksbury, MA, USA). Contrast variation emulsion systems were designed to account for the sample transmission due to the use of long pathlength sample holders in the ultrasound sample environment (1 cm). In short, two stock emulsions, one fully deuterated (high SLD, oil density = 0.88 g/mL and SLD = 6.66 $x10^{-6}$ $Å^{-2}$) and one partially deuterated (low SLD, 60 vol% hydrogenated and 40 vol% deuterated, density = 0.85 g/mL and SLD = 2.41 $x10^{-6}$ $Å^{-2}$) with equal contrast to the solvent were synthesized identically by sonicating 1 volume percent of oil in the solvent with the presence of desired concentration of SDS (e.g. 0.1 mM) using a Branson Digital Sonifier S-450 with a 3 mm sonicating microtip (Branson Ultrasonics, CT, USA) at 30% amplitude 50% duty cycle (1 seconds on and 1 seconds off) for a total of 30 minutes. The SDS used in this study was contrast matched to the solvent, which contained 26.5 vol% hydrogenated water and 73.5 vol% deuterated water. The two stock emulsions containing the same concentration of surfactants were then mixed at a 1:1 volume ratio right before starting CV-SANS data collection. The mixture was quickly loaded into a 2 mm pathlength standard NIST sample cell with quartz windows, 4 mm pathlength standard NIST sample cell (i.e. for experiments at rest), or into an *in-situ* ultrasound sample environment sample holder to monitor the oil exchange kinetics (i.e. for samples under sonication).

5.2.1 *Small Angle Neutron Scattering (SANS)*

The majority of the small angle neutron scattering experiments were performed at the National Institute of Standards and Technology Center for Neutron Research (NCNR) using the NGB 30m SANS instrument. Three detector distances were used during the experiment to acquire scattering intensities spanning a q-range from 0.0034 to 0.47 $Å^{-1}$ for samples before/after the sonication process and for the initial time point (t=0) of samples at rest (without the application of acoustic forces). On the other hand, only the 13m detector was used for scattering data collection (i.e. lowest q range) during most of the oil exchange process. Since the collection of SANS data over the whole q range requires moving the detectors during the scan, which would result in extra downtime, we decided to collect the bulk of the data at the lowest-q configuration where the largest changes in intensity were being observed. For samples that exchanged rapidly (i.e. sonicated samples), the downtime involved in moving the detectors would ultimately result in an inability to characterize initial rates of oil exchange.

Portions of the experiments were repeated and also performed at the National Institute of Standards and Technology Center for Neutron Research (NCNR) using the new 45-meter-long very small angle neutron scattering (VSANS) instrument. The main advantage of the VSANS instrument is its ability to obtain the scattering intensities over the whole q range simultaneously without having downtime due to moving the detectors. Two detectors were used simultaneously when collecting scattering data to acquire scattering intensities from a q range of $1.9x10^{-3}$ to $1.7x10^{-1}$ $Å^{-1}$. Each sample was exposed to neutrons for 5 minute intervals to collect a full-range scattering profile.

The *in-situ* sonication experiments were conducted using a custom-built ultrasound environment that has been previously described.[45,46] In short, a sample holder was sandwiched

between two water baths that could each contain a focused ultrasound transducer (1.24 MHz Sonic Concepts H-102, f-number 0.98, 64 mm diameter, Sonic Concepts Inc., Bothell, WA, USA). Perpendicular to the acoustic axis is a pair of Kapton windows that allows the neutron beam to pass. Moreover, a custom made wide-bandwidth polyvinylidene fluoride (PVDF) hydrophone was also place under the sample holder to record the acoustic signal that passes through the sample holder. One additional modification made for this study was the use of a single focused ultrasound transducer coupled to a spherical metal reflector on the opposite side of the acoustic source (Figure 5.1).[45,47] The use of the spherical metal reflector was to induce constructive interference to increase the applied acoustic pressure fields in the system. In general, the ultrasound sample environment was operated at acoustic pressures ranging from 0 to 8.6 MPa with a pulse repetition frequency (PRF) at 1250 Hz, pulse duration of 50 cycles (40 μs pulse length) and a 5 percent duty cycle. Each sample was sonicated for 3-minute intervals for each SANS time-point measurement. The experiments were then stopped when no significant changes were observed in scattering profiles or after reaching one hour of total sonication time.

5.2.2 *SANS Data Analysis*

All recorded SANS data were reduced using standard NCNR Igor reduction protocols.[48] A relaxation function (equation (5.1)) was used to express the extent of oil exchanged in the emulsion system. $I(t)$ is the integrated scattering intensity within a q range of 0.003 to 0.03 $Å^{-1}$ at any given time, I_0 is the integrated scattering intensity at time 0 (i.e. intensity prior to the application of any acoustic forces), and I_∞ is the integrated scattering intensity at infinite time, which was obtained from a 'pre-mixed' control sample. Such control samples contained mixed compositions equivalent to a 1:1 mixture of deuterated and hydrogenated emulsions that were ultrasonically processed externally to ensure full mixing of the oils. All incoherent scattering and background

signals were subtracted to account for the use of different sample pathlengths during the data analysis. One main assumption made when using the relaxation function was that there was no net emulsion size change during the duration of the experiment. For samples at rest, this assumption was confirmed by tracking the scattering profiles of a control fully deuterated hexadecane emulsion sample to measure the emulsion size change over time. Relaxation functions were then estimated accounting for the emulsion size change and also under the assumption of no size change. The differences between the two estimated relaxation decay curves were minimal. As for emulsions that were sonicated, the assumption that the emulsion size did not change over time was confirmed using dynamic light scattering (DLS) measurements. Further discussion and supporting data is provided in the result and in the supplemental information chapter (Chapter 7).

$$R(t) = \left(\frac{I(t) - I_\infty}{I_0 - I_\infty}\right)^{1/2} \tag{5.1}$$

Oil exchange kinetic parameters were estimated from fits to the relaxation functions using a single exponential decay with a plateau (equation (5.2)), where k is the decay constant, t is time, c is the equilibrium plateau.

$$R(t) = (1 - c)e^{-kt} + c \tag{5.2}$$

5.2.3 *Emulsion Size Measurement*

The emulsion size distribution was obtained either using DLS or, when possible, by fitting the recorded scattering data with a simple sphere model. Unfortunately, the distribution of the largest emulsions could not be estimated using the collected SANS scattering profiles due to the limited q range in the data. Thus, for consistency, all emulsion sizes reported in this study correspond to the hydrodynamic diameters that are estimated from DLS.

5.3 RESULTS

Oil exchange between hexadecane oil droplets without the presence of any stabilizing surfactant was first examined. Example scattering profiles of emulsion systems exchanging spontaneously at rest as well as during sonication at low/high acoustic pressures are shown in Figure 5.2. Based on the scattering profiles in Figure 5.2 (a), it can be observed that the scattering intensities decrease over time, even without the application of acoustic forces or the presence of any stabilizing surfactants. This indicates that oil molecules can indeed exchange between the oil droplets spontaneously, but at a relatively slow pace taking many hours. On the other hand, the scattering intensities decreased over a matter of minutes when the sample was sonicated at high acoustic pressures, indicating an accelerated oil exchange process. Interestingly, CV-SANS results also showed that not all sonicated samples exchanged oil molecules efficiently. Emulsion samples sonicated at low acoustic pressures showed minimal scattering changes when compared to samples exposed to higher acoustic pressures over the same time period.

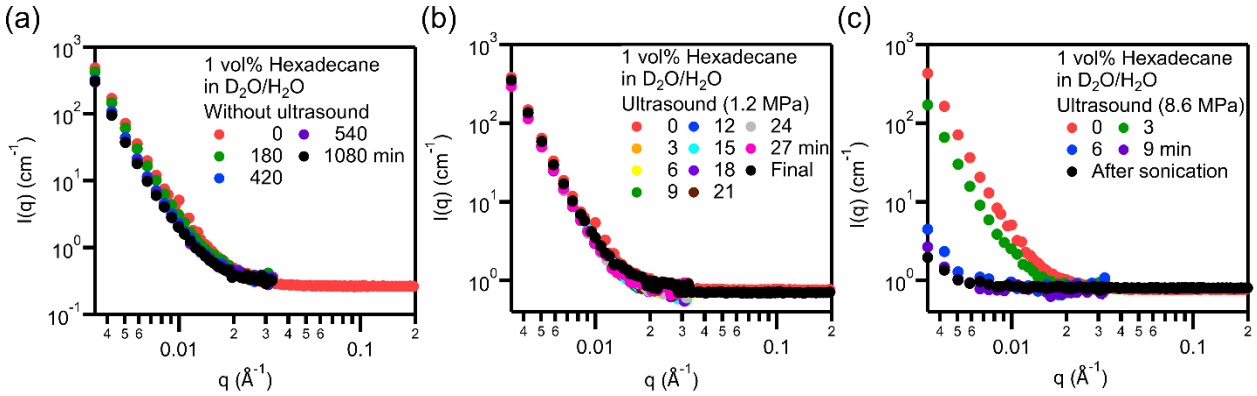

Figure 5.2. Oil exchange between bare hexadecane droplets (a) at rest (i.e. no ultrasound), (b) with application of acoustic forces at low acoustic pressures (1.2 MPa), and (c) with high acoustic pressures (8.6 MPa). The application of high acoustic pressures significantly accelerated the oil exchange process.

Based on results shown in Figure 5.2, it is clear that the applied acoustic pressure or intensity has a direct effect on oil exchange kinetics. Acoustic radiation forces and/or acoustic

cavitation events could both contribute to the observed acceleration of oil exchange kinetics. If oil exchange was primarily driven by acoustic radiation forces, by accelerating mixing and droplet advection, one would expect kinetics to scale proportionally to the applied acoustic pressures. Sonicating the sample at higher acoustic pressures would induce stronger acoustic radiation forces and the observed oil exchange would be more efficient. On the other hand, if the main driving force is based on cavitation, oil exchange kinetics would only accelerate when samples are sonicated at acoustic pressures higher than the cavitation threshold of the sample. The cavitation threshold is defined here, as well as in previous works, as the acoustic pressures necessary to achieve a 50% probability that an acoustic pulse would result in at least one cavitation event in the sample. This can be measured by acoustically monitoring cavitation events in our ultrasound sample environment with an integrated PVDF acoustic hydrophone.[45]

Bare hexadecane emulsion mixtures (i.e. in the absence of any surfactant stabilizer) were also sonicated at various acoustic pressures to explore the role of acoustic intensity on the oil exchange process. All of the CV-SANS profiles were transformed into a relaxation function (Figure 5.3 (a)) using equation (5.1). The recorded CV-SANS profiles of the samples sonicated at various acoustic pressures are also provided in the supplemental information chapter (Chapter 7) for completeness. Based on these results, it can be observed that the relaxation function decays minimally over time when the samples are sonicated at low acoustic pressures. This observation indicates that the acoustic forces provided under these conditions do not induce significant oil exchange between droplets. Increasing the applied acoustic pressure to 6.0 MPa resulted in only a minor decrease in the relaxation function over time. The only sample that showed significant oil exchange, in a manner of minutes, was the sample sonicated at the highest applied acoustic pressure of 8.6 MPa. Since the oil exchange kinetics did not scale linearly with the applied acoustic

pressure, it suggests that the acoustic radiation forces provided by the acoustic transducer were not the main driving force to the observed oil exchange.

Recorded scattering acoustic signals from the PVDF hydrophone were then examined and analyzed to determine if acoustic cavitation events were the main contributor to the observed relaxation function decay. Details on the cavitation analysis method were previously published and are also provided in Chapter 2.[47] The estimated cavitation probability curve is shown in Figure 5.3 (b).[47,49] Emulsion samples were also sonicated at additional acoustic pressures outside of the beam to obtain a more detailed cavitation probability curve and a more accurate cavitation threshold estimation. The estimated cavitation threshold for hexadecane in water emulsions is about 6.2 MPa and the oil exchange kinetics does indeed accelerate significantly when sonicated above this threshold. Results from the pressure scan experiment demonstrate that the observed acceleration in oil exchange kinetics is indeed due to acoustic cavitation and not due to acoustic radiation forces.

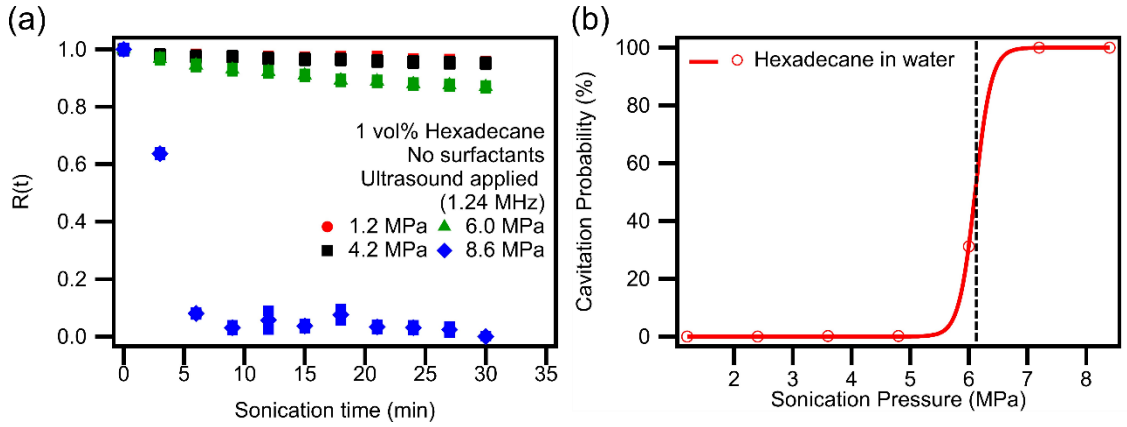

Figure 5.3. (a) Relaxation functions for bare hexadecane emulsions sonicated at various incident acoustic pressures. (b) Cavitation probability curves estimated from recorded acoustic signals from PVDF hydrophone during the sonication process.

After determining that acoustic cavitation is essential to inducing oil exchange between oil droplets, we then turn to examine how the presence of stabilizing surfactants at emulsion interfaces affects the kinetics of oil exchange during ultrasound application. As mentioned in material and methods, all emulsion stock solutions were synthesized by sonicating oil in water with the presence of a desired concentration of surfactant ranging from 0 to 20 mM SDS. Moreover, emulsion stocks were sonicated for an extended period of time (30 minutes) to ensure that samples reached an equilibrium droplet size distribution. Therefore, any further ultrasound application to emulsions during the CV-SANS measurement would not affect the droplet size distribution any further. Without this, it would be difficult to unambiguously determine if an observed decrease in scattering intensity during CV-SANS sonication was due to a change in emulsion size or to oil molecules exchanging between droplets (i.e. decrease in contrast). The size distributions of the different emulsion stocks were measured after the preparation process, before mixing deuterated and hydrogenated stocks, and are shown as box plots in Figure 5.4 (a). As a further check on the possibility of inducing size changes during the CV-SANS experiment, scattering profiles were also collected for a fully deuterated hexadecane emulsion control sample in the in-situ ultrasound environment as shown in Figure 5.4 (b). The lack of variation in intensity demonstrates that the rapid decrease that is measured with CV-SANS is due primarily to oil exchange and not to size variations. Additional examples of DLS experiments for measuring emulsion size distributions with increasing sonication time are provided in the supplemental information chapter (Chapter 7).

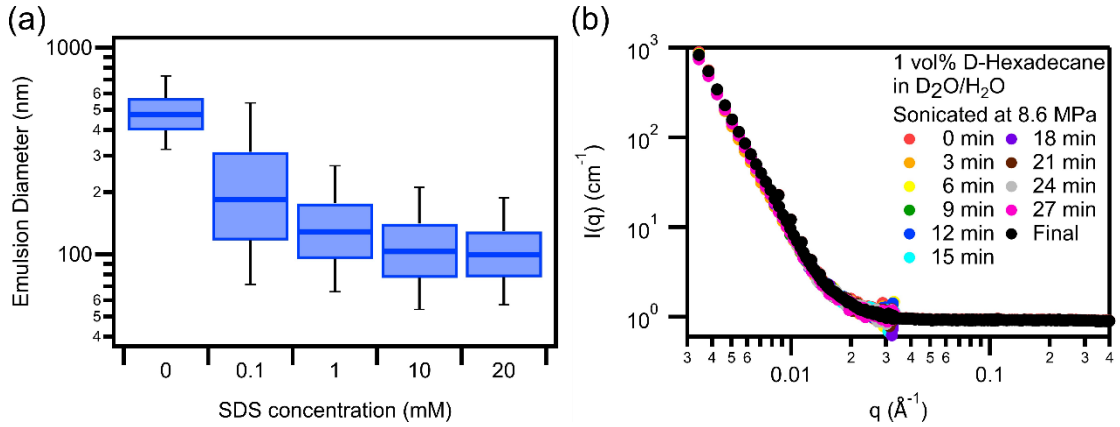

Figure 5.4. (a) Box plots of size distributions for emulsion systems synthesized using a sonication horn for 30 minutes with variable SDS concentrations. The box portion of the plot, from bottom to top, represents the 25th percentile, median, and 75th percentile of the distribution. The whisker portion represents the 5% percentile and 95% percentile. (b) CV-SANS profile during sonication of a fully deuterated hexadecane emulsion sample showing no variations due to size changes over time.

Example CV-SANS profiles corresponding to sonicating an emulsion sample containing 10 mM of SDS at high acoustic pressures is shown in Figure 5.5 (a). As can be seen in the figure, the scattering intensities decayed significantly slower than those of bare emulsions samples (i.e. no surfactant). Slower oil exchange kinetics were also observed in all emulsion samples containing surfactants and the corresponding relaxation decay curves with model fits to equation (5.2) are shown in Figure 5.5 (b). The relaxation decay rate varied non-linearly with the concentration of surfactant that was present. For example, the rate of relaxation function decay (*k* parameter) first slows down with increasing SDS concentrations (0 to 1 mM SDS). However, further increasing the SDS concentration from 1 to 20 mM resulted in slightly faster decay rates compared to the emulsion system stabilized by 1 mM of SDS.

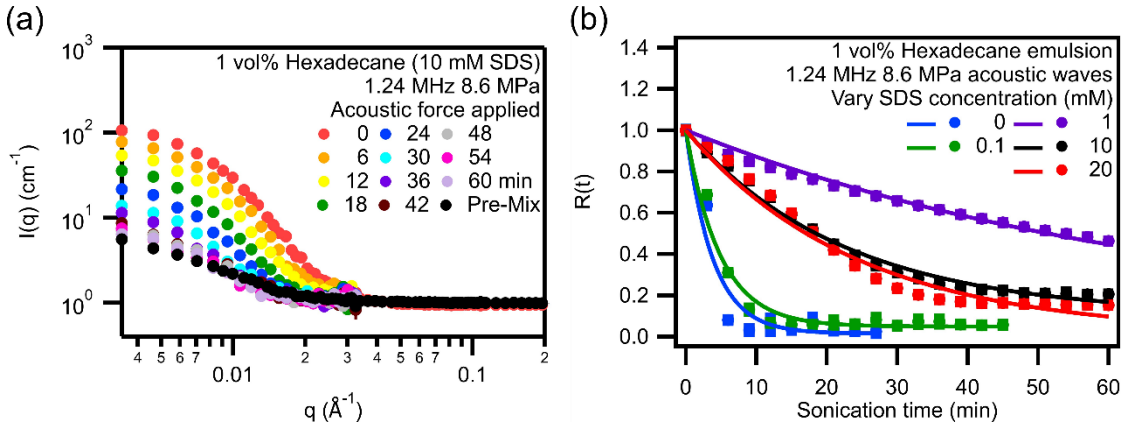

Figure 5.5. (a) CV-SANS profiles of ultrasound induced oil exchange between hexadecane droplets stabilized by 10 mM SDS. (b) Relaxation decay curves with modeled fits (equation (5.2)) for emulsion systems containing various concentration of SDS and sonicated using the in-situ ultrasound environment.

A CV-SANS profile collected for an emulsion system containing 1 mM of SDS that was allowed to exchange oil molecules at rest, without the application of ultrasound, is also shown in Figure 5.6 (a). Clearly, the presence of stabilizing surfactant resulted in a faster decay rate when no ultrasound was applied, which is opposite to results observed when acoustic fields are used to induce oil exchange. This observation also holds true for emulsion systems stabilized at other concentrations of SDS as shown in Figure 5.6 (b). A portion of the data (e.g. 5 and 10 mM SDS) was collected at a separate very small angle neutron scattering (VSANS) experiment. The results obtained from two different instruments are almost identical, showing the robustness of the experimental design. All of the relaxation curves showed that the presence of surfactants resulted in a faster oil exchange kinetics when the emulsion systems were exchanging spontaneously and without the influence of acoustic forces.

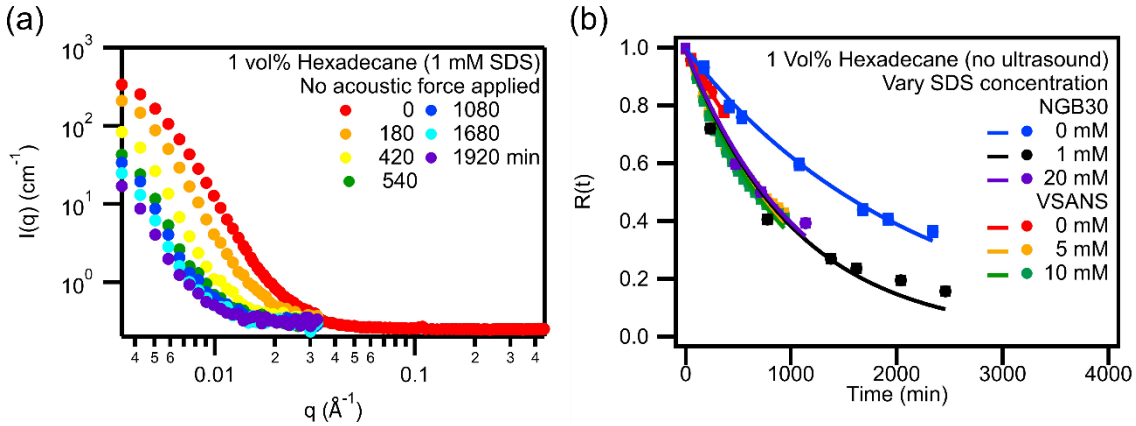

Figure 5.6. (a) CV-SANS profiles of oil exchange between hexadecane droplets stabilized by 1 mM SDS without the presence of any acoustic forces. (b) Relaxation decay curves of emulsion systems stabilized by various concentrations of SDS and the corresponding fits to equation (5.2).

The relaxation decay curves of the different emulsion systems were also fit to a single exponential decay with an equilibrium plateau model. For emulsion systems at rest (i.e. no ultrasound), the plateau was kept at 0 because these systems were still at the initial oil exchange stages and decayed similarly to a simple single exponential decay. Allowing the plateau to vary would result in obtaining an estimated exchange rate that is extremely slow and an overestimated plateau value that is high (e.g. 0.3). The estimated kinetic decay constants are shown in Figure 5.7. As can be seen in Figure 5.7, the oil exchange kinetics with and without the application of acoustic forces are on a completely different time scale and the effect of stabilizing surfactants is completely opposite. Furthermore, the estimated equilibrium plateau value is very small but it is present in all of the samples that were analyzed.

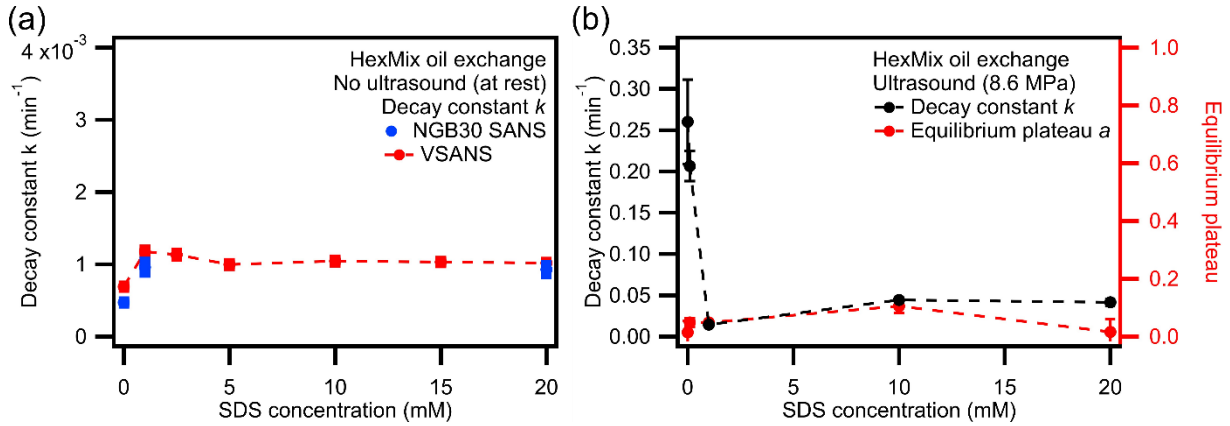

Figure 5.7.. Estimated decay constants, k, and equilibrium plateau, a, for emulsion oil exchange (a) at rest without the presence of acoustic forces and (b) sonicated at high acoustic pressure (8.6 MPa).

5.4 DISCUSSION

Based on the presented CV-SANS data, it is clear that the application of acoustic forces significantly affects how oil molecules exchange in emulsion systems. Although oil molecules can also exchange between oil droplets spontaneously and without the presence of any stabilizing surfactants, the process is extremely slow and takes on the order of hours for hexadecane due to its poor solubility in water. On the other hand, the oil exchange process was accelerated significantly when acoustic forces induced cavitation events, allowing the system to reach equilibrium within just a few minutes of sonication. In acoustics research, cavitation events are defined by the formation and abrupt collapse of vapor cavities that occur when high acoustic pressures are applied to samples. The abrupt collapse of these unstable cavities generates a powerful shock wave that can provide significant mechanical forces to the surrounding system. These forces can cause droplets to collide and coalesce with each other leading to rapid mixing of oil molecules. However, the same shear forces that are caused by local cavitation events can also induce instabilities in larger droplets causing them to rupture and break into smaller units. Since there are two different liquids in an emulsion system, the source of cavitation could come from

either the continuous (i.e. water) phase or dispersed phases (i.e. oil). In this case, however, the low volume fraction of oil and the high boiling point of hexadecane (286.8 $^{\circ}$C) make it likely that cavitation originates in the continuous water phase. In other emulsion systems, the dispersed phase may be more likely to cavitate and this could affect the kinetics of transport. A schematic depiction of ultrasound-induced oil exchange due to droplet coalescence/breakup is shown in Figure 5.8.

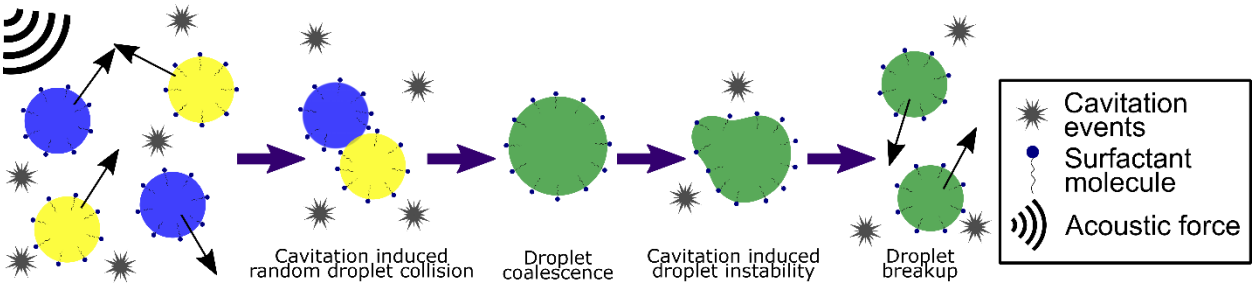

Figure 5.8.. Proposed mechanism for acoustic force induced oil exchange. Cavitation events occurring in the system induce random droplet collision/coalescence, causing rapid exchange of oil molecules between droplets. Cavitation evens can also break larger droplets down to smaller equilibrium sizes so that there is no net deviation in size distribution.

The properties of the oil-water interface are also significantly altered when surfactants are present. Interestingly, this significantly affected the rate of oil molecule exchange between droplets. When emulsions were allowed to exchange spontaneously at rest, it was observed that the presence of SDS in emulsion systems would actually enhance, though only moderately, the oil exchange process. However, after some minimum amount of surfactant was present in the system, the exchange kinetics was no longer significantly affected by further increasing the concentration of surfactant (Figure 5.7 (a)). For systems without applied ultrasound, it is hypothesized that oil exchange occurs via a combination of oil molecule diffusion through the continuous phase as well as random collisions induced by Brownian motion. Collisions in emulsions, even if they do not result in coalescence, can still induce oil exchange via direct emulsion contact through reversible

coalescence and/or permeation through thin liquid films when the droplets are close to each other.[8,9,31,50]

On the other hand, results obtained from identical samples under ultrasound showed insonation, surprisingly, a completely opposite trend. Here, oil exchange kinetics were strongly affected by the concentration of stabilizing surfactant (Figure 5.7 (b)). As mentioned previously, the primary mechanism for inducing oil exchange in sonicated emulsion systems is via droplet coalescence and breakup. Therefore, the average size of droplets could also play a significant role on oil exchange kinetics since this affects the total number concentration of droplets and the hydrodynamic forces that the droplets experience due to cavitation. Also larger oil droplets would be able to exchange more oil molecules after a single collision event and cause a faster decrease in contrast. However, since all of the emulsion samples were synthesized using the same oil volume fraction, there would also be a larger number concentration of oil droplets in smaller sized emulsion systems than in larger ones. Thus, the droplet collision frequency is also affected by the number of droplets present and one could also anticipate larger emulsion systems would experience a lower collision frequency. Therefore, the observed effect is not trivially predicted and quantitative models accounting for analyses of droplet population changes would need to be applied to properly compare collision frequency and rates of contrast decay.

Moreover, the addition of surfactant also affects the colloidal interactions that droplets experience in dispersion and this can further affect the collision efficiency in both static (i.e. rest) and in acoustic field CV-SANS experiments. The electrostatic repulsion provided by anionic surfactant head groups of SDS are likely to reduce collision efficiency for droplets at higher surfactant concentrations. Therefore, despite having more droplets in the samples due to the smaller size distribution, samples prepared at higher surfactant concentrations may also have less

frequent collisions due to the effects of stronger colloidal interaction forces. The combination of effects caused by changes in droplet size and increased electrostatic repulsion results in a net decrease in the oil exchange efficiency with increasing concentration of stabilizing surfactants. However, these effects could only explain results observed in emulsion systems containing 0 to 1 mM of SDS. When even more surfactant is added (i.e. 10 and 20 mM), synthesized droplets become even smaller and electrostatic repulsion should still be high. Yet, observed oil exchange in these systems shows an increased rate when compared to emulsion samples containing 1 mM SDS. Therefore, there is another factor that is playing a significant role in oil transport.

In addition to providing electrostatic repulsion, the presence of surfactants at oil-water interfaces have been shown to allow the interface to act as an elastic membrane. This phenomenon is known as the Gibbs-Marangoni effect and it can resist distortion, dampen capillary waves and affect drainage rates of thin liquid films as two droplets move closer to each other.[51] The ability for emulsion interfaces to resist distortion due to this effect can also cause a reduction in the collision efficiency (Figure 5.9 (a)). The Gibbs elasticity makes the draining film hydrodynamically rigid and reduces the rate of collision by preventing droplets from moving closer to each other.

The origin of the Gibbs elasticity arises from the Marangoni effect that occurs at the oil-water interface. For unsaturated interfaces, draining of the thin liquid film between droplets can change the distribution of surfactant molecules at the oil-water interface due to the viscous drag of the moving fluid. This generates an interfacial tension gradient at the interface and a restoring surface force is generated to redistribute the surfactant molecules along the interface. Since this restoring force arises from an interfacial tension gradient, it is strongly affected by the concentration of surfactants that are present at the interface (Figure 5.9 (b)). Thus, increasing the

concentration of surfactant beyond an optimum value can actually result in a decrease in the interfacial tension gradient and a reduction of the Gibbs-Marangoni elasticity. Ultimately, when they have saturated interfaces, droplets lose this elasticity and this can result in increases in the collision efficiency and coalesce rates. The nearly identical decay curve for samples with 10 and 20 mM SDS, further suggest that this is a viable explanation since it is consistent with the saturation of the interface with surfactant. Theoretical estimation of the Gibbs elasticity for a thin liquid film decorated by SDS have also been investigated by Tempel *et al.*[52] In their study, the estimated Gibbs elasticity of the interface first increases then decreases with increasing surfactant concentration, with a maximum peak elasticity found around 1.2 mM of SDS. This trend is similar to our observations of variations in exchange rates, where emulsion systems with a higher predicted Gibbs-Marangoni elasticity results in the slowest oil exchange rate.

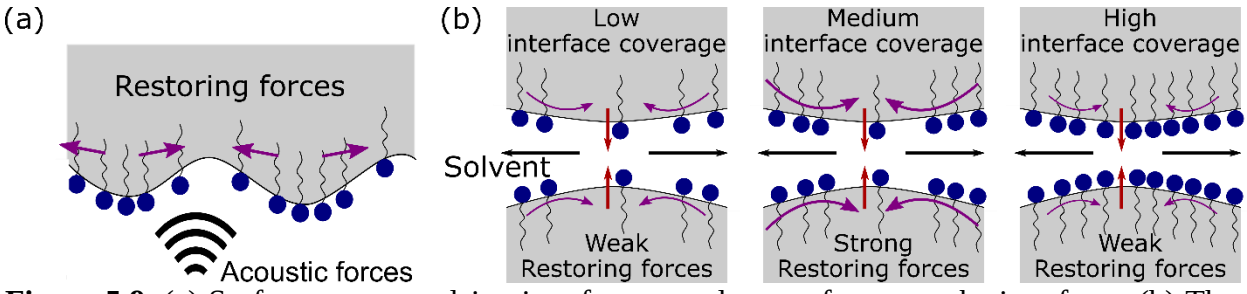

Figure 5.9. (a) Surfactants at emulsion interfaces can dampen forces on the interface. (b) The presence of surfactants also provides restoring forces that prevents the emulsions from coalescing. The Gibbs-Marangoni elasticity is affected by the amount of surfactant that is present at the interface.

When modeling oil exchange kinetics, it was observed that an exponential decay with an equilibrium plateau was required to fit the relaxation function decay. The deviation from a single exponential decay model have also been observed in several other mass transport studies. Variations of the exponential decay model have also been used for data fitting and several potential hypotheses were proposed to explain this discrepancy.[28–30,34] For our system, the deviation could

potentially be attributed to polydispersity of the droplet sizes. Other potential explanations include the possibility of the presence of a distribution of oil exchange time scales and isotope effects on the exchange rate. Additional experiments would be required to further determine the fundamental cause to this experimental observation.

5.5 CONCLUSION

In this study, contrast variation time-resolved small angle neutron scattering was used to examine the oil exchange between hexadecane in water emulsion system under the influence of acoustic forces. CV-SANS Results show that oil exchange processes could significantly accelerate from equilibrium rates that occur on the order of hours (i.e. in absence of ultrasound) to exchange rates over time scales of minutes when acoustic cavitation was induced. It was proposed that cavitation events occurring when sonicating at high acoustic pressures induce oil exchange through steady-state droplet coalescence and breakup. Moreover, it was observed that oil exchange kinetics was effectively reduced when surfactants were used to stabilize emulsions. The decay constant was found to be a non-linear a function of the stabilizing surfactant concentration. It first reduced significantly with increasing SDS concentration followed by a small increase with further increasing of the stabilizing surfactant concentration. It was proposed that the changing size of emulsions, the electrostatic repulsion, and the Gibbs-Marangoni elasticity all contribute to observed trends of oil exchange rate with concentration.

5.6 REFERENCES

(1) Ivanov, I. B.; Kralchevsky, P. A. *Colloids Surfaces A Physicochem. Eng. Asp.* **1997**, *128* (1–3), 155–175.

(2) Solans, C.; Izquierdo, P.; Nolla, J.; Azemar, N.; Garciacelma, M. *Curr. Opin. Colloid Interface Sci.* **2005**, *10* (3–4), 102–110.

(3) Weiss, J.; Herrmann, N.; McClements, D. J. *Langmuir* **1999**, *15* (20), 6652–6657.

(4) Taylor, P. *Colloids Surfaces A Physicochem. Eng. Asp.* **1995**, *99* (2–3), 175–185.

(5) Binks, B. P.; Clint, J. H.; Fletcher, P. D. I.; Rippon, S.; Lubetkin, S. D.; Mulqueen, P. J. *Langmuir* **1998**, *14* (19), 5402–5411.

(6) Nazarzadeh, E.; Anthonypillai, T.; Sajjadi, S. *J. Colloid Interface Sci.* **2013**, *397*, 154–162.

(7) Weiss, J.; McClements, D. J. *Langmuir* **2000**, *16* (14), 5879–5883.

(8) Malassagne-Bulgarelli, N.; McGrath, K. M. *Soft Matter* **2009**, *5* (23), 4804.

(9) Taisne, L.; Walstra, P.; Cabane, B. *J. Colloid Interface Sci.* **1996**, *184* (2), 378–390.

(10) Weiss, J.; Coupland, J. N.; Brathwaite, D.; McClements, D. J. *Colloids Surfaces A Physicochem. Eng. Asp.* **1997**, *121* (1), 53–60.

(11) McClements, D. J.; Dungan, S. R.; German, J. B.; Kinsella, J. E. *Top. Catal.* **1992**, *6* (5), 415–422.

(12) McClements, D. J.; Dungan, S. R.; German, J. B.; Kinsella, J. E. *Colloids Surfaces A Physicochem. Eng. Asp.* **1993**, *81* (C), 203–210.

(13) Thickett, S. C.; Gilbert, R. G. *Polymer* **2007**, *48* (24), 6965–6991.

(14) Hettiarachchi, K.; Zhang, S.; Feingold, S.; Lee, A. P.; Dayton, P. A. *Biotechnol. Prog.* **2009**, *25* (4), 938–945.

(15) Mao, L.; Roos, Y. H.; Biliaderis, C. G.; Miao, S. *Crit. Rev. Food Sci. Nutr.* **2017**, *57* (15), 3173–3187.

(16) Dan, N. *J. Food Eng.* **2016**, *175*, 136–144.

(17) Antonietti, M. *Prog. Polym. Sci.* **2002**, *27* (4), 689–757.

(18) Capek, I. *Adv. Colloid Interface Sci.* **2010**, *156* (1–2), 35–61.

(19) Jansen, T. G. T.; Lovell, P. A.; Meuldijk, J.; Van Herk, A. M. *Macromol. Symp.* **2013**, *333* (1), 24–34.

(20) Chern, C. S. *Prog. Polym. Sci.* **2006**, *31* (5), 443–486.

(21) Uno, T.; Kazui, T.; Suzuki, Y.; Hashimoto, H.; Suzuki, K.; Muhammad, B. A. M. *Lipids* **1999**, *34* (3), 249–254.

(22) Hung, C. F.; Fang, C. L.; Liao, M. H.; Fang, J. Y. *Int. J. Pharm.* **2007**, *335* (1–2), 193–202.

(23) Hauss, D. J.; Fogal, S. E.; Ficorilli, J. V; Price, C. A.; Roy, T.; Jayaraj, A. A.; Keirns, J. J. *J. Pharm. Sci.* **1998**, *87* (2), 164–169.

(24) McClements, D. J.; Dungan, S. R. *J. Phys. Chem.* **1993**, *97* (28), 7304–7308.

(25) Drelich, A.; Grossiord, J. L.; Gomez, F.; Clausse, D.; Pezron, I. *J. Colloid Interface Sci.* **2012**, *386* (1), 218–227.

(26) Fletcher, P. D. I.; Howe, A. M.; Robinson, B. H. *J. Chem. Soc. Faraday Trans. 1 Phys. Chem. Condens. Phases* **1987**, *83* (4), 985–1006.

(27) Clark, S.; Fletcher, P. D. I.; Ye, X. *Langmuir* **1990**, *6* (7), 1301–1309.

(28) Wang, Y.; Kausch, C. M.; Chun, M.; Quirk, R. P.; Mattice, W. L. *Macromolecules* **1995**, *28* (4), 904–911.

(29) Prochazka, K.; Kiserow, D.; Ramireddy, C.; Tuzar, Z.; Munk, P.; Webber, S. E.

Macromolecules **1992**, *25* (1), 454–460.

(30) Skhiri, Y.; Gruner, P.; Semin, B.; Brosseau, Q.; Pekin, D.; Mazutis, L.; Goust, V.; Kleinschmidt, F.; El Harrak, A.; Hutchison, J. B.; et al. *Soft Matter* **2012**, *8* (41), 10618.

(31) Roger, K.; Olsson, U.; Schweins, R.; Cabane, B. *Angew. Chemie Int. Ed.* **2015**, *54* (5), 1452–1455.

(32) Lund, R.; Willner, L.; Richter, D. In *Advances in Polymer Science*; 2013; pp 51–158.

(33) Lund, R.; Willner, L.; Pipich, V.; Grillo, I.; Lindner, P.; Colmenero, J.; Richter, D. *Macromolecules* **2011**, *44* (15), 6145–6154.

(34) Willner, L.; Poppe, A.; Allgaier, J.; Monkenbusch, M.; Richter, D. *Europhys. Lett.* **2001**, *55* (5), 667–673.

(35) Yang, P. W.; Lin, T. L.; Hu, Y.; Jeng, U. S. *Soft Matter* **2015**, *11* (11), 2237–2242.

(36) Nakano, M.; Fukuda, M.; Kudo, T.; Matsuzaki, N.; Azuma, T.; Sekine, K.; Endo, H.; Handa, T. *J. Phys. Chem. B* **2009**, *113* (19), 6745–6748.

(37) Gondrexon, N.; Cheze, L.; Jin, Y.; Legay, M.; Tissot, Q.; Hengl, N.; Baup, S.; Boldo, P.; Pignon, F.; Talansier, E. *Ultrason. Sonochem.* **2015**, *25* (1), 40–50.

(38) Legay, M.; Gondrexon, N.; Le Person, S.; Boldo, P.; Bontemps, A. *Int. J. Chem. Eng.* **2011**, *2011*, 1–17.

(39) Yao, Y. *Ultrason. Sonochem.* **2016**, *31*, 512–531.

(40) Del Campo, F. J.; Coles, B. A.; Marken, F.; Compton, R. G.; Cordemans, E. *Ultrason. Sonochem.* **1999**, *6* (4), 189–197.

(41) Moholkar, V. S.; Warmoeskerken, M. M. C. G. *Chem. Eng. Sci.* **2004**, *59* (2), 299–311.

(42) Bhanvase, B. A.; Sonawane, S. H. *Chem. Eng. Process. Process Intensif.* **2014**, *85*, 86–107.

(43) Teo, B. M.; Prescott, S. W.; Ashokkumar, M.; Grieser, F. *Ultrason. Sonochem.* **2008**, *15* (1), 89–94.

(44) Bhanvase, B. A.; Pinjari, D. V.; Sonawane, S. H.; Gogate, P. R.; Pandit, A. B. *Ultrason. Sonochem.* **2012**, *19* (1), 97–103.

(45) Li, D. S.; Lee, Y.-T.; Xi, Y.; Pelivanov, I.; O'Donnell, M.; Pozzo, L. D. *Soft Matter* **2018**, *14* (25), 5283–5293.

(46) Xi, Y.; Li, D. S.; Newbloom, G. M.; Tatum, W. K.; O'Donnell, M.; Luscombe, C. K.; Pozzo, L. D. *Soft Matter* **2018**, 4963–4976.

(47) Lee, Y.-T.; Li, D. S.; Ilavsky, J.; Kuzmenko, I.; Jeng, G.-S.; O'Donnell, M.; Pozzo, L. D. *J. Colloid Interface Sci.* **2019**, *536*, 281–290.

(48) Kline, S. R. *J. Appl. Crystallogr.* **2006**, *39* (6), 895–900.

(49) Fabiilli, M. L.; Haworth, K. J.; Fakhri, N. H.; Kripfgans, O. D.; Carson, P. L.; Fowlkes, J. B. *IEEE Trans. Ultrason. Ferroelectr. Freq. Control* **2009**, *56* (5), 1006–1017.

(50) Schmitt, V.; Cattelet, C.; Leal-Calderon, F. *Langmuir* **2004**, *20* (1), 46–52.

(51) Gibbs, J. W. *Trans. Connect. Acad. Arts Sci.* **1878**, *3*, 343–524.

(52) Tempel, M. van den; Lucassen, J.; Lucassen-Reynders, E. H. *J. Phys. Chem.* **1965**, *69* (6), 1798–1804.

Chapter 6. CONCLUSIONS AND OUTLOOK

6.1 KEY RESULTS

Emulsion systems are incredibly dynamic. Therefore, understanding how stabilized emulsions are synthesized as well as the kinetics of mass transport that can occur within these stabilized systems is critical when designing any new droplet-based system. In this research, we demonstrate that small angle scattering is a unique technique that can facilitate in unraveling of these phenomena in their native dispersion state. Moreover, with the combination of the use of an ultrasound sample environment, we were able to examine acoustic force induced interactions while we simultaneously characterized any structural or dynamic changes during the sonication process. These results provide some insights on the fundamental molecular scaled interactions that would be hard to characterize with other techniques.

In Chapter 3, we directly examined the role of acoustic forces in the formation of amphiphilic gold nanoparticle stabilized Pickering emulsions. Several types of perfluorocarbon and alkane oils were used as the emulsion core in this study. Ultra-small angle X-ray scattering was the primary characterization technique and we demonstrated that acoustic force induced cavitation events were required to induce the formation of Pickering emulsions when using sterically stabilized particles as stabilizers. Pickering emulsions would not form spontaneously, and no particle adsorption was observed when weak acoustic forces, where no cavitation events occurred, were applied. Moreover, we demonstrated that there would be a significant amount of oil loss when using volatile oils as the emulsion core. Furthermore, it was observed that there was also an excess amount of free un-absorbed particles in the emulsion system after the synthesis. Two potential mechanisms were proposed to describe how different cavitation sources could

induce adsorption of the gold nanoparticles onto emulsion surfaces. These results were published in the Journal of Colloid and Interface Science in 2019.

We then examined the mass transport that occurs between oil droplets using contrast variation time-resolved small angle neutron scattering. The extent of oil exchange in these emulsion systems was evaluated using a relaxation decay function and the kinetic decay rates were obtained using an exponential decay model. In Chapter 4, we examined the oil exchange kinetics that occurs between droplets when at rest. In this study, we observed that oil molecules could exchange over time even when no stabilizing surfactants were present. The oil exchange kinetics was accelerated when the emulsions were stabilized by surfactants (i.e. sodium dodecyl sulfate), held at higher temperatures, and when a more water-soluble oil was used as the emulsion phase. Moreover, the estimated decay constants follow the Arrhenius equation. On the other hand, varying the stabilizing surfactant concentration and screening the electrostatic repulsion forces showed little effect on the oil exchange kinetics.

It was hypothesized that two oil exchange mechanisms occurred in the emulsion system. The first mechanism was direct oil diffusion, where the oil molecules diffused from one droplet to another through the aqueous phase. The oil molecule diffusion-based oil exchange was observed when examining the oil exchange between Pickering emulsions, where the other oil exchange mechanisms were hindered. It was observed that emulsion systems with higher oil solubilities exchanged significantly more rapid. The other mechanism proposed was that the oil molecules exchange through direct emulsion contact, through reversible droplet coalescence and/or direct permeation of oil molecules through the thin liquid film between the oil droplets. The latter mechanism was observed in emulsion systems where the oil molecules were extremely immiscible with water.

In Chapter 5, we directly examine the acoustic force induced oil exchange using our custom-built ultrasound sample environment. We demonstrated that acoustic force induced cavitation events could induce oil exchange between oil droplets through droplet coalescence/breakup. Under the influence of the cavitation events, the oil exchange kinetics was accelerated from hours to minutes. The presence of stabilizing surfactants resulted in a deterred oil exchange kinetics compared to the oil exchange in a bare emulsion system. Moreover, it was observed that the oil exchange rate varied non-linearly with the surfactant concentrations. The oil exchange rate first decreases with increasing surfactant concentration. A minimal exchange rate value was observed at an intermediate concentration and further increasing the surfactant concentration resulted in a slight recovery of the exchange rate.

The combination of droplet size, electrostatic repulsion provided by the surfactants, and the Gibbs elasticity of the oil-water interface were hypothesized to contribute to the observed deter in the oil exchange kinetics. The latter phenomenon could resist distortion at the oil-water interface and prevent the drainage of thin liquid films, which both prevented emulsion coalescence. In addition, the Gibbs elasticity was also a function of surfactant concentration, where there was a maximum elasticity value at an intermediate surfactant concentration.

The collective results in Chapters 3 to 5 contribute to a better understanding of the dynamics in emulsion systems. We have studied three different emulsion systems and uncovered several interactions that occurred on a molecular scale. Moreover, we have demonstrated that cavitation events could greatly affect the interactions that occurred in emulsion systems. Furthermore, these results demonstrate that small angle scattering is an effective tool to examine interactions that occurs in emulsion systems.

6.2 FUTURE WORK

This research has laid the groundwork of using small angle scattering to examine fundamental interactions at emulsion interfaces. However, there are still many more projects that can be pursued further as a result of this work. Some of these potential future works are briefly discussed in this section.

6.2.1 *Oil Exchange Between Oil Droplets Stabilized by Other Surfactants*

In Chapter, 4 we examined the oil exchange kinetics of an anionic surfactant stabilized emulsion system. The same characterization technique could also be performed on emulsion systems stabilized by cationic surfactants, nonionic surfactants, or lipids. Prior studies have also examined the oil exchange kinetics in nonionic surfactant stabilized emulsion systems but used alternative techniques and dissimilar oils.[1,2] Preliminary experiments examining the oil exchange kinetics between hexadecane emulsions stabilized by nonionic surfactants (i.e. tetraethylene glycol monooctyl ether, C8E4) were also performed at the very-small angle neutron scattering (VSANS) instrument. Example scattering profiles obtained are shown in Figure 6.1 and the corresponding estimated relaxation functions are shown in Figure 6.2. As can be seen in the figures, the size of the synthesized droplets was significantly larger than of the ones used in Chapter 4. The preliminary data demonstrate that the oil exchange mechanism was surfactant micelle driven since minimal oil exchange was observed when no surfactant micelles were present at concentrations under the critical micelle concentration (~8 mM). Moreover, the oil exchange rate was faster when more surfactant micelles were present. This observation is similar to reports performed using other characterization techniques.

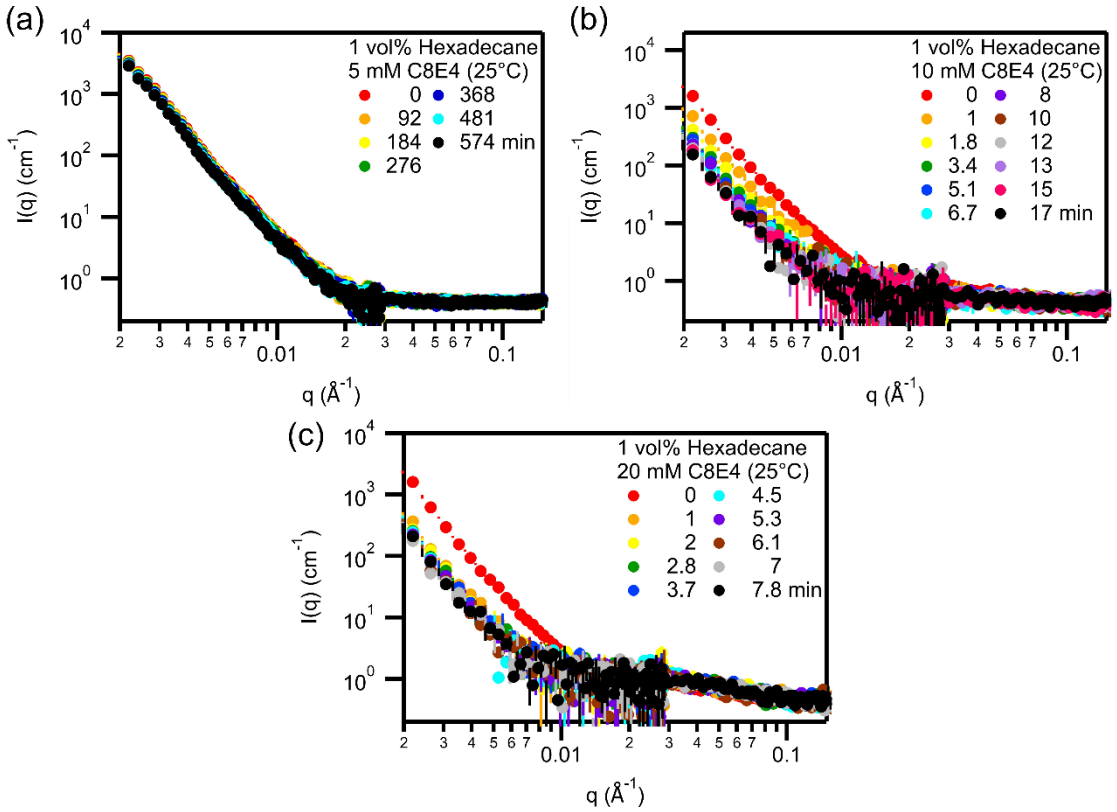

Figure 6.1. Oil exchange between emulsions stabilized by (a) 5, (b) 10, and (c) 20 mM of nonionic surfactant tetraethylene glycol monooctyl ether (C8E4). Oil molecules were only exchanged when surfactant micelles were present, and the exchange rate scales with micelle concentration.

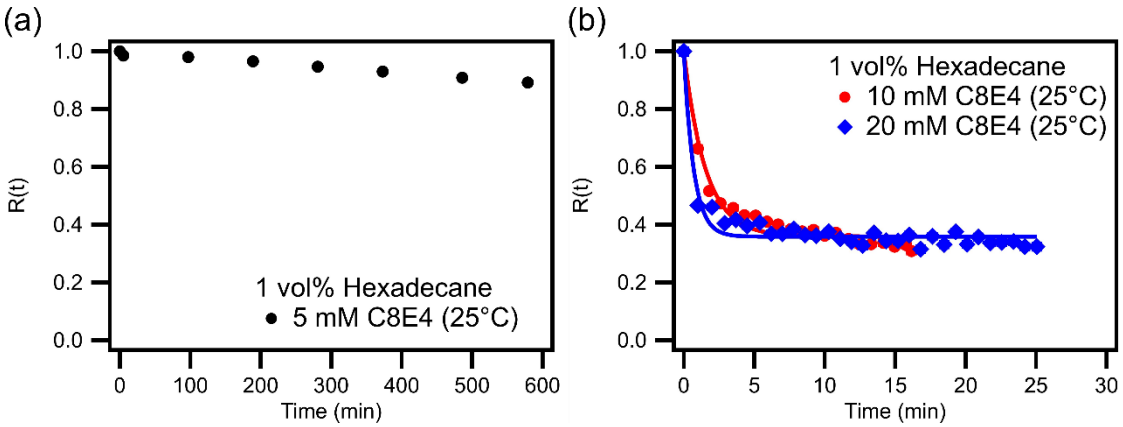

Figure 6.2. Estimated relation function oil exchange between hexadecane emulsions stabilized by C8E4 (a) below the critical micelle concentration (CMC) and (b) above the CMC.

Another observation from the preliminary results was that the estimated relaxation function seemed to be 'stuck' and minimal oil exchange occurred after 5 minutes of exchange. Using a single exponential decay with plateau function to model these relaxation functions resulted in a large estimated equilibrium plateau. However, results obtained from significantly longer time points (Figure 6.3) show that the emulsion system could reach exchange equilibrium where minimal scattering intensities were recorded. These results suggest that two oil exchange mechanisms occur in the emulsion systems. Additional experiments are required to further examine these two-step exchange mechanisms. Moreover, other experiments that could be done on nonionic surfactant stabilized emulsion systems include the design an emulsion system that exchanges oil molecules on a more manageable time scale, analyze the effects of varying the properties of the nonionic surfactant (e.g. molecular weight and ratio of the hydrophobic versus hydrophilic portion of the surfactant), and the used of multiple nonionic surfactants to examine its effects on the oil exchange rate. The experiments could be performed using the white beam mode on the VSANS instrument to obtain better statistics in the scattering profiles.

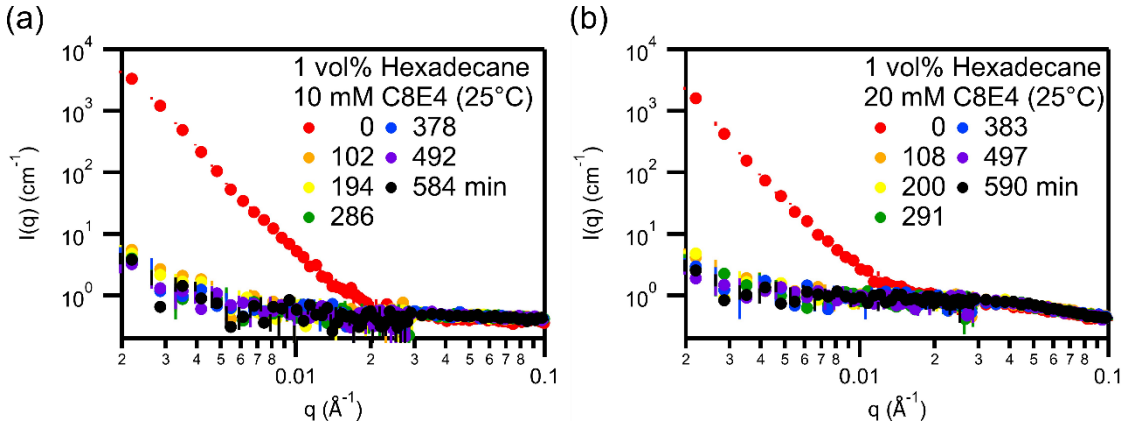

Figure 6.3. Scattering profiles of hexadecane emulsions stabilized by (a) 10 mM and (b) 20 mM C8E4 showing that the emulsion system can reach oil exchange equilibrium at longer time points.

On the other hand, the oil exchange kinetics and driving mechanism could be completely different in lipid stabilized emulsion systems. Therefore, a systematic study is required to determine the effects of lipids and vesicles on the oil exchange kinetics. Understanding the oil exchange between lipid-coated droplets may potentially be extremely impactful since there is an abundance of interest in developing a lipid-coated emulsion for biomedical applications.

6.2.2 *Drug Release in Emulsion Systems*

The primary advantage of contrast variation time-resolved SANS is that it provides the ability to track mass transport that is occurring in the system on a molecular base. Another follow up future project that could be pursued is to examine the release of chemical compounds from oil droplets into the solvent. For droplet-based drugs, the transport of oil soluble molecules would dictate the shelf-life of the product and the required method for delivering/releasing the drugs into the human body. One could design a model system where the solvent phase is contrast matched to the drug molecules that are dissolved in oil. In this system, an overall contrast increase would be observed in the emulsion system when the molecules are released from the droplets into the continuous phase. Furthermore, how the environment (e.g. pH, salinity, external force induced release) can affect the release kinetics could be investigated using this characterization technique.

6.2.3 *Demulsification of Emulsions*

As mentioned in the report, ultrasound is frequently applied to emulsion systems. While most of the presented results were focused on the emulsion synthesis and the dynamics at the equilibrium state, another phenomenon that could occur in emulsion systems is the destabilization of droplets under the influence of acoustic forces. Therefore, another project that could be pursued is the investigation of emulsion destabilization kinetics. Water in oil emulsions (W/O) are

commonly formed during crude oil extraction, transportation, and treatment.[3–6] These inverse emulsions are stabilized by solid particles or high molecular weight hydrocarbons and can be problematic for downstream processes. Thus, it is a common procedure for facilities to treat and remove water from the freshly extracted crude oil before transporting or performing any refinery operations.[4] Recently, the use of high-frequency acoustic waves (ultrasound) was investigated as a method to demulsify inverse emulsions.[7–11] It was observed that the application of demulsifiers (i.e. molecules with high hydrophilic-lipophilic balance values) and ultrasound could rapidly induce the coalescence of water droplets in inverse emulsion systems.

Preliminary experiments were performed to examine the ultrasound induced demulsification process using our ultrasound sample environment. Inverse emulsions containing 10 to 30 volume percent of water in West Texas crude oil were synthesized using high shear homogenization. Demulsification of the inverse emulsions could be observed when the samples were sonicated above the cavitation threshold and with the presence of demulsifiers (Brij® L23) as shown in Figure 6.4. Experiments were also performed on the ultra-small angle X-ray scattering instrument, but preliminary results suggest that the size of the stabilizing particles (i.e. asphaltene) and the inverse emulsions were too large for this characterization technique.

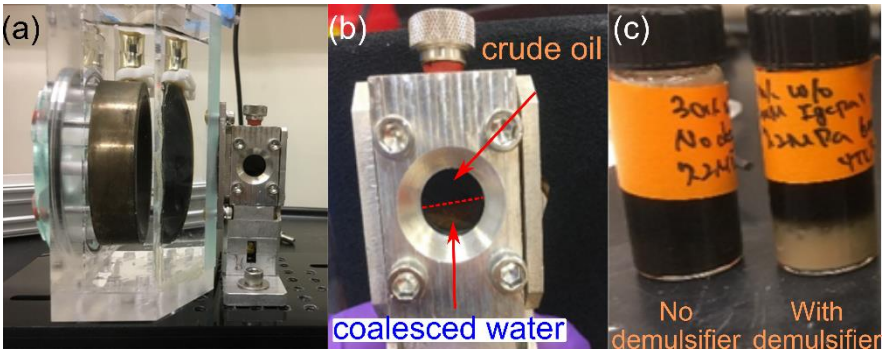

Figure 6.4. (a) Using ultrasound sample environment for demulsifying water in crude oil inverse emulsions. (b) Water droplets coalesced and sedimented in the sample holder after sonication. (c) Sedimentation of water droplets were only observed when demulsifiers were added to the inverse emulsion system

An alternative model system could be developed using smaller sized stabilizers and hydrocarbon oils. An example stabilizer that can be used to is Span® 80. Preliminary results of sonicating a 1 volume percent of water in hexadecane inverse emulsion is shown in Figure 6.5. It was observed that the inverse emulsions were stable and sonicating them did not result in emulsion size change. On the other hand, adding demulsifiers destabilized the system to forming larger inverse emulsions when dispersing the demulsifiers. Moreover, sonicating the sample resulted in further phase separation and a decrease in scattering intensities due to emulsion coalescence. Additional experiments are required to further explore this demulsification process. However, the primary hurdle for using this model system is that it is limited to examining systems with low volume fraction of inverse emulsions. Synthesizing inverse emulsions using a higher volume fraction of water (e.g. 10 vol%) resulted in observing multiple scattering and the presence of structure factors in the recorded scattering profiles.

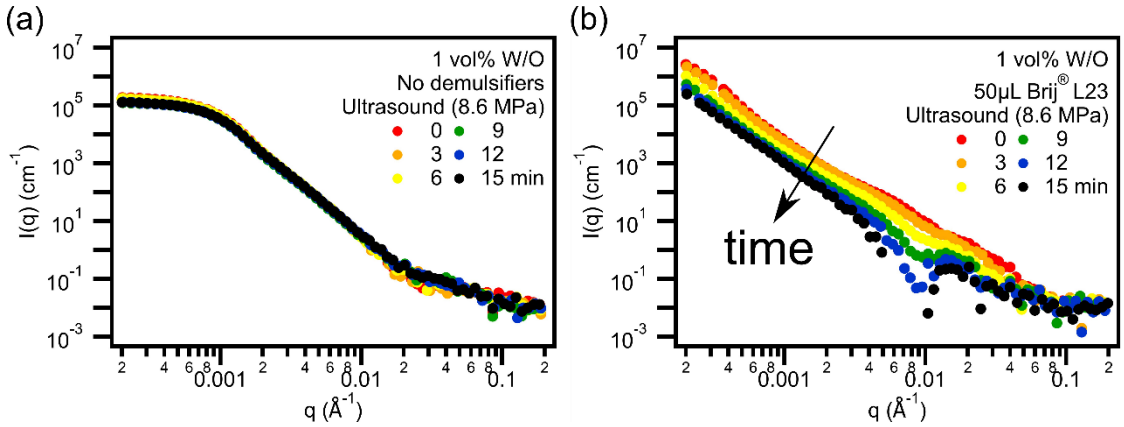

Figure 6.5. (a) Sonicating 1 vol% water in hexadecane inverse emulsion showing no significant size change over time. (b) Adding demulsifiers to the inverse emulsion sample resulted in forming larger droplets and sonicating the sample resulted in the droplets coalescing and separating from the dispersion.

6.2.4 *Design of an Acoustic System for Inducing Standing Wave/or Concentrating Samples*

Though cavitation events are extremely efficient in inducing the desired processes, the presence of cavitation events would result in the system to be chaotic and hard to control. Another direction that can be taken to induce demulsification of inverse emulsions is to design a new acoustic sample environment to induce a more controlled and less extreme acoustic field that can concentrate the samples to a desired location. One potential direction is to induce a standing wave within the sample holder where the acoustic radiation forces provided by the transducers can concentrate the droplets to either the node or antinode of the standing wave (depending on the sign of the acoustic contrast factor). The use of standing waves also has been explored and shown to be effective in inducing destabilization of the inverse emulsions.[8,10,12] Another strategy is to offset the two driving transducers such that the acoustic forces could induce fluid flow, which concentrates to the center of the sample holder. Nevertheless, extensive modeling is required to determine its feasibility and for optimizing the system design. Ultimately, this work is not limited to only

examine the demulsification process and could also be applied to other systems such as acoustic force induced assembly of nanoparticles/particles.

6.3 REFERENCES

(1) McClements, D. J.; Dungan, S. R.; German, J. B.; Kinsella, J. E. *Top. Catal.* **1992**, *6* (5), 415–422.

(2) Weiss, J.; McClements, D. J. *Langmuir* **2000**, *16* (14), 5879–5883.

(3) Wong, S. F.; Lim, J. S.; Dol, S. S. *J. Pet. Sci. Eng.* **2015**, *135*, 498–504.

(4) Kilpatrick, P. K. *Energy and Fuels* **2012**, *26* (7), 4017–4026.

(5) McLean, J. D.; Kilpatrick, P. K. *J. Colloid Interface Sci.* **1997**, *189* (2), 242–253.

(6) Kokal, S. L. *SPE Prod. Facil.* **2005**, *20* (01), 5–13.

(7) Yi, M.; Huang, J.; Wang, L. *J. Chem.* **2017**, *2017*.

(8) Trujillo, F. J.; Juliano, P.; Barbosa-Cánovas, G.; Knoerzer, K. *Ultrason. Sonochem.* **2014**, *21* (6), 2151–2164.

(9) Antes, F. G.; Diehl, L. O.; Pereira, J. S. F.; Guimarães, R. C. L.; Guarnieri, R. A.; Ferreira, B. M. S.; Dressler, V. L.; Flores, E. M. M. *Ultrason. Sonochem.* **2015**, *25* (1), 70–75.

(10) Ye, G.; Lu, X.; Han, P.; Peng, F.; Wang, Y.; Shen, X. *Chem. Eng. Process. Process Intensif.* **2008**, *47* (12), 2346–2350.

(11) Hamidi, H.; Mohammadian, E.; Asadullah, M.; Azdarpour, A.; Rafati, R. *Ultrason. Sonochem.* **2015**, *26*, 428–436.

(12) Check, G. R. *Chem. Eng. Process. Process Intensif.* **2014**, *81*, 72–78.

Chapter 7. SUPPORTING INFORMATION

7.1 SUPPORTING INFORMATION FOR CHAPTER 3

7.1.1 *Energy Barrier Calculations*

The interaction potential between a polymer coated particle and emulsion surface was calculated using the Dolan Edwards model.[1,2] Theoretical interaction energy potential between a 12 nanometer diameter particle coated with a 10 kDa molecular weight PEG-thiol and non-polymer coated emulsion droplet was estimated using Equations (7.1) and (7.2). This estimation showed that there was a significant energy barrier (relative to kT) between the two surfaces. Thus, it was not possible to induce spontaneous adsorption and would require a large force into the system to form Pickering emulsions.

$$d_{modified} < \sqrt{3} \times R_F: \quad \frac{E(d)}{kT} = \Gamma \left\{ ln \left[\left(\frac{d^2}{8\pi lL} \right)^{0.5} \right] + \frac{\pi^2}{2} \left(\frac{lL}{d^2} \right) \right\} \tag{7.1}$$

$$d_{modified} > \sqrt{3} \times R_F: \quad \frac{E(d)}{kT} = -\Gamma * ln \left\{ 1 - 2 \times exp \left[\frac{-d^2}{2lL} \right] \right\} \tag{7.2}$$

where:

- d: Separation distance
- R_F: Flory radius of the polymer chain
- k: Boltzmann constant
- T: Temperature
- l: Length of monomer in the polymer chain
- L: Contour length of the polymer chain
- Γ: Surface density of the anchored polymer chain

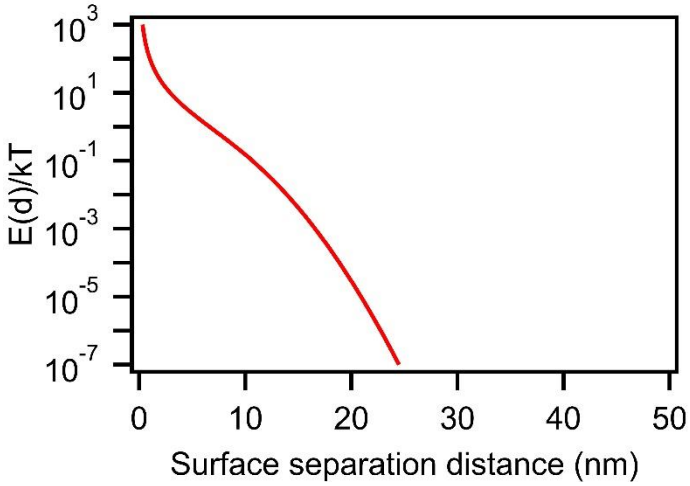

Figure 7.1. Theoretical estimation of energy barrier between a polymer grafted nanoparticle and emulsion surface using the Dolan Edwards model where R_F = 6.0 nm, l = 0.3 nm, L = 63.0 nm, and Γ = 1.2 chains/nm^2.

7.1.2 *Optimizing Hydrophobic vs Hydrophilic Forces on Synthesized GNP*

To effectively examine the role of sonication during emulsion formation, it was crucial to choose the correct type and amount of hydrophilic/hydrophobic chains used to functionalize GNPs. Based on previous experiences, increasing the grafting densities or using larger molecular weights of the dosed hydrophilic PEG-thiol to functionalize the surface of GNPs increases the stability of the particles and results in smaller nanoclusters.[3] If the additional steric repulsion force on GNPs is strong enough to overcome the hydrophobic attractive force, the GNPs will stay as a stable 'singlet' spherical particles and will not form larger structures. These stable GNPs have been shown to stay in this 'singlet' form even after sonication.

Selecting the right hydrophobic alkane thiol was also important. For these experiments, we selected the smallest amounts needed to fully coat the surface of the GNPs, avoiding a large excess of thiol. We also selected to use shorter thiol chains that have been shown to form more surface active particles and lead to more pronounced correlation peaks in the scattering profiles from Pickering emulsions.[4] If the spacing between gold nanoparticles at the emulsion interface is limited

by the length of the alkane thiol (i.e. assuming close contact), then the use of short chain alkane thiols can result in denser packing of nanoparticles on a finite emulsion interface. More particles on the emulsion would then result in more particle-particle correlations and a more pronounced characteristic peak in the mid-q regions of the scattering profiles. For a 12 nm diameter butanethiol functionalized GNP, the theoretical maximum surface coverage estimated was around 82% whereas longer chains such as octanethiol had a theoretical maximum surface coverage of 67%.[5]

7.1.3 *Ultra-small X-ray Scattering Profile of Different Components in The Pickering Emulsion Synthesis Process*

An example of the scattering profile of the different materials used for our Pickering emulsion synthesis is shown in Figure 7.2. As can be seen, emulsions had higher scattering intensities in the lower q region whereas GNP dominated the scattering intensities at high q regions. When the two materials were combined, scattering data were basically a combination of the two different components. However, when sonicated at high acoustic pressure, the scattering profile of the sample significantly alters in the mid and low q regions indicating the formation of Pickering emulsions.

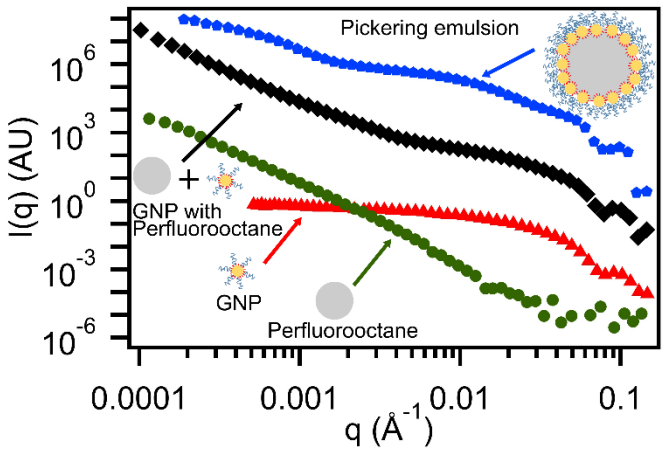

Figure 7.2. Example of desmeared USAXS data for perfluorooctane emulsions, GNP, GNP with perfluorooctane emulsions presence (no sonication), and Pickering emulsions. Scattering data are arbitrarily shifted in the y axis to show the difference in the characteristic between curves.

Figure 7.3 is an example of modeling the scattering profile of a sample sonicated at low acoustic pressure showing that the final fitted scattering curve was a combination of two spheres, one for emulsions and one for gold nanoparticles. Fits suggest that the system consisted of a polydisperse perfluorooctane with mean radius of 411.6 nanometers with a PDI of 0.5. In addition, two different size distributions of GNPs were present, where 78.5 vol% of the particles had a radius of 6.00 nm and 21.5 vol% were 13.3 nm. This model was also used to provide information on the changes of emulsion droplet size and volume fraction in the sample during sonication.

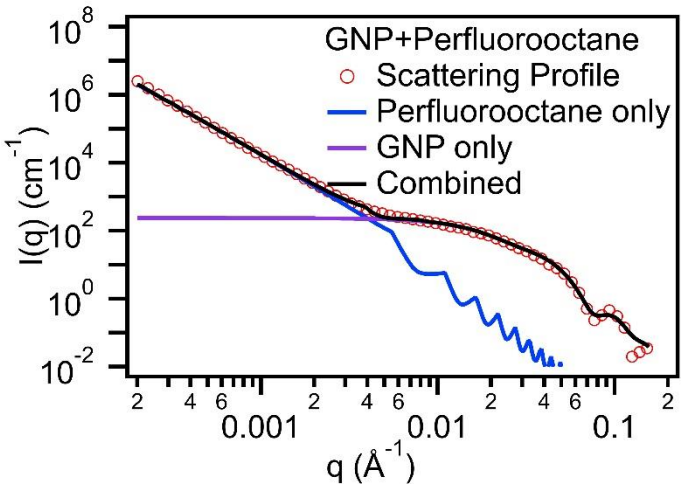

Figure 7.3. Desmeared USAXS scattering data at low acoustic pressure can be fitted with a model containing 2 spherical components, the perfluorooctane emulsion and GNP.

7.1.4 *Control Samples to Help Determine Pickering Emulsion Formation*

To investigate the role of sonication in the formation of Pickering emulsions, it was important to be sure that no false positives were observed during experiments. The first control experiment used hydrophilic gold nanoparticles (Gold-PEG) with emulsion droplets to determine whether or not Pickering emulsions could be synthesized without hydrophobic alkane thiol chains. Figure 7.4 is an example of the result of scattering data obtained showing no Pickering emulsion characteristic peaks were formed in the mid q region regardless of the acoustic pressure. The only difference was the change in slope in the low q regions suggesting that the only change in the system was the size distribution of emulsion droplets.

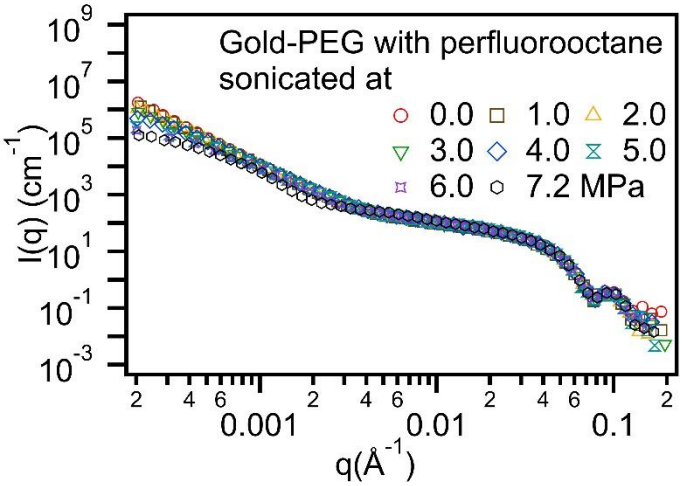

Figure 7.4. USAXS profile for Gold-PEG with perfluorooctane sonicated at different acoustic pressure showing that Gold-PEG will not adsorb onto emulsion surfaces even when sonicated at high acoustic pressures.

GNP alone was also evaluated to determine whether or not it would form a larger structure when sonicated. As mentioned in the discussion, choosing the correct parameters for synthesizing GNPs was crucial. Figure 7.5, the result of sonicating GNPs alone, showed that no larger clusters were formed even when with cavitation. These two control experiments proved that it was safe to assume that any significant changes observed in the scattering profile when sonicating a GNP with emulsion sample was from formation of Pickering emulsions.

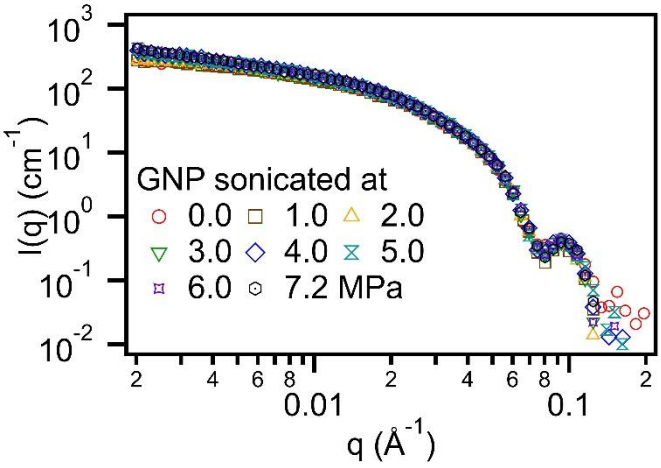

Figure 7.5. USAXS profile of GNP sonicated at different acoustic pressure showing that no larger structures will form even with cavitation.

7.1.5 *Using FTIR Spectrum to Verify the Integrity of the Ligands on the GNPs*

Fourier-transform infrared spectroscopy (FTIR) was performed on GNP with perfluorooctane samples before and after sonication. The samples were synthesized, lyophilized, mixed with dry KBr and pressed into a pellet using KBr pellet a die kit. The FTIR measurements were performed using a Bruker Vector 33 FTIR spectrophotometer (Bruker Corporation, MA, USA). This experiment was used to examine whether or not cavitation events have an effect on the ligands binding to the GNP surfaces. The obtained spectra are shown in Figure 7.6. The broad peak in the 3100-3700 cm^{-1} region corresponds to the OH group on the PEG-thiol. The peak at around 1100 cm^{-1} is from the C-O bond on the PEG-thiol and the peak in the 2800-2950 cm^{-1} region is from the alkane bonds (combination of PEG-thiol and alkanethiol). The presence of a peak at 2350 cm^{-1} is due to CO_2, which was a small background subtraction error within the instrument. Since the FTIR spectrum of the sample before and after sonication remains identical, it demonstrates that alkanethiol and PEG-thiol coatings are unaffected by the application of ultrasound.

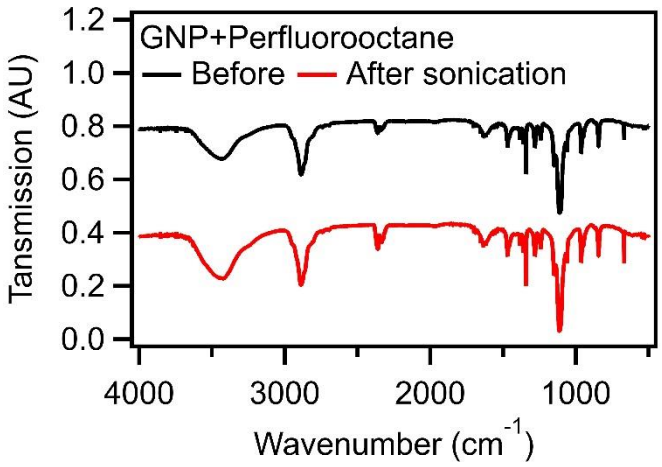

Figure 7.6. FTIR spectrum of GNP with perfluorooctane before and after sonication.

7.2 SUPPORTING INFORMATION FOR CHAPTER 4

7.2.1 *Scattering Profiles of Emulsion Oil Exchange at Various Surfactant Concentrations, Salt Concentrations, and Temperatures*

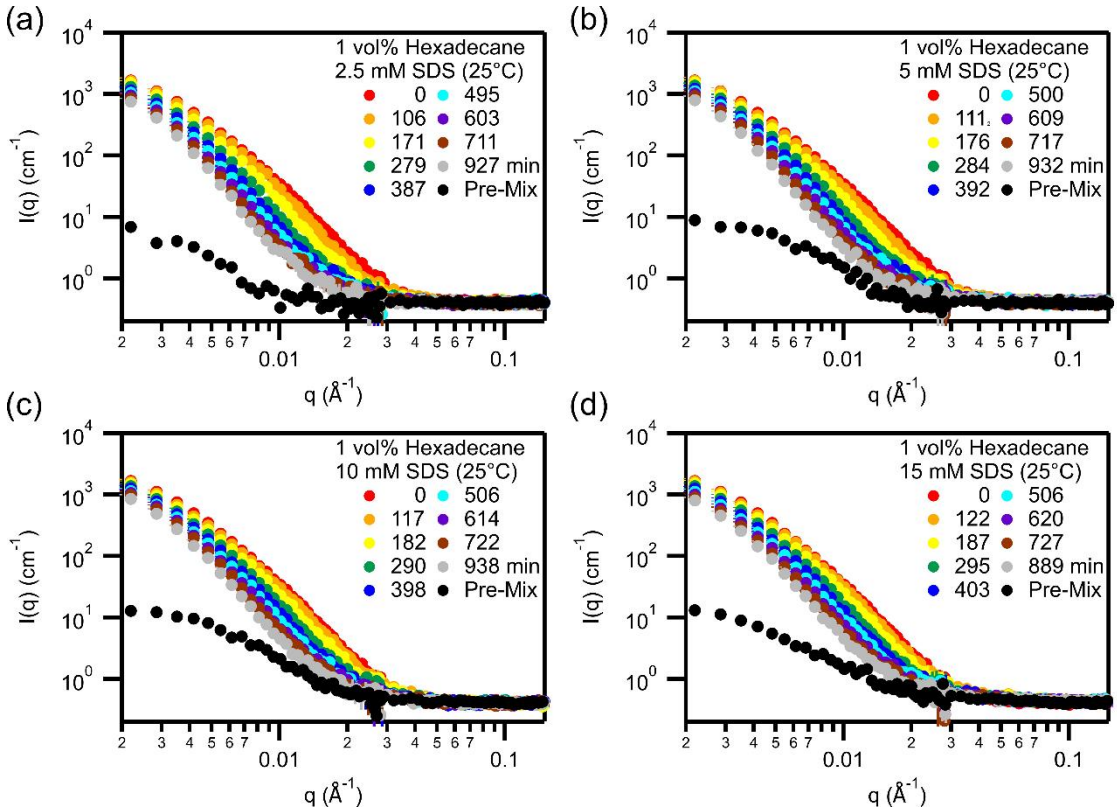

Figure 7.7. Oil exchange between hexadecane droplets stabilized by (a) 2.5, (b) 5, (c) 10, and (d) 15 mM sodium dodecyl sulfate (SDS) (25 °C). The rate of decay in scattering intensities is similar across various stabilizing surfactant concentrations.

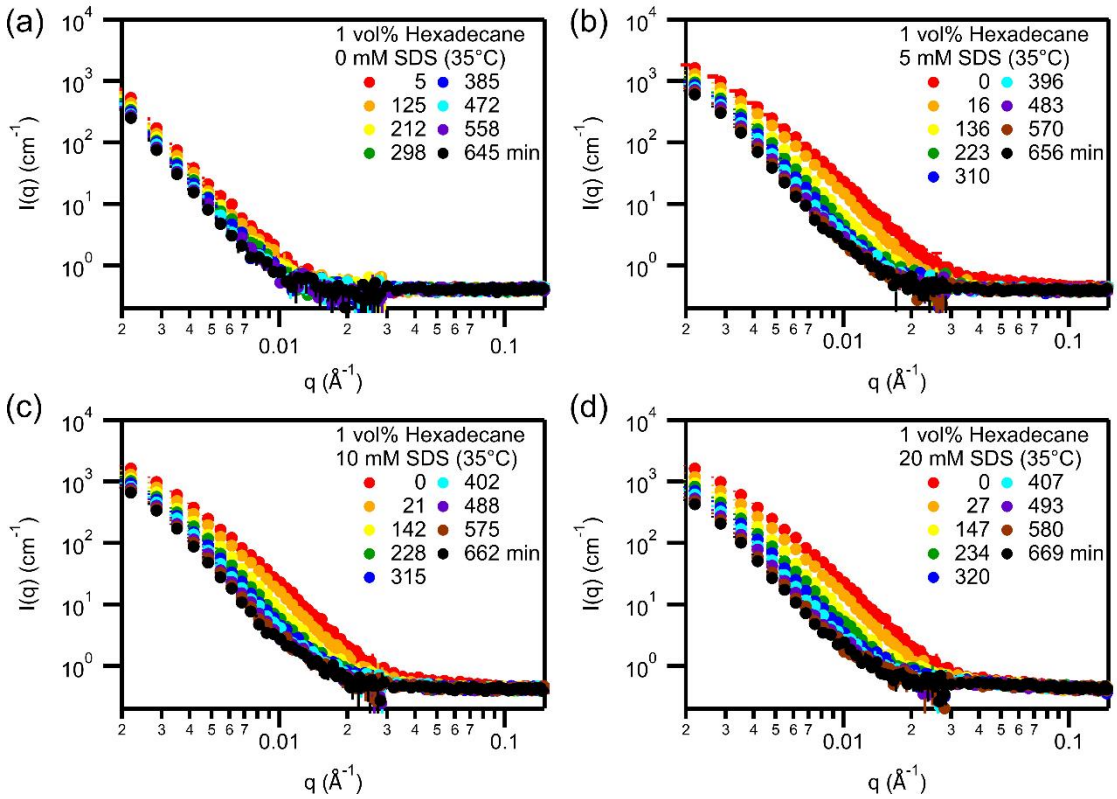

Figure 7.8. Oil exchange between hexadecane droplets with the presence of (a) 0, (b) 5, (c) 10, and (d) 20 mM SDS (35 °C).

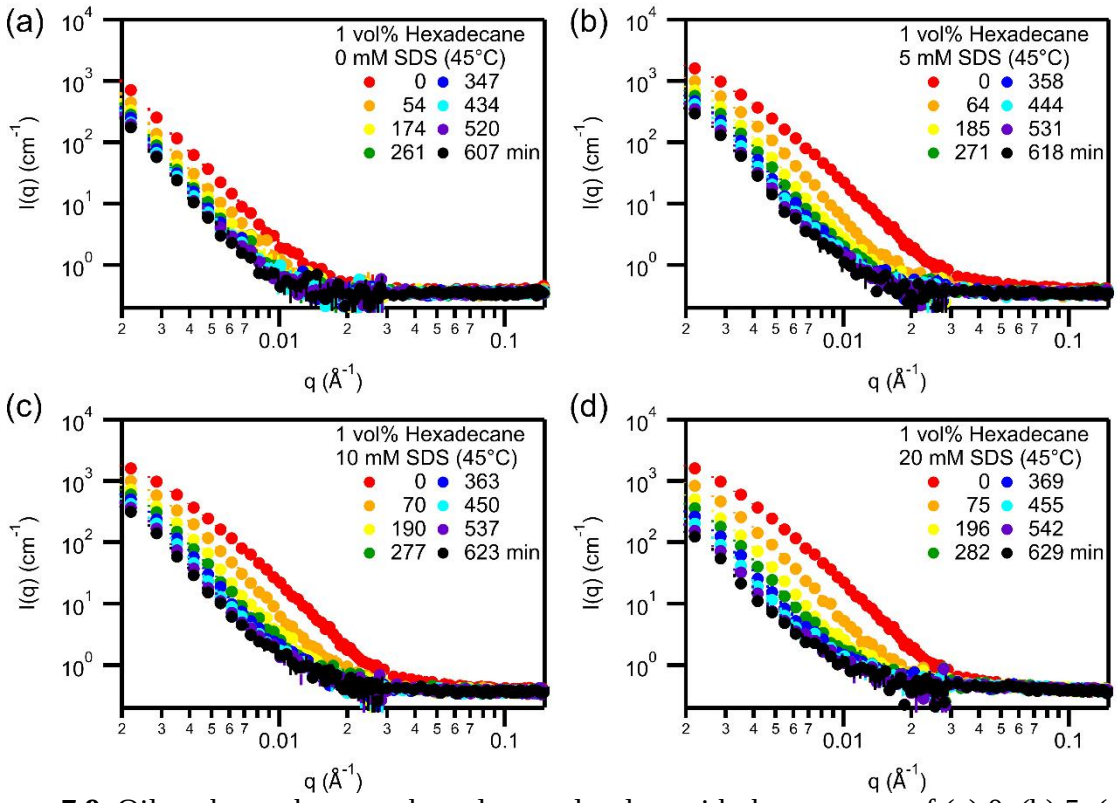

Figure 7.9. Oil exchange between hexadecane droplets with the presence of (a) 0, (b) 5, (c) 10, and (d) 20 mM SDS (45 °C).

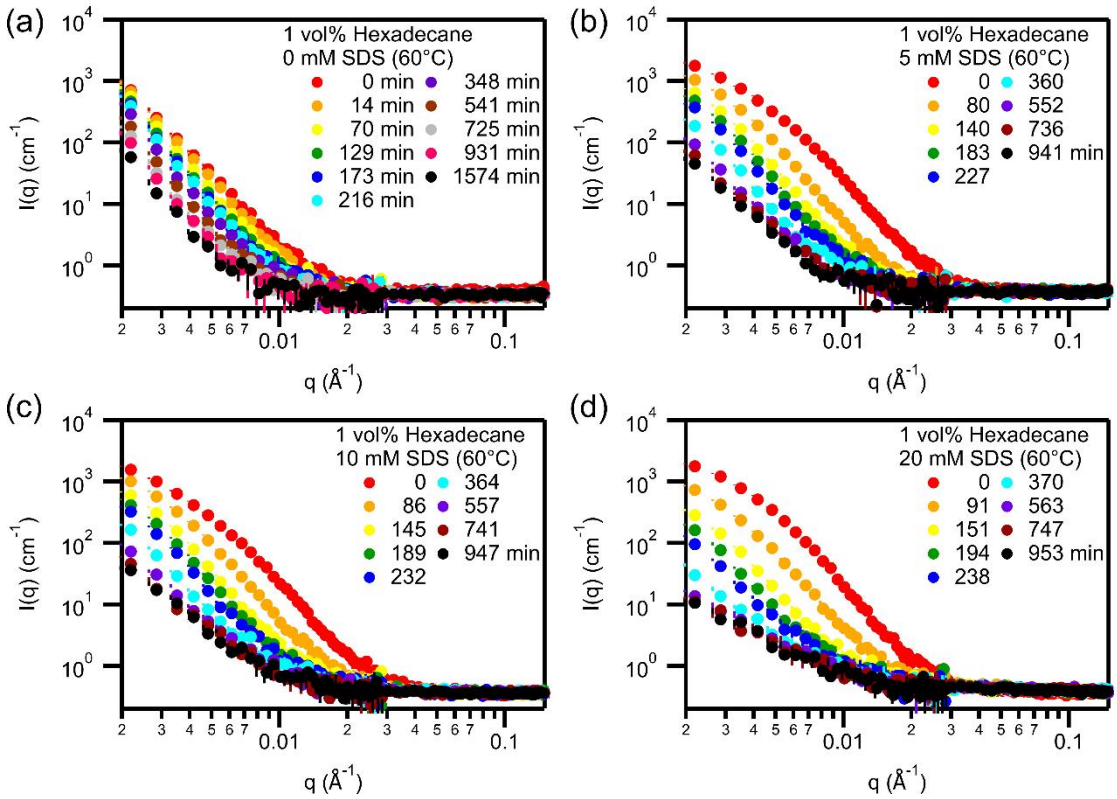

Figure 7.10. Oil exchange between hexadecane droplets with the presence of (a) 0, (b) 5, (c) 10, and (d) 20 mM SDS (60 °C).

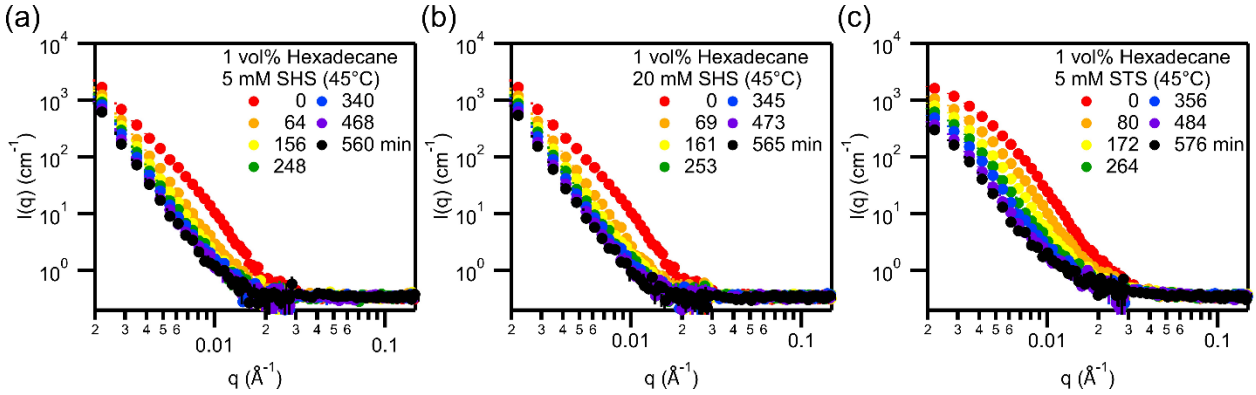

Figure 7.11.. Oil exchange between hexadecane droplets with the presence of (a) 5 mM SHS, (b) 20 mM SHS, and (c) 5 mM STS at 45 °C.

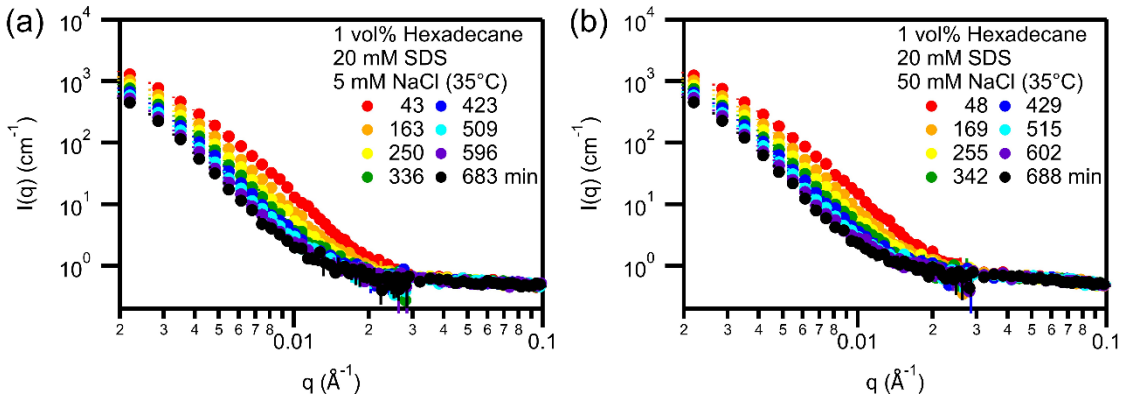

Figure 7.12.. Oil exchange between hexadecane droplets stabilized by 20 mM SDS in (a) 5 mM and (b) 50 mM NaCl at 35 °C.

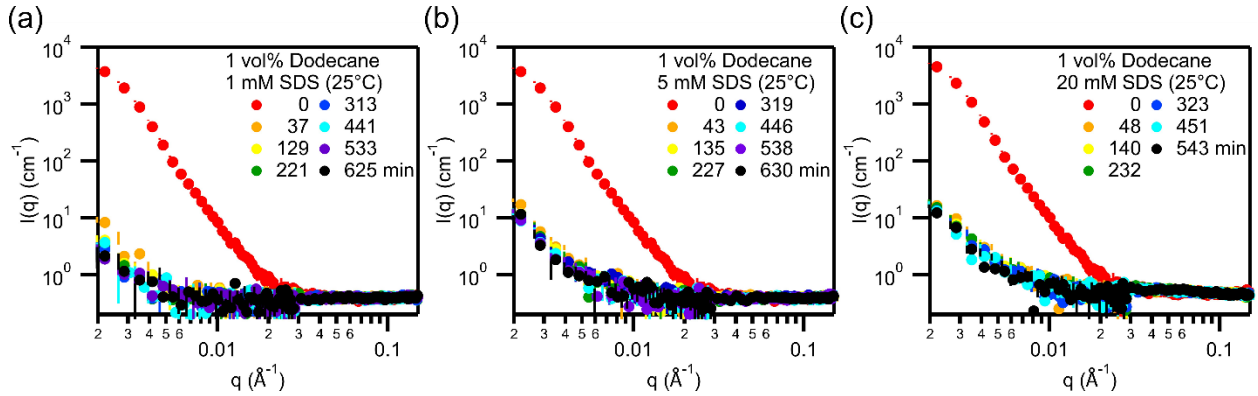

Figure 7.13.. Oil exchange between dodecane (DodeMix) droplets stabilized by (a) 1 mM, (b) 5 mM, and (c) 20 mM SDS at 25 °C.

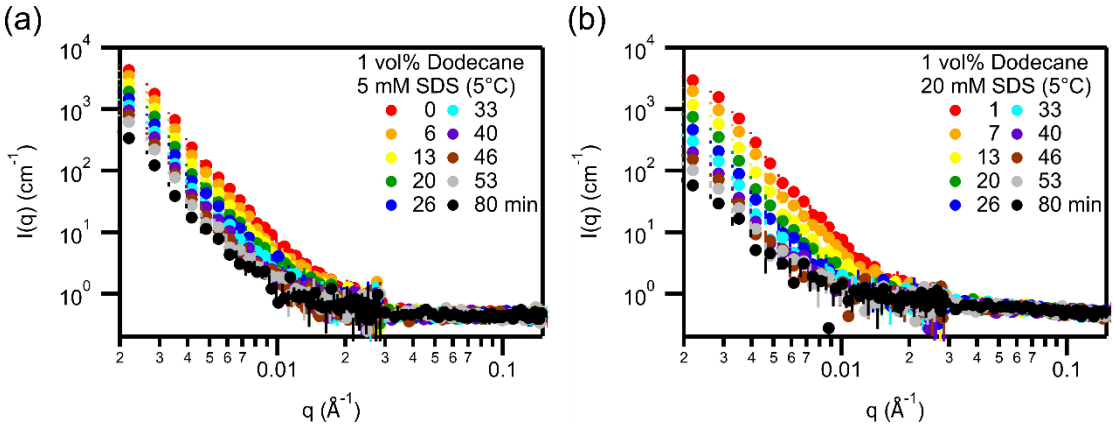

Figure 7.14.. Oil exchange between dodecane droplets stabilized in (a) 5 mM and (b) 20 mM SDS at 5 °C.

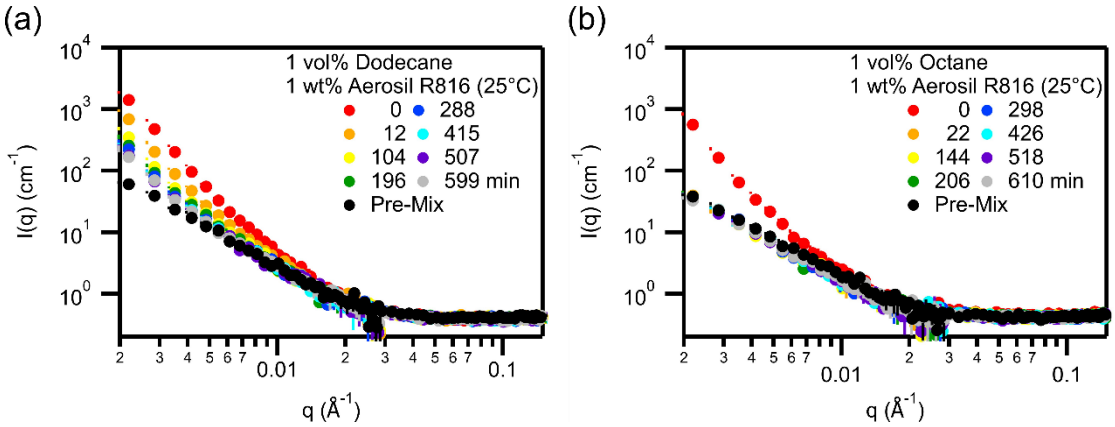

Figure 7.15.. Oil exchange between silica particle stabilized Pickering emulsions with (a) dodecane (DodeMix) and (b) octane (OctMix) as the emulsion core at 25 °C.

7.2.2 *Emulsion Size Estimation*

The hydrodynamic size distribution of emulsions was obtained using dynamic light scattering as shown in Figure 7.16. On the other hand, the size distribution of smaller emulsions could also be obtained by fitting the scattering data with a sphere model. For example, the emulsion size distribution of control samples (e.g. 1 vol% D-hexadecane with 20 mM SDS) was estimated by fitting the recorded scattering profiles with a sphere model using Irena.[6] The size distributions at different time points could be expressed using a box and whisker plot. The box portion of the plot, from bottom to top, represents the 25th percentile, median, and 75th percentile of the distribution. The whisker portion represents the 10% percentile and 90% percentile. An example of estimating the emulsion size distribution at the start and end of the experiment is shown in Figure 7.17. Based on the results, it could be observed that the overall distribution does not change significantly over the course of the experiment.

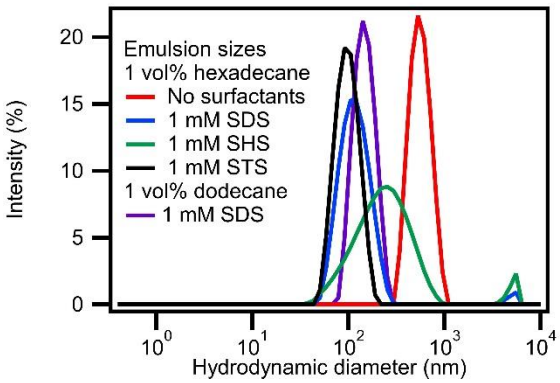

Figure 7.16.. Hydrodynamic size distribution of emulsions obtained using dynamic light scattering.

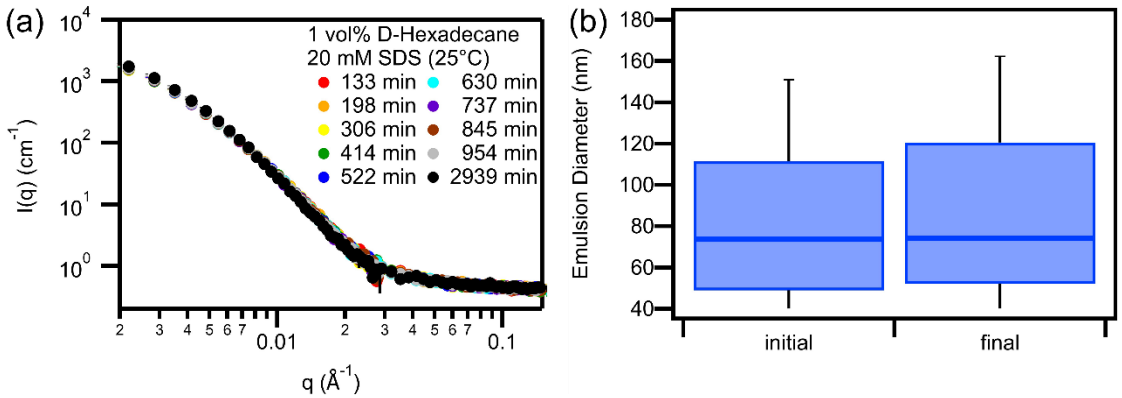

Figure 7.17. (a) Scattering profile of 1 vol% D-hexadecane with 1 mM SDS tracked over time at 25 °C. (b) Size distribution (box plot) of emulsions at the start and finish of the experiment. The scattering length densities of the emulsion system were 6.67×10^{-6} Å^{-2} (D-hexadecane) and 4.54×10^{-6} Å^{-2} (solvent)

On the other hand, the scattering profiles and emulsion size distributions change more prominently over time in samples at elevated temperature or when stabilized with a lower concentration of surfactants. An example is the emulsion sample stabilized with 1 mM of SDS held at 60 °C. The recorded scattering profile and estimated emulsion size distribution are shown in Figure 7.18. Luckily, the change in emulsion size distribution has minimal effect on the estimated relaxation function.

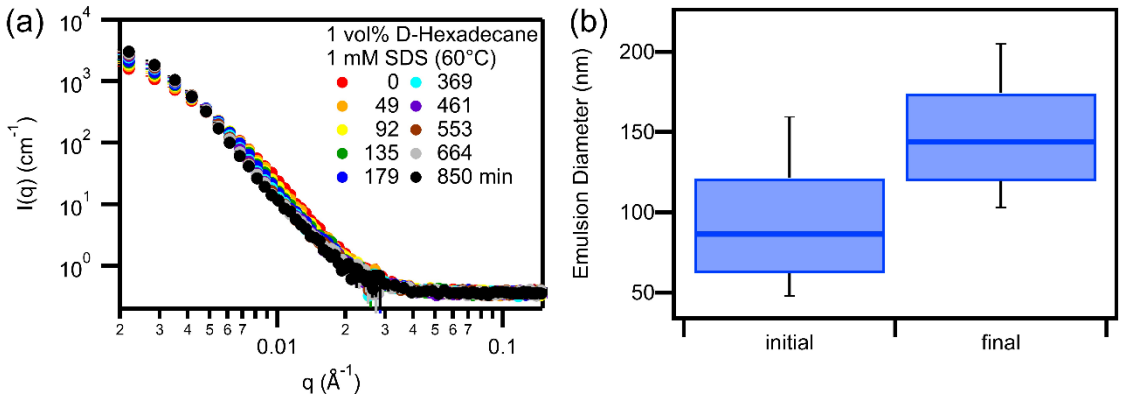

Figure 7.18. (a) Scattering profile of 1 vol% D-hexadecane with 1 mM SDS tracked over time at 60 °C. (b) Size distribution (box plot) of emulsions at the start and finish of the experiment.

7.2.3 *Estimation of Relaxation Function While Accounting for Emulsion Size Change Over Time*

For samples that showed some variations in size distributions during the time scale of the experiments, additional analysis was performed to estimate their impact on the kinetic analysis. One example of the calculation of the relaxation function with/without accounting for droplet size changes is shown in Figure 7.19. This sample was chosen because it represented a 'worst-case scenario' since it showed the most significant size change in the scattering profile due to the use of lower surfactant concentrations. Based on the figure, it can be observed that accounting for the changes in droplet size had little effect on the estimated values of the relaxation functions. However, a significant increase in uncertainty was observed at the longer time points due to increasing uncertainty in the control sample's scattering profiles and the propagation of error. Fitting the two decay curves resulted in very small changes to the plateau value, from 0.12 to 0.10. On the other hand, the estimated decay constant remained identical (6.31×10^{-3} min^{-1}). Therefore, the assumption that any changes in droplet size are small over the measured time-scales was used for all of the analysis in this report.

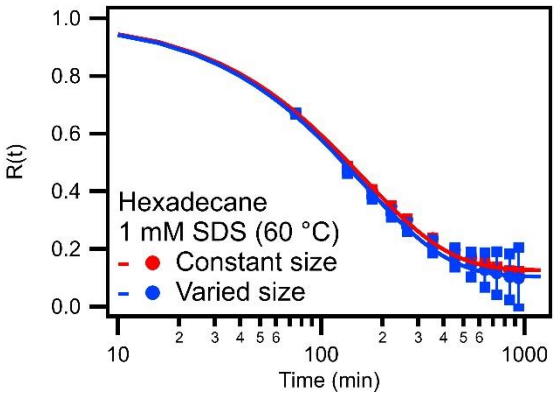

Figure 7.19. Comparison of the estimated relaxation function for a sample accounting for changes in droplet size versus assuming constant emulsion size. Accounting for emulsion size changes had a minimal effect on the estimated decay constants and plateau values.

7.2.4 *Examining the Critical Micelle Concentration with the Presence of Emulsion Droplets*

The presence of oil droplets in a system could potentially affect the critical micelle concentration (CMC) of a surfactant. Portions of the surfactants decorates the oil-water interface; therefore, the concentration of surfactants in the dispersed phase would be lower than the dosed concentration. On the other hand, the surfactant micelles have been known to solubilize oil molecules into their hydrophobic cores. This could facilitate the formation of 'swollen' micelles at lower surfactant concentrations that could also affect transport. Two experiments were performed to examine whether the surfactant's CMC was affected by the presence of oil droplets in water.

The first experiment was to use small angle neutron scattering (SANS) to determine whether the presence of dissolved oil molecules would affect the surfactant CMC. Two series of surfactant solutions were synthesized. In one series of samples, there was a layer of oil 'floating' on top of the aqueous surfactant solution. These samples were synthesized days before performing the SANS experiments such that the oil molecules were allowed to equilibrate and dissolve into

the aqueous surfactant solution. Surfactant solutions without the presence of micelles would scatter similar to a solvent only sample. On the other hand, the scattering profiles would show a significant increase in intensity if surfactant micelles were present. The results are shown in Figure 7.20 and it can be seen that no significant differences in the CMC were observed between the two series of samples. Both samples, with and without equilibrated oil, showed a similar increase in scattering between 8 and 10 mM SDS. This observation suggest that the presence of dissolved oil molecules will not significantly increase or decrease the CMC of SDS.

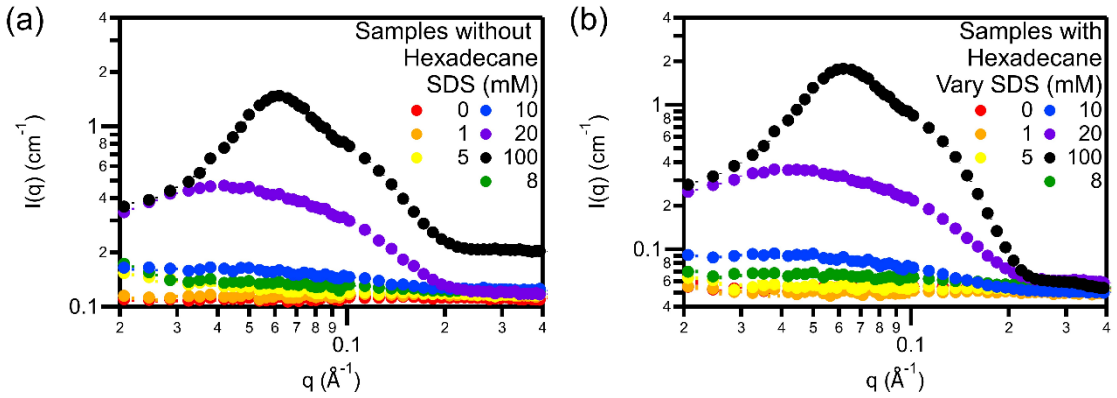

Figure 7.20. Scattering profiles for (a) SDS solutions and (b) SDS solutions after long-term stabilization (4 days) with an excess layer of hexadecane.

The second experiment was to perform conductivity measurements to obtain the CMC of surfactants in water and in surfactant-stabilized emulsion systems. The CMC of surfactants were first obtained by slowly adding high concentrations of surfactants (e.g. 200 mM SDS) into DI water and monitoring the changes in the sample conductivity (Figure 7.21 (a), (c), and (e)). A slope change was observed and the intercept of the two fit lines is the CMC. The measured CMC values for SDS (8.51 mM), STS (1.94 mM), and SHS (299.6 mM) were all close to the theoretically estimated values.

The same experiment was then performed on samples containing 1 volume percent of dispersed hexadecane oil droplets. The estimated CMC for surfactants dissolved in hexadecane emulsions were 11.94 mM for SDS and 5.93 mM for STS. These CMC values are larger than the values obtained from surfactants dissolved in pure water. The increase in CMC is likely due to the adsorption of some surfactant molecules onto the oil-water interface, resulting in a lower effective concentration in the bulk phase. Similar results were also observed by Chang *et al.*[7] Conductivity measurements for emulsions stabilized by SHS were not performed since the surfactant concentrations used in this study were well below the CMC of the surfactant (~300 mM).

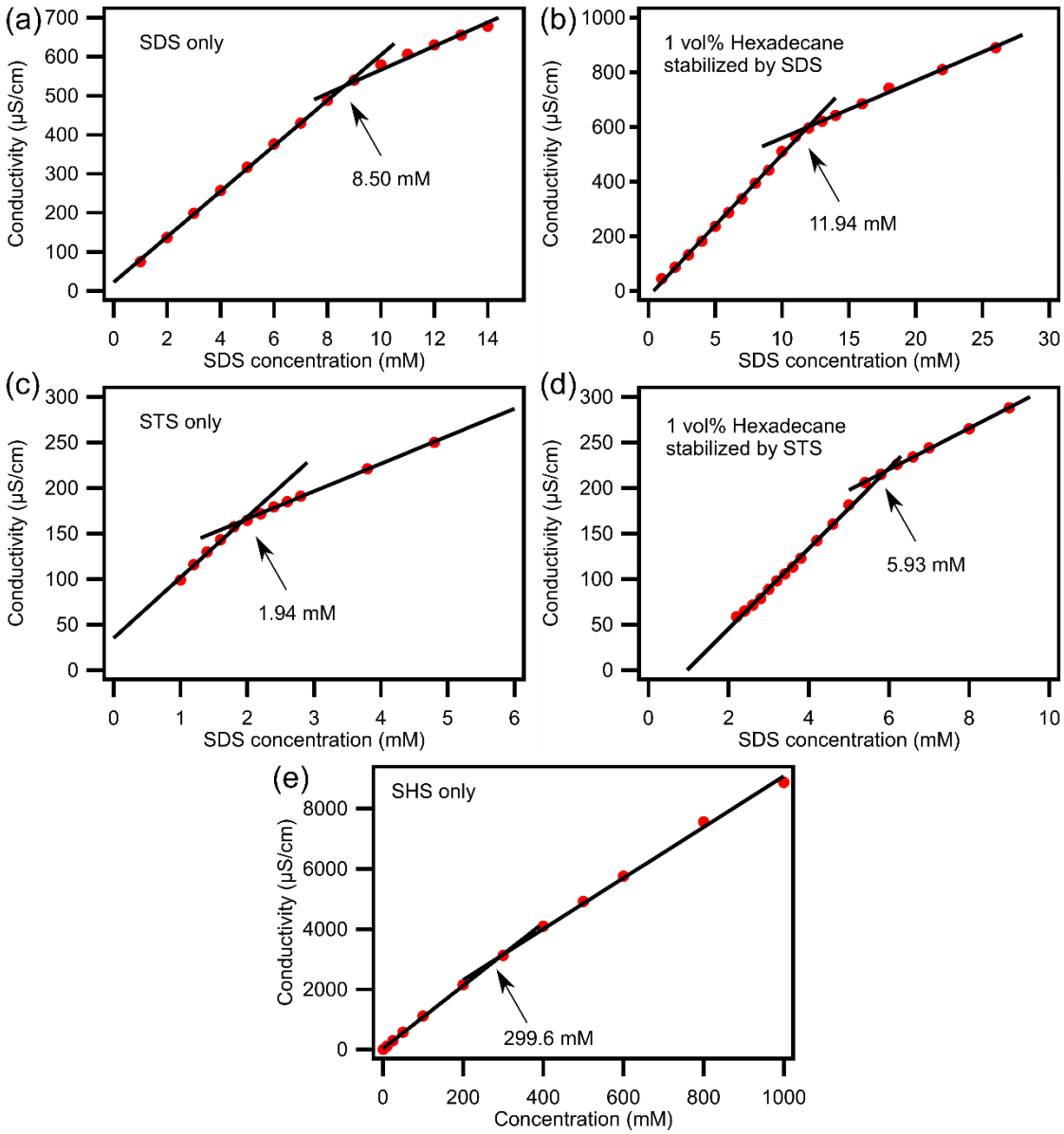

Figure 7.21. Conductivity measurements of (a) SDS, (b) SDS stabilized emulsions, (c) STS, (d) STS stabilized emulsions, and (e) SHS.

7.2.5 *Reproducibility of the Experiments*

The reproducibility of the oil exchange experiments was examined by comparing the experimental results obtained at two different beamlines, the VSANS and NGB 30 SANS. The relaxation functions estimated using data from the same q range ($3.0x10^{-3}$ to $3.0x10^{-2}$ $Å^{-1}$) of several emulsion systems are almost identical as shown in Figure 7.22.

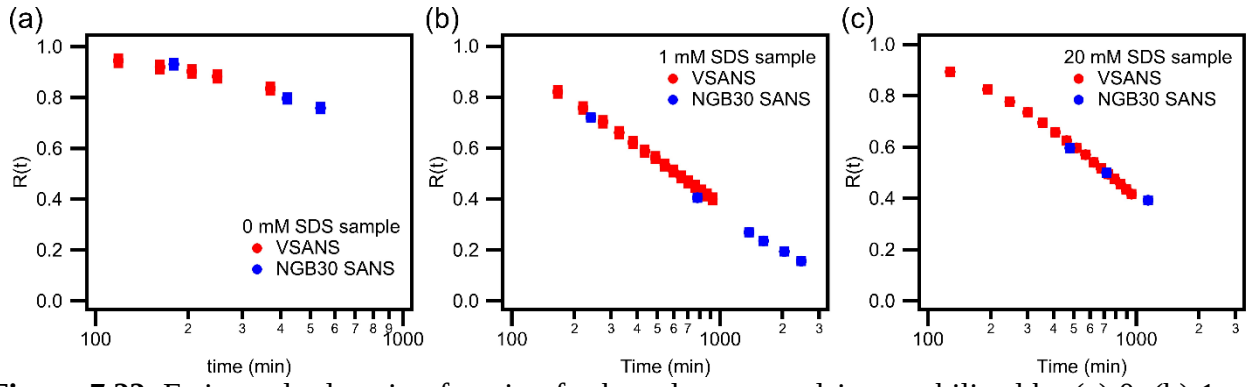

Figure 7.22. Estimated relaxation function for hexadecane emulsions stabilized by (a) 0, (b) 1, and (c) 20 mM SDS using the VSANS and NGB 30 SANS instrument at National Institute of Standards and Technology Center for Neutron Research.

7.3 SUPPORTING INFORMATION FOR CHAPTER 5

7.3.1 *Scattering Profiles of Bare Hexadecane Emulsion System Sonicated at Various Acoustic Pressures*

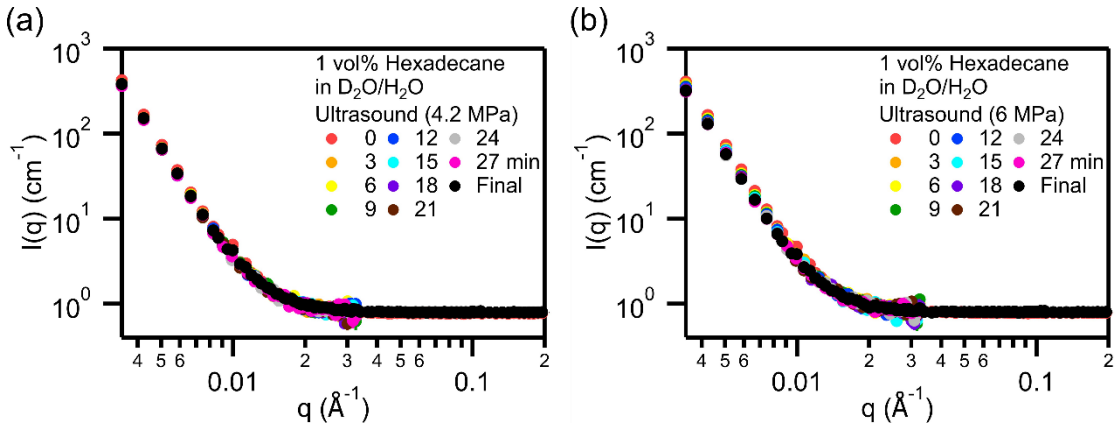

Figure 7.23. Scattering profiles of bare hexadecane emulsion mixtures sonicated at (a) 4.2 and (b) 6 MPa. Slight decrease in scattering intensities over time was only observed in the sample sonicated at 6 MPa.

7.3.2 *Scattering Profiles of Emulsion Oil Exchange While Varying the Concentration of Stabilizing Surfactant Under the Influence of Acoustic Forces*

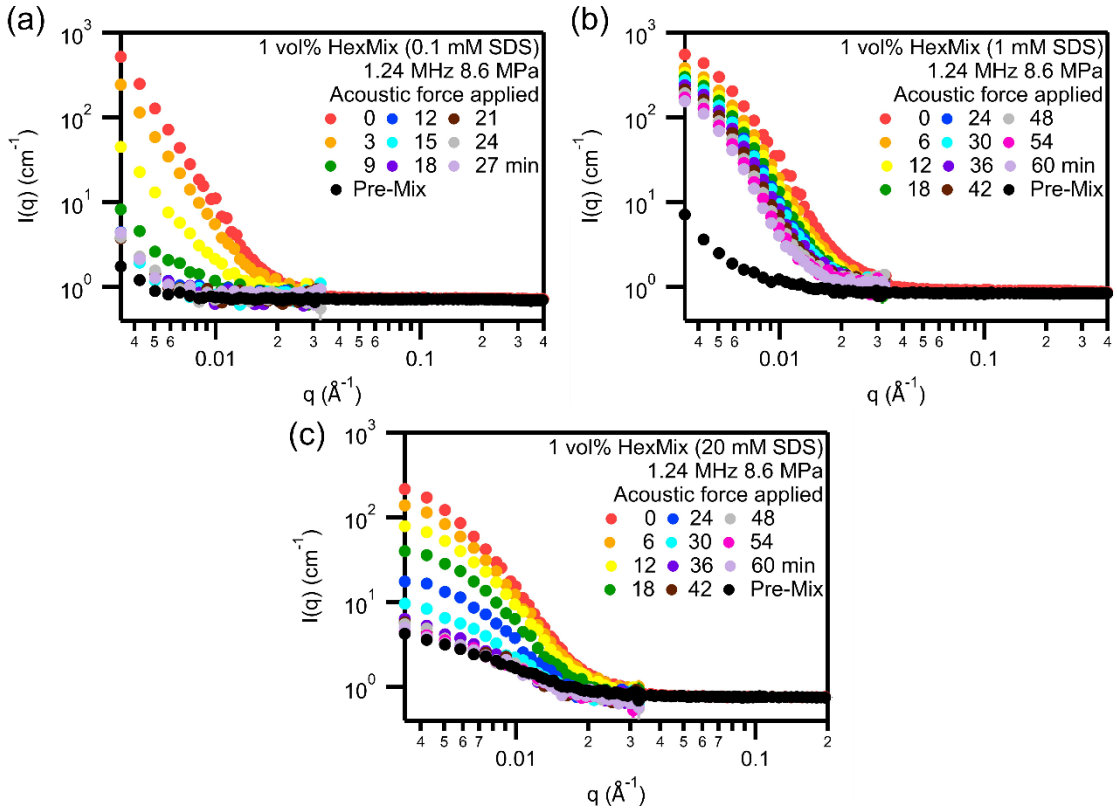

Figure 7.24. Scattering profiles of acoustic force (8.6 MPa) induced oil exchange between hexadecane emulsions stabilized by (a) 0.1, (b) 1, and (c) 20 mM of SDS.

7.3.3 *Scattering Profiles of Emulsion Oil Exchange While Varying Concentration of Stabilizing Surfactant Without the Application of Any Acoustic Forces*

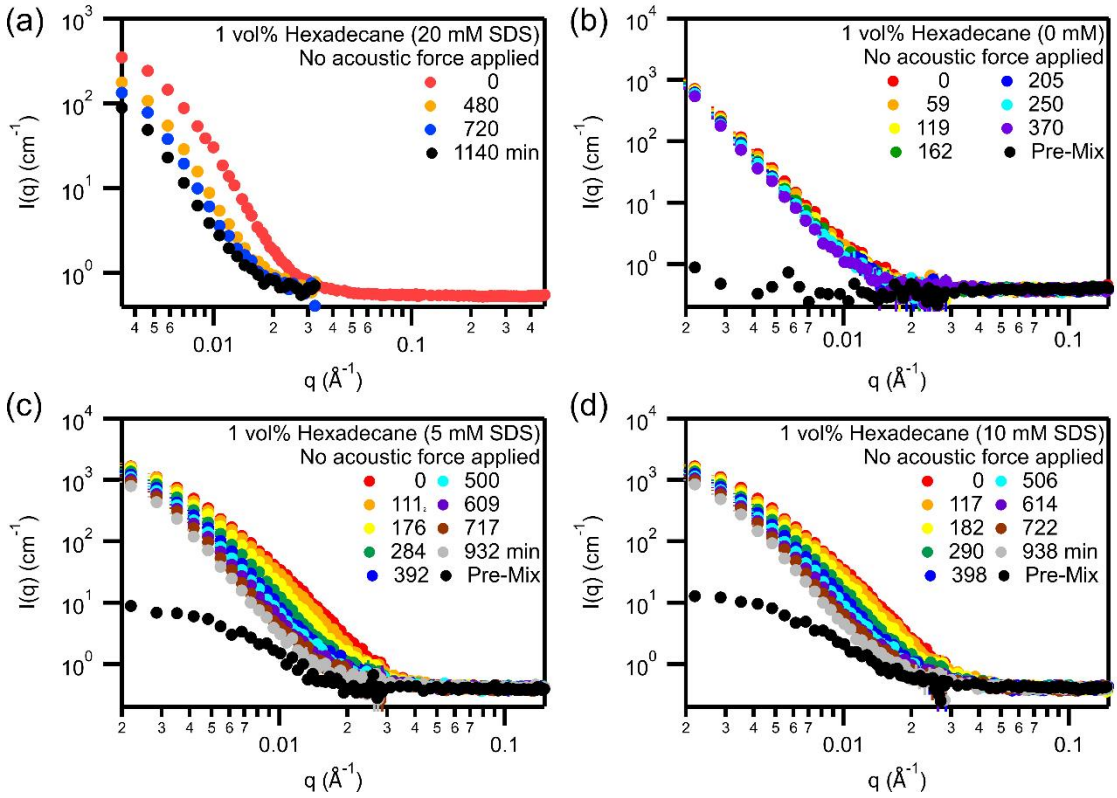

Figure 7.25. Scattering profiles of oil exchange between hexadecane droplets stabilized by (a) 20 (NGB 30 SANS), (b) 0, (c) 5, and 10 mM SDS (VSANS) without the influence of any acoustic forces.

7.3.4 *Dynamic Light Scattering Results for Observing Emulsion Size Change Over Time Under the Influence of Sonication*

The stock emulsions were sonicated using a Branson Digital Sonifier S-450 with a 3 mm sonicating microtip (Branson Ultrasonics, CT, USA) at 30% amplitude 50% duty cycle (1 seconds on and 1 seconds off). Figure 7.26 is a typical result obtained when tracking the emulsion size change during the sonication process. As can be seen in the figure, the emulsions rapidly reached an equilibrium size and additional sonication does not further decrease the size of the emulsions.

The sample shown here contained a relatively low concentration of SDS since generally it takes a longer time for samples containing less surfactants to reach the steady-state emulsion size distribution.

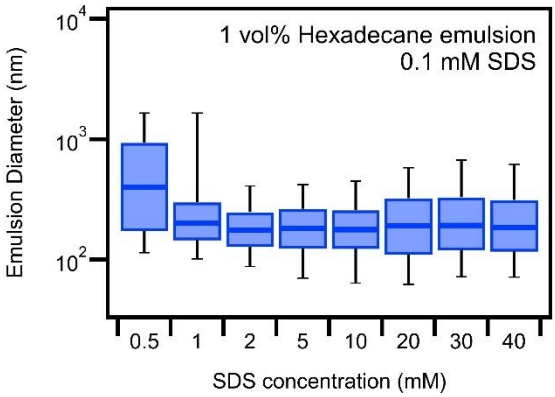

Figure 7.26. Box plot of the emulsion (0.1 mM SDS) size change over time when sonicated using a sonicating horn. The box portion of the plot, from bottom to top, represents the 25th percentile, median, and 75th percentile of the distribution. The whisker portion represents the 5% percentile and 95% percentile

7.4 REFERENCES

(1) Dolan, A. K.; Edwards, S. F. *Proc. R. Soc. A Math. Phys. Eng. Sci.* **1974**, *337* (1611), 509–516.

(2) Li, F.; Pincet, F. *Langmuir* **2007**, *23* (25), 12541–12548.

(3) Larson-Smith, K.; Pozzo, D. C. *Soft Matter* **2011**, *7* (11), 5339–5347.

(4) Larson-Smith, K.; Pozzo, D. C. *Langmuir* **2012**, *28* (32), 11725–11732.

(5) Porter, M. D.; Bright, T. B.; Allara, D. L.; Chidsey, C. E. *J. Am. Chem. Soc.* **1987**, *109* (12), 3559–3568.

(6) Ilavsky, J.; Zhang, F.; Andrews, R. N.; Kuzmenko, I.; Jemian, P. R.; Levine, L. E.; Allen, A. J. *J. Appl. Crystallogr.* **2018**, *51* (3), 867–882.

(7) Chang, H.-C.; Lin, Y.-Y.; Chern, C.-S.; Lin, S.-Y. *Langmuir* **1998**, *14* (23), 6632–6638.

BIBLIOGRAPHY

A Issaka, S. Review on the Fundamental Aspects of Petroleum Oil Emulsions and Techniques of Demulsification. *J. Pet. Environ. Biotechnol.* **2015**, *06* (02).

Ahn, J.-H.; Kim, H.-S.; Lee, K. J.; Jeon, S.; Kang, S. J.; Sun, Y.; Nuzzo, R. G.; Rogers, J. A. Heterogeneous Three-Dimensional Electronics by Use of Printed Semiconductor Nanomaterials. *Science.* **2006**, *314* (5806), 1754–1757.

Antes, F. G.; Diehl, L. O.; Pereira, J. S. F.; Guimarães, R. C. L.; Guarnieri, R. A.; Ferreira, B. M. S.; Dressler, V. L.; Flores, E. M. M. Feasibility of Low Frequency Ultrasound for Water Removal from Crude Oil Emulsions. *Ultrason. Sonochem.* **2015**, *25* (1), 70–75.

Anton, N.; Benoit, J. P.; Saulnier, P. Design and Production of Nanoparticles Formulated from Nano-Emulsion Templates-A Review. *J. Control. Release* **2008**, *128* (3), 185–199.

Anton, N.; Vandamme, T. F. The Universality of Low-Energy Nano-Emulsification. *Int. J. Pharm.* **2009**, *377* (1–2), 142–147.

Antonietti, M. Polyreactions in Miniemulsions. *Prog. Polym. Sci.* **2002**, *27* (4), 689–757.

Apfel, R. E.; Holland, C. K. Gauging the Likelihood of Cavitation from Short-Pulse, Low-Duty Cycle Diagnostic Ultrasound. *Ultrasound Med. Biol.* **1991**, *17* (2), 179–185.

Arnal, B.; Perez, C.; Wei, C.; Xia, J.; Lombardo, M.; Pelivanov, I.; Matula, T. J.; Pozzo, L. D.; Donnell, M. O. Photoacoustics Sono-Photoacoustic Imaging of Gold Nanoemulsions : Part I . Exposure Thresholds. *Photoacoustics* **2015**, *3* (1), 3–10.

Arnal, B.; Wei, C.; Perez, C.; Nguyen, T.; Lombardo, M.; Pelivanov, I.; Pozzo, L. D.; Donnell, M. O. Photoacoustics Sono-Photoacoustic Imaging of Gold Nanoemulsions : Part II . Real Time Imaging. *Photoacoustics* **2015**, *3* (1), 11–19.

Arnal, B.; Wei, C.-W.; Xia, J.; Pelivanov, I. M.; Lombardo, M.; Perez, C.; Matula, T. J.; Pozzo, D.; O'Donnell, M. Inertial Cavitation in Theranostic Nanoemulsions with Simultaneous Pulsed Laser and Low Frequency Ultrasound Excitation. In *SPIE BiOS*; Oraevsky, A. A., Wang, L. V., Eds.; 2014; Vol. 8943, p 89433E.

Aronson, M. P.; Princen, H. M. Contact Angles Associated with Thin Liquid Films in Emulsions. *Nature* **1980**, *286* (5771), 370–372.

Aveyard, R.; Binks, B. P.; Clint, J. H. Emulsions Stabilised Solely by Colloidal Particles. *Adv. Colloid Interface Sci.* **2003**, *100–102*, 503–546.

Aveyard, R.; Clint, J. H. Foam and Thin Film Breakdown Processes. *Curr. Opin. Colloid Interface Sci.* **1996**, *1* (6), 764–770.

Berg, J. C. *An Introduction to Interfaces and Colloids*; WORLD SCIENTIFIC, **2009.**

Berton-Carabin, C. C.; Schroën, K. Pickering Emulsions for Food Applications: Background, Trends, and Challenges. *Annu. Rev. Food Sci. Technol.* **2015**, *6* (1), 263–297.

Bhanvase, B. A.; Pinjari, D. V.; Sonawane, S. H.; Gogate, P. R.; Pandit, A. B. Analysis of Semibatch Emulsion Polymerization: Role of Ultrasound and Initiator. *Ultrason. Sonochem.* **2012**, *19* (1), 97–103.

Bhanvase, B. A.; Sonawane, S. H. Ultrasound Assisted in Situ Emulsion Polymerization for Polymer Nanocomposite: A Review. *Chem. Eng. Process. Process Intensif.* **2014**, *85*, 86–107.

Bibette, J.; Mason, T. G.; Gang, H.; Weitz, D. A.; Poulin, P. Structure of Adhesive Emulsions. *Langmuir* **1993**, *9* (12), 3352–3356.

Binks, B. P. Particles as Surfactants—Similarities and Differences. *Curr. Opin. Colloid Interface Sci.* **2002**, *7* (1–2), 21–41.

Binks, B. P.; Clint, J. H. Solid Wettability from Surface Energy Components: Relevance to Pickering Emulsions. *Langmuir* **2002**, *18* (4), 1270–1273.

Binks, B. P.; Clint, J. H.; Fletcher, P. D. I.; Lees, T. J. G.; Taylor, P. Growth of Gold Nanoparticle Films Driven by the Coalescence of Particle-Stabilized Emulsion Drops. *Langmuir* **2006**, *22* (9), 4100–4103.

Binks, B. P.; Clint, J. H.; Fletcher, P. D. I.; Rippon, S.; Lubetkin, S. D.; Mulqueen, P. J. Kinetics of Swelling of Oil-in-Water Emulsions. *Langmuir* **1998**, *14* (19), 5402–5411.

Binks, B. P.; Lumsdon, S. O. Catastrophic Phase Inversion of Water-in-Oil Emulsions Stabilized by Hydrophobic Silica. *Langmuir* **2000**, *16* (6), 2539–2547.

Bondy, C.; Söllner, K. On the Mechanism of Emulsification by Ultrasonic Waves. *Trans. Faraday Soc.* **1935**, *31*, 835–843.

Bondy, C.; Söllner, K. The Influence of Gases on Mercury Emulsions Prepared by Ultrasonic Waves. *Trans. Faraday Soc.* **1935**, *31* (C), 843–846.

Bradley, M.; Grieser, F. Emulsion Polymerization Synthesis of Cationic Polymer Latex in an Ultrasonic Field. *J. Colloid Interface Sci.* **2002**, *251* (1), 78–84.

Bruce J. Berne, R. P. *Dynamic Light Scattering: With Applications to Chemistry, Biology, and Physics*; **1976**.

Burguera, J. L.; Burguera, M. Analytical Applications of Emulsions and Microemulsions. *Talanta* **2012**, *96*, 11–20.

Canselier, J. P.; Delmas, H.; Wilhelm, A. M.; Abismaïl, B. Ultrasound Emulsification—An Overview. *J. Dispers. Sci. Technol.* **2002**, *23* (1–3), 333–349.

Capek, I. On Inverse Miniemulsion Polymerization of Conventional Water-Soluble Monomers. *Adv. Colloid Interface Sci.* **2010**, *156* (1–2), 35–61.

Chang, H.-C.; Lin, Y.-Y.; Chern, C.-S.; Lin, S.-Y. Determination of Critical Micelle Concentration of Macroemulsions and Miniemulsions. *Langmuir* **1998**, *14* (23), 6632–6638.

Check, G. R. Two-Stage Ultrasonic Irradiation for Dehydration and Desalting of Crude Oil: A Novel Method. *Chem. Eng. Process. Process Intensif.* **2014**, *81*, 72–78.

Chern, C. S. Emulsion Polymerization Mechanisms and Kinetics. *Prog. Polym. Sci.* **2006**, *31* (5), 443–486.

Chevalier, Y.; Bolzinger, M.-A. Emulsions Stabilized with Solid Nanoparticles: Pickering Emulsions. *Colloids Surfaces A Physicochem. Eng. Asp.* **2013**, *439*, 23–34.

Choi, S. H.; Lodge, T. P.; Bates, F. S. Mechanism of Molecular Exchange in Diblock Copolymer Micelles: Hypersensitivity to Core Chain Length. *Phys. Rev. Lett.* **2010**, *104* (4), 1–4.

Christov, N. C.; Danov, K. D.; Zeng, Y.; Kralchevsky, P. A.; von Klitzing, R. Oscillatory Structural Forces Due to Nonionic Surfactant Micelles: Data by Colloidal−Probe AFM vs Theory. *Langmuir* **2010**, *26* (2), 915–923.

Clark, S.; Fletcher, P. D. I.; Ye, X. Interdroplet Exchange Rates of Water-in-Oil and Oil-in-Water Microemulsion Droplets Stabilized by Pentaoxyethylene Monododecyl Ether. *Langmuir* **1990**, *6* (7), 1301–1309.

Cucheval, A.; Chow, R. C. Y. A Study on the Emulsification of Oil by Power Ultrasound. *Ultrason. Sonochem.* **2008**, *15* (5), 916–920.

Dan, N. Transport and Release in Nano-Carriers for Food Applications. *J. Food Eng.* **2016**, *175*, 136–144.

David B. Williams, C. B. C. *The Transmission Electron Microscope*; **1996**.

Debye, P. Molecular-Weight Determination by Light Scattering. *J. Phys. Colloid Chem.* **1946**, *18* (1), 18–32.

Debye, P. Zerstreuung von Röntgenstrahlen. *Ann. Phys.* **1915**, *351* (6), 809–823.

Del Campo, F. J.; Coles, B. A.; Marken, F.; Compton, R. G.; Cordemans, E. High-Frequency Sonoelectrochemical Processes: Mass Transport, Thermal and Surface Effects Induced by Cavitation in a 500 KHz Reactor. *Ultrason. Sonochem.* **1999**, *6* (4), 189–197.

Destribats, M.; Rouvet, M.; Gehin-Delval, C.; Schmitt, C.; Binks, B. P. Emulsions Stabilised by Whey Protein Microgel Particles: Towards Food-Grade Pickering Emulsions. *Soft Matter* **2014**, *10* (36), 6941–6954.

Doktycz, S.; Suslick, K. Interparticle Collisions Driven by Ultrasound. *Science* **1990**, *247* (4946), 1067–1069.

Dolan, A. K.; Edwards, S. F. Theory of the Stabilization of Colloids by Adsorbed Polymer. *Proc. R. Soc. A Math. Phys. Eng. Sci.* **1974**, *337* (1611), 509–516.

Drelich, A.; Grossiord, J. L.; Gomez, F.; Clausse, D.; Pezron, I. Mixed O/W Emulsions Stabilized by Solid Particles: A Model System for Controlled Mass Transfer Triggered by Surfactant Addition. *J. Colloid Interface Sci.* **2012**, *386* (1), 218–227.

Entezari, M. H.; Ghows, N. Micro-Emulsion under Ultrasound Facilitates the Fast Synthesis of Quantum Dots of CdS at Low Temperature. *Ultrason. Sonochem.* **2011**, *18* (1), 127–134.

Fabiilli, M. L.; Haworth, K. J.; Fakhri, N. H.; Kripfgans, O. D.; Carson, P. L.; Fowlkes, J. B. The Role of Inertial Cavitation in Acoustic Droplet Vaporization. *IEEE Trans. Ultrason. Ferroelectr. Freq. Control* **2009**, *56* (5), 1006–1017.

Fletcher, P. D. I.; Horsup, D. I. Droplet Dynamics in Water-in-Oil Microemulsions and Macroemulsions Stabilised by Non-Ionic Surfactants. Correlation of Measured Rates with Monolayer Bending Elasticity. *J. Chem. Soc. Faraday Trans.* **1992**, *88* (6), 855–864.

Fletcher, P. D. I.; Howe, A. M.; Robinson, B. H. The Kinetics of Solubilisate Exchange between Water Droplets of a Water-in-Oil Microemulsion. *J. Chem. Soc. Faraday Trans. 1 Phys. Chem. Condens. Phases* **1987**, *83* (4), 985–1006.

Flint, E. B.; Suslick, K. S. The Temperature of Cavitation. *Science* **1991**, *253* (5026), 1397–1399.

Frens, G. Controlled Nucleation for the Regulation of the Particle Size in Monodisperse Gold Suspensions. *Nat. Phys. Sci.* **1973**, *241* (105), 20–22.

Gaikwad, S. G.; Pandit, A. B. Ultrasound Emulsification: Effect of Ultrasonic and Physicochemical Properties on Dispersed Phase Volume and Droplet Size. *Ultrason. Sonochem.* **2008**, *15* (4), 554–563.

Garbin, V.; Crocker, J. C.; Stebe, K. J. Nanoparticles at Fluid Interfaces: Exploiting Capping Ligands to Control Adsorption, Stability and Dynamics. *J. Colloid Interface Sci.* **2012**, *387* (1), 1–11.

Gerelli, Y.; Porcar, L.; Lombardi, L.; Fragneto, G. Lipid Exchange and Flip-Flop in Solid Supported Bilayers. *Langmuir* **2013**, *29* (41), 12762–12769.

Gibbs, J. W. On the Equilibrium of Heterogeneous Substances. *Trans. Connect. Acad. Arts Sci.* **1878**, *3*, 343–524.

Giesecke, T.; Hynynen, K. Ultrasound-Mediated Cavitation Thresholds of Liquid Perfluorocarbon Droplets in Vitro. *Ultrasound Med. Biol.* **2003**, *29* (9), 1359–1365.

Gondrexon, N.; Cheze, L.; Jin, Y.; Legay, M.; Tissot, Q.; Hengl, N.; Baup, S.; Boldo, P.; Pignon, F.; Talansier, E. Intensification of Heat and Mass Transfer by Ultrasound: Application to Heat Exchangers and Membrane Separation Processes. *Ultrason. Sonochem.* **2015**, *25* (1), 40–50.

Gould, J.; Garcia-Garcia, G.; Wolf, B. Pickering Particles Prepared from Food Waste. *Materials (Basel).* **2016**, *9* (9), 791.

Guillot, S.; Bergaya, F.; de Azevedo, C.; Warmont, F.; Tranchant, J.-F. Internally Structured Pickering Emulsions Stabilized by Clay Mineral Particles. *J. Colloid Interface Sci.* **2009**, *333* (2), 563–569.

Guinier, A and Fournet, G. Small-Angle Scattering of X-Rays. *John Wiley & Sons, Inc*. 1955.

Haiss, W.; Thanh, N. T. K.; Aveyard, J.; Fernig, D. G. Determination of Size and Concentration of Gold Nanoparticles from UV - Vis Spectra. **2007**, *79* (13), 4215–4221.

Hamidi, H.; Mohammadian, E.; Asadullah, M.; Azdarpour, A.; Rafati, R. Effect of Ultrasound Radiation Duration on Emulsification and Demulsification of Paraffin Oil and Surfactant Solution/Brine Using Hele-Shaw Models. *Ultrason. Sonochem.* **2015**, *26*, 428–436.

Hammouda, B. Probing Nanoscale Structures: The SANS Toolbox. **2008**.

Hauss, D. J.; Fogal, S. E.; Ficorilli, J. V; Price, C. A.; Roy, T.; Jayaraj, A. A.; Keirns, J. J. Lipid-Based Delivery Systems for Improving the Bioavailability and Lymphatic Transport of a Poorly Water-Soluble LTB4 Inhibitor. *J. Pharm. Sci.* **1998**, *87* (2), 164–169.

Hettiarachchi, K.; Zhang, S.; Feingold, S.; Lee, A. P.; Dayton, P. A. Controllable Microfluidic Synthesis of Multiphase Drug-Carrying Lipospheres for Site-Targeted Therapy. *Biotechnol. Prog.* **2009**, *25* (4), 938–945.

Hoang, T. K. N.; La, V. B.; Deriemaeker, L.; Finsy, R. Ostwald Ripening and Solubilization in Alkane in Water Emulsions Stabilized by Different Surfactants. *Phys. Chem. Chem. Phys.* **2004**, *6* (7), 1413–1422.

Holt, Ø.; Sˆther, Ø.; Sjo¨blom, J.; Dukhin, S. S.; Mishchuk, N. A. Video Enhanced Microscopic Investigation of Reversible Brownian Coagulation in Dilute Oil-in-Water Emulsions. *Colloids Surfaces A Physicochem. Eng. Asp.* **1997**, *123–124*, 195–207.

Hung, C. F.; Fang, C. L.; Liao, M. H.; Fang, J. Y. The Effect of Oil Components on the Physicochemical Properties and Drug Delivery of Emulsions: Tocol Emulsion versus Lipid Emulsion. *Int. J. Pharm.* **2007**, *335* (1–2), 193–202.

Ilavsky, J.; Jemian, P. R. Irena: Tool Suite for Modeling and Analysis of Small-Angle Scattering. *J. Appl. Crystallogr.* **2009**, *42* (2), 347–353.

Ilavsky, J.; Zhang, F.; Andrews, R. N.; Kuzmenko, I.; Jemian, P. R.; Levine, L. E.; Allen, A. J. Development of Combined Microstructure and Structure Characterization Facility for in Situ and Operando Studies at the Advanced Photon Source. *J. Appl. Crystallogr.* **2018**, *51* (3), 867–882.

Ivanov, I. B.; Kralchevsky, P. A. Stability of Emulsions under Equilibrium and Dynamic Conditions. *Colloids Surfaces A Physicochem. Eng. Asp.* **1997**, *128* (1–3), 155–175.

Jain, P. K.; Lee, K. S.; El-Sayed, I. H.; El-Sayed, M. A. Calculated Absorption and Scattering Properties of Gold Nanoparticles of Different Size, Shape, and Composition: Applications in Biological Imaging and Biomedicine. *J. Phys. Chem. B* **2006**, *110*, 7238–7248.

Jansen, T. G. T.; Lovell, P. A.; Meuldijk, J.; Van Herk, A. M. Mass Transfer in Miniemulsion Polymerisation. *Macromol. Symp.* **2013**, *333* (1), 24–34.

Joscelyne, S. M.; Trägårdh, G. Membrane Emulsification — a Literature Review. **2000**, *169* (April 1999), 107–117.

Kabalnov, A.; Makarov, K.; Pertzov, A.; Shchukin, E. . Ostwald Ripening in Emulsions. *J. Colloid Interface Sci.* **1990**, *138* (1), 98–104.

Kabalnov, A. S. Can Micelles Mediate a Mass Transfer between Oil Droplets? *Langmuir* **1994**, *10* (3), 680–684.

Kaci, M.; Arab-Tehrany, E.; Desjardins, I.; Banon-Desobry, S.; Desobry, S. Emulsifier Free Emulsion: Comparative Study between a New High Frequency Ultrasound Process and Standard Emulsification Processes. *J. Food Eng.* **2017**, *194*, 109–118.

Kaci, M.; Meziani, S.; Arab-Tehrany, E.; Gillet, G.; Desjardins-Lavisse, I.; Desobry, S. Emulsification by High Frequency Ultrasound Using Piezoelectric Transducer: Formation and Stability of Emulsifier Free Emulsion. *Ultrason. Sonochem.* **2014**, *21* (3), 1010–1017.

Kaewsaneha, C.; Tangboriboonrat, P.; Polpanich, D.; Eissa, M.; Elaissari, A. Preparation of Janus Colloidal Particles via Pickering Emulsion: An Overview. *Colloids Surfaces A Physicochem. Eng. Asp.* **2013**, *439*, 35–42.

Kentish, S.; Wooster, T. J.; Ashokkumar, M.; Balachandran, S.; Mawson, R.; Simons, L. The Use of Ultrasonics for Nanoemulsion Preparation. *Innov. Food Sci. Emerg. Technol.* **2008**, *9* (2), 170–175.

Kilpatrick, P. K. Water-in-Crude Oil Emulsion Stabilization: Review and Unanswered Questions. *Energy and Fuels* **2012**, *26* (7), 4017–4026.

Kline, S. R. Reduction and Analysis of SANS and USANS Data Using IGOR Pro. *J. Appl. Crystallogr.* **2006**, *39* (6), 895–900.

Köhler, K.; Santana, A. S.; Braisch, B.; Preis, R.; Schuchmann, H. P. High Pressure Emulsification with Nano-Particles as Stabilizing Agents. *Chem. Eng. Sci.* **2010**, *65* (10), 2957–2964.

Kokal, S. L. Crude Oil Emulsions: A State-Of-The-Art Review. *SPE Prod. Facil.* **2005**, *20* (01), 5–13.

Koo, O. M.; Rubinstein, I.; Onyuksel, H. Role of Nanotechnology in Targeted Drug Delivery and Imaging: A Concise Review. *Nanomedicine Nanotechnology, Biol. Med.* **2005**, *1* (3), 193–212.

Lamprecht, B.; Schider, G.; Lechner, R. T.; Ditlbacher, H.; Krenn, J. R.; Leitner, A.; Aussenegg, F. R. Metal Nanoparticle Gratings: Influence of Dipolar Particle Interaction on the Plasmon Resonance. *Phys. Rev. Lett.* **2000**, *84* (20), 4721–4724.

Larson-Smith, K.; Jackson, A.; Pozzo, D. C. SANS and SAXS Analysis of Charged Nanoparticle Adsorption at Oil–Water Interfaces. *Langmuir* **2012**, *28* (5), 2493–2501.

Larson-Smith, K.; Jackson, A.; Pozzo, D. C. Small Angle Scattering Model for Pickering Emulsions and Raspberry Particles. *J. Colloid Interface Sci.* **2010**, *343* (1), 36–41.

Larson-Smith, K.; Pozzo, D. C. Pickering Emulsions Stabilized by Nanoparticle Surfactants. *Langmuir* **2012**, *28* (32), 11725–11732.

Larson-Smith, K.; Pozzo, D. C. Scalable Synthesis of Self-Assembling Nanoparticle Clusters Based on Controlled Steric Interactions. *Soft Matter* **2011**, *7* (11), 5339–5347.

Leal-Calderon, F.; Poulin, P. Progress in Understanding Emulsion Metastability and Surface Forces. *Curr. Opin. Colloid Interface Sci.* **1999**, *4* (3), 223–230.

Lee, Y.-T.; Li, D. S.; Ilavsky, J.; Kuzmenko, I.; Jeng, G.-S.; O'Donnell, M.; Pozzo, L. D. Ultrasound-Based Formation of Nano-Pickering Emulsions Investigated via in-Situ SAXS. *J. Colloid Interface Sci.* **2019**, *536*, 281–290.

Legay, M.; Gondrexon, N.; Le Person, S.; Boldo, P.; Bontemps, A. Enhancement of Heat Transfer by Ultrasound: Review and Recent Advances. *Int. J. Chem. Eng.* **2011**, *2011*, 1–17.

Li, D. S.; Lee, Y.-T.; Xi, Y.; Pelivanov, I.; O'Donnell, M.; Pozzo, L. D. A Small-Angle Scattering Environment for in Situ Ultrasound Studies. *Soft Matter* **2018**, *14* (25), 5283–5293.

Li, D. S.; Yoon, S. J.; Pelivanov, I.; Frenz, M.; O'Donnell, M.; Pozzo, L. D. Polypyrrole-Coated Perfluorocarbon Nanoemulsions as a Sono-Photoacoustic Contrast Agent. *Nano Lett.* **2017**, *17* (10), 6184–6194.

Li, F.; Pincet, F. Confinement Free Energy of Surfaces Bearing End-Grafted Polymers in the Mushroom Regime and Local Measurement of the Polymer Density. *Langmuir* **2007**, *23* (25), 12541–12548.

Li, M. K.; Fogler, H. S. Acoustic Emulsification. Part 2. Breakup of the Large Primary Oil Droplets in a Water Medium. *J. Fluid Mech.* **1978**, *88* (03), 513.

Link, S.; Mohamed, M. B.; El-Sayed, M. A. Simulation of the Optical Absorption Spectra of Gold Nanorods as a Function of Their Aspect Ratio and the Effect of the Medium Dielectric Constant. *J. Phys. Chem. B* **1999**, *103* (16), 3073–3077.

Lu, J.; Choi, S.; Bates, F. S.; Lodge, T. P. Molecular Exchange in Diblock Copolymer Micelles: Bimodal Distribution in Core-Block Molecular Weights. *ACS Macro Lett.* **2012**, *1* (8), 982–985.

Lucassen-Reynders, E. H.; Cagna, A.; Lucassen, J. Gibbs Elasticity, Surface Dilational Modulus and Diffusional Relaxation in Nonionic Surfactant Monolayers. *Colloids Surfaces A Physicochem. Eng. Asp.* **2001**, *186* (1–2), 63–72.

Lund, R.; Willner, L.; Pipich, V.; Grillo, I.; Lindner, P.; Colmenero, J.; Richter, D. Equilibrium Chain Exchange Kinetics of Diblock Copolymer Micelles: Effect of Morphology. *Macromolecules* **2011**, *44* (15), 6145–6154.

Lund, R.; Willner, L.; Richter, D. Kinetics of Block Copolymer Micelles Studied by Small-Angle Scattering Methods. In *Advances in Polymer Science*; **2013;** pp 51–158.

Lund, R.; Willner, L.; Richter, D.; Dormidontova, E. E. Equilibrium Chain Exchange Kinetics of Diblock Copolymer Micelles: Tuning and Logarithmic Relaxation. *Macromolecules* **2006**, *39* (13), 4566–4575.

Malassagne-Bulgarelli, N.; McGrath, K. M. Dynamics of Oil Transfer in Oil-in-Water Emulsions. *Soft Matter* **2009**, *5* (23), 4804.

Malassagne-Bulgarelli, N.; McGrath, K. M. Emulsion Ageing: Effect on the Dynamics of Oil Exchange in Oil-in-Water Emulsions. *Soft Matter* **2013**, *9* (1), 48–59.

Manor, O.; Chau, T. T.; Stevens, G. W.; Chan, D. Y. C.; Grieser, F.; Dagastine, R. R. Polymeric Stabilized Emulsions: Steric Effects and Deformation in Soft Systems. *Langmuir* **2012**, *28* (10), 4599–4604.

Mao, L.; Roos, Y. H.; Biliaderis, C. G.; Miao, S. Food Emulsions as Delivery Systems for Flavor Compounds: A Review. *Crit. Rev. Food Sci. Nutr.* **2017**, *57* (15), 3173–3187.

Marinova, K. G.; Gurkov, T. D.; Dimitrova, T. D.; Alargova, R. G.; Smith, D. Role of Oscillatory Structural Forces for Interactions in Thin Emulsion Films Containing Micelles. *Langmuir* **1998**, *14* (8), 2011–2019.

Marto, J.; Ascenso, A.; Gonçalves, L. M.; Gouveia, L. F.; Manteigas, P.; Pinto, P.; Oliveira, E.; Almeida, A. J.; Ribeiro, H. M. Melatonin-Based Pickering Emulsion for Skin's Photoprotection. *Drug Deliv.* **2016**, *23* (5), 1594–1607.

Matsunaga, T. O.; Sheeran, P. S.; Luois, S.; Streeter, J. E.; Mullin, L. B.; Banerjee, B.; Dayton, P. A. Phase-Change Nanoparticles Using Highly Volatile Perfluorocarbons: Toward a Platform for Extravascular Ultrasound Imaging. *Theranostics* **2012**, *2* (12), 1185–1198.

McClements, D. J. Nanoemulsions versus Microemulsions: Terminology, Differences, and Similarities. *Soft Matter* **2012**, *8* (6), 1719–1729.

McClements, D. J.; Dungan, S. R. Factors That Affect the Rate of Oil Exchange between Oil-in-Water Emulsion Droplets Stabilized by a Nonionic Surfactant: Droplet Size, Surfactant Concentration, and Ionic Strength. *J. Phys. Chem.* **1993**, *97* (28), 7304–7308.

McClements, D. J.; Dungan, S. R.; German, J. B.; Kinsella, J. E. Factors Which Affect Oil Exchange between Oil-in-Water Emulsion Droplets Stabilized by Whey Protein Isolate: Protein Concentration, Droplet Size and Ethanol. *Colloids Surfaces A Physicochem. Eng. Asp.* **1993**, *81* (C), 203–210.

McClements, D. J.; Dungan, S. R.; German, J. B.; Kinsella, J. E. Oil Exchange between Oil-in-Water Emulsion Droplets Stabilised with a Non-Ionic Surfactant. *Top. Catal.* **1992**, *6* (5), 415–422.

McLean, J. D.; Kilpatrick, P. K. Effects of Asphaltene Solvency on Stability of Water-in-Crude-Oil Emulsions. *J. Colloid Interface Sci.* **1997**, *189* (2), 242–253.

Moholkar, V. S.; Warmoeskerken, M. M. C. G. Investigations in Mass Transfer Enhancement in Textiles with Ultrasound. *Chem. Eng. Sci.* **2004**, *59* (2), 299–311.

Mondain-Monval, O.; Leal-Calderon, F.; Phillip, J.; Bibette, J. Depletion Forces in the Presence of Electrostatic Double Layer Repulsion. *Phys. Rev. Lett.* **1995**, *75* (18), 3364–3367.

Moroi, Y.; Motomura, K.; Matuura, R. The Critical Micelle Concentration of Sodium Dodecyl Sulfate-Bivalent Metal Dodecyl Sulfate Mixtures in Aqueous Solutions. *J. Colloid Interface Sci.* **1974**, *46* (1), 111–117.

Mountford, P. A.; Borden, M. A. On the Thermodynamics and Kinetics of Superheated Fluorocarbon Phase-Change Agents. *Adv. Colloid Interface Sci.* **2016**, *237*, 15–27.

Mujumdar, S.; Senthil Kumar, P.; Pandit, A. B. Emulsification by Ultrasound: Relation between Intensity and Emulsion Quality. *Indian J. Chem. Technol.* **1997**, *4* (6), 277–284.

Nakano, M.; Fukuda, M.; Kudo, T.; Endo, H.; Handa, T. Determination of Interbilayer and Transbilayer Lipid Transfers by Time-Resolved Small-Angle Neutron Scattering. *Phys. Rev. Lett.* **2007**, *98* (23), 30–33.

Nakano, M.; Fukuda, M.; Kudo, T.; Matsuzaki, N.; Azuma, T.; Sekine, K.; Endo, H.; Handa, T. Flip-Flop of Phospholipids in Vesicles: Kinetic Analysis with Time-Resolved Small-Angle Neutron Scattering. *J. Phys. Chem. B* **2009**, *113* (19), 6745–6748.

Nazarzadeh, E.; Anthonypillai, T.; Sajjadi, S. On the Growth Mechanisms of Nanoemulsions. *J. Colloid Interface Sci.* **2013**, *397*, 154–162.

Neutron, X-Rays and Light: Scattering Methods Applied to Soft Condensed Matter, 1st ed.; Lindner, P., Zemb, T., Eds.; North Holland, 2002.

Nguyen, M. H. L.; DiPasquale, M.; Rickeard, B. W.; Stanley, C. B.; Kelley, E. G.; Marquardt, D. Methanol Accelerates DMPC Flip-Flop and Transfer: A SANS Study on Lipid Dynamics. *Biophys. J.* **2019**, *116* (5), 755–759.

NIST neutron activation and scattering calculator
https://www.ncnr.nist.gov/resources/activation/.

Peña, A. A.; Miller, C. A. Solubilization Rates of Oils in Surfactant Solutions and Their Relationship to Mass Transport in Emulsions. *Adv. Colloid Interface Sci.* **2006**, *123–126* (SPEC. ISS.), 241–257.

Petsev, D. N.; Denkov, N. D.; Kralchevsky, P. A. Flocculation of Deformable Emulsion Droplets. Ii. Interaction Energy. *J. Colloid Interface Sci.* **1995**, *176* (1), 201–213.

Pickering, S. U. CXCVI.—Emulsions. *J. Chem. Soc., Trans.* **1907**, *91*, 2001–2021.

Porter, M. D.; Bright, T. B.; Allara, D. L.; Chidsey, C. E. Spontaneously Organized Molecular Assemblies. 4. Structural Characterization of n-Alkyl Thiol Monolayers on Gold by Optical Ellipsometry, Infrared Spectroscopy, and Electrochemistry. *J. Am. Chem. Soc.* **1987**, *109* (12), 3559–3568.

Poulin, P.; Nallet, F.; Cabane, B.; Bibette, J. Evidence for Newton Black Films between Adhesive Emulsion Droplets. *Phys. Rev. Lett.* **1996**, *77* (15), 3248–3251.

Prochazka, K.; Kiserow, D.; Ramireddy, C.; Tuzar, Z.; Munk, P.; Webber, S. E. Time-Resolved Fluorescence Studies of the Chain Dynamics of Naphthalene-Labeled Polystyrene-Block-Poly(Methacrylic Acid) Micelles in Aqueous Media. *Macromolecules* **1992**, *25* (1), 454–460.

Roger, K.; Olsson, U.; Schweins, R.; Cabane, B. Emulsion Ripening through Molecular Exchange at Droplet Contacts. *Angew. Chemie Int. Ed.* **2015**, *54* (5), 1452–1455.

Rose, P. F. *ENDF-201: ENDF/B-VI Summary Documentation*; Upton, NY, **1991.**

Schad, K. C.; Hynynen, K. In Vitro Characterization of Perfluorocarbon Droplets for Focused Ultrasound Therapy. *Phys. Med. Biol.* **2010**, *55* (17), 4933–4947.

Schmitt, V.; Cattelet, C.; Leal-Calderon, F. Coarsening of Alkane-in-Water Emulsions Stabilized by Nonionic Poly(Oxyethylene) Surfactants: The Role of Molecular Permeation and Coalescence. *Langmuir* **2004**, *20* (1), 46–52.

Sheeran, P. S.; Matsunaga, T. O.; Dayton, P. A. Phase Change Events of Volatile Liquid Perfluorocarbon Contrast Agents Produce Unique Acoustic Signatures. *Phys. Med. Biol.* **2014**, *59* (2), 379–401.

Shinoda, K.; Saito, H. The Effect of Temperature on the Phase Equilibria and the Types of Dispersions of the Ternary System Composed of Water, Cyclohexane, and Nonionic Surfactant. *J. Colloid Interface Sci.* **1968**, *26* (1), 70–74.

Simovic, S.; Prestidge, C. A. Hydrophilic Silica Nanoparticles at the PDMS Droplet−Water Interface. *Langmuir* **2003**, *19* (9), 3785–3792.

Skelhon, T. S.; Grossiord, N.; Morgan, A. R.; Bon, S. A. F. Quiescent Water-in-Oil Pickering Emulsions as a Route toward Healthier Fruit Juice Infused Chocolate Confectionary. *J. Mater. Chem.* **2012**, *22* (36), 19289.

Skerget, M.; Kotnik, P.; Hadolin, M.; Hras, A. R.; Simonic, M.; Knez, Z. Phenols, Proanthocyanidins, Flavones and Flavonols in Some Plant Materials and Their Antioxidant Activities. *Food Chem.* **2005**, *89* (2), 191–198.

Skhiri, Y.; Gruner, P.; Semin, B.; Brosseau, Q.; Pekin, D.; Mazutis, L.; Goust, V.; Kleinschmidt, F.; El Harrak, A.; Hutchison, J. B.; et al. Dynamics of Molecular Transport by Surfactants in Emulsions. *Soft Matter* **2012**, *8* (41), 10618.

Solans, C.; Izquierdo, P.; Nolla, J.; Azemar, N.; Garciacelma, M. Nano-Emulsions. *Curr. Opin. Colloid Interface Sci.* **2005**, *10* (3–4), 102–110.

Stocco, A.; Rio, E.; Binks, B. P.; Langevin, D. Aqueous Foams Stabilized Solely by Particles. *Soft Matter* **2011**, *7* (4), 1260.

Suslick, K. S.; Price, G. J. APPLICATIONS OF ULTRASOUND TO MATERIALS CHEMISTRY. *Annu. Rev. Mater. Sci.* **1999**, *29* (1), 295–326.

Taisne, L.; Cabane, B. Emulsification and Ripening Following a Temperature Quench. *Langmuir* **1998**, *14* (17), 4744–4752.

Taisne, L.; Walstra, P.; Cabane, B. Transfer of Oil between Emulsion Droplets. *J. Colloid Interface Sci.* **1996**, *184* (2), 378–390.

Tang, J.; Quinlan, P. J.; Tam, K. C. Stimuli-Responsive Pickering Emulsions: Recent Advances and Potential Applications. *Soft Matter* **2015**, *11* (18), 3512–3529.

Taylor, P. Ostwald Ripening in Emulsions. *Adv. Colloid Interface Sci.* **1998**, *75* (2), 107–163.

Taylor, P. Ostwald Ripening in Emulsions. *Colloids Surfaces A Physicochem. Eng. Asp.* **1995**, *99* (2–3), 175–185.

Tempel, M. van den; Lucassen, J.; Lucassen-Reynders, E. H. Application of Surface Thermodynamics to Gibbs Elasticity. *J. Phys. Chem.* **1965**, *69* (6), 1798–1804.

Teo, B. M.; Prescott, S. W.; Ashokkumar, M.; Grieser, F. Ultrasound Initiated Miniemulsion Polymerization of Methacrylate Monomers. *Ultrason. Sonochem.* **2008**, *15* (1), 89–94.

Thickett, S. C.; Gilbert, R. G. Emulsion Polymerization: State of the Art in Kinetics and Mechanisms. *Polymer* **2007**, *48* (24), 6965–6991.

Trujillo, F. J.; Juliano, P.; Barbosa-Cánovas, G.; Knoerzer, K. Separation of Suspensions and Emulsions via Ultrasonic Standing Waves - A Review. *Ultrason. Sonochem.* **2014**, *21* (6), 2151–2164.

Tu, F.; Park, B. J.; Lee, D. Thermodynamically Stable Emulsions Using Janus Dumbbells as Colloid Surfactants. *Langmuir* **2013**, *29* (41), 12679–12687.

Uno, T.; Kazui, T.; Suzuki, Y.; Hashimoto, H.; Suzuki, K.; Muhammad, B. A. M. Pharmacokinetic Advantages of a Newly Developed Tacrolimus Oil-in- Water-Type Emulsion via the Enteral Route. *Lipids* **1999**, *34* (3), 249–254.

Valkovska, D. S.; Ivanov, I. B. Effect of Surfactants on the Film Drainage. *J. Colloid Interface Sci.* **1999**, *211* (2), 291–303.

Vitale, S. a.; Katz, J. L. Liquid Droplet Dispersions Formed by Homogeneous Liquid-Liquid Nucleation: “The Ouzo Effect.” *Langmuir* **2003**, *19* (10), 4105–4110.

Voorhees, P. W. The Theory of Ostwald Ripening. *J. Stat. Phys.* **1985**, *38* (1–2), 231–252.

Wah, B.; Breidigan, J. M.; Adams, J.; Horbal, P.; Garg, S.; Porcar, L.; Perez-Salas, U. Reconciling Differences between Lipid Transfer in Free-Standing and Solid Supported Membranes: A Time-Resolved Small-Angle Neutron Scattering Study. *Langmuir* **2017**, *33* (14), 3384–3394.

Wang, X.; Shi, Y.; Graff, R. W.; Lee, D.; Gao, H. Developing Recyclable PH-Responsive Magnetic Nanoparticles for Oil–Water Separation. *Polymer (Guildf).* **2015**, *72*, 361–367.

Wang, Y.; Kausch, C. M.; Chun, M.; Quirk, R. P.; Mattice, W. L. Exchange of Chains between Micelles of Labeled Polystyrene-Block-Poly(Oxyethylene) As Monitored by Nonradiative Singlet Energy Transfer. *Macromolecules* **1995**, *28* (4), 904–911.

Wei, C. W.; Lombardo, M.; Larson-Smith, K.; Pelivanov, I.; Perez, C.; Xia, J.; Matula, T.; Pozzo, D.; O’Donnell, M. Nonlinear Contrast Enhancement in Photoacoustic Molecular Imaging with Gold Nanosphere Encapsulated Nanoemulsions. *Appl. Phys. Lett.* **2014**, *104*, 0–4.

Wei, C.; Xia, J.; Lombardo, M.; Perez, C.; Arnal, B.; Larson-Smith, K.; Pelivanov, I.; Matula, T.; Pozzo, L.; O’Donnell, M. Laser-Induced Cavitation in Nanoemulsion with Gold Nanospheres for Blood Clot Disruption: In Vitro Results. *Opt. Lett.* **2014**, *39* (9), 2599–2602.

Weiss, J.; Canceliere, C.; McClements, D. J. Mass Transport Phenomena in Oil-in-Water Emulsions Containing Surfactant Micelles: Ostwald Ripening. *Langmuir* **2000**, *16* (17), 6833–6838.

Weiss, J.; Coupland, J. N.; Brathwaite, D.; McClements, D. J. Influence of Molecular Structure of Hydrocarbon Emulsion Droplets on Their Solubilization in Nonionic Surfactant Micelles. *Colloids Surfaces A Physicochem. Eng. Asp.* **1997**, *121* (1), 53–60.

Weiss, J.; Herrmann, N.; McClements, D. J. Ostwald Ripening of Hydrocarbon Emulsion Droplets in Surfactant Solutions. *Langmuir* **1999**, *15* (20), 6652–6657.

Weiss, J.; McClements, D. J. Mass Transport Phenomena in Oil-in-Water Emulsions Containing Surfactant Micelles: Solubilization. *Langmuir* **2000**, *16* (14), 5879–5883.

Whitby, C. P.; Djerdjev, A. M.; Beattie, J. K.; Warr, G. G. Nanoparticle Adsorption and Stabilisation of Surfactant-Free Emulsions. *J. Colloid Interface Sci.* **2006**, *301* (1), 342–345.

Willner, L.; Poppe, A.; Allgaier, J.; Monkenbusch, M.; Richter, D. Time-Resolved SANS for the Determination of Unimer Exchange Kinetics in Block Copolymer Micelles. *Europhys. Lett.* **2001**, *55* (5), 667–673.

Wong, S. F.; Lim, J. S.; Dol, S. S. Crude Oil Emulsion: A Review on Formation, Classification and Stability of Water-in-Oil Emulsions. *J. Pet. Sci. Eng.* **2015**, *135*, 498–504.

Wu, J.; Ma, G.-H. Recent Studies of Pickering Emulsions: Particles Make the Difference. *Small* **2016**, *12* (34), 4633–4648.

Xi, Y.; Li, D. S.; Newbloom, G. M.; Tatum, W. K.; O'Donnell, M.; Luscombe, C. K.; Pozzo, L. D. Sonocrystallization of Conjugated Polymers with Ultrasound Fields. *Soft Matter* **2018**, 4963–4976.

Xu, H.; Zeiger, B. W.; Suslick, K. S. Sonochemical Synthesis of Nanomaterials. *Chem. Soc. Rev.* **2013**, *42* (7), 2555–2567.

Yamanaka, K.; Nishino, S.; Naoe, K.; Imai, M. Preparation of Highly Uniform Pickering Emulsions by Mercaptocarboxylated Gold Nanoparticles. *Colloids Surfaces A Physicochem. Eng. Asp.* **2013**, *436*, 18–25.

Yang, P. W.; Lin, T. L.; Hu, Y.; Jeng, U. S. A Time-Resolved Study on the Interaction of Oppositely Charged Bicelles - Implications on the Charged Lipid Exchange Kinetics. *Soft Matter* **2015**, *11* (11), 2237–2242.

Yang, Y.; Fang, Z.; Chen, X.; Zhang, W.; Xie, Y.; Chen, Y.; Liu, Z.; Yuan, W. An Overview of Pickering Emulsions: Solid-Particle Materials, Classification, Morphology, and Applications. *Front. Pharmacol.* **2017**, *8* (MAY), 1–20.

Yao, Y. Enhancement of Mass Transfer by Ultrasound: Application to Adsorbent Regeneration and Food Drying/Dehydration. *Ultrason. Sonochem.* **2016**, *31*, 512–531.

Ye, G.; Lu, X.; Han, P.; Peng, F.; Wang, Y.; Shen, X. Application of Ultrasound on Crude Oil Pretreatment. *Chem. Eng. Process. Process Intensif.* **2008**, *47* (12), 2346–2350.

Yi, M.; Huang, J.; Wang, L. Research on Crude Oil Demulsification Using the Combined Method of Ultrasound and Chemical Demulsifier. *J. Chem.* **2017**, *2017*.

Zapryanov, Z.; Malhotra, A. K.; Aderangi, N.; Wasan, D. T. Emulsion Stability: An Analysis of the Effects of Bulk and Interfacial Properties on Film Mobility and Drainage Rate. *Int. J. Multiph. Flow* **1983**, *9* (2), 105–129.

Zhang, F.; Ilavsky, J.; Long, G. G.; Quintana, J. P. G.; Allen, A. J.; Jemian, P. R. Glassy Carbon as an Absolute Intensity Calibration Standard for Small-Angle Scattering. *Metall. Mater. Trans. A* **2010**, *41* (5), 1151–1158.

Zhang, T.; Marchant, R. E. Novel Polysaccharide Surfactants: The Effect of Hydrophobic and Hydrophilic Chain Length on Surface Active Properties. *J. Colloid Interface Sci.* **1996**, *177* (2), 419–426.

Zinn, T.; Willner, L.; Lund, R.; Pipich, V.; Richter, D. Equilibrium Exchange Kinetics in N-Alkyl-PEO Polymeric Micelles: Single Exponential Relaxation and Chain Length Dependence. *Soft Matter* **2012**, *8* (3), 623–626.

Zinn, T.; Willner, L.; Pipich, V.; Richter, D.; Lund, R. Molecular Exchange Kinetics of Micelles: Corona Chain Length Dependence. *ACS Macro Lett.* **2016**, *5* (7), 884–888.

CURRICULUM VITAE

Yi-Ting Lee

EDUCATION

University of Washington, Seattle, WA

Ph.D.	*Chemical Engineering*	Aug. 2019
	Thesis Title: Unravelling Synthesis and Transport Phenomena in Emulsion Systems with Small Angle Scattering	
	Advisor: Prof. Lilo D. Pozzo	
M.S.	*Chemical Engineering*	Aug. 2016

University of Michigan, Ann Arbor, MI

M.S.	*Biomedical Engineering*	May 2013

National Taiwan University, Taipei, Taiwan

B.S.	*Chemical Engineering*	June 2010
B.S.	*Bioenvironmental Systems Engineering*	June 2010

Awards

Runstad Family Endowed Fellowship (2014)

RELEVANT EXPERIENCE

University of Washington, Chemical Engineering Department, Seattle, WA

Graduate Research Assistant Advisor: Dr. Lilo D. Pozzo **Jan. 2015-Present**

- Designed and fundamentally examined the formation of gold nanoparticle stabilized Pickering emulsions and polypyrrole stabilized emulsions as a potential novel sonophotoacoustic theranostic agent for blood clot lysis.
- Studied/characterized/experimentally investigated mass transport between stabilized emulsions either at rest or induced by acoustic forces.
- Facilitated in developing a novel sample environment for X-ray and neutron scattering. The setup allows the application of acoustic forces (and/or) laser energies to the samples while simultaneously performing X-ray/neutron scattering experiments.

Teaching Assistant **Jan. 2015-Present**

- In charge of Unit Operations Lab and Surface & Colloids Science Lab operations. Responsible for setting up/maintaining various lab instruments, guiding experimental design, execution, and data analysis.

Zimmer Biomet, Warsaw, IN **Jan. 2014- June 2014**
Manufacturing Engineer

- Designed and performed test method validations for various orthopedic implant packages. Examples of test method validations includes high altitude package test and determining gross leaks in packages.
- Implemented installation validations on new and operational/performance validation of existing packaging equipment.

University of Michigan, Biomedical Engineering Department, Ann Arbor, MI

Biomedical Instrumentation and Design **Jan. 2013 – July 2013**

- Designed and built a prototype for an arthroscopic visualization device in team of 5. Collaborated effectively as a team and provided other teams constructive suggestions on various design topic reviews.
- Represented the University of Michigan to attend the NCIIA BMEidea competition in 2013.
- Designed prototype lead to a patent and start-up company Arthroptics, LLC.

Spine Research Laboratory
Graduate Research Assistant, Advisor: Dr. Chia-Ying Lin **Aug. 2012- July 2013**

- Investigate particle/protein interactions for targeted cancer therapy
- Conduct and interpret viability assay studies using novel nanoparticles

Active and Functional Soft Matter Lab
Graduate Research Assistant, Advisor: Dr. Brian Love **Nov. 2011- Aug. 2012**

- Investigated crosslinking of collagen to develop effective treatment method for Keratoconus.
- Used photorheology to probe UV induced crosslinking kinetics with different photo-sensitizers

National Taiwan University, Chemical Engineering Department, Taipei, Taiwan

Undergraduate Research Assistant, Advisor: Steven S.-S. Wang **Feb. 2008-June 2010**

- Investigate natural substances as potential inhibitors against amyloid formation using spectroscopy
- Applied kinetic models to quantify and describe the effects of inhibitors on amyloid formation.

PUBLICATIONS

Lee, Y.-T.; Li, D. S.; Pozzo, L. D., "Kinetic Analysis of Ultrasound induced oil exchange in oil-in-water emulsions through contrast-variation time-resolved SANS" In preparation, available on request.
Lee, Y.-T.; Pozzo, L. D., "Contrast-variation time-resolved SANS analysis of oil exchange kinetics between oil-in-water emulsions stabilized by anionic surfactants" In preparation, available on request.
Lee, Y.-T.; Li, D. S.; Ilavsky, J.; Kuzmenko, I.; Jeng, G.-S.; O'Donnell, M.; Pozzo, L. D., "Ultrasound-based formation of nano-Pickering emulsions investigated via in-situ SAXS", *J. Colloid Interface Sci. 2018, 536, 281–290.*

Xi, Y.; Li, D. S.; **Lee, Y.-T.**; Pozzo, L. D., "In-situ ultrasound sample environment for small angle scattering studies", *Accomplishments and Opportunities, 2019, 47*
Li, D. S.; **Lee, Y.-T.**; Xi, Y.; Pelivanov, I.; O'Donnell, M.; Pozzo, L. D., "A small-angle scattering environment for in situ ultrasound studies", *Soft Matter 2018, 14 (25), 5283–5293.*
Liu, K. N.; Lai, C. M.; **Lee, Y. T**.; Wang, S. N.; Chen, R. P. Y.; Jan, J. S.; Liu, H. S.; Wang, S. S. S., "Curcumin's pre-incubation temperature affects its inhibitory potency toward amyloid fibrillation and fibril-induced cytotoxicity of lysozyme", *Biochim. Biophys. Acta - Gen. Subj. 2012, 1820 (11), 1774–1786.*

PRESENTATIONS

Lee, Y.-T.; Pozzo, L. D., "Time-resolved SANS Analysis of Oil Exchange Kinetics Between Oil-in-water Emulsions Stabilized by Anionic Surfactants" ACS Colloid & Surface Science Symposium, June, 2019
Lee, Y.-T.; Li, D. S.; O'Donnell, M.; Matula, T.; Pozzo, L. D., "Gold Pickering emulsions as a phase-change contrast agent for photoacoustic imaging" IEEE International Ultrasonics Symposium (IUS), Sept. 2017
Lee, Y.-T.; Li, D. S.; Pozzo, L. D., "Ultrasound synthesis of nano-Pickering emulsions investigated via in-situ SAXS" ACS Colloid & Surface Science Symposium, July, 2017
Li, D. S.; **Lee, Y.-T.;** Matula, T; O'Donnell, M.; Pozzo, L. D., "Self-assembly of nanoparticle surfactants and their use as theranostic agents" 2015 MRS Fall Meeting & Exhibit, Nov. 2015, *Poster*
Lee, Y.-T.; Li, D. S.; O'Donnell, M.; Matula, T.; Pozzo, L. D., "Amphiphilic gold nanoparticle stabilized Pickering emulsions as a contrast agent for photoacoustic imaging" UW Chemical Engineering Graduate Student Symposium, Sept. 2015, *Poster*
Lee, Y.-T.; Pozzo, L. D, "Recanilization of blood clots using amphiphilic gold nanoparticle stabilized Pickering emulsions" Thirteenth International Nanomedicine and Drug Delivery Symposium, Sept. 2015, *Poster*

PATENTS

U.S. Patent 9839344: "Cannula assembly" **December 12, 2017**
Patent application: "Nanoemulsion agent" **Filed in April 2019**

LEADERSHIP

Taiwan Military Service- Second Lieutenant **Aug. 2010-July 2011**

- Communication between veterans and military.

SKILLS

Technical: UV-vis, small angle X-ray scattering (SAXS), small angle neutron scattering (SANS), dynamic light scattering (DLS), transmission electron microscopy (TEM), scanning electron microscopy (SEM), thermo-gravimetric analysis (DSC/TGA), Fourier-transform infrared spectroscopy (FTIR), pendant drop and sessile contact angle, surface tensiometry, rheology, Matlab, Python, Igor Pro